AD _____

Award Number: W81XWH-13-2-0039

TITLE: Spectroscopic Biomarkers for Monitoring Wound Healing and Infection in Wounds

PRINCIPAL INVESTIGATOR: Dr. Eric Elster

CONTRACTING ORGANIZATION: The Geneva Foundation
Tacoma, WA 98402

REPORT DATE: June 2015

TYPE OF REPORT: Annual

PREPARED FOR: U.S. Army Medical Research and Materiel Command
Fort Detrick, Maryland 21702-5012

DISTRIBUTION STATEMENT: Approved for Public Release;
Distribution Unlimited

The views, opinions and/or findings contained in this report are those of the author(s) and should not be construed as an official Department of the Army position, policy or decision unless so designated by other documentation.

REPORT DOCUMENTATION PAGE

Form Approved
OMB No. 0704-0188

1. REPORT DATE	2. REPORT TYPE	3. DATES COVERED
June 2015	Annual	15 May 2013 – 14 May 2014

4. TITLE AND SUBTITLE

Spectroscopic Biomarkers for Monitoring Wound Healing and Infection in Wounds

5a. CONTRACT NUMBER

5b. GRANT NUMBER
W81XWH-13-2-0039

5c. PROGRAM ELEMENT NUMBER

6. AUTHOR(S)

Dr. Eric Elster, Dr. Nicole Crane

E-Mail: eric.elster@usuhs.edu, nicole.crane@med.navy.mil

5d. PROJECT NUMBER

5e. TASK NUMBER

5f. WORK UNIT NUMBER

7. PERFORMING ORGANIZATION NAME(S) AND ADDRESS(ES) AND ADDRESS(ES)

The Geneva Foundation
917 Pacific Ave, Suite 600
Tacoma, WA 98402

8. PERFORMING ORGANIZATION REPORT NUMBER

9. SPONSORING / MONITORING AGENCY NAME(S) AND ADDRESS(ES)
U.S. Army Medical Research and Materiel Command
Fort Detrick, Maryland 21702-5012

10. SPONSOR/MONITOR'S ACRONYM(S)

11. SPONSOR/MONITOR'S REPORT NUMBER(S)

12. DISTRIBUTION / AVAILABILITY STATEMENT
Approved for Public Release; Distribution Unlimited

13. SUPPLEMENTARY NOTES

14. ABSTRACT

The complexity and severity of the extremity wounds seen in recent military operations have necessitated the demand for improved wound assessment, before, during and after medical treatment. We have quantified parameters such as tissue oxygenation, tissue temperature and the molecular environment at specific locations within the wound, to better understand the wound healing process in various wound phenotypes. This has helped us to establish which parameters are most important for a correct initial assessment of the wound along with a more accurate wound healing prediction. We will apply the same research strategy to wound healing in a civilian trauma center. The parameters bearing the most weight will be used to diagnose trauma wounds and predict patient outcome.

15. SUBJECT TERMS
Wound healing; biomarkers; Raman spectroscopy; 3CCD imaging; infrared imaging; tissue oxygenation

16. SECURITY CLASSIFICATION OF:			17. LIMITATION OF ABSTRACT	18. NUMBER OF PAGES	19a. NAME OF RESPONSIBLE PERSON
a. REPORT	b. ABSTRACT	c. THIS PAGE			USAMRMC
U	U	U	UU	319	19b. TELEPHONE NUMBER *(include area code)*

Standard Form 298 (Rev. 8-98)
Prescribed by ANSI Std. Z39.18

Table of Contents

INTRODUCTION

Casualties in Operation Iraqi Freedom (OIF) and Operation Enduring Freedom (OEF) have experienced a high rate of extremity injuries with nearly ubiquitous diffuse tissue damage and compromised local circulation often associated with overt vascular injury. These injuries include traumatic amputations, open fractures, crush injuries, burns, acute vascular disruption, blastwave-associated pressure injuries, air, thrombotic, and fat embolism, and compartment syndrome. In the treatment of such complex traumatic injuries, improved assessment of global and regional perfusion, extent of infection, location and development of necrotic tissue, as well as location and development of early heterotopic ossification would facilitate the resuscitation and definitive treatment of these patients. Noninvasive spectroscopic methods may fulfill such a role, particularly Raman spectroscopy, infrared imaging, and visible reflectance spectroscopic imaging. These technologies are capable of monitoring tissue temperature (1), perfusion (2) and associated hypoxia (3-6), collagen deposition (7, 8), and development of calcified tissue (9-18).

The complexity and severity of the extremity wounds seen in recent military operations have necessitated the demand for improved wound assessment, before, during and after medical treatment. We have quantified parameters such as tissue oxygenation, tissue temperature and the molecular environment at specific locations within the wound, to better understand the wound healing process in various wound phenotypes. This has helped us to establish which parameters are most important for a correct initial assessment of the wound along with a more accurate wound healing prediction. The parameters bearing the most weight will be used to diagnose trauma wounds and predict patient outcome. Improved objective assessment of acute wounds would be conducive to improved treatment of the wounds which may result in faster healing times, decreased infection rates, and decreased local and systemic complications of injury.

KEYWORDS

Wound healing; biomarkers; Raman spectroscopy; 3CCD imaging; infrared imaging; tissue oxygenation

OVERALL PROJECT SUMMARY

Our hypothesis is that the development of an integrated prediction model (using spectroscopy and spectroscopic imaging data in addition to clinical data) will allow for more accurate assessment of tissue perfusion and oxygenation in extremity injuries, as well as the precise biochemical composition of the wound bed, providing improved diagnosis and prognosis of the affected tissue. Improved objective assessment of acute wounds would be conducive to improved treatment of the wounds which may result in faster healing times, decreased infection rates, and decreased local and systemic complications of injury.

This proposal will serve to validate these prediction models, developed from a military population of acute combat wounds, in civilian acute wounds. We have initiated a collaboration with Emory University to expand this study at a civilian Level 1 trauma center.

The goal of this proposal is to comprehensively address key decision points for critically ill trauma and surgical patients including: 1) timing of wound closure; 2) assessment of bacterial bioburden; 3) techniques of wound management; 4) amputee-specific issues including, timing of wound closure, management of infection, ischemia and peripheral nerve injury; 5) early identification and monitoring of heterotopic ossification.

Aim 1

Aim 1 is comprised of four tasks:

a) Collect 3-CCD and IR images of extremity wounds in the operating room.

b) Collect serum, wound exudates, and tissue biopsies from each wound during the surgical debridement process.

c) Perform quantitative bacteriology on wound effluent and tissue, RT-PCR on tissue biopsies, protein analysis on serum, and Raman spectroscopy on tissue biopsies and wound effluent.

d) Correlate the presence of necrotic tissue (depth and breadth), wound infection (serial quantitative bacteriology, development of heterotopic ossification, physician and pathologist observations, and serum cytokine levels and wound cytokine and gene expression levels. (n=100)

To date, we have enrolled 35 patients at Grady Memorial Hospital through Emory University. Only one eligible patient has declined enrollment. Initial enrollment was extremely slow and limited our ability to complete Tasks 1a-d during the first year. Slow enrollment was due to inclusion criteria not being met by patients that were not vulnerable persons, and an inability to enroll patients that did not speak English. Since amending the clinical protocol to include a consent form in Spanish, we have been able to almost double our enrollment. We anticipate that enrollment numbers will continue to grow, particularly through the summer months, hopefully reaching our target enrollment of 50 patients.

A summary of the samples obtained during the performance period is presented in Table 1.

Number of newly enrolled patients	20
Number of wounds	32
Number of samples collected (all types)	516
Number of tissue biopsies	237
Number of serum samples	68
Number of effluent samples	211
Number of wound images	>150

Table 1. Summary of samples obtained at Grady Memorial Hospital between May 15th, 2014 and May 14th, 2015.

As outlined in Task 1a, to date a total of 126 3CCD images from 32 patients have been analyzed. A preliminary analysis is presented below in Figure 1. While there do appear to be differences in the camera channels between normal healing wounds (green bars) and dehisced wounds (yellow bars), the differences are not statistically significant.

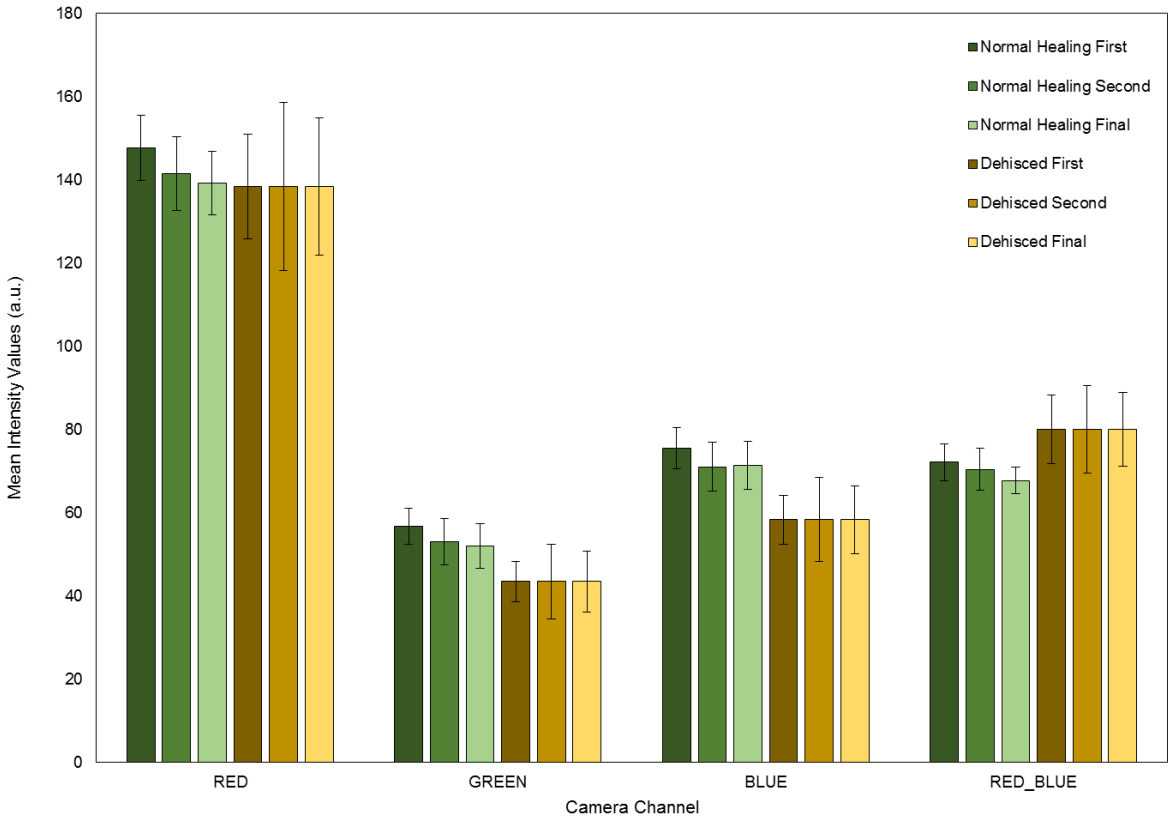

Figure 1. Comparison of the response of camera channels for normal healing and dehisced wounds at first, second, and final debridements.

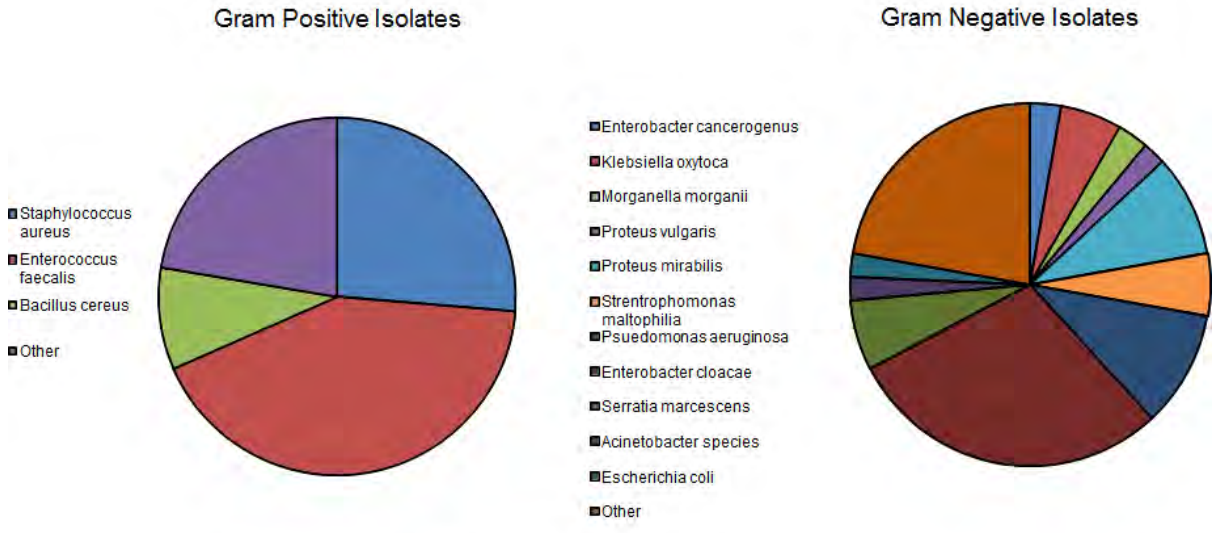

Figure 2. Summary of bacterial isolates present in wound effluent and tissue biopsy specimens obtained from the first 25 patients enrolled at Grady Memorial Hospital.

As outlined in Task 1b, serum, wound exudate, and tissue biopsies have been collected for each patient enrolled in the study to date. To date, all effluent and tissue samples have been processed for quantitative bacteriology for all 35 patients enrolled. To date, of the 516 samples collected, one effluent and one tissue biopsy for each debridement for each wound has been submitted for microbiological analysis. Figure 2 demonstrates the prevalence of Gram-positive and –negative bacterial isolates present in wound effluent and/or tissue biopsies of the first 25 patients enrolled at Grady Memorial Hospital.

As a preliminary step for identification of bacterial isolates in wound effluent using Raman spectroscopy, we have collected Raman spectra of 42 bacterial isolates, including ESKAPE pathogens *Escherichia coli*, *Stapylococcus aureus*, *Klebsiella pneumonia*, *Acinetobacter baumannii*, *Pseudomonas aeruginosa*, and *Enterococcus faecium*. A hierarchical model has been generated for bacterial isolates for differentiation of the following based on Raman spectra: 1) Gram status (+/-) – Figure 2; 2) Family – Figures 3A & B. Classification models based on Raman spectroscopic data have been compared to classification models based on biochemistries, antibiotic sensitivities and resistance, 16S PCR, and high resolution melting data.

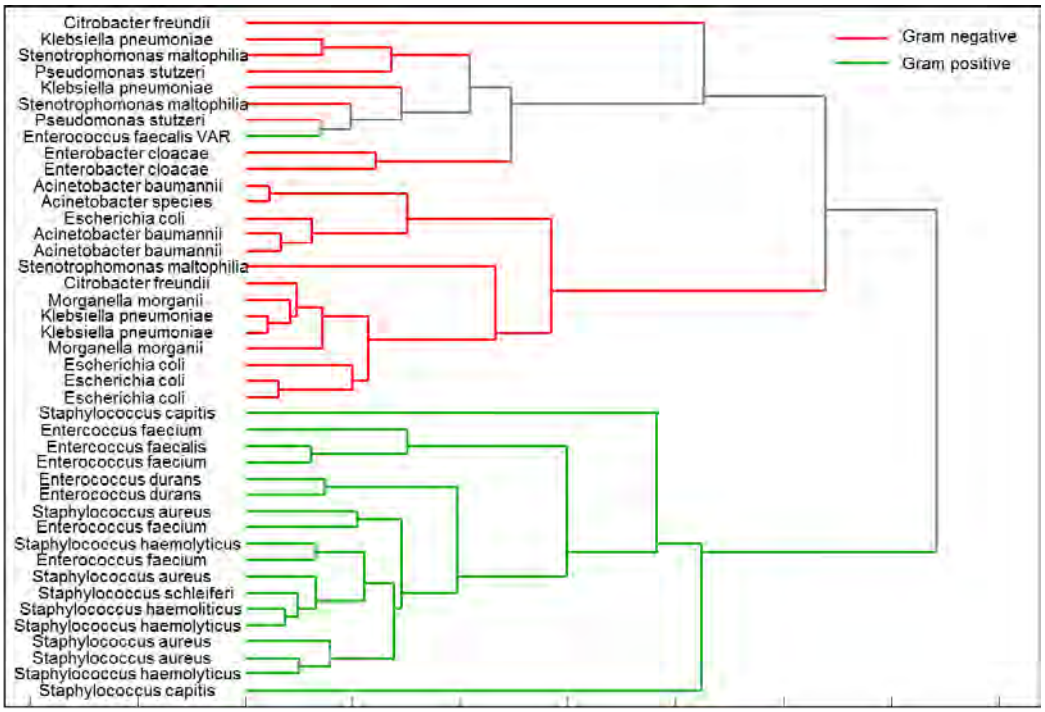

Figure 2. Classification model for Gram status of bacterial isolates. The model performs with 98% accuracy.

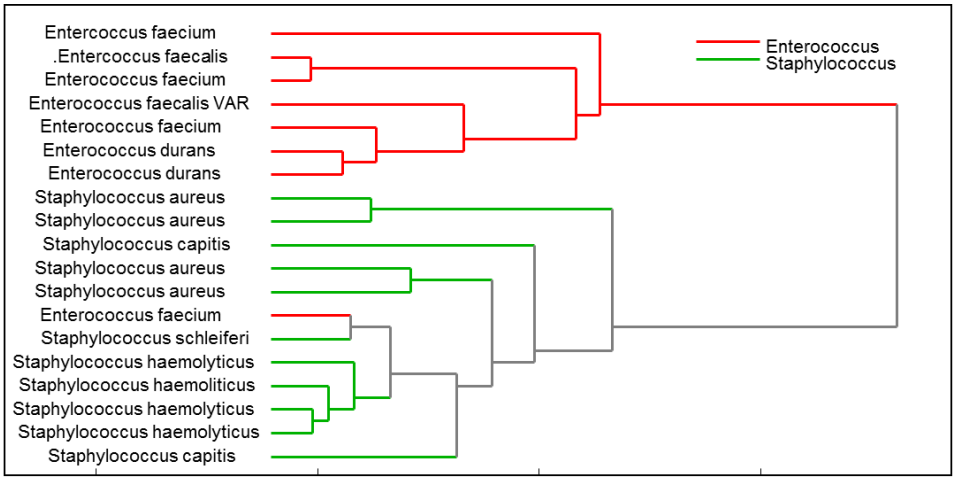

Figure 3A. Family classification model for Gram positive bacterial isolates. The model performs with 95% accuracy.

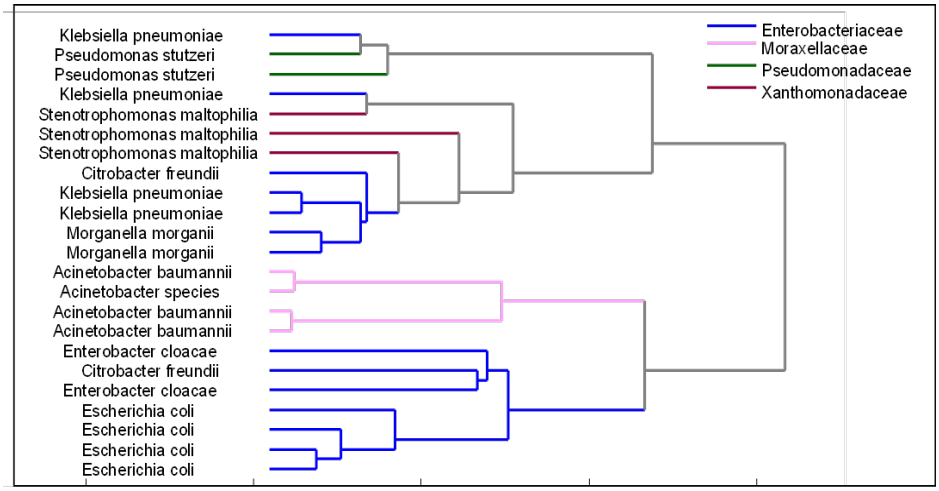

Figure 3B. Family classification model for Gram negative bacterial isolates. The model performs with 91% accuracy.

In addition, as samples are received from Grady Memorial Hospital/Emory University and processed, we are performing protein analysis on serum and effluent via Luminex, and preparing samples for gene expression analysis via Taqman (Task 1c). To date, 175 of the effluent and serum samples have been processed for analysis via Luminex and Luminex analysis has been completed for 124 of the samples processed. Preliminary analysis of serum and effluent samples from the first 19 patients reveals a similar trend in cytokine and chemokine expression when compared to military trauma patients – Figure 4 (next page).

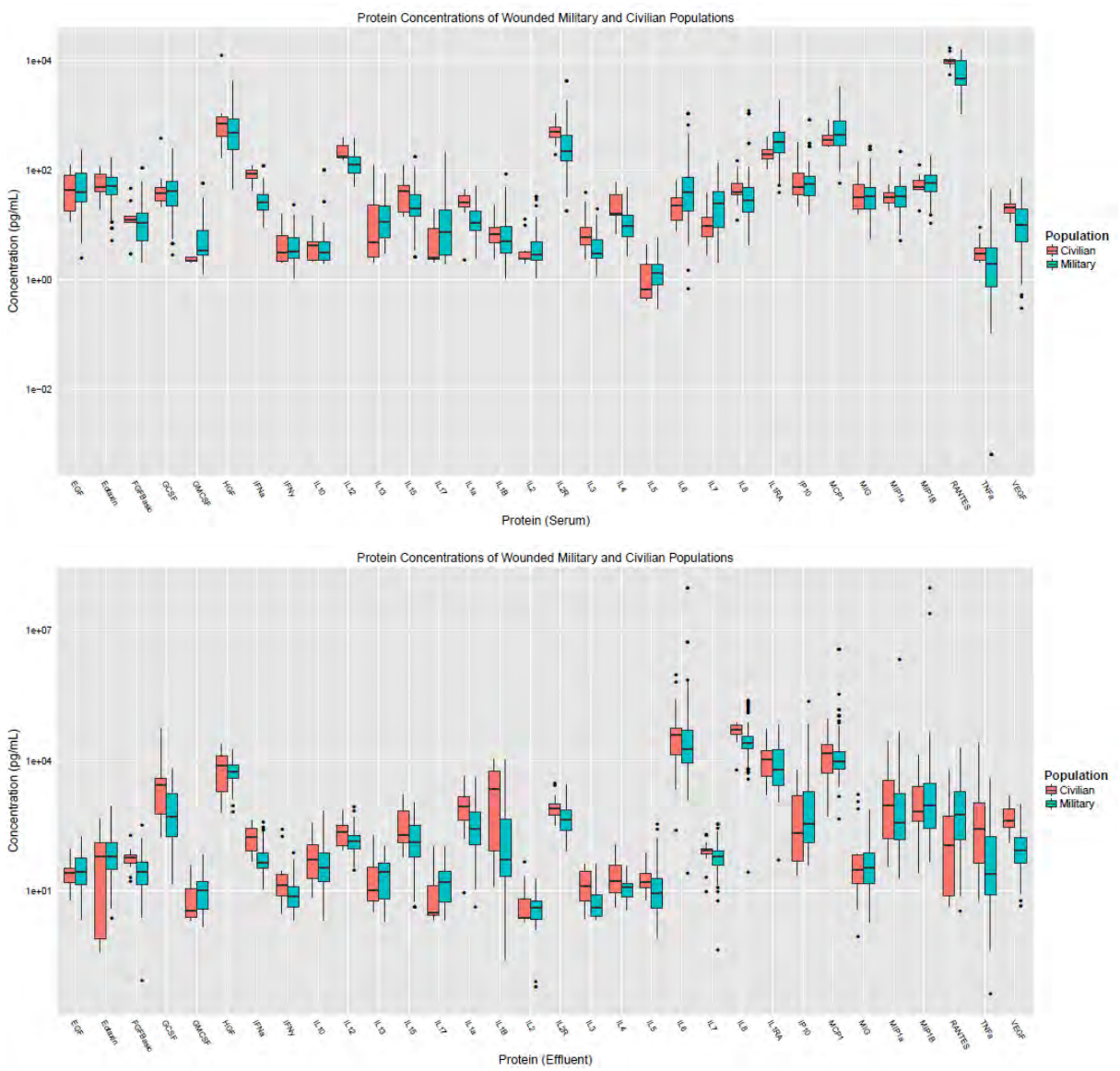

Figure 4. Comparison of protein expression of cytokines and chemokines from military and civilian patients in both serum (A) and wound effluent (B).

Though Task 1c also specifies the collection of Raman spectra of tissue biopsies and wound effluent, the 830 nm Raman spectroscopic system necessary to collect the spectra was not installed until April 2014. Since the instrument's installation, however, Raman spectra have been collected (5 replicates per wound biopsy and three replicates per effluent sample) for all wound biopsies collected to date. We are still collecting Raman spectra of wound effluent, and anticipate the completion of that task by the end of the grant cycle (September 30th, 2015).

Directly in line with the work performed for Task 1c, in an effort to achieve lower limits of detection for detection of bioburden, we have begun utilizing surface enhanced Raman spectroscopy (SERS). We have successfully synthesized silver nanoparticles for surface enhanced Raman spectroscopy (SERS). Below is a transmission emission microscopy image of a sample of the silver nanoparticles, synthesized via the methods outlined in a manuscript published in Analytical Chemistry by White and coworkers in 2010. Note, the nanoparticles have a rod-like shape (Figure 5).

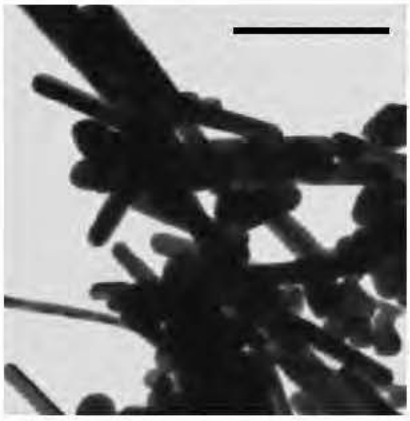

Figure 5. Transmission emission microscopy image of silver nanoparticles synthesized. Scale bar = 500 nm.

Briefly, silver nitrate was added to ultrapure water, which was then brought to a boil in a flask under vigorous stirring. Sodium citrate was added, and the solution was left to boil for an additional 10 - 60 minutes. After the solution turned greenish brown, which indicated the formation of silver colloid, it was then removed from heat. The solution was immediately cooled on ice to prevent aggregation of the silver nanoparticles. After varying several variables of the nanoparticle synthesis, we have found that more rapid boiling and longer boiling times result in smaller nanoparticles, which is preferred. Once silver nanoparticles are formed, they can be aliquoted into solution (such as wound effluent), deposited onto a traditional substrate for Raman spectroscopy (such as a gold-coated slide), or printed onto paper for "test strip" testing. Currently, we are testing all formats for optimal signal enhancement and reproducibility.

We have collected SERS spectra of all bacterial isolates for comparison with performance of standard Raman spectroscopy. In Figure 6, Raman spectra are displayed of nanoparticles alone (green), *Cornyebacterium striatum* alone, and nanoparticles with *Cornyebacterium striatum* (purple). All spectra were acquired using an 830 nm excitation with a 10 second exposure and 5 accumulations. Raman spectral features on the traditional Raman spectra of the bacteria (red) demonstrate a very low signal to noise ratio (SNR). SERS spectra of the bacteria show clear enhancement of the SNR. While the Raman spectral features of the SERS spectra of bacteria do not align with the non-SERS spectra of bacteria, this is expected; it should not, however, impair spectral classification of bacteria. Rather, the enhanced SNR in the SERS spectra of bacteria is expected to improve spectral classification and identification.

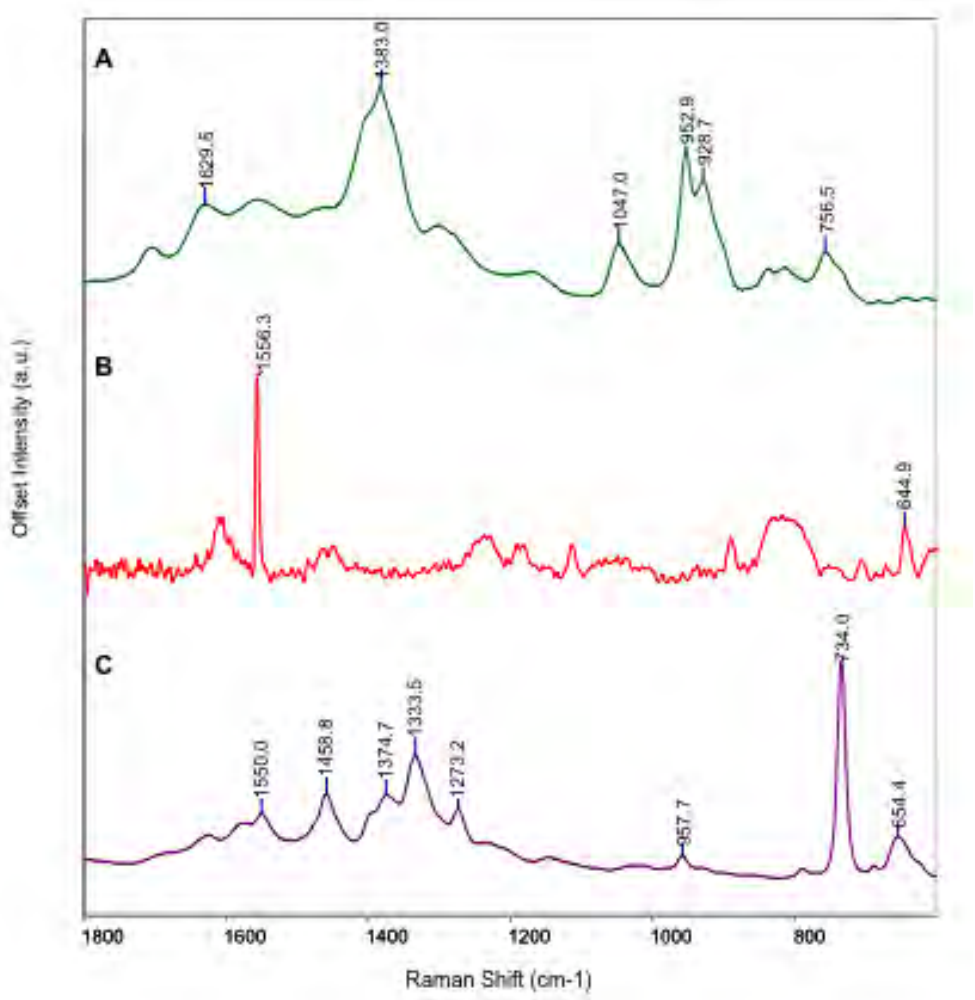

Figure 6. Raman spectra are displayed for A) nanoparticles alone (green), B) *Cornyebacterium striatum* alone (red), and C) nanoparticles with *Cornyebacterium striatum* (purple).

Work on Task 1d has begun in an effort to better characterize tissue that may develop heterotopic ossification. We have further characterized heterotopic ossification (HO) tissue, in an attempt to push the limits of Raman spectroscopic detection of early HO development. Recent research suggests that substance P (SP) is a necessary intermediate signal for HO formation. We asked whether Raman spectral changes, measured *ex vivo*, could be associated with histologic evidence of the earliest signs of HO formation and substance P (SP) expression in tissue biopsies from the wounds of combat casualties.

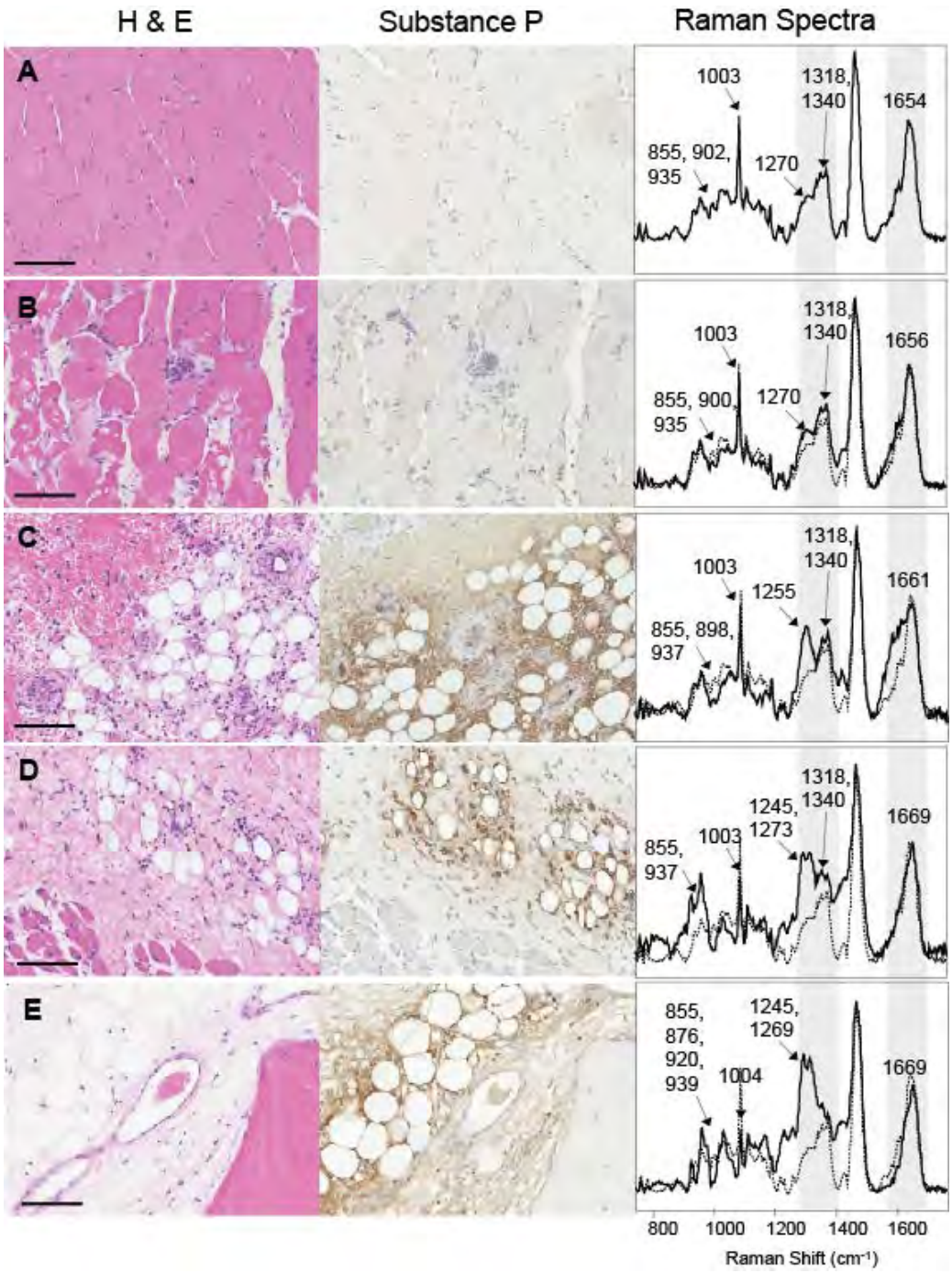

Figure 7. Comparison of serial tissue sections (H&E stained tissue – left; substance P IHC stained tissue – middle; Raman spectrum of unstained tissue – right) for: A) control muscle, B) injured muscle, C) very early HO (< 16 days post-injury), D) early HO (> 16 days post-injury), and E) mature HO (> 100 days post-injury). Scale bar = 100 μm.

In this pilot study, we compared normal muscle tissue, injured muscle tissue, very early HO lesions (< 16 days post-injury), early HO lesions (> 16 days post-injury), and mature HO lesions (Figure 1). SP expression in the HO lesions appears to peak between 16

and 30 days post-injury, as determined by SP immunohistochemistry of corresponding tissue sections, potentially indicating optimal timing for administration of therapeutics.

Raman spectra displayed in Figure 7 are representative of the indicated tissue type and overlaid with the normal muscle Raman spectrum (dashed) in subsequent panels. Gray boxes in the right panels highlight changes in the Amide III and Amide I regions of the Raman spectra. Raman spectroscopic bands of interest and their band assignments are as follows: 855 and 876 cm^{-1} – ν(C-C) hydroxyproline; 920 cm^{-1} – ν(C-C) proline; 898 and 937 cm^{-1} – ν(C-C) protein backbone; 1003 cm^{-1} – C-C ring breathing phenylalanine; 1245 cm^{-1} – ν(C-N) Amide III, disordered; ~1270 cm^{-1} – δ(N-H), ν(C-N) Amide III, ordered; 1318 cm^{-1} - $\gamma(CH_2, CH_3)$ twist; 1340 cm^{-1} – $\gamma(CH_2, CH_3)$ wag; ~1650-1670 cm^{-1} – ν(C=O), Amide I. The dissimilarity between the Raman spectrum of muscle and HO tissue is obvious in panels C-E, even at the earliest stage of HO development.

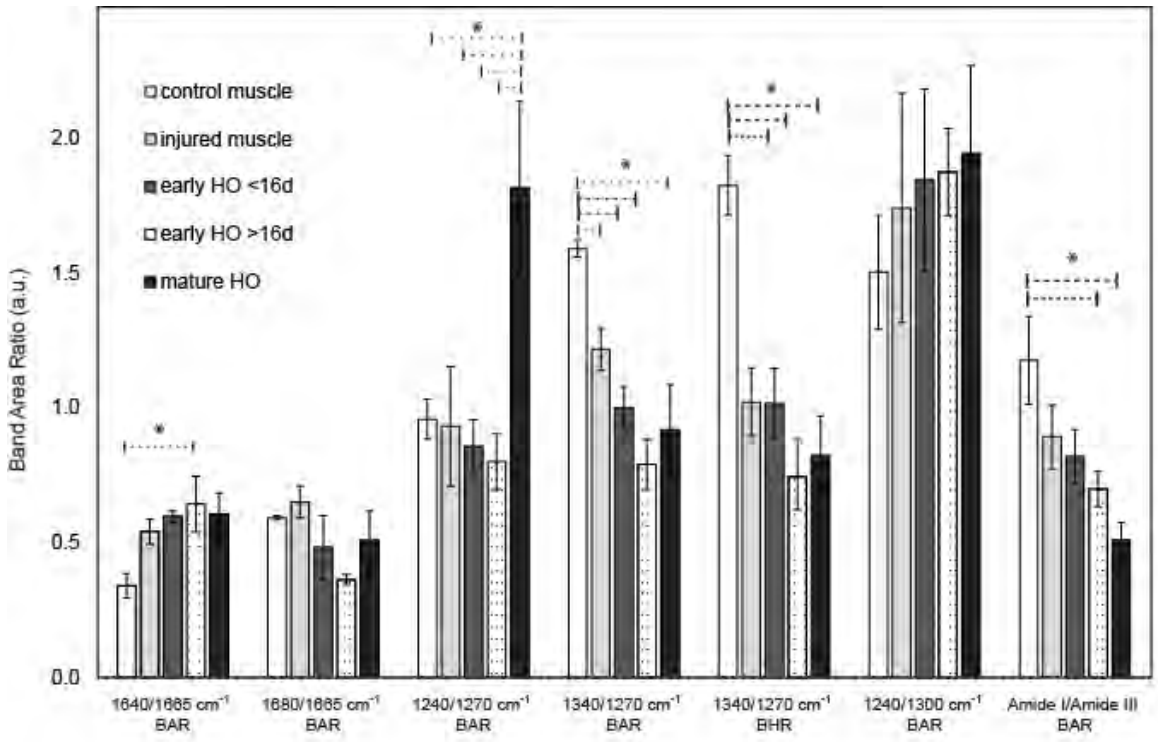

Figure 8. A comparison of band area ratios calculated from Raman spectra to assess tissue quality are presented for control muscle (white), injured muscle (light gray), very early HO (gray, < 16 days post-injury), early HO (spotted white, > 16 days post-injury), mature HO (black). Vertical bars = standard deviation. Dashed horizontal bars = relationship for statistically significant differences. An asterisk (*) indicates a p-value $\leq$ *0.05*.

The Raman spectra of these tissues demonstrate clear differences in the amide I and III spectral regions of HO lesions compared to normal tissue, denoted by changes in the Amide I band center (*p<0.01*) and the 1340/1270 cm^{-1} (*p<0.05*) band area and band height ratios, displayed in Figure 8.

Finally, there is a shift in the Amide I band in the Raman spectra from 1659.1 ± 0.5 cm^{-1} to 1668.1 ± 0.6 cm^{-1} – this is likely due to increased collagen content (*p<0.01*).

	Control muscle	Injured muscle	Very Early HO <16d	Early HO >16d	Mature HO
Amide I BC	1659.1 (± 0.5) c,d,e	1661.0 (± 0.5) c,d,e	1664.3 (± 1.3) a,b,d,e	1668.0 (± 0.6) a,b,c	1668.1 (± 0.6) a,b,c

P-values ≤ 0.05 compared to a = control muscle, b = injured muscle, c = early HO <16d, d = early HO >16d, and/or e = mature HO.

Table 2. Comparison of Amide I band center (BC) ± standard error of mean (SEM).

In general, when comparing muscle (normal or injured) to HO tissue (early or mature), we noted an increase in Raman shift in the Amide I BC, an increase in the 1640/1665 cm^{-1} BAR and the 1240/1300 cm^{-1} BAR, and a decrease in the 1340/1270 cm^{-1} BAR and the Amide I/Amide III BAR. These changes in Raman metrics can also be examined as a progression of the development of heterotopic ossification.

The 1640/1665 cm^{-1} BAR shows a statistically significant difference between control muscle and early HO lesions (*p=0.03*), and approaches statistical significance when comparing control muscle (0.34 ± 0.04) and very early HO (0.60 ± 0.02) and mature HO lesions (0.61 ±0.08, *p=0.08* and *p=0.07* respectively). The 1340/1270 cm^{-1} BAR and BHR are sensitive metrics for differentiating control muscle from injured muscle and HO lesions (*p<0.01*). The 1240/1270 cm^{-1} band area ratio is a discriminating Raman metric for distinguishing mature HO lesions (1.82 ± 0.32) from all other HO lesions and muscle (0.86 ± 0.10, 0.80 ± 0.10, and 0.96 ±0.07, 0.93 ± 0.22, respectively; *p<0.05*). However, the Amide I BC is the best Raman metric at individuating all of the tissue categories (*p<0.01*).

Finally, the category of biopsy (i.e. control muscle, very early HO, etc.) was significantly correlated with the 1665 cm^{-1} BC, 1340/1270 cm^{-1} BAR and BHR, and Amide I/Amide III BAR (*p<0.01*). Substance P expression in tissue expressions correlated with only one Raman metric, the 1680/1665 cm^{-1} BAR (*p<0.01*).

In this study, we used Raman spectroscopy to discern molecular changes in the matrix components that occur prior to and during the formation of HO, in conjunction with substance P expression in the tissue. We compared normal muscle to injured muscle, very early, early, and mature HO lesions. For mature HO, the clinical sequelae of HO formation is usually readily apparent on physical and/or radiologic examination. In

contrast, immature and largely unmineralized HO lesions are not as clinically obvious, which is why we are exploring non-invasive means by which to identify it. Raman Spectroscopy correlates with histologic appearance of tissues within combat wounds, and can identify the earliest signs in patients who are actively developing HO.

Aim 2

Aim 2 is comprised of one task - use machine learning to validate spectroscopic and clinical results with patient outcome as a predictor. In this aim, we will predict patient outcomes based on correlations between spectroscopic and clinical parameters and wound grade and healing. (n=100 patients). Based on current enrollment, we anticipate a final enrollment of 50 patients.

A preliminary wound outcome prediction model was generated from Raman spectra (collected on the 785nm Raman system) of wound biopsies collected from patients enrolled into a sister protocol at Walter Reed National Military Medical Center (WRNMMC protocol 352334) using a partial least squares discriminant analysis (PLSDA). The receiver operating curve (ROC) for the prediction model, which can be used to assess the success of the prediction, is displayed below in Figure 9.

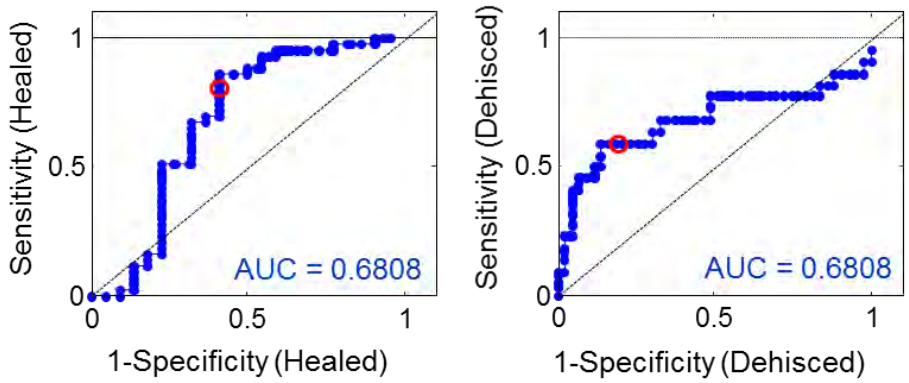

Figure 9. Preliminary model generated from Raman spectra (254 wound biopsies collected from 81 wounds, spectra collected on 785 nm Raman system) of combat wound biopsies to predict wound dehiscence. The PLSDA model performs with 77.3% sensitivity, 81.4% specificity, and 80% accuracy.

While the PLSDA model of the 785nm Raman spectra demonstrates >70% sensitivity, specificity, and accuracy for predicting wound dehiscence, the performance is less than optimal.

We have generated a second PLSDA model for predicting wound outcome, including normal healing, delayed healing, and wound dehiscence, using replicates of 830nm Raman spectra of the same wound biopsies. There is a clear improvement in the performance of the prediction model for normal and impaired healing wounds (including both delayed and dehisced wounds) – Figure 10 (next page).

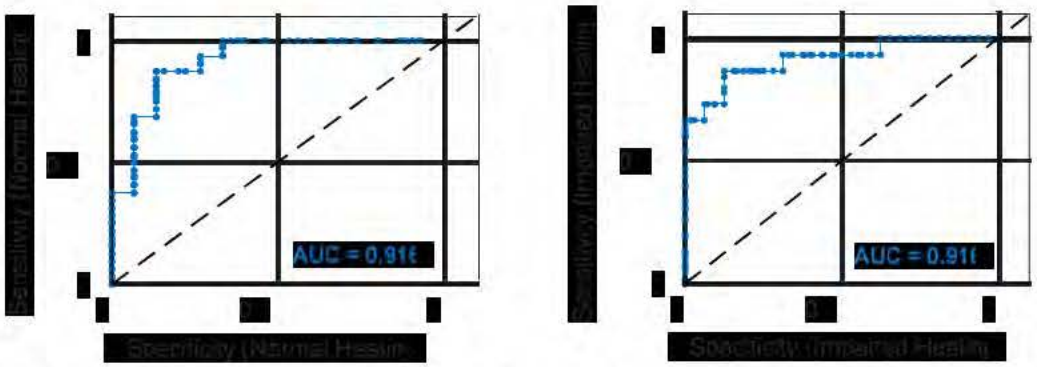

Figure 10. Preliminary model generated from Raman spectra (254 wound biopsies collected from 81 wounds, spectra collected on 830 nm Raman system) of combat wound biopsies to predict impaired wound healing. The PLSDA model performs with 86.7% sensitivity, 81.3% specificity, and 83.0% accuracy.

As a next step towards completing Task 2, we will validate the PLSDA model on an external validation data set comprised of 830 nm Raman spectra of the Grady Memorial Hospital/Emory University wound biopsies.

In addition, we will start a preliminary analysis of meta-datasets (comprised of 3CCD image values, Raman spectra, microbiological data, clinical data, protein expression data, and gene expression data over the next 3 months, prior to the grant close date.

KEY RESEARCH ACCOMPLISHMENTS

- We have received serum, wound exudate, and tissue biopsies from 35 patients to date.
- 3CCD images have been analyzed for the first 32 patients.
- Microbiological analysis of all effluent and tissue samples from patients 1-35 has been completed.
- Raman spectra have been collected in triplicate of all wound biopsies through patient 35.
- Both traditional Raman spectra and SERS spectra have been collected for 42 clinically relevant bacterial isolates, including those observed in both our combat wounded and civilian trauma patients.
- Efforts to collect Raman spectra of colonized wound effluent samples advances.
- Luminex analysis for serum and effluent samples has been performed on patients 1-19 and will be completed through patients 1-35 by end of July 2015.
- Early heterotopic ossification (prior to mineralization and radiographic evidence) has been further characterized by histology and Raman spectroscopy.

CONCLUSION

This project was significantly delayed due to slow enrollment and late receipt of the new 830 nm Raman spectroscopic system. Both of these issues have since been mitigated. We have since enrolled 35 patients and continue to move forward the research. Having received a no cost extension of the award, anticipate meeting our originally stated goal of addressing key decision points for critically ill trauma and surgical patients including: 1) timing of wound closure; 2) assessment of bacterial bioburden; 3) techniques of wound management; and 4) amputee-specific issues including, timing of wound closure, management of infection, ischemia and heterotopic ossification, and peripheral nerve injury; 5) risk stratification of heterotopic ossification.

PUBLICATIONS, ABSTRACTS, AND PRESENTATIONS:

Lay Press
NOTHING TO REPORT.

Peer-Reviewed Scientific Journals
1. M. Harris, K. E. Cilwa, E. A. Elster, B. K. Potter, J. A. Forsberg, N. J. Crane. *Pilot study for detection of early changes in tissue associated with heterotopic ossification: moving toward clinical use of Raman spectroscopy*. Conn. Tiss. Res., 56(2): 144-152, 2015.
2. J. Radowsky, J. Caruso, R. Luthra, M. Bradley, E. A. Elster, J. A. Forsberg, N. J. Crane. *Noninvasive Multimodal Imaging to Predict Recovery of Locomotion after Extended Limb Ischemia*. PLOS One (accepted).

Invited Articles
NOTHING TO REPORT.

Abstracts
1. K. E. Cilwa, T. Slaughter, E. A. Elster, J. A. Forsberg, N. J. Crane. *Surveying Tourniquet-Induced Nerve Damage in Swine using Raman Spectroscopy*. MHSRS, Fort Lauderdale, FL: August 2014.
2. N. J. Crane. *Multivariate Approaches to Predicting Wound Outcome Using Multimodal Data*. SciX, Reno, NV: September 2014.
3. K. E. Cilwa, T. Slaughter, E. A. Elster, J. A. Forsberg, N. J. Crane. *Surveying Tourniquet-Induced Nerve Damage in Swine using Raman Spectroscopy*. SciX, Reno, NV: September 2014.
4. M. Ghebremedhin, S. Yesupriya, N. J. Crane. *Evaluation of Raman Spectroscopic Discrimination between Bacterial Strains and Species using Hierarchical Cluster Analysis*. SciX, Reno, NV: September 2014.
5. K. E. Cilwa, T. Slaughter, E. Elster, J. Forsberg, N. J. Crane. *Raman spectroscopy of non-penetrating peripheral nerve damage in swine: a tool for spectral pathology of nerves*. Photonics West, San Francisco, CA: February 2015.
6. M. Ghebremedhin, S. Yesupriya, J. Luka, N. J. Crane. *Validation of hierarchical cluster analysis for identification of bacterial species using 42 bacterial isolates*. Photonics West, San Francisco, CA: February 2015.

Presentations
1. K. E. Cilwa, T. Slaughter, E. A. Elster, J. A. Forsberg, N. J. Crane. *Surveying Tourniquet-Induced Nerve Damage in Swine using Raman Spectroscopy*. MHSRS, Fort Lauderdale, FL: August 2014.
2. N. J. Crane. *The Spectroscopist: An Unexpected Journey*. Gordon Research Seminar, Biomineralization, New London, NH: August 2014. (invited)
3. N. J. Crane. *Multivariate Approaches to Predicting Wound Outcome Using Multimodal Data*. SciX, Reno, NV: September 2014. (invited)
4. K. E. Cilwa, T. Slaughter, E. A. Elster, J. A. Forsberg, N. J. Crane. *Surveying Tourniquet-Induced Nerve Damage in Swine using Raman Spectroscopy*. SciX, Reno, NV: September 2014.

5. M. Ghebremedhin, S. Yesupriya, N. J. Crane. *Evaluation of Raman Spectroscopic Discrimination between Bacterial Strains and Species using Hierarchical Cluster Analysis*. SciX, Reno, NV: September 2014.
6. K. E. Cilwa, T. Slaughter, E. Elster, J. Forsberg, N. J. Crane. *Raman spectroscopy of non-penetrating peripheral nerve damage in swine: a tool for spectral pathology of nerves*. Photonics West, San Francisco, CA: February 2015.
7. M. Ghebremedhin, S. Yesupriya, J. Luka, N. J. Crane. *Validation of hierarchical cluster analysis for identification of bacterial species using 42 bacterial isolates*. Photonics West, San Francisco, CA: February 2015.
8. N. J. Crane. *Raman Spectroscopic Analysis of Combat Wounds*. University of Maryland: February 2015. (invited)
9. N. Crane. *Spectroscopy and Imaging for Combat Related Medicine*. University of Tampa Bay: March 2015. (invited)
10. J. Prieto, N. Crane, S. M. Mock. *To Heal or Not to Heal? Monitoring Combat Wound Outcome Using Raman Spectroscopy*. USU Research Days, Bethesda, MD: May 2015.
11. S. M. Mock, J. A. Forsberg, B. K. Potter, N. J. Crane. *Total Tourniquet Time and Successful Wound Healing in Acute Combat Wounds*. USU Research Days, Bethesda, MD: May 2015.

INVENTIONS, PATENTS AND LICENSES

Nothing to report.

REPORTABLE OUTCOMES

Nothing to report.

OTHER ACHIEVEMENTS

Nothing to report.

REFERENCES

1. Hanna B, Gorbach A, Gage F, et al. Intraoperative assessment of critical biliary structures with visible range/infrared image fusion. In: American Transplant Congress; 2007; San Francisco, CA; 2007.
2. Gorbach A, Heiss J, Kufta C, et al. Intraoperative infrared functional imaging. Annals of Neuorology 2003;54:297-309.
3. Watson J, Gorbach A, Pluta R, Rak R, Heiss J, Oldfield E. Real-time detection of vascular occlusion and reperfusion of the brain during surgery by using infrared imaging. Journal of Neurosurgery 2002;96:918-23.
4. Gorbach A, Simonton D, Hale DA, Swanson SJ, Kirk AD. Objective, real-time, intraoperative assessment of renal perfusion using infrared imaging. Am J Transplant 2003;3:988-93.
5. Robson MC, Krizek TJ. The effect of human amniotic membranes on the bacteria population of infected rat burns. Ann Surg 1973;177:144-9.
6. Loebl EC, Marvin JA, Heck EL, Curreri PW, Baxter CR. The method of quantitative burn-wound biopsy cultures and its routine use in the care of the burned patient. Am J Clin Pathol 1974;61:20-4.
7. Stojadinovic A, Eberhardt J, Brown TS, et al. Development of a Bayesian model to estimate health care outcomes in the severely wounded. J Multidiscip Healthc;3:125-35.
8. Adamina M, Tomlinson G, Guller U. Bayesian statistics in oncology: a guide for the clinical investigator. Cancer 2009;115:5371-81.
9. Cheng SH, Horng CF, Clarke JL, et al. Prognostic index score and clinical prediction model of local regional recurrence after mastectomy in breast cancer patients. Int J Radiat Oncol Biol Phys 2006;64:1401-9.
10. Damato B, Eleuteri A, Fisher AC, Coupland SE, Taktak AF. Artificial neural networks estimating survival probability after treatment of choroidal melanoma. Ophthalmology 2008;115:1598-607.
11. Heriot AG, Tekkis PP, Smith JJ, et al. Prediction of postoperative mortality in elderly patients with colorectal cancer. Dis Colon Rectum 2006;49:816-24.
12. Jerez-Aragones JM, Gomez-Ruiz JA, Ramos-Jimenez G, Munoz-Perez J, Alba-Conejo E. A combined neural network and decision trees model for prognosis of breast cancer relapse. Artif Intell Med 2003;27:45-63.
13. Levitt SH, Aeppli DM, Nierengarten ME. The importance of local control in the conservative treatment of breast cancer. Acta Oncol 1995;34:839-44.
14. Lisboa P, Taktak A. The use of artificial neural networks in decision support in cancer: a systematic review. . Neural Networks 2006;19:408-15.
15. Orr RK. The impact of prophylactic axillary node dissection on breast cancer survival--a Bayesian meta-analysis. Ann Surg Oncol 1999;6:109-16.

16. Taktak AF, Fisher AC, Damato BE. Modelling survival after treatment of intraocular melanoma using artificial neural networks and Bayes theorem. Phys Med Biol 2004;49:87-98.

17. van den Hout A, Matthews FE. Estimating dementia-free life expectancy for Parkinson's patients using Bayesian inference and microsimulation. Biostatistics 2009;10:729-43.

18. Forsberg J. Modeling survival in patients with operative bony metastases--a new look at an old problem. In: Musculoskeletal Tumor Society Annual Meeting Philadelphia, PA; 2010.

APPENDICES

1. Presentations and manuscripts

connective tissue research

http://informahealthcare.com/cts
ISSN: 0300 8207 (print), 1607 8438 (electronic)

Connect Tissue Res, Early Online: 1 9
 DOI: 10.3109/03008207.2015.1013190

informa healthcare

Pilot study for detection of early changes in tissue associated with heterotopic ossification: moving toward clinical use of Raman spectroscopy

Mitchell Harris[1], Katherine Cilwa[2], Eric A. Elster[1,3], Benjamin K. Potter[1,2,4], Jonathan A. Forsberg[1,2,4], and Nicole J. Crane[1,2]

[1]*Department of Surgery, Uniformed Services University of Health Science, Bethesda, MD, USA,* [2]*Regenerative Medicine Department, Naval Medical Research Center, Silver Spring, MD, USA,* [3]*Department of Surgery, Walter Reed National Military Medical Center, Bethesda, MD, USA, and* [4]*Department of Orthopedics, Walter Reed National Military Medical Center, Bethesda MD, USA*

Abstract

Over 60% of combat-wounded patients develop heterotopic ossification (HO). Nearly 33% of them require surgical excision for symptomatic lesions, a procedure that is both fraught with complications and can delay or regress functional rehabilitation. Relative medical contraindications limit widespread use of conventional means of primary prophylaxis, such as nonspecific nonsteroidal anti-inflammatory medications and radiotherapy. Better methods for risk stratification are needed to both mitigate the risk of current means of primary prophylaxis as well as to evaluate novel preventive strategies currently in development. We asked whether Raman spectral changes, measured *ex vivo*, could be associated with histologic evidence of the earliest signs of HO formation and substance P (SP) expression in tissue biopsies from the wounds of combat casualties. In this pilot study, we compared normal muscle tissue, injured muscle tissue, very early HO lesions (<16 d post-injury), early HO lesions (>16 d post-injury) and mature HO lesions. The Raman spectra of these tissues demonstrate clear differences in the Amide I and III spectral regions of HO lesions compared to normal tissue, denoted by changes in the Amide I band center ($p<0.01$) and the 1340/1270 cm^{-1} ($p<0.05$) band area and band height ratios. SP expression in the HO lesions appears to peak between 16 and 30 d post-injury, as determined by SP immunohistochemistry of corresponding tissue sections, potentially indicating optimal timing for administration of therapeutics. Raman spectroscopy may therefore prove a useful, non-invasive and early diagnostic modality to detect HO formation before it becomes evident either clinically or radiographically.

Keywords

Heterotopic ossification, muscle, Raman spectroscopy, substance P, war wounds

History

Received 31 October 2014
Revised 15 January 2015
Accepted 24 January 2015
Published online 24 February 2015

Introduction

Heterotopic ossification (HO) is defined as the aberrant formation of mature, lamellar bone in non-osseous tissue and is common in war-related trauma of the extremities. The entity commonly produces deformity of soft tissues, difficulty with the use of prosthetics, joint ankylosis, skin ulceration and/or nerve entrapment (1,2). HO occurs in the setting of familial conditions, such as fibrodysplasia ossificans progressive (FOP), or as a complication of surgery, such as hip arthroplasty (3,4). However, HO is more common in military casualties, presumably due to the unique trauma resulting from blasts and high-velocity projectiles. In fact, HO developed in 65% of service members with combat-related extremity trauma in a study conducted at the National Naval Medical Center between 2003 and 2006 (5). This is very high in comparison to civilian populations, in which the prevalence of HO varies between 2 and 20% with central nervous system or orthopedic injury alone (6,7). However, civilians who have a combined orthopedic injury and central nervous system injury have rates similar to the military population, presumably because many military casualties experience simultaneous orthopedic and traumatic brain injuries due to blasts, the most frequent mechanism of injury in both Iraq and Afghanistan (8,9).

Recent research suggests that substance P (SP) is a necessary intermediate signal for HO formation (10,11). SP and other neuropeptides are released from peripheral sensory nerves after high-velocity injuries and traumatic brain injuries (10,12). Bone morphogenetic protein-2 is released during soft tissue injury and also stimulates peripheral nerves to release neuropeptides such as SP (10,12). SP and other neuropeptides attract leukocytes and stimulate mast cells to release proteases that activate metalloproteinases (10,13). The activated metalloproteinases then cause remodeling of local peripheral nerves, allowing progenitor cells to escape from the nerve (12,14). The origin of HO progenitor cells is somewhat controversial and has also been theorized to

Correspondence: Nicole J. Crane, PhD, Regenerative Medicine, Naval Medical Research Center, 503 Robert Grant Ave, Silver Spring, MD, USA. Tel: (301) 319 7304. E mail: nicole.j.crane4.ctr@mail.mil

originate from muscle and endothelial cells (12,15). SP receptors, neurokinin 1, have been found on chondrocytes, osteocytes, osteoblasts and osteoclasts, indicating that SP may also induce HO by direct interaction with these cells (11,16 20). This signaling pathway is considered to be essential for the formation of HO, since blocking any component has been shown to minimize or completely prevent HO in mouse models (10,11). In a paper by Salisbury et al., neural reserves of SP were depleted using capsaicin, a neural ligand frequently used for pain relief, thus preventing HO in a mouse model. This study also demonstrated that cromolyn, a mast cell stabilizer, substantially decreases HO formation (10). The ability to inhibit this pathway, or otherwise identify and inhibit early HO before mineralization occurs, is paramount to reducing patient morbidity and healthcare costs for combat casualties returning with orthopedic injuries.

Raman spectroscopy has been shown to be an effective means of identifying early HO lesions (21 25). It has also become a useful tool in many areas of research, including mineralization analysis, biomedical assays, cellular analysis, cancer detection and other areas (26 32). The benefits of this spectroscopic modality are numerous and include minimum sample preparation, noninvasive examination and the ability to detect both organic and inorganic components (26,33). Perhaps most important is the ability to analyze biological specimens with very little interference from water. Raman is also well suited for the analysis of biological tissues because it can quantitatively detect the complex primary and secondary molecular structures *in vivo* or *in vitro*. The utility of Raman spectroscopy in mineralization research was elucidated when it was used to detect a transient precursor to carbonated apatite in tooth and bone mineralization, a feat that was previously elusive because of the inability of other methods to test tissue *in vivo* (34,35). In this study, we examine both SP expression and molecular matrix changes at several time points during the development of combat-related HO, as well as characterizing the molecular changes that accompany increased SP expression in early HO formation. *In vivo* Raman analysis of combat wounds could eventually guide therapeutic options in the operating room, to include NSAID therapy, radiation therapy, resection of early HO or targeted delivery of novel local therapies. This ability to identify and treat early HO is paramount to optimizing the rapid and uncomplicated recovery of veterans with combat-related orthopedic injuries.

Methods

Clinical studies

The clinical studies were approved by the institutional review boards of our institutions. All injured muscle specimens were obtained from US service members evacuated following high-energy combat-related extremity injuries sustained abroad.

Sample collection

''Normal'' muscle samples ($n = 7$) were collected from excess, discarded muscle tissue harvested during hamstring autograft preparation following routine, elective and anterior cruciate ligament reconstruction. Injured muscle ($n = 8$) was collected from combat-injured patients sustaining high-energy extremity injuries, during the initial debridement upon arrival to our institution, prior to definitive wound closure or coverage. All injured patients were treated with negative pressure wound therapy. HO tissue biopsies were collected during the surgical removal of symptomatic lesions from 20 different injured patients and were subdivided into very early lesions (<16 d post-injury, $n = 8$), early lesions (> 16 d post-injury, $n = 7$) and mature lesions (>100 d post-injury, $n = 8$). Kaplan and coworkers clinically define early HO lesions as ''early'' within the first four weeks of development clinically, as ''intermediate'' within 5 8 weeks of development clinically, and as ''late'' within 9 12 weeks of development clinically (36,37). In this study, we further define ''very early'' HO lesions as those that develop within approximately the first two weeks post-injury, and ''mature'' HO lesions as those that develop beyond 12 weeks post-injury. Early stage HO lesions were classified as such by the attending surgeon excising the tissue. Often, early HO tissue presents a tactile profile distinct from surrounding musculoskeletal tissue and feels ''woody''. Tissue biopsies, approximately 1 cm^3, were obtained during surgical procedures and immediately fixed in neutral buffered formalin for at least 48 h before fixation in 70% ethanol for long-term storage.

Sample histology

Prior to histopathological or immunohistochemical processing, all HO samples were decalcified and then paraffin-embedded. Each biopsy was serial sectioned in the following order: unstained (10 μm thick), SP immunohistochemistry (IHC 5 μm thick) and hematoxylin and eosin (5 μm thick). Stained tissue sections were examined by standard histologic evaluation.

Immunohistochemistry

IHC was performed using standard protocols. Samples were fixed with neutral buffered formalin, decalcified with EDTA and paraffin embedded. Sectioned, unstained slides (5 μm thick) were then deparaffinized and used for IHC staining. Slides were incubated with mouse SP primary monoclonal antibody (R&D Systems, Inc., Minneapolis, MN), at 1:100 dilution, to which horseradish peroxidase was conjugated. SP antibody controls are presented in Supplementary Figure 1. Stained tissue sections were examined using a NanoZoomer 2.0-RS (Hamamatsu Co., Bridgewater, NJ) capable of 20 × magnification. Tissue sections that were positive for SP staining were scored with a ''1'' and tissue sections negative for SP staining were scored with a ''0''.

Raman spectroscopy

Unstained, 10 μm paraffin-embedded tissue sections were placed on gold-coated glass slides (EMF Corp., Ithaca, NY). Tissue sections were deparaffinized with a 48 72 h 40 °C cyclohexane bath (38). Spectra of deparaffinized tissue sections were collected using an 830 nm Raman PhAT probe system (Kaiser Optical Systems, Inc., Ann Arbor, MI) with a 1 mm excitation spot size. Dark subtracted and intensity-corrected spectra were acquired at multiple locations

Table 1. Raman vibrational band assignments (58,63,65,69 74).

ν (cm^{-1})	Band assignment	Component
821	ν(CC) of backbone	Collagen; muscle
856	ν(CC) of hydroxyproline ring	Collagen; muscle
873	ν_3 P OH stretching	Bone
876	ν(CC) of hydroxyproline ring	Collagen; protein
921	ν(CC) of proline ring	Collagen; protein
938	ν(CC) of protein backbone	Collagen; muscle; protein
945 952	ν_1 PO_4^{3-} stretch	Amorphous calcium phosphate
959	ν_1 PO_4^{3-} stretch	Hydroxyapatite
1004	ν(CC) aromatic ring	Phe; collagen; muscle
1032	ν_3 PO_4^{3-}; ν(CC) skeletal; C O stretch	Bone; collagen; muscle
1071	$\nu_1(CO_3^{2-})$	Bone
1075	ν_3 PO_4^{3-} stretch	Hydroxyapatite
1080	ν(CC) and ν(CN) skeletal	Collagen; muscle
1159	ν(CC) and ν(CN) skeletal	Carotenoid
1178	ν(CC) and ν(CN) skeletal	Collagen; muscle
1244	$\delta(CH_2)$ wagging; ν(CN) Amide III disordered/β sheet	Collagen; muscle
1274	ν(CN) and δ(NH) Amide III α helix	Collagen; muscle
1297	$\delta(CH_2)$ twisting	Collagen; muscle
1343	$\gamma(CH_2, CH_3)$ wagging	Collagen; muscle
1385	$\delta(CH_3)$ symmetric	Collagen
1448	$\delta(CH_2)$ scissoring	Collagen; muscle
1524	carotenoid	Collagen; muscle
1552	ν(CC) ring stretch	Collagen; muscle; Trp
1665	ν(CO) Amide I	Collagen; muscle

within each tissue section (up to five spectra per tissue section, dependent on section size) using five second acquisitions and 20 accumulations each. Preprocessing of spectra was conducted using in-house MATLAB® scripts. Spectra were truncated to 400 1800 cm^{-1}; summed for each sample; and room light, paraffin and gold slide subtracted. Baseline subtraction was achieved using an in-house MATLAB® script based on a polynomial fitting routine described in Cao and Freeman (39). Finally, spectra were intensity normalized to the CH_2 scissoring band at 1445 cm^{-1}. Following preprocessing, spectra were curve fit over two spectra regions, 1500 1720 cm^{-1} and 1185 1500 cm^{-1}, using mixed Gaussian/Lorentzian bands in GRAMS/AI software (Thermo Fisher Scientific, Madison, WI). Band area ratios (BARs) and band height ratios (BHRs) were calculated, and band centers (BCs) noted, using curve fit derived band parameters of peaks of interest. Raman vibrational band assignments are listed in Table 1. Raman metrics examined include the Raman BC of the largest Amide I band ($\sim$ 1665 cm^{-1}), unordered protein content (1640/1665 cm^{-1}), reducible collagen crosslinks (1680/1665 cm^{-1}), protein disorder/order (1240/1270 cm^{-1}), helical structure (1340/1270 cm^{-1}) and β-sheet protein content (1240/1300 cm^{-1}) and secondary structural changes in proteins (Amide I/Amide III).

Statistical analysis

BARs were compared between groups (normal muscle control, injured muscle, very early HO < 16 d post-injury, early HO > 16 d post-injury and mature HO) using ANOVA with a Bonferroni correction. p Values less than 0.05 were considered to indicate statistical significance. Bivariate correlations were assessed using Spearman's correlation coefficient. Correlation coefficients greater than 0.5 (positive or negative) were considered important. Statistical analyses were performed using SPSS software (SPSS 22.0, SPSS Inc., Chicago, IL).

Results

Histopathologic characterization of tissue

Stained tissue sections of normal and injured muscle exhibit typical skeletal muscle histological attributes. Normal myofibers (Figure 1A, left) are uniform, whereas the injured muscle myofibers are swollen, atrophied and infiltrated with neutrophils (Figure 1B, left). Injured muscle was a mixture of degenerated myocytes, coagulative necrosis and new granulation tissue, but was devoid of osteoid and cartilage. Early HO lesions appear disorganized, hypercellular and fibrotic, with both acute and chronic inflammatory cells (40). In all early HO specimens, lesion development begins adjacent to injured muscle or fat and is surrounded by fibrous connective tissue heavily besieged with neutrophils and macrophages (Figures 1C and D, left). Only one of the eight very early HO lesions (<16 d post-injury) had cartilage with an ossifying periphery, whereas four of the seven early HO lesions (>16 d post-injury) demonstrated cartilage, sometimes independent of an ossifying edge. Mature HO osteoid contains osteocytes surrounded by woven bone (Figure 1E, left). Mature HO tissue more closely resembles lamellar bone where cement lines are obvious and bone marrow elements were prevalent throughout the lesions. While osteoblasts and osteoclasts are prevalent in early HO formation, the presence of osteoblasts and osteoclasts in mature HO were not routinely evident, indicative of little if any active remodeling; this is supported by the lack of scalloped edges along the trabeculae, which appear smooth.

All control and injured muscle tissue sections were negative for SP IHC staining. SP positive staining (Figures 1C E, middle) were present in two of the eight very early HO lesions (<16 d post-injury), in five of the seven early HO lesions (>16 days post-injury) and in three of the eight mature HO lesions. SP positive staining was significantly increased in early HO lesions (>16 d post-injury) compared to all other tissue categories ($p < 0.05$).

Raman spectroscopy of tissue biopsies

Raman spectroscopic examination was conducted for 38 tissue sections collected from 38 patients, including control or ''normal'' muscle ($n = 7$), injured muscle ($n = 8$) and HO tissue ($n = 23$). Representative Raman spectra of each samples category, i.e. uninjured (or control) muscle, injured muscle and surgically excised HO, were compared (Figures 1A E, right). Spectral differences were prominent in the Amide I, Amide III and fingerprint regions of the Raman spectra. These changes directly reflect variation in the composition of the tissue.

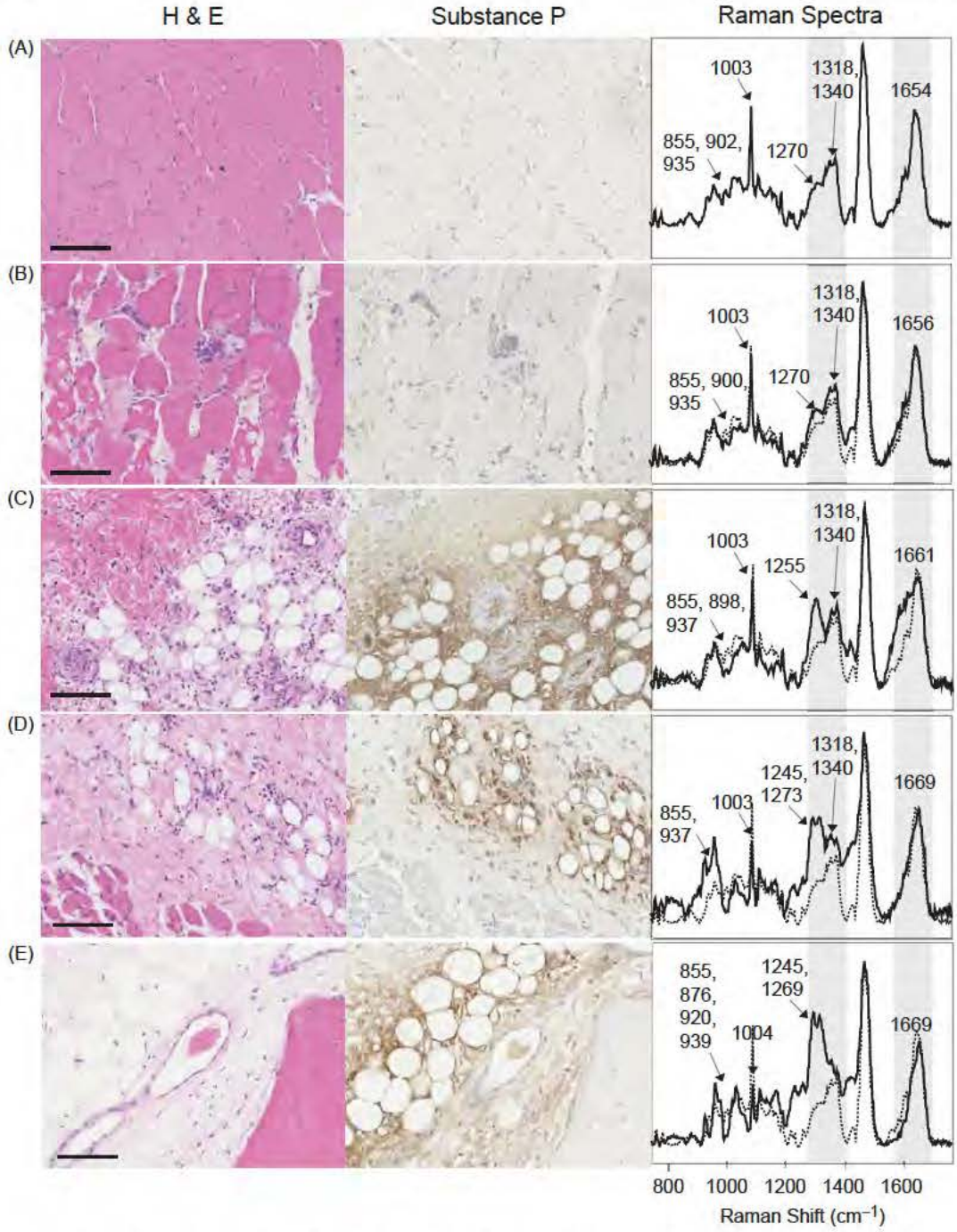

Figure 1. Comparison of serial tissue sections (H&E stained tissue left; substance P IHC stained tissue middle; Raman spectrum of unstained tissue right) for: (A) control muscle, (B) injured muscle, (C) very early HO (<16 d post injury), (D) early HO (>16 d post injury) and (E) mature HO (>100 d post injury). Scale bar 100 μm.

Table 2 displays the calculated BCs for the Amide I band, while the BHRs and BARs for the Raman spectra of control muscle, injured muscle, very early HO lesions, early HO lesions and mature HO lesions for matrix bands are presented in Figure 2. In general, when comparing muscle (normal or injured) to HO tissue (early or mature), we noted an increase in Raman shift in the Amide I BC, an increase in the 1640/1665 cm^{-1} BAR and the 1240/1300 cm^{-1} BAR and a decrease in the 1340/1270 cm^{-1} BAR and the Amide I/Amide III BAR. These changes in Raman metrics can also be examined as a progression of the development of HO.

The 1640/1665 cm^{-1} BAR shows a statistically significant difference between control muscle and early HO lesions ($p = 0.03$) and approaches statistical significance when compared to control muscle (0.34 ± 0.04) and very early HO (0.60 ± 0.02) and mature HO lesions (0.61 ± 0.08, $p = 0.08$ and $p = 0.07$, respectively). The 1340/1270 cm^{-1} BAR and BHR are sensitive metrics for differentiating control muscle from injured muscle and HO lesions ($p < 0.01$). The 1240/1270 cm^{-1} BAR is a discriminating Raman metric for distinguishing mature HO lesions (1.82 ± 0.32) from all other HO lesions and muscle (0.86 ± 0.10, 0.80 ± 0.10 and 0.96 ± 0.07, 0.93 ± 0.22, respectively; $p < 0.05$).

Table 2. Comparison of Amide I band center (BC) ± standard error of mean (SEM).

	Control muscle	Injured muscle	Very early HO < 16 d	Early HO > 16 d	Mature HO
Amide I BC	1659.1 (±0.5)[c,d,e]	1661.0 (±0.5)[c,d,e]	1664.3 (±1.3)[a,b,d,e]	1668.0 (±0.6)[a,b,c]	1668.1 (±0.6)[a,b,c]

p Values ≤ 0.05 compared to a control muscle, b injured muscle, c early HO < 16 d, d early HO > 16 d and/or e mature HO.

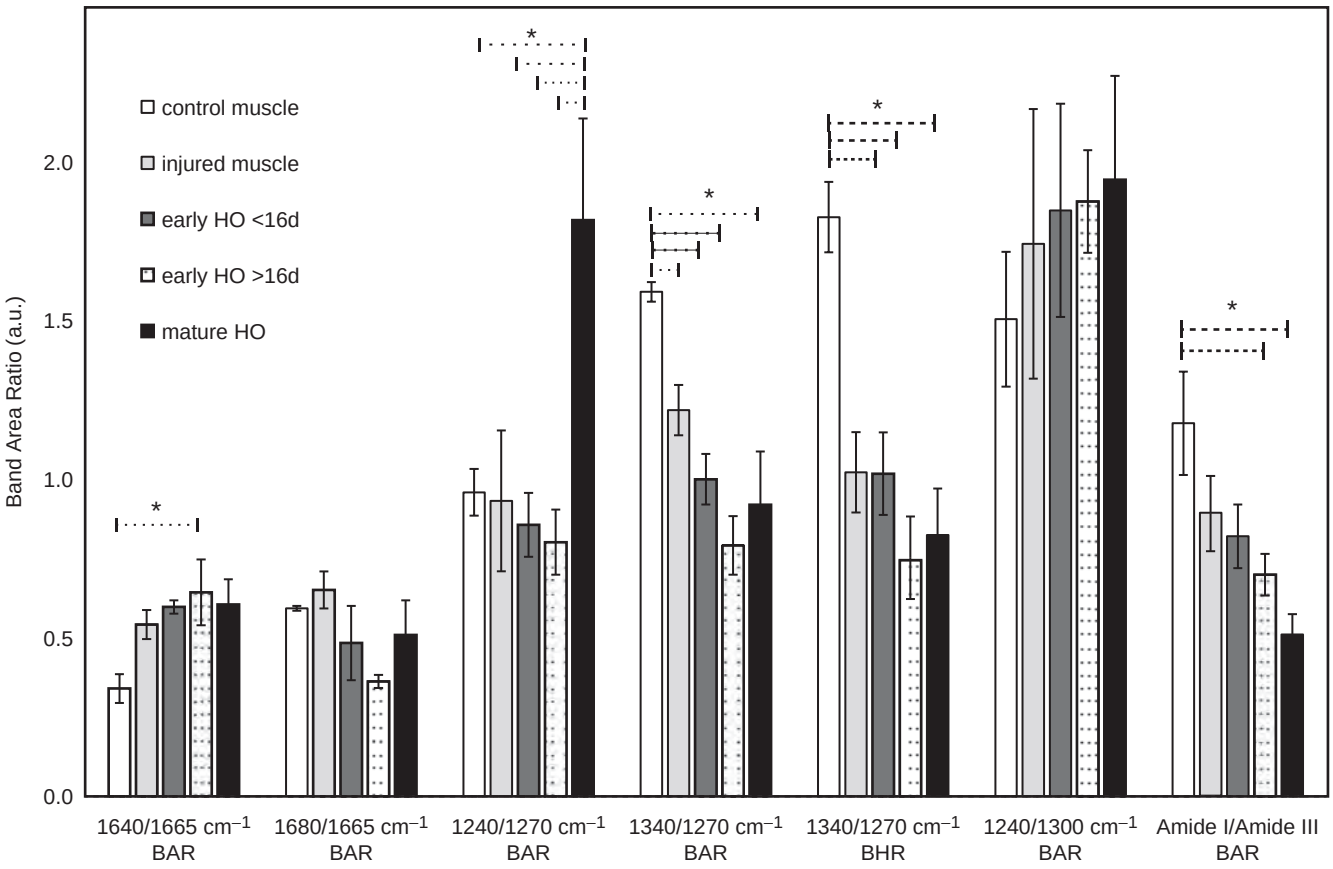

Figure 2. A comparison of band area ratios calculated from Raman spectra to assess tissue quality are presented for control muscle (white), injured muscle (light gray), very early HO (gray, < 16 days post injury), early HO (spotted white, > 16 days post injury) and mature HO (black). Vertical bars standard deviation. Dashed horizontal bars relationship for statistically significant differences. An asterisk (*) indicates a *p* value ≤ 0.05.

However, the Amide I BC is the best Raman metric at individuating all of the tissue categories ($p < 0.01$).

Finally, the category of biopsy (i.e. control muscle, very early HO, etc.) was significantly correlated with the 1665 cm ^{1} BC, 1340/1270 cm ^{1} BAR and BHR and Amide I/Amide III BAR ($p < 0.01$). SP expression in tissue expressions correlated with only one Raman metric, the 1680/1665 cm ^{1} BAR ($p < 0.01$).

Discussion

Combat-related HO formation is theorized to follow a common sequence of events (41). The first of these events is an induction signal (41 43), which, in our patient population, is the creation of a high-energy penetrating wound, usually from a blast. This leads to a pronounced and prolonged systemic and local inflammatory response (44 47). The second of these events is a population of progenitor cells (48,49), previously identified in our patients (49,50), which expands and is primed to undergo osteogenic differentiation in an environment conducive to osteogenesis. Neuroinflammatory factors, such as SP, recruit immune cells, including neutrophils, which ultimately allow for regranulation of tissue (51). Ossification then proceeds by either an endochondral bone formation (as with FOP) or intramembranous bone formation (as with progressive osseous heteroplasia) or both (as with myositis ossificans circumscripta) (52). Finally, the subsequent neoangiogenesis allows for the matrix mineralization and eventual ossification.

In this study, we observed the temporal changes of SP expression as HO develops in soft tissue. This is the first study that profiles SP expression in combat-related HO. None of the control muscle or injured muscle (collected between 7 and 20 d post-injury) samples were positive for SP IHC staining. Only two of the eight very early HO lesions, collected 10 and 13 d post-injury, demonstrate positive SP staining in connective tissue; the sample collected 13 d post-injury also contained cartilage, ossifying around its periphery. Time points after 16 d post-injury (between 22 and 30 d post-injury) also exhibit marked SP expression in early

HO lesions, as we observed the highest level of SP expression in connective tissue surrounding fat, as well as inflammatory cells and some osteoclasts in all but one sample. SP is expressed in three of the eight mature HO lesions, but focally in bone marrow fat and not to the same extent as in early HO lesions. Kan et al. also observed the highest SP expression in early HO lesions collected from FOP patients and patients with traumatic brain injuries and spinal cord injuries (11). These early HO lesions demonstrated muscle fiber degeneration and inflammatory cell infiltration, similar to the pathology exhibited in our very early and early HO lesions. Though SP is often depicted as having neuronal origins, its production has been observed in inflammatory cells, including macrophages, eosinophils, lymphocytes and dendritic cells (53). In addition, SP has been implicated in the upregulation of osteogenic differentiation potential, a necessary precursory step for HO development (54,55). Understanding the timing and role of SP expression in combat-related HO development can aid in the development of therapeutics such as tachykinin receptor antagonists, which prevent the proinflammatory effects of SP (53).

In this study, we also used Raman spectroscopy to discern molecular changes in the matrix components that occur prior to and during the formation of HO, in conjunction with SP expression in the tissue. We compared normal muscle to injured muscle, very early, early and mature HO lesions. For mature HO, the clinical sequelae of HO formation is usually readily apparent on physical and/or radiologic examination. In contrast, immature and largely unmineralized HO lesions are not as clinically obvious, which is why we are exploring non-invasive means by which to identify it. We show that Raman spectra of various tissues demonstrate clear differences in the Amide I and Amide III spectral regions of HO lesions compared to normal and injured muscle, which may indicate whether or not muscle and adjacent connective tissue will develop HO. These differences include a significant shift in the Amide I BC and an increase/decrease in some of the Amide III bands.

As injured muscle transitions to mineralized tissue, significant changes in many matrix bands (Figure 1B E, right) are apparent. First, there is a shift in the Amide I band in the Raman spectra from $1659.1 \pm 0.5\,cm^{-1}$ to $1668.1 \pm 0.6\,cm^{-1}$ this is likely due to increased collagen content ($p < 0.01$). Following skeletal muscle injury and during the formation of granuloma, the granulation tissue produces predominantly type I collagen after about five days post-injury (56). Next, the bandwidth of Amide I band increases, evidenced by an increase in $1640/1665\,cm^{-1}$ BAR (Figure 2). Bands at 1640 and $1665\,cm^{-1}$ are assigned to non-helical protein secondary structure (57 59). Muscle is composed largely of actin and myosin, both of which are more alpha helical in structure than collagen (60). As collagen content increases and muscle myofibers degenerate, the BC and width more closely resemble that of collagen, specifically type I collagen. As scar tissue forms, there is an increase in collagen turnover, thus an increase in reducible collagen crosslinks; as the fibers within the scar tissue mature, reducible crosslinks in collagen are converted to a more stable nonreducible crosslink (61). This is mirrored in the $1680/1665\,cm^{-1}$ BAR, which demonstrates an initial increase in reducible collagen crosslinks in injured muscle, followed by an increase in nonreducible crosslinks in very early and early HO lesions (62). In addition, the intensity of Amide III bands change, most notably with a decrease in the helical structure ($1340/1270\,cm^{-1}$) BAR and BHR. The Raman band at $1240\,cm^{-1}$ is attributed to more disordered protein structures, such as those containing a large number of β-pleats or random coils, while the $1270\,cm^{-1}$ Raman band is assigned to more ordered protein structures, such as those containing a large number of helical coils (63,64). In fact, Raman bands below $1270\,cm^{-1}$ are very weak in protein with a large proportion of helical structure (63), while increased Amide III scattering intensity above $1300\,cm^{-1}$ is indicative of highly helical proteins (65), such as myosin in muscle. Finally, the Amide I/Amide III BAR is indicative of general secondary protein structural changes (66). In fact, the Raman spectrum of early HO lesions in particular closely resembles the Raman spectrum of type I collagen. Type I collagen not only plays an important role in the process of wound healing but also in the formation of osseous tissue, such as HO. Osteoblasts secrete and deposit type I collagen, which comprises 90% of bone matrix prior to mineralization (67). In some cases, the same collagen that serves as an initiator of wound healing may also act as the scaffold for the deposition of bone mineral.

This study further demonstrates that Raman spectroscopy may be useful to identify early wound-specific changes that portend eventual HO formation. It is true that the examination of decalcified tissue presented in this study limited our study of early mineralization in fact, it prevented the investigation of mineralized tissue in these samples. However, we have previously explored the possibility that the mineral signature of these samples can be discriminating as well (21). In this study, we were particularly interested in identifying the earliest matrix changes that precursor mineralization; by identifying these changes in tissue composition, we will likely be able to identify HO development before other imaging techniques such as radiographs, computed tomography and ultrasound.

As an intraoperative modality, Raman spectroscopy may have distinct advantages over other techniques of assessing tissue during surgery such as histology or visual or tactile inspection by the surgeon. Though not widely used, frozen section and/or permanent pathologic analysis can be used to identify early stages associated with eventual HO formation. This technique requires multiple wound biopsies, is time and labor intensive and may not be sufficiently precise with regard to overall HO precursor location and potential severity to guide surgical decision-making. Furthermore, the ability of a surgeon to identify early HO tissue during a debridement is subjective and relies heavily on personal experience; however, the complexity and heterogeneity of blast wounds makes them difficult to evaluate, even for experienced surgeons (43). Conversely, the Raman technique described above could be adapted as an objective, intraoperative non-invasive means by which to risk stratify wounds, without significant preparation or bias on the part of the interpreter (21,24). If Raman spectroscopy demonstrates that a wound has Raman spectral features associated with the formation of HO, prophylaxis could be employed in these select cases. Alternatively, in areas that appear prone to HO development, which can be

mapped with Raman spectroscopy more precisely than gross clinical assessment, the clinician can consider early preferential excision of pre-HO tissue while the patient is undergoing debridement, local means of primary prophylaxis currently in development and/or amputation revision before final closure. Raman spectroscopy may also be useful for monitoring the development and progression of HO non-invasively and without radiation. For example, tomography techniques currently in development are able to model bone mineral density in three-dimensional space (68). With such a model, based on the Raman spectroscopic parameters presented in this study, the clinician may also be able visualize areas of HO formation as well as monitor the maturation of the each portion of the lesion(s) over time.

Conclusions

Raman Spectroscopy correlates with histologic appearance of tissues within combat wounds and can identify the earliest signs in patients who are actively developing HO. All data acquisition and analysis in this study were performed *ex vivo* and outside of the surgical suite. We plan to optimize existing Raman spectroscopic equipment, such as fiber-probe coupled systems, for use in the operating room during surgical debridements to perform Raman spectroscopic analysis of HO development, similar to the *ex vivo* analysis presented in this study. This technology will provide treating surgeons and researchers with an accurate, non-invasive means by which to risk stratify individual wounds to receive systemic and local means of primary prophylaxis currently in development.

Acknowledgments

The authors would like to thank Dr. Maryann Klassen-Fisher for her evaluation of tissue slides as a pathologist. In addition, the authors would also to thank Yingjie Song for her assistance preparing tissue sections and Adam Berger for his assistance in collecting data.

Declaration of interest

The authors report no conflict of interest. The authors alone are responsible for the content and writing of the paper. The views expressed in this manuscript are those of the authors and do not reflect the official policy of the Department of the Army, Department of the Navy, the Department of Defense or the United States Government. We are military service members (or employee of the US Government). This work was prepared as part of our official duties. Title 17 U.S.C. 105 provides the ''Copyright protection under this title is not available for any work of the United States Government''. Title 17 U.S.C. 101 defines a US Government work as a work prepared by a military service member or employee of the US Government as part of that person's official duties. Drs. Nicole Crane and Katherine Cilwa are employees of the Henry M. Jackson Foundation for the Advancement of Military Medicine.

We certify that all individuals who qualify as authors have been listed; each has participated in the conception and design of this work, the analysis of data (when applicable), the writing of the document and the approval of the submission of this version; that the document represents valid work; that if we used information derived from another source, we obtained all necessary approvals to use it and made appropriate acknowledgements in the document; and that each takes public responsibility for it.

This effort was supported (in part) by the US Navy Bureau of Medicine and Surgery under the Medical Development Program and Office of Naval Research work unit number (602115HP.3720.001.A1015), USAMRMC Military Medical Research and Development award OR090136, as well as the Orthopedic Trauma Research Program grant # OTRP W81XWH-07-1-0222. This study was approved by the Walter Reed Military Medical Center Institutional Review Board in compliance with all Federal regulations governing the protection of human subjects. The WRNMMC IRB approved protocol numbers are 352334 and 374863, and the protocol titles are ''The Use of the Vacuum Assisted Wound Closure Device in Treating Extremity Wounds'' and ''The Orthopedic Discarded Tissue Protocol''. The multidisciplinary care of these patients would not have been possible without the dedicated efforts of everyone at the Walter Reed National Military Medical Center. Both civilian and military personnel have rendered skilled and compassionate care for these casualties. All of our efforts are dedicated to those who have been placed in harm's way for the good of our nation.

References

1. Potter BK, Forsberg JA, Davis TA, Evans KN, Hawksworth JS, Tadaki D, Brown TS, Crane NJ, Burns TC, O'Brien FP, Elster EA. Heterotopic ossification following combat related trauma. J Bone Joint Surg Am 2010;92:74 89.
2. Melcer T, Belnap B, Walker GJ, Konoske P, Galarneau M. Heterotopic ossification in combat amputees from Afghanistan and Iraq wars: five case histories and results from a small series of patients. J Rehabil Res Dev 2011;48:1 12.
3. Tippets DM, Zaryanov AV, Vincent Burke W, Patel PD, Suarez JC, Ely EE, Figueroa NM. Incidence of heterotopic ossification in direct anterior total hip arthroplasty: a retrospective radiographic review. J Arthroplasty 2014;29:1835 8.
4. Regis D, Sandri A, Sambugaro E. Incidence of heterotopic ossification after surface and conventional total hip arthroplasty: a comparative study using anterolateral approach and indomethacin prophylaxis. Biomed Res Int 2013;2013:293528.
5. Forsberg JA. Heterotopic ossification in high energy wartime extremity injuries: prevalence and risk factors. J Bone Joint Surg Am 2009;91:1084 91.
6. Garland DE. Clinical observations on fractures and heterotopic ossification in the spinal cord and traumatic brain injured popu lations. Clin Orthop Relat Res 1988;233:86 101.
7. Seipel R, Langner S, Platz T, Lippa M, Kuehn JP, Hosten N. Neurogenic heterotopic ossification: epidemiology and morphology on conventional radiographs in an early neurological rehabilitation population. Skeletal Radiol 2012;41:61 6.
8. Sullivan MP, Torres SJ, Mehta S, Ahn J. Heterotopic ossification after central nervous system trauma: a current review. Bone Joint Res 2013;2:51 7.
9. Belmont Jr PJ, McCriskin BJ, Sieg RN, Burks R, Schoenfeld AJ. Combat wounds in Iraq and Afghanistan from 2005 to 2009. J Trauma Acute Care Surg 2012;73:3 12.
10. Salisbury E, Rodenberg E, Sonnet C, Hipp J, Gannon FH, Vadakkan TJ, Dickinson ME, Olmsted Davis EA, Davis AR. Sensory nerve induced inflammation contributes to heterotopic ossification. J Cell Biochem 2011;112:2748 58.
11. Kan L, Lounev VY, Pignolo RJ, Duan L, Liu Y, Stock SR, McGuire TL, Lu B, Gerard NP, Shore EM, Kaplan FS, Kessler JA. Substance

P signaling mediates BMP dependent heterotopic ossification. J Cell Biochem 2011;112:2759 72.
12. Reichel LM, Salisbury E, Moustoukas MJ, Davis AR, Olmsted Davis E. Molecular mechanisms of heterotopic ossification. J Hand Surg 2014;39:563 6.
13. Rodenberg E, Azhdarinia A, Lazard ZW, Hall M, Kwon SK, Wilganowski N, Salisbury EA, Merched Sauvage M, Olmsted Davis EA, Sevick Muraca EM, Davis AR. Matrix metalloprotei nase 9 is a diagnostic marker of heterotopic ossification in a murine model. Tissue Eng Part A 2011;17:2487 96.
14. Adameyko I, Lallemend F, Aquino JB, Pereira JA, Topilko P, Muller T, Fritz N, Beljajeva A, Mochii M, Liste I, Usoskin D, Suter U, Birchmeier C, Ernfors P. Schwann cell precursors from nerve innervation are a cellular origin of melanocytes in skin. Cell 2009;139:366 79.
15. Jackson WM, Aragon AB, Bulken Hoover JD, Nesti LJ, Tuan RS. Putative heterotopic ossification progenitor cells derived from traumatized muscle. J Orthop Res 2009;27:1645 51.
16. Wang L, Zhao R, Shi X, Wei T, Halloran BP, Clark DJ, Jacobs CR, Kingery WS. Substance P stimulates bone marrow stromal cell osteogenic activity, osteoclast differentiation, and resorption activ ity in vitro. Bone 2009;45:309 20.
17. Goto T, Kido MA, Yamaza T, Tanaka T. Substance P and substance P receptors in bone and gingival tissues. Med Electron Microsc 2001;34:77 85.
18. Goto T, Yamaza T, Kido MA, Tanaka T. Light and electron microscopic study of the distribution of axons containing substance P and the localization of neurokinin 1 receptor in bone. Cell Tissue Res 1998;293:87 93.
19. Okada T, Hirayama Y, Kishi S, Miyayasu K, Hiroi J, Fujii T. Functional neurokinin NK 1 receptor expression in rat peritoneal mast cells. Inflamm Res 1999;48:274 9.
20. Millward Sadler SJ, Mackenzie A, Wright MO, Lee H S, Elliot K, Gerrard L, Fiskerstrand CE, Salter DM, Quinn JP. Tachykinin expression in cartilage and function in human articular chondrocyte mechanotransduction. Arthritis Rheum 2003;48: 146 56.
21. Crane NJ, Polfer E, Elster EA, Potter BK, Forsberg JA. Raman spectroscopic analysis of combat related heterotopic ossification development. Bone 2013;57:335 42.
22. Potter BK, Forsberg JA, Davis TA, Evans KN, Hawksworth JS, Tadaki D, Brown TS, Crane NJ, Burns TC, O'Brien FP, Elster EA. Heterotopic ossification following combat related trauma. J Bone Joint Surg Am 2010;92:74 89.
23. Peterson JR, Eboda ON, Brownley RC, Cilwa KE, Pratt LE, De La Rosa S, Agarwal S, Buchman SR, Cederna PS, Morris MD, Wang SC, Levi B. Effects of aging on osteogenic response and heterotopic ossification following burn injury in mice. Stem Cells Dev 2015;24:205 13.
24. Peterson JR, Okagbare PI, De La Rosa S, Cilwa KE, Perosky JE, Eboda ON, Donneys A, Su GL, Buchman SR, Cederna PS, Wang SC, Kozloff KM, Morris MD, Levi B. Early detection of burn induced heterotopic ossification using transcutaneous Raman spectroscopy. Bone 2013;54:28 34.
25. Perosky JE, Peterson JR, Eboda ON, Morris MD, Wang SC, Levi B, Kozloff KM. Early detection of heterotopic ossification using near infrared optical imaging reveals dynamic turnover and progression of mineralization following Achilles tenotomy and burn injury. J Orthop Res 2014;32:1416 23.
26. Wachsmann Hogiu S, Weeks T, Huser T. Chemical analysis in vivo and in vitro by Raman spectroscopy from single cells to humans. Curr Opin Biotechnol 2009;20:63 73.
27. Morris MD, Mandair GS. Raman assessment of bone quality. Clin Orthop Relat Res 2011;469:2160 9.
28. Edwards HG, Munshi T. Diagnostic Raman spectroscopy for the forensic detection of biomaterials and the preservation of cultural heritage. Anal Bioanal Chem 2005;382:1398 406.
29. Huang Z, Lui H, McLean DI, Korbelik M, Zeng H. Raman spectroscopy in combination with background near infrared auto fluorescence enhances the in vivo assessment of malignant tissues. Photochem Photobiol 2005;81:1219 26.
30. Ellis DI, Goodacre R. Metabolic fingerprinting in disease diagno sis: biomedical applications of infrared and Raman spectroscopy. Analyst 2006;131:875 85.
31. Diem M, Romeo M, Boydston White S, Miljkovic M, Matthaus C. A decade of vibrational micro spectroscopy of human cells and tissue (1994 2004). Analyst 2004;129:880 5.
32. Choo Smith LP, Edwards HG, Endtz HP, Kros JM, Heule F, Barr H, Robinson Jr JS, Bruining HA, Puppels GJ. Medical applications of Raman spectroscopy: from proof of principle to clinical implementation. Biopolymers 2002;67:1 9.
33. Owen CA, Notingher I, Hill R, Stevens M, Hench LL. Progress in Raman spectroscopy in the fields of tissue engineering, diagnostics and toxicological testing. J Mater Sci Mater Med 2006;17:1019 23.
34. Crane NJ, Popescu V, Morris MD, Steenhuis P, Ignelzi Jr MA,. Raman spectroscopic evidence for octacalcium phosphate and other transient mineral species deposited during intramembranous min eralization. Bone 2006;39:434 42.
35. Crane NJ, Morris MD, Ignelzi MA, Yu G. Raman imaging demonstrates FGF2 induced craniosynostosis in mouse calvaria. J Biomed Opt 2005;10:031119.
36. Kaplan FS, Glaser DL, Hebela N, Shore EM. Heterotopic ossification. J Am Acad Orthop Surg 2004;12:116 25.
37. Kaplan FS, Hahn GV, Zasloff MA. Heterotopic ossification: two rare forms and what they can teach us. J Am Acad Orthop Surg 1994;2:288 96.
38. Faolain EO, Hunter MB, Byrne JM, Kelehan P, Lambkin HA, Byrne HJ, Lyng FM. Raman spectroscopic evaluation of efficacy of current paraffin wax section dewaxing agents. J Histochem Cytochem 2005;53:121 9.
39. Cao A, Pandya AK, Serhatkulu GK, Weber RE, Dai H, Thakur JS, Naik VM, Naik R, Auner GW, Rabah R, Freeman DC. A robust method for automated background subtraction of tissue fluores cence. J Raman Spectros 2007;38:1199 205.
40. Vigorita V. Orthopaedic pathology. Philadelphia: Lippincott Williams & Wilkins; 1999.
41. Chalmers J, Gray DH, Rush J. Observations on the induction of bone in soft tissues. J Bone Joint Surg Br 1975;57:36 45.
42. Lounev VY, Ramachandran R, Wosczyna MN, Yamamoto M, Maidment AD, Shore EM, Glaser DL, Goldhamer DJ, Kaplan FS. Identification of progenitor cells that contribute to heterotopic skeletogenesis. J Bone Joint Surg Am 2009;91:652 63.
43. Nelson ER, Wong VW, Krebsbach PH, Wang SC, Levi B. Heterotopic ossification following burn injury: the role of stem cells. J Burn Care Res 2012;33:463 70.
44. Evans KN, Forsberg JA, Potter BK, Hawksworth JS, Brown TS, Andersen R, Dunne JR, Tadaki D, Elster EA. Inflammatory cytokine and chemokine expression is associated with heterotopic ossification in high energy penetrating war injuries. J Orthop Trauma 2012;26:e204 13.
45. Forsberg JA, Potter BK, Polfer EM, Safford SD, Elster EA. Do inflammatory markers portend heterotopic ossification and wound failure in combat wounds? Clin Orthop Relat Res 2014;472: 2845 54.
46. Hahm G, Glaser JJ, Elster EA. Biomarkers to predict wound healing: the future of complex war wound management. Plast Reconstr Surg 2011;127:21S 6S.
47. Hawksworth JS, Stojadinovic A, Gage FA, Tadaki DK, Perdue PW, Forsberg J, Davis TA, Dunne JR, Denobile JW, Brown TS, Elster EA. Inflammatory biomarkers in combat wound healing. Ann Surg 2009;250:1002 7.
48. Suda RK, Billings PC, Egan KP, Kim JH, McCarrick Walmsley R, Glaser DL, Porter DL, Shore EM, Pignolo RJ. Circulating osteogenic precursor cells in heterotopic bone formation. Stem Cells 2009;27:2209 19.
49. Davis TA, O'Brien FP, Anam K, Grijalva S, Potter BK, Elster EA. Heterotopic ossification in complex orthopaedic combat wounds: quantification and characterization of osteogenic precursor cell activity in traumatized muscle. J Bone Joint Surg Am 2011;93: 1122 31.
50. Davis TA, O'Brien FP, Anam K, Grijalva S, Potter BK, Elster EA. Heterotopic ossification in complex orthopaedic combat wounds: quantification and characterization of osteogenic precursor cell activity in traumatized muscle. J Bone Joint Surg Am 2011;93: 1122 31.

51. Reichel LM, Salisbury E, Moustoukas MJ, Davis AR, Olmsted Davis E. Molecular mechanisms of heterotopic ossification. J Hand Surg Am 2013;39:563 6.
52. McCarthy EF, Sundaram M. Heterotopic ossification: a review. Skeletal Radiol 2005;34:609 19.
53. O'Connor TM, O'Connell J, O'Brien DI, Goode T, Bredin CP, Shanahan F. The role of substance P in inflammatory disease. J Cell Physiol 2004;201:167 80.
54. Dubon MJ, Byeon Y, Jung N, Son Y, Park K S. Substance P modulates properties of bone marrow derived mesenchymal stem cells. Tissue Eng Regenerat Med 2014;11:217 23.
55. Qian M, Liu M, Duan M, Zhang H, Wu Z, Zhou Y. Substance P induce osteogenic differentiation in human adipose derived stem cells. J Anim Vet Adv 2013;12:863 7.
56. Lehto M, Duance VC, Restall D. Collagen and fibronectin in a healing skeletal muscle injury. An immunohistological study of the effects of physical activity on the repair of injured gastrocnemius muscle in the rat. J Bone Joint Surg Br 1985;67:820 8.
57. Sane SU, Cramer SM, Przybycien TM. A holistic approach to protein secondary structure characterization using amide I band Raman spectroscopy. Anal Biochem 1999;269:255 72.
58. Maiti NC, Apetri MM, Zagorski MG, Carey PR, Anderson VE. Raman spectroscopic characterization of secondary structure in natively unfolded proteins: alpha synuclein. J Am Chem Soc 2004; 126:2399 408.
59. Spiro TG, Gaber BP. Laser Raman scattering as a probe of protein structure. Annu Rev Biochem 1977;46:553 72.
60. Tiaho F, Recher G, Rouede D. Estimation of helical angles of myosin and collagen by second harmonic generation imaging microscopy. Opt Express 2007;15:12286 95.
61. Lehto M, Sims TJ, Bailey AJ. Skeletal muscle injury molecular changes in the collagen during healing. Res Exp Med (Berl) 1985; 185:95 106.
62. Paschalis EP, Verdelis K, Doty SB, Boskey AL, Mendelsohn R, Yamauchi M. Spectroscopic characterization of collagen cross links in bone. J Bone Miner Res 2001;16:1821 8.
63. Lippert JL, Tyminski D, Desmeules PJ. Determination of the secondary structure of proteins by laser Raman spectroscopy. J Am Chem Soc 1976;98:7075 80.
64. Carew EB, Stanley HE, Seidel JC, Gergely J. Studies of myosin and its proteolytic fragments by laser Raman spectroscopy. Biophys J 1983;44:219 24.
65. Pezolet M, Pigeon M, Menard D, Caille JP. Raman spectroscopy of cytoplasmic muscle fiber proteins. Orientational order. Biophys J 1988;53:319 25.
66. Paschalis EP, Verdelis K, Doty SB, Boskey AL, Mendelsohn R, Yamauchi M. Spectroscopic characterization of collagen cross links in bone. J Bone Miner Res 2001;16:1821 8.
67. Kaplan FS, Hayes WC, Keaveny TM, Boskey A, Einhorn TA, Iannotti JP. Form and function of bone. Chapter 4. Rosemont (IL): American Academy of Orthopaedic Surgeons; 1994: 127 84.
68. Schulmerich MV, Cole JH, Dooley KA, Morris MD, Kreider JM, Goldstein SA, Srinivasan S, Pogue BW. Noninvasive Raman tomographic imaging of canine bone tissue. J Biomed Opt 2008; 13:020506.
69. Chrit L, Hadjur C, Morel S, Sockalingum G, Lebourdon G, Leroy F, Manfait M. In vivo chemical investigation of human skin using a confocal Raman fiber optic microprobe. J Biomed Opt 2005;10: 44007.
70. Wood BR, McNaughton D. Raman excitation wavelength investi gation of single red blood cells in vivo. J Raman Spectros 2002;33: 517 23.
71. Sane SU, Cramer SM, Przybycien TM. A holistic approach to protein secondary structure characterization using amide I band Raman spectroscopy. Anal Biochem 1999;269: 255 72.
72. Wohlrab J, Vollmann A, Wartewig S, Marsch WC, Neubert R. Noninvasive characterization of human stratum corneum of undiseased skin of patients with atopic dermatitis and psoriasis as studied by Fourier transform Raman spectroscopy. Biopolymers 2001;62:141 6.
73. Frushour BG, Koenig JL. Raman scattering of collagen, gelatin, and elastin. Biopolymers 1975;14:379 91.
74. Maquelin K, Kirschner C, Choo Smith LP, van den Braak N, Endtz HP, Naumann D, Puppels GJ. Identification of medically relevant microorganisms by vibrational spectroscopy. J Microbiol Methods 2002;51:255 71.

Supplementary material available online
Supplementary Figure 1.

PLOS ONE

Noninvasive Multimodal Imaging to Predict Recovery of Locomotion after Extended Limb Ischemia

--Manuscript Draft--

Manuscript Number:	PONE-D-15-17746
Article Type:	Research Article
Full Title:	Noninvasive Multimodal Imaging to Predict Recovery of Locomotion after Extended Limb Ischemia
Short Title:	Noninvasive Multimodal Imaging for Extended Limb Ischemia
Corresponding Author:	Nicole J. Crane, Ph.D. Naval Medical Research Center Silver Spring, MD UNITED STATES
Keywords:	extremity; ischemia/reperfusion injury; tourniquet; occlusion; infrared imaging; 3CCD imaging; oxygenation; perfusion; post-occlusive hyperemia
Abstract:	Acute limb ischemia is a common cause of morbidity and mortality following trauma both in civilian centers and in combat related injuries. Rapid determination of tissue viability and surgical restoration of blood flow are desirable, but not always possible. We sought to characterize the response to increasing periods of hind limb ischemia in a porcine model such that we could define a period of critical ischemia (the point after which irreversible neuromuscular injury occurs), evaluate non-invasive methods for characterizing that ischemia, and establish a model by which we could predict whether or not the animal's locomotion would return to baselines levels post-operatively. Ischemia was induced by either application of a pneumatic tourniquet or vessel occlusion (performed by clamping the proximal iliac artery and vein at the level of the inguinal ligament). The limb was monitored for the duration of the procedure with both 3-charge coupled device (3CCD) and infrared (IR) imaging for tissue oxygenation and perfusion, respectively. The experimental arms of this model are effective at inducing histologically evident muscle injury with some evidence of expected secondary organ damage, particularly in animals with longer ischemia times. Noninvasive imaging data shows excellent correlation with post-operative functional outcomes, validating its use as a non-invasive means of viability assessment, and directly monitors post-occlusive reactive hyperemia. A classification model, based on partial-least squares discriminant analysis (PLSDA) of imaging variables only, successfully classified animals as "returned to normal locomotion" or "did not return to normal locomotion" with 87.5% sensitivity and 66.7% specificity after cross-validation. PLSDA models generated from non-imaging data were not as accurate (AUC of 0.53) compared the PLSDA model generated from only imaging data (AUC of 0.76). With some modification, this limb ischemia model could also serve as a means on which to test therapies designed to prolong the time before critical ischemia.
Order of Authors:	Jason S. Radowsky
	Joseph D. Caruso
	Matthew J. Bradley
	Rajiv Luthra
	Eric A. Elster
	Jonathan A. Forsberg
	Nicole J. Crane, Ph.D.
Opposed Reviewers:	
Additional Information:	
Question	**Response**
Financial Disclosure	This work was supported/funded by work unit number 602115HP.3720.001.A1015. Funding support includes Congressionally Directed Medical Research Program award

Please describe all sources of funding that have supported your work. A complete funding statement should do the following: Include **grant numbers and the URLs** of any funder's website. Use the full name, not acronyms, of funding institutions, and use initials to identify authors who received the funding. **Describe the role** of any sponsors or funders in the study design, data collection and analysis, decision to publish, or preparation of the manuscript. If they had no role in any of the above, include this sentence at the end of your statement: "*The funders had no role in study design, data collection and analysis, decision to publish, or preparation of the manuscript*." If the study was **unfunded**, provide a statement that clearly indicates this, for example: "*The author(s) received no specific funding for this work*." * typeset	number W81XWH-10-2-0162.
Competing Interests You are responsible for recognizing and disclosing on behalf of all authors any competing interest that could be perceived to bias their work, acknowledging all financial support and any other relevant financial or non-financial competing interests. Do any authors of this manuscript have competing interests (as described in the PLOS Policy on Declaration and Evaluation of Competing Interests)? **If yes**, please provide details about any and all competing interests in the box below. Your response should begin with this statement: *I have read the journal's policy and the authors of this manuscript have the following competing interests:* **If no** authors have any competing interests to declare, please enter this statement in the box: "*The authors have*	The authors have declared that no competing interests exist.

declared that no competing interests exist." * typeset	
Ethics Statement You must provide an ethics statement if your study involved human participants, specimens or tissue samples, or vertebrate animals, embryos or tissues. All information entered here should also **be included in the Methods section** of your manuscript. Please write "N/A" if your study does not require an ethics statement. **Human Subject Research (involved human participants and/or tissue)** All research involving human participants must have been approved by the authors' Institutional Review Board (IRB) or an equivalent committee, and all clinical investigation must have been conducted according to the principles expressed in the Declaration of Helsinki. Informed consent, written or oral, should also have been obtained from the participants. If no consent was given, the reason must be explained (e.g. the data were analyzed anonymously) and reported. The form of consent (written/oral), or reason for lack of consent, should be indicated in the Methods section of your manuscript. Please enter the name of the IRB or Ethics Committee that approved this study in the space below. Include the approval number and/or a statement indicating approval of this research. **Animal Research (involved vertebrate animals, embryos or tissues)** All animal work must have been conducted according to relevant national and international guidelines. If your study involved non-human primates, you must provide details regarding animal welfare and steps taken to ameliorate suffering; this is in accordance with the recommendations of the Weatherall report, "The use of non-human primates in research." The relevant guidelines followed and the committee that approved	The study protocol was approved by the Institutional Animal Care and Use Committees at the Uniformed Services University of Health Sciences and the Naval Medical Research Center (protocols SUR-11-816 and 11-OUMD-13, respectively) in compliance with all Federal regulations governing the protection of animal subjects. Animals were euthanized by intravenous injection of sodium pentabarbital (100 mg/kg, Beuthanasia®, Merck Animal Health, Madison, NJ).

the study should be identified in the ethics statement. If anesthesia, euthanasia or any kind of animal sacrifice is part of the study, please include briefly in your statement which substances and/or methods were applied. Please enter the name of your Institutional Animal Care and Use Committee (IACUC) or other relevant ethics board, and indicate whether they approved this research or granted a formal waiver of ethical approval. Also include an approval number if one was obtained. **Field Permit** Please indicate the name of the institution or the relevant body that granted permission.	
Data Availability PLOS journals require authors to make all data underlying the findings described in their manuscript fully available, without restriction and from the time of publication, with only rare exceptions to address legal and ethical concerns (see the PLOS Data Policy and FAQ for further details). When submitting a manuscript, authors must provide a Data Availability Statement that describes where the data underlying their manuscript can be found. Your answers to the following constitute your statement about data availability and will be included with the article in the event of publication. **Please note that simply stating 'data available on request from the author' is not acceptable.** ***If, however, your data are only available upon request from the author(s), you must answer "No" to the first question below, and explain your exceptional situation in the text box provided.*** Do the authors confirm that all data underlying the findings described in their manuscript are fully available without restriction?	No - some restrictions will apply
Please describe where your data may be found, writing in full sentences. **Your answers should be entered into the box below and will be published in the form you provide them, if your manuscript is**	All relevant data are within the paper and its Supporting Information files.

accepted. If you are copying our sample text below, please ensure you replace any instances of XXX with the appropriate details. If your data are all contained within the paper and/or Supporting Information files, please state this in your answer below. For example, “All relevant data are within the paper and its Supporting Information files.” If your data are held or will be held in a public repository, include URLs, accession numbers or DOIs. For example, “All XXX files are available from the XXX database (accession number(s) XXX, XXX)." If this information will only be available after acceptance, please indicate this by ticking the box below. If neither of these applies but you are able to provide details of access elsewhere, with or without limitations, please do so in the box below. For example: “Data are available from the XXX Institutional Data Access / Ethics Committee for researchers who meet the criteria for access to confidential data.” “Data are from the XXX study whose authors may be contacted at XXX.” * typeset	
Additional data availability information:	

23 April 2015

Editorial Director
PLOS ONE
Dr. Damian Pattison
1160 Battery Street
Koshland Building East, Suite 100
San Francisco, CA 94111, USA

Dear Dr. Pattison:

On behalf of my coauthors, I would like to thank you for reviewing our manuscript entitled, "Noninvasive Multimodal Imaging to Predict Recovery of Locomotion after Extended Limb Ischemia."

Today, over 90% of extremity injuries endured in combat have tourniquets applied to limit blood loss on the battlefield as well as in the operating room. The local physiologic and pathologic effects of vascular injury to a limb have been well studied and there is substantial evidence that longer ischemia times correlate with reduced functional outcomes. Assessment of limb perfusion is commonly subjective during operative evaluation and experienced surgeons apply the "four Cs" in an effort to determine whether tissue is adequately perfused and likely to recover (color, consistency, capacity, contractility); however, the absence of one or more is commonly encountered. Imaging modalities, which can ascertain perfusion and oxygenation non-invasively, would lend insight into the viability of tissue and could help direct further vascular interventions or surgical debridement including the role of limb salvage in borderline cases.

The imaging technologies we present here, in general, are low in cost, non-invasive, rapid, and reliable. By combining available and inexpensive technologies, such as 3CCD and IR imaging cameras, we hypothesized that information concerning the perfusion, metabolism, and oxygenation of tissue can be ascertained in real-time. The following large animal study in swine is designed to discover the characteristics of limb tissue, and more specifically of the entire limb, following variable ischemic periods as evaluated with 3CCD and IR imaging.

If successful, this technology could be used in a variety of settings to help identify the point of critical ischemia, which, in turn would guide surgical decision-making.

Thank you, once again, for considering this important work.

Sincerely,

Nicole J. Crane, PhD
Senior Scientist
Advanced Surgical Imaging Program
Naval Medical Research Center
Silver Spring, MD 20910

Noninvasive Multimodal Imaging to Predict Recovery of Locomotion after Extended Limb Ischemia

Jason S. Radowsky[1], Joseph D. Caruso[2], Matthew J. Bradley[1,2,3], Rajiv Luthra[3], Eric A. Elster[1,2], Jonathan A. Forsberg[1,3,4], Nicole J. Crane*[1,3,5]

[1]Department of Surgery, Uniformed Services University of Health Sciences, Bethesda, MD, USA

[2] General Surgery, Walter Reed National Military Medical Center, Bethesda, MD, USA

[3] Regenerative Medicine Department, Naval Medical Research Center, Silver Spring, MD, USA

[4] Orthopaedics and Rehabilitation, Walter Reed National Military Medical Center, Bethesda, MD, USA

[5] Henry M. Jackson Foundation for the Advancement of Military Medicine, Bethesda, MD, USA

***Corresponding author:**

Nicole J. Crane, Ph.D.

Regenerative Medicine Department, Naval Medical Research Center, 503 Robert Grant Avenue, Silver Spring, MD, 20910.

Tel.: (301) 319-7304 office, (734) 358-3099 cell; E-mail: nicole.j.crane@gmail.com,

Keywords: extremity, ischemia/reperfusion injury, tourniquet, infrared imaging, 3CCD imaging, oxygenation, perfusion, post-occlusive hyperemia

Abstract

Acute limb ischemia is a common cause of morbidity and mortality following trauma both in civilian centers and in combat related injuries. Rapid determination of tissue viability and surgical restoration of blood flow are desirable, but not always possible. We sought to characterize the response to increasing periods of hind limb ischemia in a porcine model such that we could define a period of critical ischemia (the point after which irreversible neuromuscular injury occurs), evaluate non-invasive methods for characterizing that ischemia, and establish a model by which we could predict whether or not the animal's locomotion would return to baselines levels post-operatively. Ischemia was induced by either application of a pneumatic tourniquet or vessel occlusion (performed by clamping the proximal iliac artery and vein at the level of the inguinal ligament). The limb was monitored for the duration of the procedure with both 3-charge coupled device (3CCD) and infrared (IR) imaging for tissue oxygenation and perfusion, respectively. The experimental arms of this model are effective at inducing histologically evident muscle injury with some evidence of expected secondary organ damage, particularly in animals with longer ischemia times. Noninvasive imaging data shows excellent correlation with post-operative functional outcomes, validating its use as a non-invasive means of viability assessment, and directly monitors post-occlusive reactive hyperemia. A classification model, based on partial-least squares discriminant analysis (PLSDA) of imaging variables only, successfully classified animals as "returned to normal locomotion" or "did not return to normal locomotion" with 87.5% sensitivity and 66.7% specificity after cross-validation. PLSDA models generated from non-imaging data were not as accurate (AUC of 0.53) compared the PLSDA model generated from only imaging data (AUC of 0.76). With some modification,

this limb ischemia model could also serve as a means on which to test therapies designed to prolong the time before critical ischemia.

Introduction

Tourniquets are regularly applied to lower limbs to limit blood loss in the operating room from surgical procedures as well as on the battlefield following blast injuries. The local physiologic and pathologic effects of vascular injury to a limb have been well studied [1,2] and there is substantial evidence that longer ischemia times correlate with reduced functional outcomes. Furthermore, the deleterious effects of ischemia and reperfusion are not limited to the affected limb alone, but have systemic sequelae from released myoglobin and inflammatory cytokines, to including multi-organ dysfunction and even death.[3]

Commonly, the time to release of tourniquets and vascular clamps, with the subsequent restoration of blood flow to the limb, is the only identified information about limb reperfusion. Little is known, however, about the oxygenation of the distal tissue following release of vessel occlusion. Assessment is commonly subjective during operative evaluation and experienced surgeons apply the "four Cs" in an effort to determine whether tissue is adequately perfused and likely to recover. In this fashion surgeons assess the 'color' and 'consistency' of the tissue, while also observing 'capacity' by sharply excising tissue until bleeding is encountered. Then 'contractility' of muscle is assessed using electrocautery stimulation. The presence of all "four Cs" is generally thought to portend viability and eventual healing, however, the absence of one or more is commonly encountered. Recently, Forsberg and coworkers demonstrated that, for combat wounds, the "four Cs" are not adequate for portending wound outcome.[4] However, imaging modalities, which can ascertain perfusion and oxygenation, would lend insight into the viability of tissue and could help direct further vascular interventions or surgical debridement including the role of limb salvage in borderline cases.

Recently, imaging techniques have been employed in the operating room to ascertain adequacy of perfusion, including indocyanine green angiography, laser Doppler imaging, and laser speckle contrast imaging. Indocyanine green angiography requires the injection of a dye, such as indocyanine green, and the use of specialized near-infrared cameras to capture the extent of vascularity within flaps during reconstructive procedures.[5,6] Unfortunately, dye might not be readily available in austere environments and injection may cause anaphylactic reactions.[7] The potential disadvantages of using indocyanine green angiography include high cost, increased duration of surgical procedure, and inferiority of performance when compared to clinical assessment.[8] Additionally, while indocyanine green-based imaging modalities may discern whether or not tissue is being perfused, there is no avenue for determining actual tissue oxygenation which may result in false conclusions regarding the viability of certain tissues.[9] Laser Doppler imaging (LDI), founded on the idea that changes in blood flow can be measured via backscattering of a laser beam when it interacts with moving red blood cells, has been utilized extensively over the past 30 years to visualize tissue perfusion; while the non-invasive nature of LDI is highly desirable, it suffers from lack of standardization.[10] In laser speckle contrast imaging (LSCI), light from a laser beam is scattered by red blood cells, producing random interference patterns called speckle. As the movement of the red blood cells changes with changes in blood flow, the speckle pattern subsequently changes.[10] LSCI presents an index of blood flow not unlike LDI, but is able to provide near real-time feedback while LDI scanning suffers from a reduction in temporal resolution[11]; however, LSCI only penetrates approximately 300 microns into tissue while LDI will provide details about tissue approximately

1 cm below the surface.[10,11] Further investigation of other imaging modalities to ascertain tissue viability is warranted.

The imaging technologies we present here, in general, are low in cost, non-invasive, rapid, and reliable. 3CCD (charge coupled device) imaging, a relatively ubiquitous imaging technology, provides chemically specific information (oxygenated/deoxygenated hemoglobin), a large field of view, and *in vivo* detection simultaneously. 3CCD cameras are widely used in operating room suites due to better color sensitivity and increased color palette range. Briefly, a color image is reconstructed and recorded using red, green, and blue bandpass filters in front of three separate monochrome charge coupled devices (CCDs). The individual colors can be combined, subtracted and otherwise manipulated to enhance the contrast of an image so that detection is sensitive to molecules of interest. Here, 3CCD imaging enhancement arises directly from the absorption properties of oxygenated and deoxygenated hemoglobin (HbO_2 and Hb, respectively).[12] We have proven experimentally that 3CCD imaging is a viable technbology to monitor intraoperative renal parenchymal oxygenation [13] and bowel ischemia.[14,15] Intraoperative vessel identification has also been enhanced with this technology.[16] Long wave infrared (IR) imaging in the range of 7.5 - 13.5μm provides data for overall tissue perfusion and has been proven experimentally to assess tissue function and metabolism.[17] IR imaging assessment of tissue perfusion can be determined based on the principles of thermography: the two-dimensional mapping of temperature differences by detecting the natural emission from tissue that is warmer (or cooler) than surrounding structures.[18] These differences can be quantified using a digital IR camera in a non-invasive manner. We have previously studied the application of noninvasive digital IR imaging in models of cerebral and renal perfusion.[19,20] In addition to their low cost

in comparison to other imaging technologies, both 3CCD imaging and long wave IR imaging do not rely on extrinsic enhancement with injectable dyes or contrast agents.

By combining available and inexpensive technologies, such as 3CCD and long wave IR imaging cameras, we hypothesized that information concerning the perfusion, metabolism, and oxygenation of tissue can be ascertained in real-time. The following study is designed to discover the characteristics of limb tissue following variable ischemic periods as evaluated with 3CCD and IR imaging. Ischemia times included 3.5 and 4.7 hours, yielding moderate to severe ischemia/reperfusion injury (IRI). In a previous study by Burkhardt et al, ischemia times of 1, 3, and 6 hours were investigated; the investigators postulated that critical ischemia would be achieved with 4.7 hours of ischemia.[21] If successful, this technology could be used in a variety of settings to help identify the point of critical ischemia, which, in turn would guide surgical decision-making.

Materials and Methods

Ethics Statement

The study protocol was approved by the Institutional Animal Care and Use Committees at the Uniformed Services University of Health Sciences and the Naval Medical Research Center (protocols SUR-11-816 and 11-OUMD-13, respectively) in compliance with all Federal regulations governing the protection of animal subjects.

In vivo studies

In this protocol, 26 adolescent female swine (*Sus scrofa*) ranging from 45-55 pounds were randomized to sham (n=5), 3.5 hour tourniquet (n=5), 3.5 hour occlusion (n=5), 4.7 hour tourniquet (n=5), and 4.7 hour occlusion (n=6) experiment arms (Table 1). Each animals was housed in a single run and provided regular access to food and water, as well as environmental enrichment.

In all cases, the animals were anesthetized using intramuscular Telazol (4-6mg/kg IM, Fort Dodge Animal Health, Overland, KS, USA) and Dexdomitor (0.05 mg/m^2 IM, Zoetis, Madison, NJ, USA) for initial sedation and then maintained with inhaled isofluorane (1.5%-3% with approximately 30% FiO_2). A Foley catheter was inserted to collect urine and a tunneled central venous catheter (CVC) was placed in the right external jugular vein to allow for regular collection of blood samples. To reduce the risk of thrombosis formation during ischemia, unfractionated heparin (100U/kg) was administered prior to limb occlusion. Additonally, all animals received intravenous antibiotics (5 mg/kg, Baytril 100, Bayer Healthcare LLC, Shawnee

Mission, KS) at the beginning of the surgical procedure and 3 days post-operatively. All animals in the sham and tourniquet groups had an incision in the right inguinal crease with exposure, but not clamping of the femoral vasculature to control for any amount of inflammation observed from the incision itself. The incision was made on the right hind limb because tourniquets were placed on the left hind limb (in the appropriate groups). For animals in the tourniquet experimental groups (later termed tourniquet animals), a pneumatic tourniquet (PediFit, Delfi Medical Innovations, Vancouver BC, Canada) was placed as proximally as possible on the left lower extremity and connected to a portable inflation system (PTSii, Delfi Medical Innovations, Vancouver BC, Canada) and inflated to 250 mm Hg. For animals in the 3.5-hour occlusion group (later termed 3.5 hour occlusion animals), occlusion was achieved by direct clamping of the proximal femoral artery and vein at the level of the inguinal ligament. Both the artery and vein were occluded to approximate the complete occlusion of efferent and afferent flow induced by the tourniquet. With the assistance of the thermal camera we adjusted the vascular clamp proximally, if needed, until collateral flow was absent; swine, however, have an extremely redundant vascular supply in their hind limbs and complete ischemia (100%) of the limb was often not achieved as perfusion was sometimes observed in small proximal and lateral vessels of the limb. Occlusion in the 4.7-hour group was accomplished by clamping both the internal and external iliac vasculature at their branch-point from the aorta via a left lower quadrant incision and extraperitoneal dissection, required to ensure complete ischemia of the limb (these animals are termed 4.7 hour occlusion animals). Note, all efforts were made to minimize suffering throughout the duration of the study; animals were administered Fentanyl (75-100 μg/kg/hr transdermal patches) and buprenorphine (0.03 mg/kg intramuscular injections) operatively and post-operatively for analgesia.

Clinical and Laboratory Data Acquisition

Heart rate, body temperature, respiratory rate, end tidal CO_2 and oxygen saturation were monitored throughout the procedure. Blood and urine samples were collected at every hour and after reperfusion the day of the procedure, as well as on Day 1 (D1), Day 3 (D3) and Day 7 (D7). Whole blood was used for a complete blood count (CBC) and blood serum was used for chemistry analysis as well as serum cytokine analysis. The blood chemistry panel included a basic metabolic panel, calcium, phosphorus, cholesterol, triglycerides, total protein, albumin, AST, ALT, LDH, creatine kinase, ALKP, GGT, and total bilirubin. Blood urea nitrogen was first converted to serum urea content (mmol/L) prior to normalizing analytes of interest to serum urea content (U/mmol). Urine was analyzed for urea, creatinine, pH, specific gravity, and presence of blood or protein.

Serum cytokines were analyzed using multiplex ELISA kits (Aushon Biosystems, Billerica, MA). Cytokines measured included IFNα, IFNγ, IL-1β, IL-2, IL-4, IL-6, IL-8, IL-10, and TNFα. Core needle biopsies (14g) were taken from the injured leg at baseline, 30 minutes post-reperfusion, D1, D3 and D7; each was stored in 10% neutral buffered formalin prior to histologic preparation. Clinical observations were recorded twice daily for seven days. Each animal was evaluated by general clinical appearance, food and water consumption, and provoked behavior. The resulting extremity injuries were scored during clinical observations with a modified Tarlov scale[22] to determine how ischemia affected locomotion (0: complete paralysis, 1: minimal movement, 2: stands with assistance, 3: stands alone, 4: weak walk, 5: normal gait). A Tarlov score of 5 indicated normal mobility while a Tarlov score of 2 was manifested by significantly impaired mobility.

After collection of D7 blood and urine samples, animals were euthanized by intravenous injection of sodium pentabarbital (100 mg/kg, Beuthanasia®, Merck Animal Health, Madison, NJ). Muscle samples were taken from predetermined proximal, mid, and distal sections of the bilateral hind-limbs, both from the medial and lateral aspect. Pieces of the porcine liver, kidney, proximal stomach and esophagus and lung were also collected and submitted for pathologic analysis. Samples were graded from 0-5 based on the presence of edema, non-suppurative inflammation, degeneration, necrosis, and regeneration in the submitted tissue by veterinary pathologists attached to Naval Medical Research Center; pathology scores are the sum of each category (i.e. 1-edema + 1-inflammation + 1-degenration + 1-necrosis + 1-regeneration = 5). A pathology score of 25 indicates the highest level of injury in tissue; a pathology score of 0 indicates no injury in tissue.

The animals were observed twice a day for seven days. Their behavior was rated on general clinical appearance, food and water consumption, and provoked behavior. The Tarlov scale was also used to determine how ischemia affected locomotion. Additionally, a drop foot score was used to monitor neuropathy in the affected limb.

At study endpoint (D7) a necropsy was performed to harvest tissue (kidney, liver and skeletal muscle) and placed in 10% neutral buffered formalin. Other organs were harvested if evidence of damage was observed, indicated by gross pathology. The tissues were then submitted for paraffin embedding, sectioning, mounting of sections and staining of slides with hematoxylin and eosin (H&E) to monitor morphological change in tissue.

Non-invasive Imaging

Throughout the procedure, images and spectral data were collected using both 3CCD and infrared (IR) modalities. Surface oxygenation was measured based on the spectral response of hemoglobin in the visible region of the spectrum. 3CCD imaging utilizes a trichroic prism to split incoming light into red, blue, and green channels, each of which has its own charge-coupled device. 3CCD technology is commercially available, at low cost, with high color sensitivity and dynamic range. For this study, a commercially available 3CCD camcorder (HDC-HS9) was used to document the entirety of the procedure. The camera was white balanced at the beginning of the procedure, and frames of interest were extracted from the video files. Additionally, IR images were collected using a FLIR Tau640 (Santa Barbara, CA, USA) camera and transferred to a PC using a frame grabber card (Frame Link Express, VCE-CLEX01, Imprex, Boca Raton, FL). Images were collected at five-minute intervals during the entire procedure. An in-house developed tool allowed for tracking of a region of interest (ROI) over the duration of the procedure. Representative images are displayed in Figure 1 (top panels) for 4 time points (t=0, t=210, t=220, and t=240 minutes, respectively). ROIs are indicated by a white box. The normalized change in 3CCD values was plotted as a function of time (Figure 1, bottom left panel). A similar process was used to track changes in IR values (Figure 1, bottom right panel). Equipment malfunctioned during two of the cases and 3CCD imaging data was not collected.

Data Analysis

All image data acquired was processed using custom Matlab ® (Mathworks, Nattick, MA, USA) programs. Images were registered and subsequently processed, tracking a selected ROI in both

the IR and 3CCD image frames. In the infrared frames, a mean intensity value for the ROI was used to assess limb perfusion.[23] Values were converted to temperature using a calibration for mean IR values and temperature. For the 3CCD frames, mean R-B values correlated to tissue oxygenation.[12,13,16,24,25] The percent difference of R-B values from the baseline R-B value was calculated for each time point.

The slope of reperfusion was determined by the difference between the 3CCD and IR maximum ischemia values and their corresponding maximum reperfusion values divided by the duration of reperfusion. The slope of post-occlusive reactive hyperemia (PORH) was calculated from the difference between the 3CCD and IR maximum reperfusion values and their corresponding 5 or 10 minute post-reperfusion values divided by the duration of the post-reperfusion period.

Statistical Analysis

One-way analysis of variance (ANOVA) was used to compare differences across groups for normally distributed continuous data, with the post-hoc Bonferroni correction employed to compare differences between individual groups. For comparisons of tourniquet and occlusion animals or a comparison of fully recovered and not fully recovered animals, a Kruskal-Wallis ANOVA was used. P-values less than 0.05 were considered statistically significant and are indicated by an asterisk (*); p-values < 0.01 were considered very statistically significant and are indicated by a double asterisk (**); p-values < 0.001 were considered the most statistically significant and are indicated by a triple asterisk (***). Bivariate correlations were assessed using Spearmans correlation coefficient. Correlation coefficients greater than 0.7 (positive or

negative) were considered important. All univariate statistics were analyzed using IBM SPSS v.22 (IBM Corp, Armonk, NY).

Partial-least squares discriminant analysis (PLSDA) was performed in PLS_Toolbox (Eigenvector Research Inc., Wenatchee, WA). Briefly, PLSDA is a classification algorithm that places samples into two groups and then places a line between the two groups to discriminate the two groups of samples. In this study, we use multiple variables to create this discrimination and the line becomes a hyperplane separating the two groups of samples in a multidimensional space. Here, the two groups are 1) returned to normal locomotion and 2) did not return to normal locomotion. Variables were mean-centered and one or two principal components. Cross-validation was performed with random subsets of samples, including 4 data splits and 10 iterations. Samples with excessive missing data points were excluded from the model.

Results

Two animals expired before the one-week survival period (one sham and one 4.7 hour occlusion) and one animal was euthanized prematurely (3.5 hour tournuiquet) on post-operative day 5; data points for intraoperative and post-reperfusion were retained in the data set, if collected.

Blood Chemistries Exhibit End Organ Stress

Blood samples were analyzed with the standard Chem20 panel. Blood urea nitrogen (BUN) served as a marker of renal injury. In Figure 2A, BUN levels begin to increase towards the end of ischemia and continue to increase post-operatively, peaking at 3 hours post-reperfusion, however, these values are not appreciably different from BUN levels in sham animals. Lactate dehydrogenase (LDH) in this study served as a marker of general tissue damage and injury. LDH increased at 3 hours post-reperfusion and peaked on D1 (Figure 2B). Aminotransferases, specifically alanine aminotransferase (ALT) and aspartate aminotransferase (AST), were used to monitor liver function and were elevated post-operatively in tourniquet and occlusion animals (Figures 2C and 2D). ALT levels increased at D1 for all tourniquet and occlusion animals, reached its apex at D3, but continued to stay elevated to D7 for tourniquet animals only. AST levels began to increase at 3 hours port-reperfusion, peak at D1, and returned to baseline levels by D7. Creatine kinase (CK) is a ubiquitous enzyme present in muscle, the brain, the heart, and other tissues; CK is released into the bloodstream when damage is incurred in muscle and thus is used as a serum marker of skeletal muscle injury. CK levels have a similar profile to AST levels; CK levels increase by 3 hours post-reperfusion, peak at D1, and return to near baseline levels by D7 (Figure 2E). Finally, bicarbonate levels (measured as CO_2) in the blood can be a determinant of oxidative damage after IRI. In occlusion and tourniquet animals, bicarbonate levels decreased

at 30 minutes post-reperfusion and continued to decrease within the first 24 hours, but return to baseline levels by 24 hours post-reperfusion (Figure 2F).

As expected, animals in all experimental groups demonstrated higher levels of AST ($p<0.05$), ALT ($p<0.001$), LDH ($p<0.05$), and CK ($p<0.03$) at post-operative D1 when compared to sham animals. Animals in the 4.7 hour tourniquet group demonstrated higher levels of AST ($p<0.03$) and CK ($p<0.03$) on D3 compared with sham animals. Potassium was elevated in all experimental animals compared to sham animals 1 week post-operatively ($p<0.01$). Hematologic and renal parameters were not significantly different across groups. BUN levels at maximum ischemia were significantly higher in animals that did not fully recover locomotion when compared to animals that did fully recover locomotion ($p=0.05$). All other blood chemistry levels showed no significant difference between animals without fully recovered locomotion and animals with fully recovered locomotion (Table 2).

Serum Cytokines Reveal Little Regarding Return to Full Locomotion

Serum cytokine levels were measured in all sham and experimental animals and included a panel of nine cytokines and chemokines associated with inflammation (pro-inflammatory and anti-inflammatory). Cytokines levels were highly variable within experimental groups, making an accurate comparison difficult. Few statistically significant differences were observed between experimental groups (data not shown). IL-13 was significantly elevated in tourniquet animals compared to occlusion and sham animals ($p<0.02$).

Evidence of IRI and Attenuated Locomotion

Mean pathology scores for the left and right kidneys and liver are presented in Figure 3A. Some end organ damage was observed in both the left and right kidneys of the 4.7 hour occlusion animals and the kidneys and liver of the 4.7 hour tourniquet animals. A small degree of damage was also observed in the liver of the 3.5 hour tourniquet animals, though not consistently. When comparing the mean pathology scores for muscle and sciatic nerve, we saw increased pathology scores for all tourniquet animals compared to occlusion animals – Figure 3B. The patterns of damage to the skeletal muscle were not, however, consistent across both cohorts of occlusion and tourniquet animals. Note the lack of magnitude in the pathology scores for sham animals.

All animals in the 4.7 hour occlusion and 4.7 hour tourniquet groups had an increased drop foot score when compared to sham animals ($p<0.03$) – Figure 4A. All but one of the ten 4.7 hour ischemia animals, which included both occlusion and tourniquet animals, exhibited drop foot for at least 2 days post-operatively. None of the 3.5 hour animals demonstrate drop foot after D1. Tarlov scores were decreased in 3.5 hour occlusion and 4.7 hour tourniquet animals at post-operative time points days 1 through 3 when compared with sham animals ($p<0.03$) – Figure 4B. This decrease in function was most significant in the 4.7 hour tourniquet animals, and remained depressed throughout the entire survival period, compared to other experimental groups. Interestingly, 4.7 hour occlusion animals demonstrate similar locomotion to 3.5 hour tourniquet animals. The 3.5 hour occlusion animals demonstrate little to no decrease in function/locomotion. Finally, only 25% of the animals in the 4.7 hour ischemia group fully recover by D7; in comparison, 75% of the 3.5 hour ischemia animals fully recover by D7.

Intraoperative Imaging Directly Observes Post-Occlusive Reactive Hyperemia

Representative 3CCD and infrared (IR) images for baseline, maximum ischemia, 10 minutes post-reperfusion, and 30 minutes post-reperfusion are displayed in Figure 1 (top panels – 3CCD images; middle panels – IR imaging). Both 3CCD and IR mean ROI values are plotted in the bottom two panels (left and right, respectively). 3CCD values (calculated as R-B values) show an almost immediate drop after induction of ischemia, and continue to decrease over the duration of ischemia but at a slow rate. 3CCD values exceed baseline values within the first 10 minutes post-reperfusion and return to almost baseline levels at 30 minutes post-reperfusion. Here, 3CCD imaging (Figure 1 - bottom left) clearly illustrates PORH – an increase in blood flow after release of arterial occlusion either by unclamping of the artery or releasing of the tourniquet. IR imaging values (Figure 1 - bottom right) demonstrate a more progressive and almost linear decrease over the duration of ischemia and do not exhibit the hallmark of PORH after reperfusion, but do return to baseline levels by 30 minutes post-reperfusion.

When comparing the 3CCD imaging profiles of the occlusion and tourniquet experimental groups, there are several notable differences. The degree of severity of the ischemia is evidenced by the decreased R-B values at maximum ischemia for both the 3.5 hour and 4.7 hour tourniquet groups (Figure 5A). Correspondingly, the difference between the R-B vales at maximum ischemia and 10 minutes post-reperfusion is greatest in the tourniquet experimental groups. Here also, we observed PORH, exposed in Figure 5A as an increase in R-B values at 10 minutes reperfusion compared to baseline R-B values.

Though the data was collected on the same animals from the four experimental groups, the IR imaging profiles (Figure 5B) are substantially different from the 3CCD imaging profiles. The

degree of severity of the ischemia, exhibited by a decrease in the mean temperature of the leg, is not only noted most significantly in the tourniquet animals but also in the 4.7 hour occlusion animals. Additionally, the magnitude of the difference between the IR values at maximum ischemia and 10 minutes post-reperfusion is not as great as the difference between the IR values at maximum ischemia and 30 minutes post-reperfusion. The mean leg temperature of the 4.7 hour ischemia animals does not return to baseline values and remains significantly less than that of the 3.5 hour ischemia animals ($p<0.005$). There is also a significant difference between the mean leg temperature at both 5 and 10 minutes post-reperfusion between 3.5 hour ischemia and 4.7 hour ischemia animals ($p<0.002$).

These changes can also be described by plotting the slopes of reperfusion for both 3CCD and IR imaging (Figures 6 A and 6B) and the slopes of PORH at 5 and 10 minutes post-reperfusion for 3CCD imaging (Figure 6A). The 3CCD imaging slope of reperfusion is greatest in tourniquet animals. There is a significant difference between the 3CCD imaging slope reperfusion in the 4.7 hour tourniquet animals and the slope of reperfusion in the 4.7 hour occlusion and 3.5 hour occlusion animals ($p<0.05$); furthermore, the IR slope of reperfusion in the 4.7 hour tourniquet animals is significantly higher than the IR slopes of reperfusion in all other animal groups ($p<0.001$). This trend persists for the 3CCD imaging slopes of PORH at both 5 minutes and 10 minutes post-reperfusion ($p<0.05$).

Based on Pearson's correlation coefficients, both IR and 3CCD imaging values and slopes are highly correlated with function and mobility and pathology ($\rho>0.65$ – Table 3). This is less so

when comparing IR and 3CCD imaging values and slopes to blood chemistry values ($\rho>0.65$ – Table 4).

Predicting Full Recovery of Locomotion Post-operatively after I/R Injury

Finally, as demonstrated in Figures 7A-C, we were able to predict whether or not the affected limb would fully recover by post-operative D7. In a PLSDA model based on all parameters but excluding outcome parameters (Figure 7A), the training model performed decently (62.5% sensitivity and 88.9% specificity) but the same was not true for the cross-validated model (62.5% sensitivity and 55.6% specificity). Next, we calculated a PLSDA model based on only imaging parameters (Figure 7B); the training model and the cross-validated model both performed very well with 87.5% sensitivity and 77.8% specificity for the training model and 87.5% sensitivity and 66.7% specificity for the cross-validated model. Lastly, we generated a PLSDA model using all non-imaging parameters but excluding outcome parameters (Figure 7C). The training model performed comparably to the training model with all parameters (62.5% sensitivity and 88.9% specificity), but the cross-validation model did not perform as well as the cross-validation model using imaging parameters only (62.5% sensitivity and 66.7% specificity). An area under the curve (AUC) of greater than 0.8 was observed in all training models; only the cross-validation model made from imaging parameters only approached an AUC of 0.8.

Discussion

Parameters derived from 3CCD and IR imaging show promise as surrogate outcome measures for tissue oxygenation and perfusion, as it relates to ischemia/reperfusion injury and return to normal locomotion. In addition, we confirmed that 4.7 hours is the upper limit for tolerated critical ischemia before disability is permanent in swine. Translating this information into clinical scenarios will be an important next step to determine the upper limit of ischemia in humans as it relates to function. Likewise, using these imaging technologies to identify the extent of ischemia and reperfusion in a clinical setting will have important implications.

The hind limb ischemia model utilized in this study validates our development of a critical acute limb ischemia model. Interestingly, the 4.7 hour tourniquet animals had more profound and prolonged disability compared to the 4.7 occlusion animals despite complete proximal vessel occlusion; both experimental arms demonstrated a meager 25% recovery to full locomotion post-operatively. The difference in disability between the 4.7 hour tourniquet group and the 4.7 hour occlusion group could be attributable to direct vascular injury from the vascular clamp, but most likely is the result of reduced or nonexistent collateral flow below the tourniquet compared to direct vessel occlusion. This may also be due in part to direct tissue injury from the tourniquet itself (focal crush injury where tourniquet was applied). This additional, direct injury in the tourniquet animals is particularly evidenced by the slope of reperfusion as determined by 3CCD imaging. We postulate that the 3CCD imaging slope of reperfusion is greatest in tourniquet animals because vessel occlusion of all vessels in the limb is more complete in the tourniquet animals compared to the occlusion animals; that is, some collateral flow was maintained below

vessel occlusion compared to the more distally placed tourniquet. As such, vessel recovery and reperfusion was more prolonged in the tourniquet groups as compared to the occlusion groups.

Recovery from tissue ischemia is largely dependent on tissue microcirculation. Though microcirculation consists of the smallest blood vessels, including arterioles, capillaries, and venules, it is responsible for tissue oxygenation and ultimately tissue (and organ) health.[26] Capillaries facilitate nutrient and gas exchanges between blood and tissue, arterioles regulate blood flow, and venules allow blood to return from the capillaries serve as a conduit to larger blood vessels. During critical ischemia, microcirculatory endothelial cells fail to perform their regulatory function, smooth muscle cells lining arterioles lose their ability to regulate perfusion, red blood cells aggregate, and the nitric oxide system is greatly impaired resulting in reduced vasodilation. Additionally, ischemia activated leukocytes generate reactive oxygen species that barrier function in the microcirculation. It is the agglomerate of these impairments to the microvasculature that contribute to acute ischemia and in more severe cases, organ failure and death. In a study by Sakr et al., a lower percentage of perfused microcirculation was associated with poorer outcome, i.e. multiple organ failure and death.[27]

Post-occlusive reactive hyperemia (PORH) can be used to detect overall changes in microcirculation by measuring the response of distal microcirculation after a period of proximal occlusion, where the applied pressure of the cuff exceeds the systolic pressure of the patient. The extent to which the blood flow increases following cuff release can be used to quantify several microcirculation parameters, including the peak raw value, peak minus baseline, percentage increase from baseline, area under the curve, and time to peak hyperemia.[28] PORH monitoring

has been used to evaluate microcirculation in arterial occlusive disease [29-31], peripheral vascular disease [32-34], and spinal cord injury [35-37]. PORH measurements are often made on the forearm.[28,38] Previous studies of PORH have used laser Doppler imaging, laser speckle imaging, ultrasonic imaging, photoacoustic microscopy, and near-infrared imaging to monitor changes in microcirculation non-invasively.[10,39-42] Using 3CCD and IR technology our data shows that we can now successfully monitor PORH in acute and critical limb ischemia.

The comparison of 3CCD imaging and IR imaging in this study demonstrates our ability to monitor dysfunction of the microcirculation in a model of acute ischemia but in entire limb as well. In this study, the slope of reperfusion (a variation of time to peak hyperemia) for both 3CCD imaging and IR imaging could be utilized as a surrogate measure for severity of acute limb ischemia. There is currently no PORH parameter that closely resembles what we term the slope of PORH, i.e. the difference between the 3CCD and IR imaging maximum reperfusion values and their corresponding 5 or 10 minute post-reperfusion values divided by the duration of the post-reperfusion period; however, the slope of PORH values for both 3CCD and IR imaging are most correlated to locomotion within the first 48 hours post-operatively as shown in Table 3. Importantly, to our knowledge, this is the first demonstration of whole limb monitoring for tissue perfusion and oxygenation measurements simultaneously.

Perhaps the PLSDA model developed with imaging parameters in this study most eloquently demonstrates the potential of non-invasive imaging, specifically 3CCD and IR imaging, to predict full recovery of locomotion after a potential critical ischemic injury. This has important clinical implications as these imaging capabilities will allow clinicians to determine the extent of

reperfusion injury and tissue necrosis, which can help guide surgical debridement. In addition, 3CCD and IR imaging may have a role in determining if a limb requires amputation should there be no functional recovery. Finally, these imaging techniques can assist clinicians in discussions with patients regarding functional outcome after IRI. We have also confirmed the development of a large animal hind limb model for critical ischemia using both a tourniquet and direct vessel occlusion technique. The results presented herein are preliminary and would need to be further demonstrated on a larger scale with more animals over a longer period of recovery and validated with a clinical trial. This model will serve as the basis for further studies on ischemia-reperfusion injury and ways to mitigate its effects using 3CCD and IR imaging to guide treatment.

In summary, as suspected, 4.7 hour tourniquet animals demonstrated the most significant decrease in limb recovery, as evaluated by function/mobility (Tarlov score and drop foot score) and muscle histopathology. This supports the previously postulated critical ischemia of approximately 4.7 hours. In animals that were subjected to a shorter duration of ischemia, the injury was not severe enough to impair function/locomotion for the entire survival period. While there is evidence that end organs such as the liver and kidneys are affected by the IRI, the effect is not deleterious to survival. Furthermore, non-invasive 3CCD and IR imaging technologies accurately monitor whole limb perfusion and oxygenation, enabling visualization of PORH; this in turn enables accurate prediction of full function/locomotion recovery post-operatively. While IR imaging correlates with immediate outcome (≤ 24 hours post-operative), 3CCD imaging correlates with longer term outcome (≥ 48 hours post-operative). This indicates the need for the complementary use of both imaging technologies, which outperform standard clinical parameters

when identifying highest risk for debilitating ischemia/reperfusion injury as it relates to tissue perfusion and oxygenation.

Acknowledgements

The authors would like to thank Tiffani Slaughter and Maricela Rodriguez, as well as ENS Mitchell Harris, MAJ Gwen Kinley, and MAJ Earl Lee for their invaluable contribution to this work. This work was supported by work unit number 602115HP.3720.001.A1015. The views expressed in this presentation are those of the author and do not necessarily reflect the official policy or position of the Department of the Navy, the Department of Defense, nor the U.S. Government. We are military service members (or employee of the U.S. Government). This work was prepared as part of our official duties. Title 17 U.S.C. 105 provides the "Copyright protection under this title is not available for any work of the United States Government." Title 17 U.S.C. 101 defines a U.S. Government work as a work prepared by a military service member or employee of the U.S. Government as part of that person's official duties. We certify that the document represents valid work; that if we used information derived from another source, we obtained all necessary approvals to use it and made appropriate acknowledgements in the document; and we take public responsibility for it.

Figure Legends

Figure 1. 3CCD and infrared (IR) imaging.

Top) Representative grayscale 3CCD images of a hind limb, and Middle) representative grayscale infrared images of a hind limb at (1) baseline, (2) maximum ischemia, (3) 10 minutes post-reperfusion, and (4) 30 minutes post-reperfusion. Bottom left) Profile of R-B values, derived from 3CCD imaging, over the course of 3.5 hours of ischemia and 30 minutes of reperfusion. Bottom right) Profile of IR values and corresponding mean leg temperature over the course of 3.5 hours of ischemia and 30 minutes of reperfusion. The time points mentioned previously (1-4) are noted.

Figure 2. Comparison of blood chemistries in sham and experimental ischemia animals.

Comparison of blood chemistries (A-E) for sham animals (black circles) and experimental, or ischemic, animals (white squares). The dashed window indicates the region of maximum ischemia and reperfusion, while the gray window highlights post-operative time points. All time points are plotted as minutes; 1440 min = D1, 4320 min = D3, and 10,080 min = D7. All blood chemistries have been normalized to blood urea with the exception of CO_2, which prevents erroneous data trends due to dehydration. A) BUN = blood urea nitrogen; B) LDH = lactate dehydrogenase; U = urea; C) ALT = alanine aminotransferase; D) AST = aspartate aminotransferase; E) CK = creatinine kinase; F) CO_2 = carbon dioxide = bicarbonate.

Figure 3. Mean pathology scores for all experimental groups.

Mean total pathology scores for all experimental groups: A) organs (kidneys and liver), and B) sciatic nerve and skeletal muscle. 3_5O = 3.5 hour occlusion; 3_5T = 3.5 hour tourniquet; 4_7O = 4.7 hour occlusion; 4_7T = 4.7 hour tourniquet.

Figure 4. **Functional outcomes in sham and experimental ischemia groups.**

A) Mean drop foot scores for all experimental groups. A drop foot score of 0 meant that no neuropathy was observed post-operatively. A drop foot score of 1 was consistent with neuropathy in the affected limb for at least one day post-operatively. A drop foot score of 2 was consistent with neuropathy in the affected limb for at least three days post-operatively. A drop foot score of 3 was indicative of neuropathy in the affected limb beyond 5 days post-operatively. B) Mean Tarlov scores for all experimental groups. The dashed line at 5.0 is reflective of normal locomotion. The asterisks indicate statistically significant differences when compared to sham and 3.5 hour occlusion animals - ** = p-value < 0.01, *** = p-value < 0.001.

Figure 5. Profiles of operative 3CCD and IR imaging values.

Bar plots of mean R-B values derived from 3CCD imaging (A) and mean leg temperatures in °F (B) for all experimental groups at baseline, maximum ischemia, 10 minutes post-reperfusion, and 30 minutes post-reperfusion. Error bars = SEM (standard error of the mean). 3_5O = 3.5 hour occlusion; 3_5T = 3.5 hour tourniquet; 4_7O = 4.7 hour occlusion; 4_7T = 4.7 hour tourniquet.

Figure 6. Slopes of reperfusion and post-occlusive reactive hyperemia for 3CCD and IR imaging.

Bar plots comparing the IR slopes of reperfusion for all experimental groups (A) and 3CCD slopes of reperfusion, slopes of PORH at 5 minutes reperfusion, and slopes of PORH at 10 minutes reperfusion for all experimental groups (B). Statistically significant differences between 4.7 hour tourniquet animals and other experimental groups are designated by an asterisk (*) – p-value<0.05. Note, for each set of slopes presented in (B), the data is plotted by lowest Tarlov score (i.e. least normal locomotion) and increases to the highest Tarlov score (i.e. most normal locomotion). 3_5O = 3.5 hour occlusion; 3_5T = 3.5 hour tourniquet; 4_7O = 4.7 hour occlusion; 4_7T = 4.7 hour tourniquet.

Figure 7. PLSDA models to predict return to normal locomotion for all data, imaging only data, and non-imaging data sets.

Receiver operating curves for both calibration and cross-validation data sets. Area under the curve (AUC), a surrogate for accuracy, is displayed for each curve. A) PLSDA model generated from all parameters, but excluding outcome parameters. B) PLSDA model calculated from only imaging parameters. C) PLSDA model generated from all non-imaging parameters, but excluding outcome parameters. The calibration data is plotted in black and the cross-validation data is plotted in gray.

Table 1. Summary of experimental design.

Table 2. Outcome based comparison of various metrics.

Values are means +/- the standard deviation for animals that 1) recovered full locomotion, and 2) did not recover full locomotion. Differences approaching statistical significance (p-value ≈ 0.1)

are indicated by (†). Statistically significant differences (p-value<0.05) are indicated by an asterisk (*).

Table 3. Correlation of imaging parameters with function and pathology.

Pearson's correlation coefficients (ρ) for parameters involving function and pathology. IR = infrared imaging; Rpf = Rpfusion; 3CCD = 3CCD imaging; PORH = post-occlusive reactive hyperemia; D = day.

Table 4. Correlation of imaging parameters with blood chemistries.

Pearson's correlation coefficients (ρ) for parameters involving blood chemistries. IR = infrared imaging; Rpf = Rpfusion; 3CCD = 3CCD imaging; PORH = post-occlusive reactive hyperemia; D = day.

Tables

Table 1.

Group	Ischemia Time (hours)	Ischemia Mode	N
1	0	none	5
2	3.5	occlusion	5
3	3.5	tourniquet	5
4	4.7	occlusion	6
5	4.7	tourniquet	5
		Animals expired	2
		Equipment Malfunction	2
		Total Animals	22

Table 2.

Metric	Mean +/- σ Recovered Fully	Mean +/- σ Did not Recover Fully	p- value
Tarlov D1	4.42 ± 1.16	3.50 ± 0.76	0.07†
Tarlov D2	4.67 ± 0.49	3.81 ± 0.37	0.0006*
Tarlov D3	4.75 ± 0.45	3.88 ± 0.35	0.0002*
Tarlov D7	5.00 ± 0.00	3.94 ± 0.82	0.0004*
Left Kidney Pathology	0.08 ± 0.29	0.50 ± 0.53	0.04*
Right Kidney Pathology	0.08 ± 0.29	0.50 ± 0.53	0.04*
Liver Pathology	0.17 ± 0.39	0.13 ± 0.35	0.81
Drop Foot	0.08 ± 0.29	1.13 ± 0.99	0.003*
ALT Max Isc	70.6 ± 13.8	63.3 ± 11.1	0.22
AST Max Isc	37.3 ± 11.4	35.1 ± 18.0	0.75
Creatinine Max Isc	1.13 ± 0.17	1.18 ± 0.28	0.63
BUN Max Isc	9.00 ± 2.66	11.3 ± 1.83	0.05*
K^+ Max Isc	5.24 ± 0.85	5.68 ± 0.93	0.30
LDH Max Ischemia	1072 ± 367	984 ± 217	0.54
CK Max Isc	1010 ± 1765	631 ± 309	0.56
ALT Rpf	70.3 ± 11.8	63.6 ± 10.9	0.22
AST Rpf	42.6 ± 14.8	43.1 ± 13.1	0.93
Creatinine Rpf	1.16 ±0.18	1.10 ± 0.33	0.61
BUN Rpf	9.75 ± 2.86	11.00 ± 3.02	0.36
K+ Rpf	5.44 ± 0.78	6.01 ± 0.89	0.15
LDH Rpf	1126 ± 388	1053 ± 288	0.65
CK Rpf	732 ± 463	1077 ± 545	0.15
O_2 Sat Max Isc	96.3 ± 2.6	98.0 ± 2.0	0.13
O_2 Sat Rpf 5min	96.2 ± 2.2	97.6 ± 1.5	0.12
Temp Max Isc	99.5 ± 5.9	101.9 ± 1.0	0.27
Temp Rpf 5 min	99.6 ± 5.9	101.9 ± 1.0	0.28
Pulse Max Isc	101.8 ± 14.5	99.1 ± 5.7	0.62
Pulse Rpf	101.9 ± 14.8	99.0 ± 5.9	0.60
sO_2 Max Isc	77.1 ± 4.5	81.4 ± 3.5	0.06†
sO_2 Rpf 30 min	78.3 ± 4.2	78.1 ± 7.0	0.95
IR Slope Rpf	3.71 ± 8.98	10.60 ± 13.64	0.25
IR Whole Leg Rpf5	155.6 ± 48.1	105.8 ± 32.3	0.04*
IR Whole Leg Rpf10	187.3 ± 24.3	152.0 ± 36.3	0.05*
IR Whole Leg Rpf30	203.4 ± 13.5	191.6 ± 16.9	0.17
IR PORH Slope Rpf5	4.74 ± 3.91	2.55 ± 6.91	0.46
IR PORH Slope Rpf10	3.82 ± 4.79	5.82 ± 4.28	0.44

IR PORH Slope Rpf30	2.09 ± 1.25	4.07 ± 1.14	0.01*
3CCD Slope Rpf	0.44 ± 0.73	0.90 ± 0.62	0.18
3CCD Whole Leg Rpf10	29.3 ± 10.3	30.8 ± 8.4	0.75
3CCD Whole Leg Rpf30	26.7 ± 11.6	27.6 ± 6.4	0.85
3CCD PORH Slope Rpf5	-0.11 ± 0.36	-0.38 ± 0.28	0.10†
3CCD PORH Slope Rpf10	-0.28 ± 0.22	-0.36 ± 0.21	0.48

Table 3.

Imaging	Function/Locomotion				Pathology		
	Tarlov D1	Tarlov D2	Tarlov D7	Drop Foot	Lateral Middle	Medial Middle	Medial Distal
IR Slope Rpf	**-0.672**	**-0.677**	-0.532	0.519	0.364	0.225	**0.728**
IR Whole Leg Rpf10	0.505	0.566	0.391	**-0.775**	0.228	0.400	-0.028
IR Whole Leg Rpf30	0.511	0.532	0.337	**-0.753**	0.088	0.392	-0.094
IR PORH Slope Rpf5	**-0.848**	**-0.848**	-0.525	-0.466	0.526	**0.760**	0.352
IR PORH Slope Rpf10	**-0.764**	-0.398	-0.250	0.220	0.078	0.196	0.386
IR PORH Slope Rpf30	-0.516	**-0.730**	**-0.737**	**0.651**	0.376	0.154	0.363
3CCD Slope Rpf	-0.446	-0.540	-0.609	**0.710**	0.204	0.286	0.574
3CCD Whole Leg Rpf10	0.624	**0.771**	**0.739**	0.342	0.144	0.054	0.077
3CCD Whole Leg Rpf30	0.601	**0.755**	**0.730**	0.272	0.137	0.008	0.031
3CCD PORH Slope Rpf5	**0.652**	**0.889**	0.517	-0.462	-0.158	-0.395	-0.361
3CCD PORH Slope Rpf10	**0.652**	**0.889**	0.517	-0.461	-0.153	-0.395	-0.361
3CCD Whole Leg D1	-0.242	-0.641	-0.633	0.179	**0.776**	0.486	**0.756**
3CCD Whole Leg D3	-0.459	-0.425	-0.384	-0.007	**0.737**	0.603	**0.712**

Table 4.

Imaging	Blood Chemistry									
	BUN Max Isc	ALT Max Isc	Creatine Max Isc	LDH Max Isc	CK Max Isc	BE Max Isc	BUN Rpf	Creatine Rpf	CK Rpf	BE Rpf
IR Slope Rpf	0.441	-0.448	-0.399	-0.084	-0.105	0.399	0.480	-0.359	0.411	0.619
IR Whole Leg Rpf10	**-0.663**	0.343	-0.418	-0.186	0.241	-0.460	-0.614	-0.454	0.018	**-0.761**
IR Whole Leg Rpf30	**-0.666**	0.432	-0.361	-0.164	0.219	-0.590	-0.604	-0.371	-0.072	**-0.890**
IR PORH Slope Rpf5	-0.374	0.347	-0.567	0.095	0.114	-0.188	-0.315	-0.527	0.320	-0.513
IR PORH Slope Rpf10	0.501	0.343	-0.401	0.082	-0.166	0.216	0.532	-0.344	0.144	0.251
IR PORH Slope Rpf30	0.534	0.432	-0.452	-0.015	-0.390	0.326	0.571	-0.399	0.072	0.379
3CCD Slope Rpf	0.034	-0.141	-0.404	0.046	-0.178	0.318	0.112	-0.281	0.207	0.473
3CCD Whole Leg Rpf10	0.635	0.444	0.166	0.508	-0.107	0.343	**0.660**	0.160	0.351	**0.824**
3CCD Whole Leg Rpf30	0.589	0.408	0.236	0.484	-0.067	0.411	0.622	0.230	0.382	**0.803**
3CCD PORH Slope Rpf5	-0.648	-0.026	-0.034	-0.149	0.381	-0.324	-0.644	-0.048	-0.025	-0.349
3CCD PORH Slope Rpf10	-0.642	-0.040	-0.045	-0.141	0.367	-0.319	-0.635	-0.059	-0.038	-0.355
3CCD Whole Leg D1	0.263	-0.541	**-0.790**	**-0.741**	**0.658**	0.067	0.392	**-0.740**	**0.838**	0.264
3CCD Whole Leg D3	0.629	**-0.755**	**-0.839**	**-0.663**	**0.722**	-0.053	**0.756**	**-0.830**	**0.812**	0.200

References

1. Malan E, Tattoni G (1963) Physio- and anatomo-pathology of acute ischemia of the extremities. J Cardiovasc Surg (Torino) 4: 212-225.

2. Scully RE, Hughes CW (1956) The pathology of ischemia of skeletal muscle in man; a description of early changes in muscles of the extremities following damage to major peripheral arteries on the battlefield. Am J Pathol 32: 805-829.

3. Gifford SM, Eliason JL, Clouse WD, Spencer JR, Burkhardt GE, et al. (2009) Early versus delayed restoration of flow with temporary vascular shunt reduces circulating markers of injury in a porcine model. J Trauma 67: 259-265.

4. Forsberg JA, Potter BK, Polfer EM, Safford SD, Elster EA (2014) Do inflammatory markers portend heterotopic ossification and wound failure in combat wounds? Clin Orthop Relat Res 472: 2845-2854.

5. Liu DZ, Mathes DW, Zenn MR, Neligan PC (2011) The application of indocyanine green fluorescence angiography in plastic surgery. J Reconstr Microsurg 27: 355-364.

6. Nguyen JT, Ashitate Y, Buchanan IA, Ibrahim AM, Gioux S, et al. (2012) Bone flap perfusion assessment using near-infrared fluorescence imaging. J Surg Res 178: e43-50.

7. Hope-Ross M, Yannuzzi LA, Gragoudas ES, Guyer DR, Slakter JS, et al. (1994) Adverse reactions due to indocyanine green. Ophthalmology 101: 529-533.

8. Wu C, Kim S, Halvorson EG (2013) Laser-assisted indocyanine green angiography: a critical appraisal. Ann Plast Surg 70: 613-619.

9. Moyer HR, Losken A (2012) Predicting mastectomy skin flap necrosis with indocyanine green angiography: the gray area defined. Plast Reconstr Surg 129: 1043-1048.

10. Roustit M, Cracowski J-L (2012) Non-invasive Assessment of Skin Microvascular Function in Humans: An Insight Into Methods. Microcirculation 19: 47-64.
11. Boas DA, Dunn AK (2010) Laser speckle contrast imaging in biomedical optics. J Biomed Opt 15: 011109.
12. Crane NJ, Schultz ZD, Levin IW (2007) Contrast enhancement for in vivo visible reflectance imaging of tissue oxygenation. Appl Spectrosc 61: 797-803.
13. Crane NJ, Pinto PA, Hale D, Gage FA, Tadaki D, et al. (2008) Non-invasive monitoring of tissue oxygenation during laparoscopic donor nephrectomy. BMC Surg 8: 8.
14. Kiyatkin EA, Brown PL, Wise RA (2002) Brain temperature fluctuation: a reflection of functional neural activation. Eur J Neurosci 16: 164-168.
15. Millendez MB, Crane NJ, Elster EA, Safford SD (2012) Evaluation of intestinal viability using 3-charge coupled device image enhancement technology in a pediatric laparoscopic appendectomy model. J Pediatr Surg 47: 142-147.
16. Crane NJ, McHone B, Hawksworth J, Pearl JP, Denobile J, et al. (2008) Enhanced surgical imaging: laparoscopic vessel identification and assessment of tissue oxygenation. J Am Coll Surg 206: 1159-1166.
17. Joyal CC, Henry M (2013) Long-wave infrared functional brain imaging in human: a pilot study. Open Neuroimag J 7: 1-3.
18. Cadeddu JA, Jackman SV, Schulam PG (2001) Laparoscopic infrared imaging. J Endourol 15: 111-116.
19. Gorbach A, Heiss J, Kufta C, Sato S, Fedio P, et al. (2003) Intraoperative infrared functional imaging. Ann Neuorol 54: 297-309.

20. Watson J, Gorbach A, Pluta R, Rak R, Heiss J, et al. (2002) Real-time detection of vascular occlusion and reperfusion of the brain during surgery by using infrared imaging. J Neurosurg 96: 918-923.
21. Burkhardt GE, Spencer JR, Gifford SM, Propper B, Jones L, et al. (2010) A large animal survival model (Sus scrofa) of extremity ischemia/reperfusion and neuromuscular outcomes assessment: a pilot study. J Trauma 69 S146-153.
22. Tarlov IM, Klinger H, Vitale S (1953) Spinal cord compression studies. I. Experimental techniques to produce acute and gradual compression. AMA Arch Neurol Psychiatry 70: 813-819.
23. Love TJ (1980) Thermography as an indicator of blood perfusion. Ann N Y Acad Sci 335: 429-437.
24. Millendez MB, Crane NJ, Elster EA, Safford SD Evaluation of intestinal viability using 3-charge coupled device image enhancement technology in a pediatric laparoscopic appendectomy model. J Pediatr Surg 47: 142-147.
25. Crane NJ, Gillern SM, Tajkarimi K, Levin IW, Pinto PA, et al. (2010) Visual enhancement of laparoscopic partial nephrectomy with 3-charge coupled device camera: assessing intraoperative tissue perfusion and vascular anatomy by visible hemoglobin spectral response. J Urol 184: 1279-1285.
26. Ince C (2005) The microcirculation is the motor of sepsis. Crit Care 9 Suppl 4: S13-19.
27. Sakr Y, Dubois MJ, De Backer D, Creteur J, Vincent JL (2004) Persistent microcirculatory alterations are associated with organ failure and death in patients with septic shock. Crit Care Med 32: 1825-1831.

28. Roustit M, Cracowski JL (2013) Assessment of endothelial and neurovascular function in human skin microcirculation. Trends Pharmacol Sci 34: 373-384.

29. Fronek A, Johansen K, Dilley RB, Bernstein EF (1973) Ultrasonographically Monitored Postocclusive Reactive Hyperemia in the Diagnosis of Peripheral Arterial Occlusive Disease. Circulation 48: 149-152.

30. Criqui MH, Fronek A, Barrett-Connor E, Klauber MR, Gabriel S, et al. (1985) The prevalence of peripheral arterial disease in a defined population. Circulation 71: 510-515.

31. Wahlberg E, Jörneskog G, Olofsson P, Swedenborg J, Fagrell B (1990) The influence of reactive hyperemia and leg dependency on skin microcirculation in patients with peripheral arterial occlusive disease (PAOD), with and without diabetes. VASA Zeitschrift fur Gefasskrankheiten 19: 301-306.

32. Cheng X, Mao JM, Xu X, Elmandjra M, Bush R, et al. (2004) Post-occlusive reactive hyperemia in patients with peripheral vascular disease. Clin Hemorheol Microcirc 31: 11-21.

33. Kragelj R, Jarm T, Erjavec T, Presern-Strukelj M, Miklavcic D (2001) Parameters of postocclusive reactive hyperemia measured by near infrared spectroscopy in patients with peripheral vascular disease and in healthy volunteers. Ann Biomed Eng 29: 311-320.

34. Jarm T, Kragelj R, Liebert A, Lukasiewitz P, Erjavec T, et al. (2003) Postocclusive reactive hyperemia in healthy volunteers and patients with peripheral vascular disease measured by three noninvasive methods. Adv Exp Med Biol 530: 661-669.

35. Hagisawa S, Ferguson-Pell M, Cardi M, Miller SD (1994) Assessment of skin blood content and oxygenation in spinal cord injured subjects during reactive hyperemia. J Rehabil Res Dev 31: 1-14.

36. Schubert V, Fagrell B (1991) Postocclusive reactive hyperemia and thermal response in the skin microcirculation of subjects with spinal cord injury. Scand J Rehabil Med 23: 33-40.

37. Sae-Sia W, Wipke-Tevis DD, Williams DA (2007) The Effect of Clinically Relevant Pressure Duration on Sacral Skin Blood Flow and Temperature in Patients After Acute Spinal Cord Injury. Arch Phys Med Rehab 88: 1673-1680.

38. Cracowski J-L, Minson CT, Salvat-Melis M, Halliwill JR (2006) Methodological issues in the assessment of skin microvascular endothelial function in humans. Trends Pharmacol Sci 27: 503-508.

39. Cheng R, Zhang X, Daugherty A, Shin H, Yu G (2013) Noninvasive quantification of postocclusive reactive hyperemia in mouse thigh muscle by near-infrared diffuse correlation spectroscopy. Appl Opt 52: 7324-7330.

40. Gurley K, Shang Y, Yu G (2012) Noninvasive optical quantification of absolute blood flow, blood oxygenation, and oxygen consumption rate in exercising skeletal muscle. J Biomed Opt 17: 075010.

41. Favazza CP, Cornelius LA, Wang LV (2011) In vivo functional photoacoustic microscopy of cutaneous microvasculature in human skin. J Biomed Opt 16: 026004.

42. Thomas KN, Cotter JD, Lucas SJ, Hill BG, van Rij AM (2015) Reliability of contrast-enhanced ultrasound for the assessment of muscle perfusion in health and peripheral arterial disease. Ultrasound Med Biol 41: 26-34.

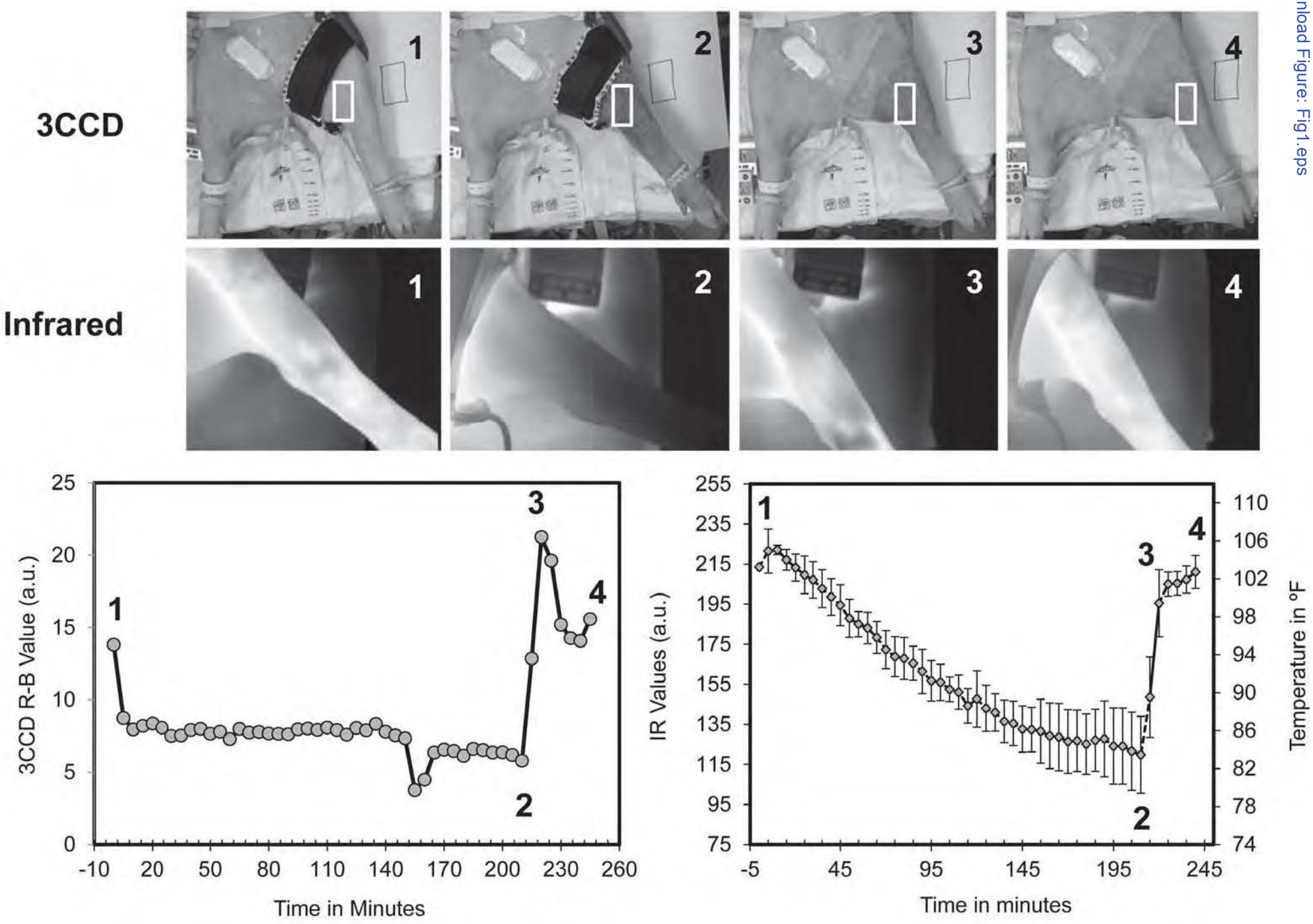

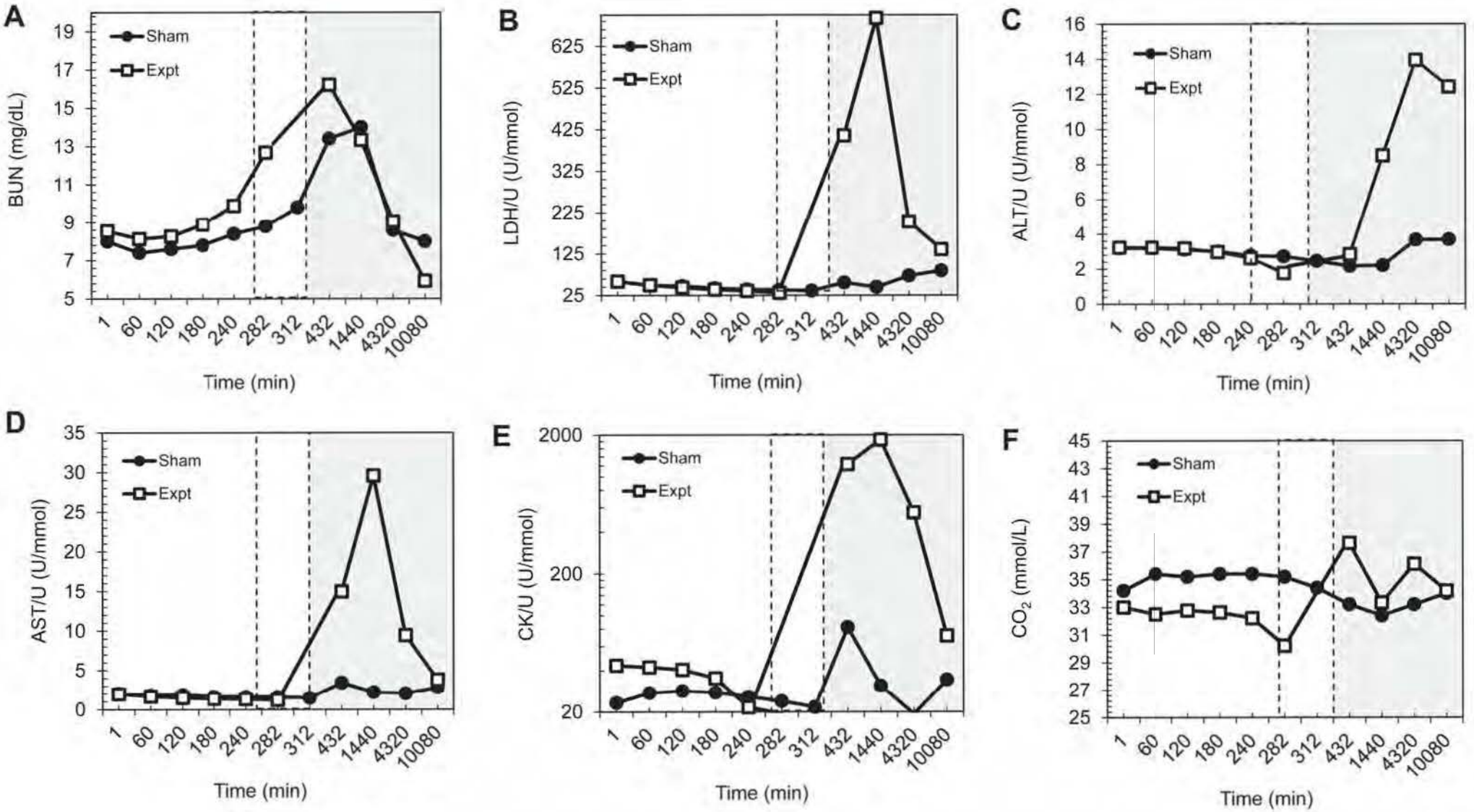

Figure
Click here to download Figure: Fig3.eps

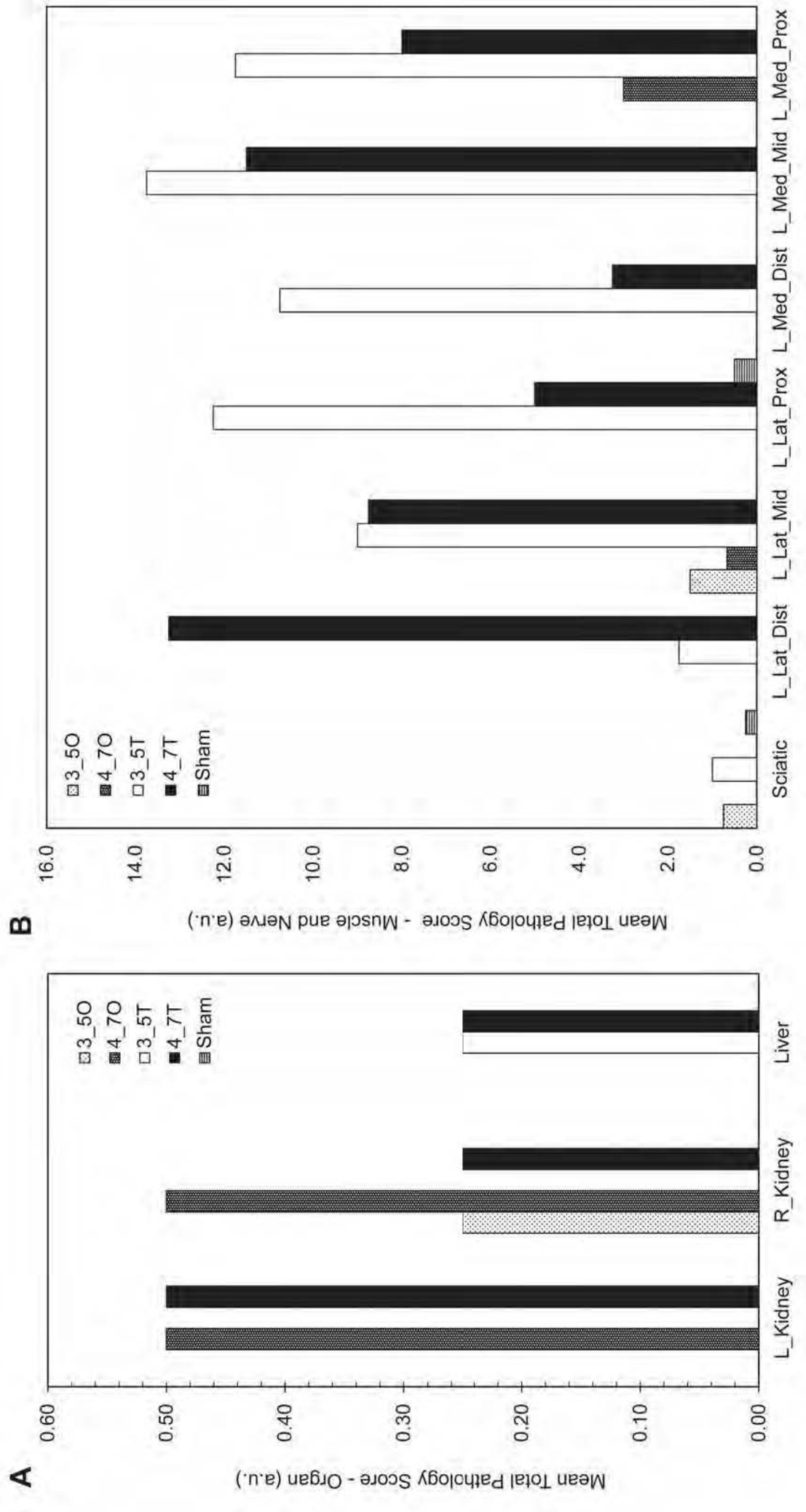

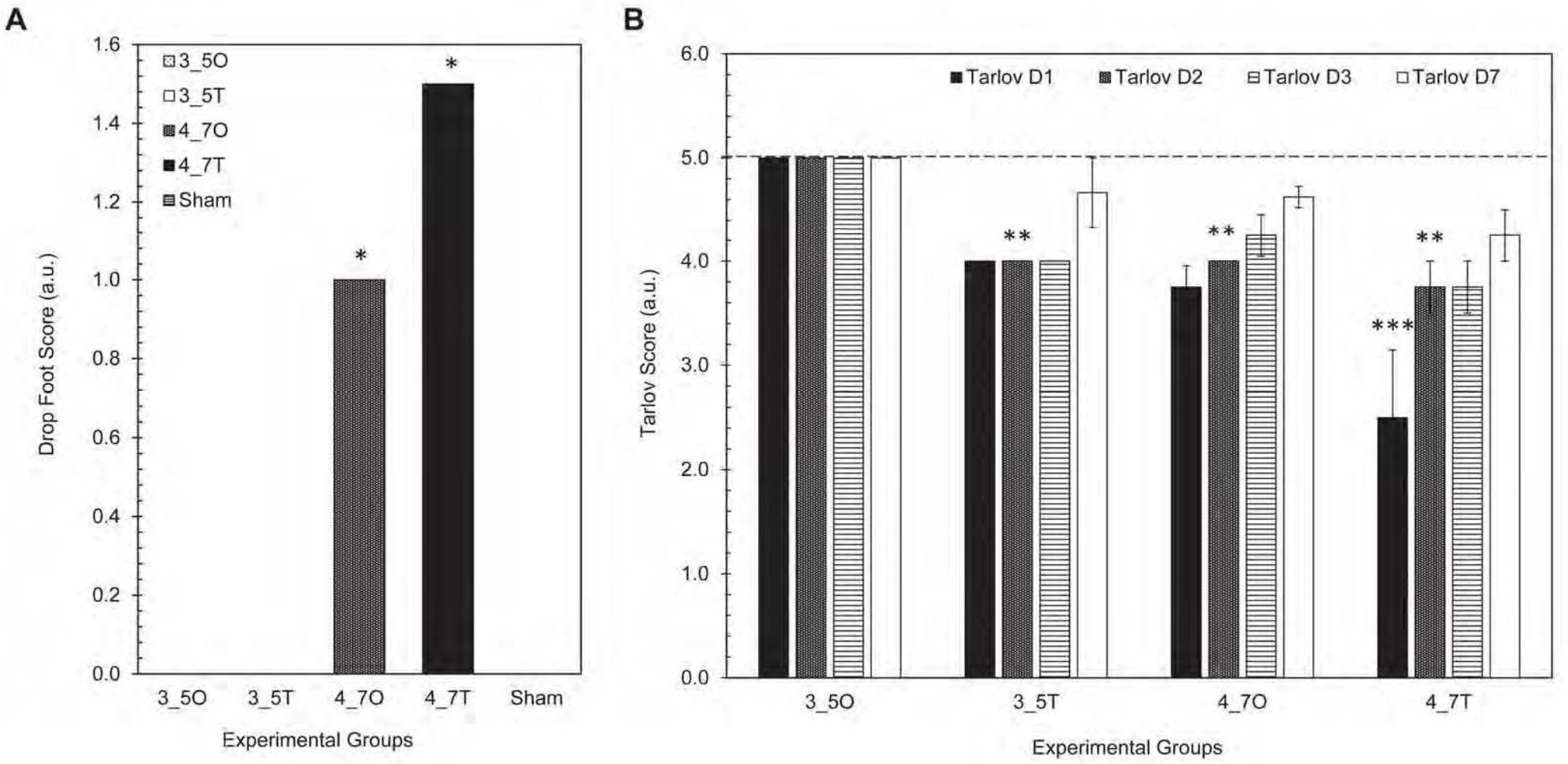

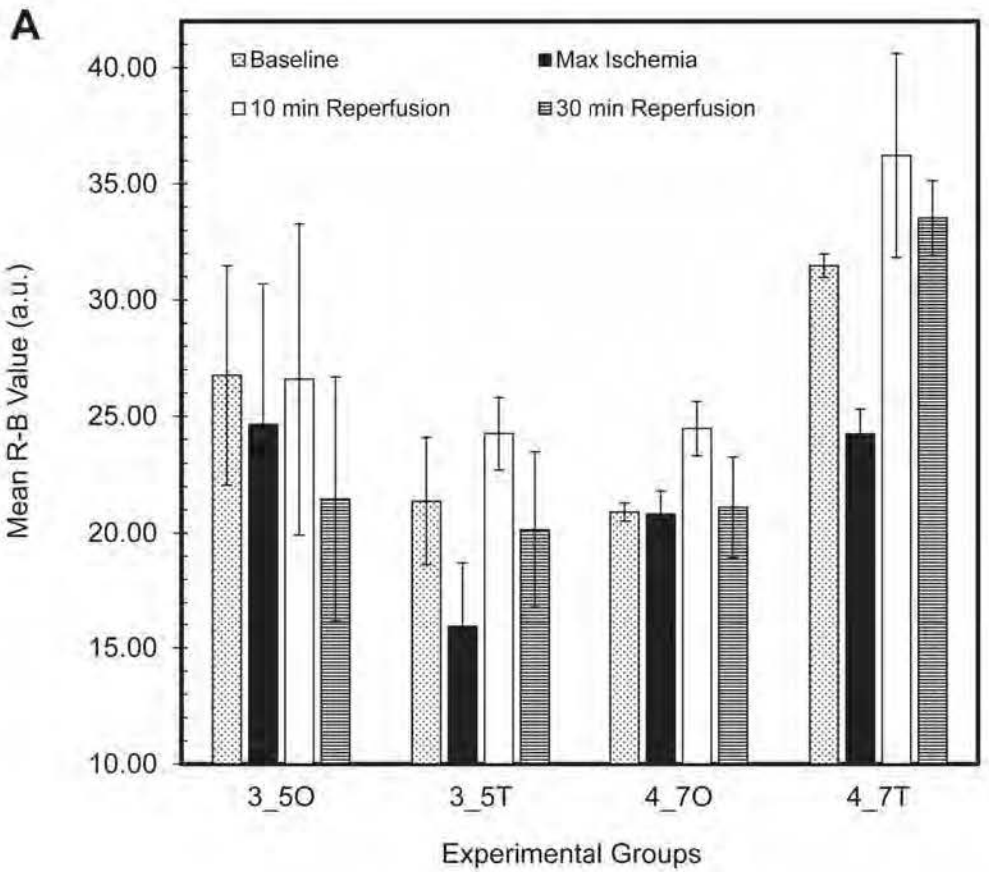

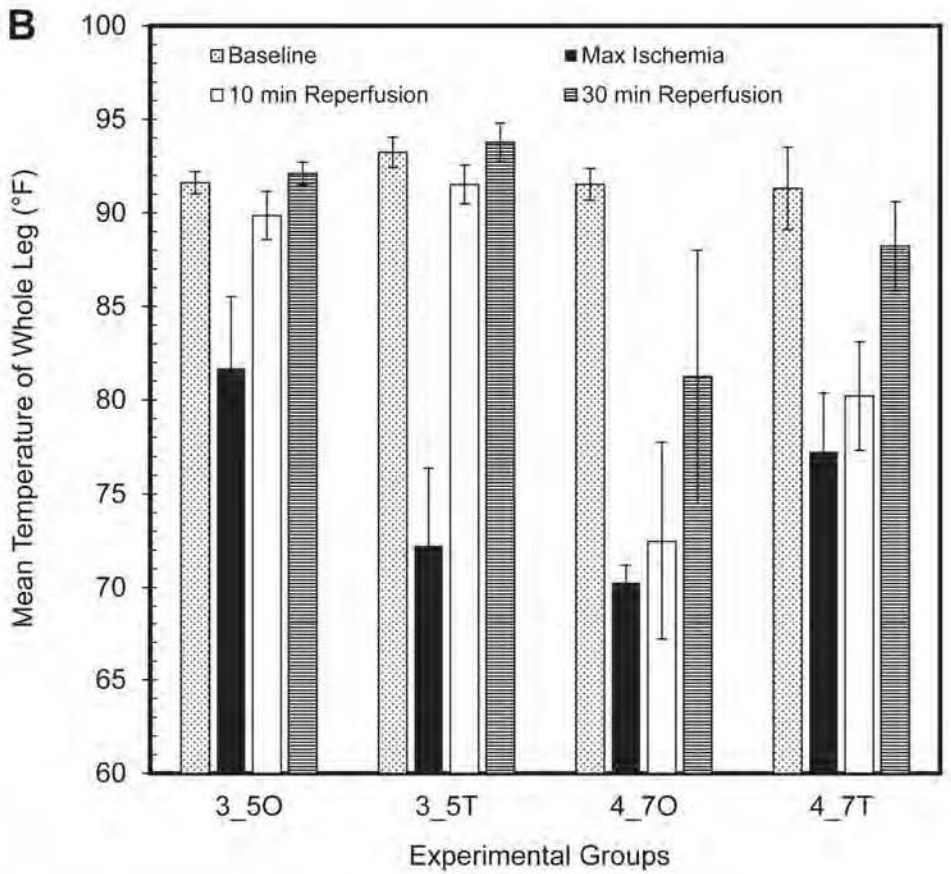

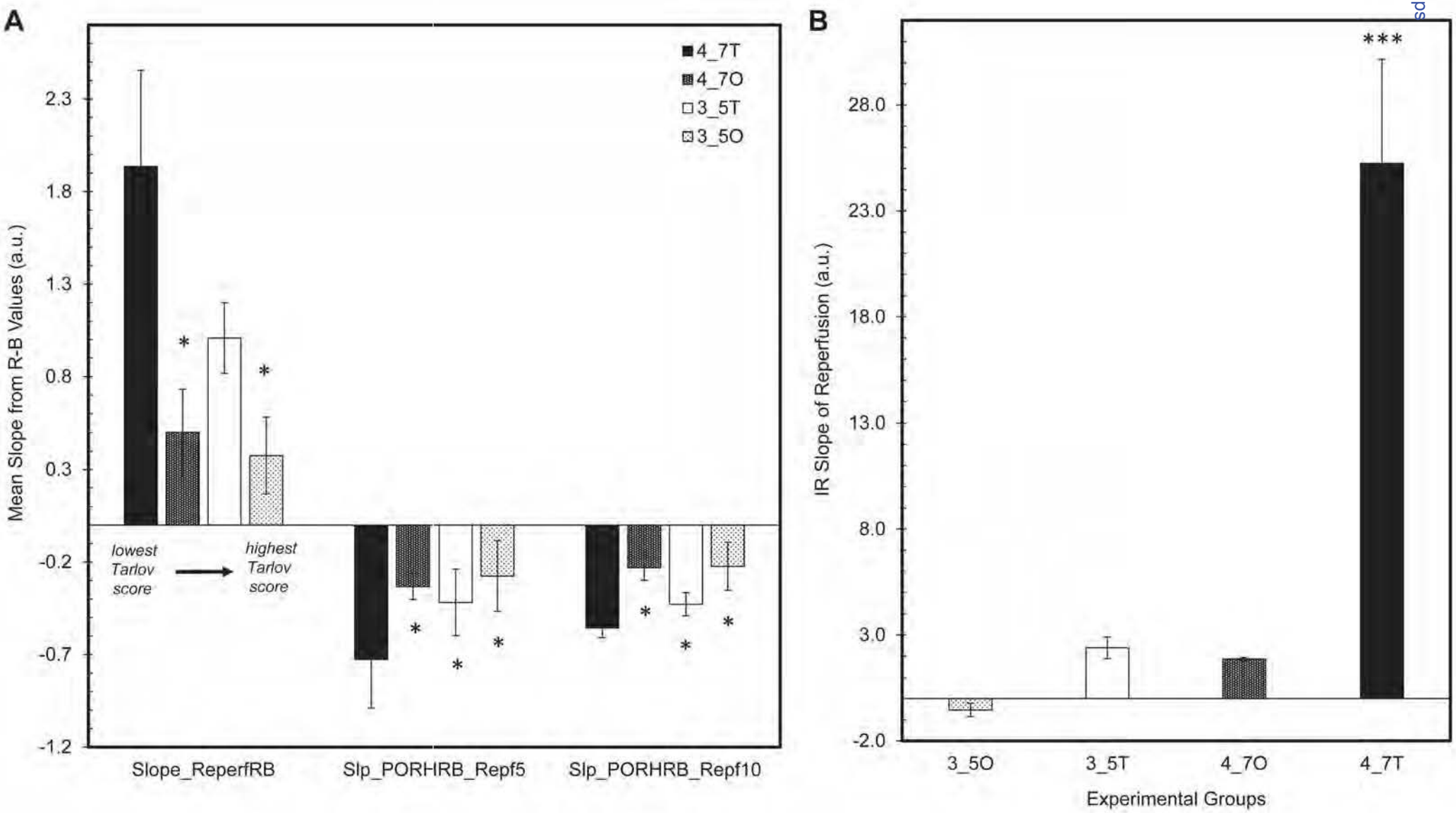

Figure
Click here to download Figure: Fig7.eps

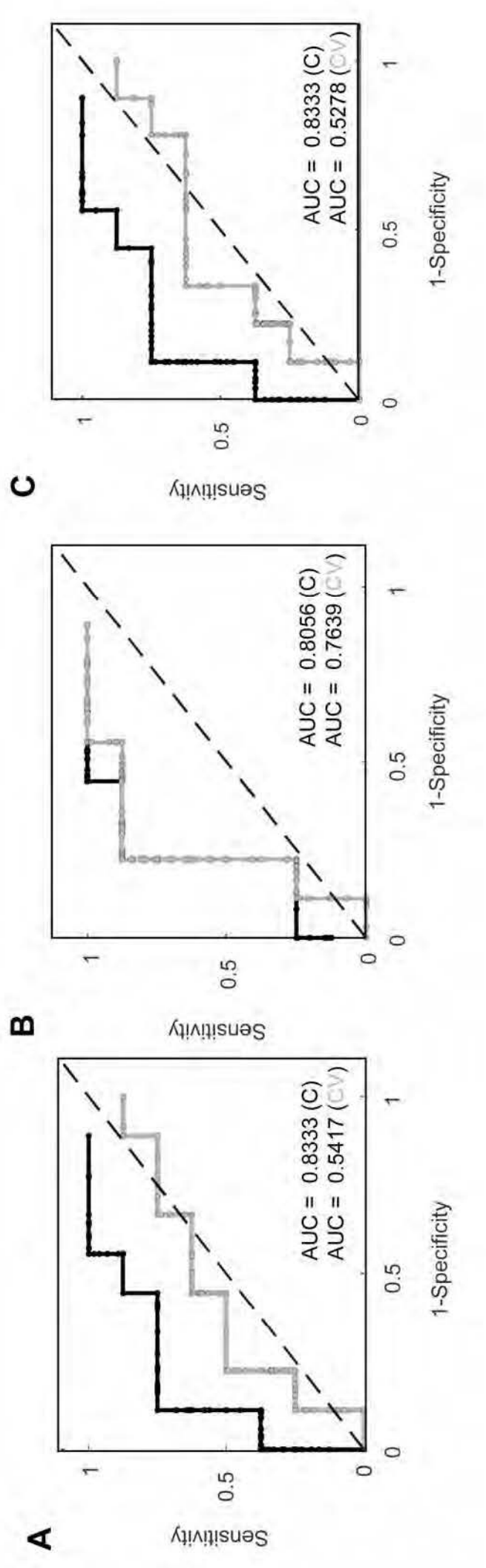

Striking Image

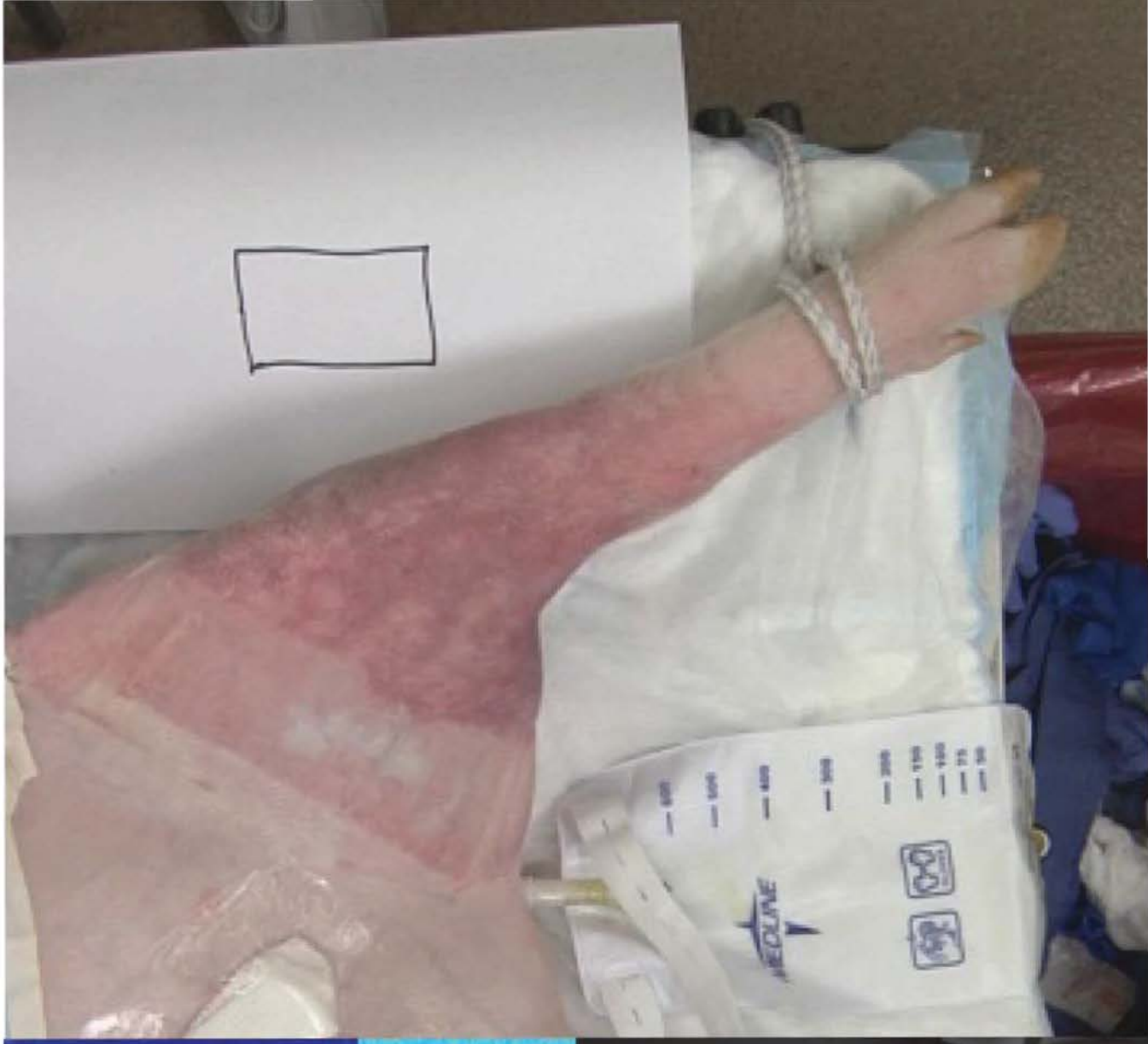

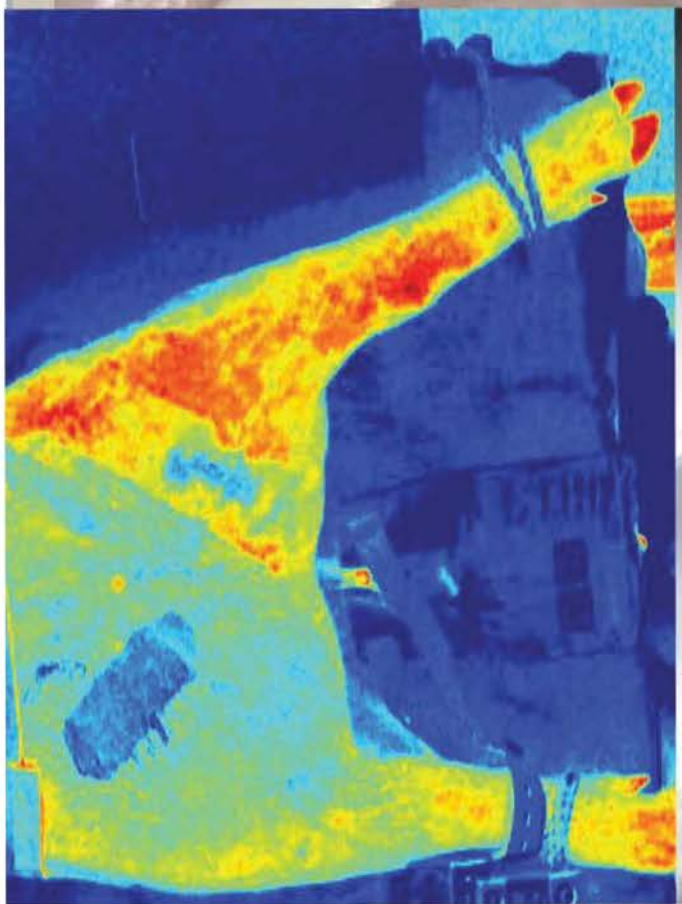

Validation of Hierarchical Cluster Analysis for Identification of Bacterial Species Using 42 Bacterial Isolates

Meron Ghebremedhin[1,3], Shubha Yesupriya[1], Janos Luka[1,2], Nicole J. Crane[1,2,3]
[1]Regenerative Medicine Department, Naval Medical Research Center, Silver Spring, MD, USA 20910; [2]Department of Surgery, Uniformed Services University of Health Sciences, Bethesda, MD, USA 20814; [3]Henry M. Jackson Foundation for the Advancement of Military Medicine, Bethesda, MD, 20817

ABSTRACT

Recent studies have demonstrated the potential advantages of the use of Raman spectroscopy in the biomedical field due to its rapidity and noninvasive nature. In this study, Raman spectroscopy is applied as a method for differentiating between bacteria isolates for Gram status and *Genus species*. We created models for identifying 28 bacterial isolates using spectra collected with a 785 nm laser excitation Raman spectroscopic system. In order to investigate the groupings of these samples, partial least squares discriminant analysis (PLSDA) and hierarchical cluster analysis (HCA) was implemented. In addition, cluster analyses of the isolates were performed using various data types consisting of, biochemical tests, gene sequence alignment, high resolution melt (HRM) analysis and antimicrobial susceptibility tests of minimum inhibitory concentration (MIC) and degree of antimicrobial resistance (SIR). In order to evaluate the ability of these models to correctly classify bacterial isolates using solely Raman spectroscopic data, a set of 14 validation samples were tested using the PLSDA models and consequently the HCA models. External cluster evaluation criteria of purity and Rand index were calculated at different taxonomic levels to compare the performance of clustering using Raman spectra as well as the other datasets. Results showed that Raman spectra performed comparably, and in some cases better than, the other data types with Rand index and purity values up to 0.933 and 0.947, respectively. This study clearly demonstrates that the discrimination of bacterial species using Raman spectroscopic data and hierarchical cluster analysis is possible and has the potential to be a powerful point-of-care tool in clinical settings.

Keywords: Raman Spectroscopy, Multivariate Statistical Analysis, Hierarchical Cluster Analysis, Partial Least Squares-Discriminant Analysis, Rand Index, Bacterial Isolates.

1. INTRODUCTION

Infections are common complications of combat wounds and affect not only quality of life but also whether or not a wound heals normally. At the beginning of the twentieth century, improvements in military hygiene and disease control significantly reduced the number of war-time deaths due to pestilence[(1)]. Though "war time" deaths from pestilence are not common in recent conflicts such as Operation Iraqi Freedom (OIF) and Operation Enduring Freedom (OEF), infection control of multi-drug resistant organisms such as *Acinetobacter*, *Klebsiella*, and *Pseudomonas* has presented a challenge[(2)]. Multi-drug resistant infections can be problematic due to the small number of effective drugs for treatment. Thus, accurate identification of the species and strain of the infecting organism becomes important.

Raman spectroscopy is a molecularly specific technique that is capable of probing samples noninvasively and nondestructively. It has been used to assess tissues at the molecular level with diverse clinical and diagnostic applications with high specificity [(3-19)] and this is one of the attributes that makes Raman spectroscopy an ideal technology for evaluating clinical infections. There have been numerous Raman spectroscopic studies of microorganisms, many focusing on rapid identification of the microorganisms [(20-28)]. In these studies, bacteria were successfully identified at the strain level by utilizing a Raman spectral database of the microorganisms. However, many of these studies have been limited to only Gram positive or only Gram negative bacterial species, and have not attempted to evaluate a dataset consisting of both Gram positive and Gram negative bacteria species.

Current methods of identifying bacterial infection rely on culturing microbes from patient material and performing biochemical tests, which together can take 2-3 days to complete. If Raman spectroscopy could detect bacterial infection from patient material directly, physicians would be able to determine course of treatment and drug administration in a matter of hours. Reliable application of Raman spectroscopy in a clinical setting could revolutionize routine identification of pathogenic organisms. Here, we target the identification of bacterial isolates responsible for infections in combat-related wounds specifically. In this preliminary study, a number of bacteria known to cause clinical infections are examined using Raman spectroscopy. Additionally, various types of data are analyzed for comparison: biochemical tests, high resolution melting points, DNA sequences, antimicrobial susceptibility, and degree of microbial resistance tests.

2. METHODS

2.1 Raman Spectroscopy

In Table 1, the 42 bacterial isolates examined are listed: 28 reference isolates and 14 validation isolates.

Gram +/-	Family	Genus	Species	Number of reference isolates	Number of validation isolates
-	Enterobacteri- ceae	*Klebsiella*	*pneumoniae*	2	2
-	Enterobacteriaceae	*Enterobacter*	*cloacae*	2	0
-	Enterobacteriaceae	*Morganella*	*morganii*	2	0
-	Enterobacteriaceae	*Escherichia*	*coli*	2	2
-	Enterobacteriaceae	*Citrobacter*	*freundii*	2	0
-	Pseudomonadaceae	*Pseudomonas*	*stutzeri*	2	0
-	Moraxellaceae	*Acinetobacter*	*baumannii*	2	2
-	Xanthomonadaceae	*Stenotro homonas*	*maltophilia*	2	1
+	Enterococcaceae	*Enterococcus*	*faecalis*	1	1
+	Enterococcaceae	*Enterococcus*	*durans*	2	0
+	Enterococcaceae	*Enterococcus*	*faecium*	2	2
+	Sta hlococcaceae	*Sta h lococcus*	*schleiferi*	1	0
+	Sta hlococcaceae	*Sta h lococcus*	*haemolyticus*	2	2
+	Sta hlococcaceae	*Sta h lococcus*	*aureus*	2	2
+	Staphlococcaceae	*Staphylococcus*	*ca itis*	2	0
			Totals	**28**	**14**

Table 1. Complete list of bacterial isolates from which all data types were acquired.

Sample identities were blinded for the validation dataset. Each bacterial isolate was grown for 48 hours on a lysogeny broth agar (LBA) and a blood agar plate. Raman spectra were collected using a 785 nm Raman PhAT system (Kaiser Optical Systems, Inc., Ann Arbor, MI, USA). Spectra were collected using a 3mm spot size lens with 50 accumulations of 2 second exposures. Nine spectra were collected from each of the 42 isolates (5 from the LBA plate and 4 from the blood agar plate). During spectral collection, sample fluorescence overwhelmed the Raman scattering of some isolates. To overcome this, particularly fluorescent bacterial isolates were transferred to a 0.5 mL centrifuge vial, rinsed with deionized water, and centrifuged at 2,000 rpm for 3 minutes. The supernatant was discarded and the bacteria samples were submitted for spectral recollection. This process was repeated until fluoresce was significantly reduced and the spectral quality improved (minimum signal to noise ratio of 10).

2.2 Biochemical and antimicrobial resistance (MIC and SIR) data

Biochemical and antimicrobial resistance data were acquired using the BD Phoenix™, a fully automated system for the rapid identification of bacteria and antimicrobial susceptibility testing (AST) [29]. Samples were prepped following the manufacturer's instruction and loaded in to BD phoenix panels. The system gives positive or negative results for an array of enzymatic and biochemical substrates providing the biochemical data for each isolate. Antimicrobial resistance data was also acquired using BD Phoenix™ for Antimicrobial Susceptibility Test (AST) results. This test determines the resistance of infectious agents by labeling them as Susceptible, Intermediate or Resistant (SIR). It also provides the Minimum Inhibitory Concentrations (MICs) data, which is the lowest concentration of an antimicrobial that will inhibit the visible growth of a microorganism after overnight incubation[30] and notes any other resistance markers found. The results of these tests were then numerically coded for cluster analysis.

2.3 DNA sequences

The extraction of DNA from culture colonies was performed using the UltraClean Microbial DNA Isolation Kit (Mo Bio Laboratories, Carlsbad, CA, USA). 16S polymerase chain reactions (PCRs) were performed in 50 µL reaction mixtures using Q5® High-Fidelity DNA Polymerase (NEB, Ipswich, MA, USA). Reactions were performed in triplicate and amplified on a GenAmp 9700 PCR System (Applied Biosystems, Grand Island, NY, USA) under the following conditions: 96°C for 1 minute, followed by 35 cycles of 96°C for 15 seconds, 60°C for 45 seconds, and 72°C for 45 seconds. Final extension at 72°C was done for 2 minutes. Then, 10 µL of amplified products from the samples were analyzed by agarose gel electrophoresis to identify if single PCR products were present. Amplified PCR products were purified from each sample using Purelink Quick PCR purification kit (Invitrogen, Grand Island, Ny, USA) prior to nucleic acid sequencing. DNA sequencing was performed at ID Genomics, Inc. (Seattle, WA, USA).

2.4 High Resolution Melt (HRM) analysis

Extracted DNA from each bacterial organism was subjected to two PCR amplifications of the V3 hypervariable region. Reactions were performed in triplicate and amplified on a LightCycler 480 Instrument II (Roche, Indianapolis, IN, USA). Each PCR sample was examined in duplicate for high resolution melting analysis (HRMA) and analyzed using the Gene Scanner software version 2.0 (Roche, Indianapolis, IN, USA). Melting curves generated from HRMA were analyzed by generating derivative plots to assess the number of melting peaks. "Autogrouping" was performed on the difference plots to group all positive samples with similar curve shape within the same analysis subset. A unique letter code was assigned for each group identified, starting with the letter 'A' and progressing alphabetically. The HRMA melting curves generated from V3 target region for each sample were then compared to sequence data.

2.5 Data analysis

Spectra were imported into MATLAB® and preprocessed. Spectral differences observed between the Raman spectra of the mean Gram positive and mean Gram negative bacterial isolates were subtle (Figure 1).

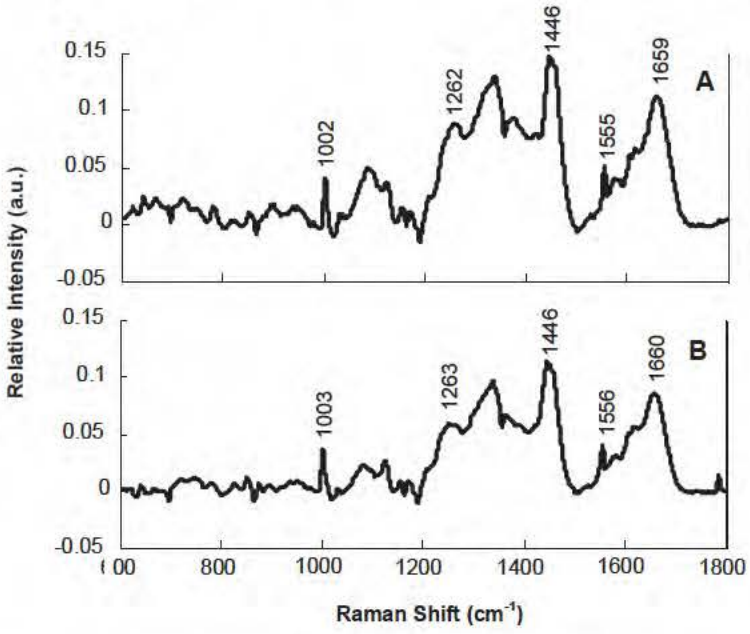

Figure 1. Mean of preprocessed Raman spectra for Gram positive bacterial isolates (A) Gram negative bacterial isolates (B).

In an attempt to visualize and highlight spectral differences between Gram positive and negative isolates, and to select the most discriminative regions, mean spectra were subject to baseline removal with a sixth order polynomial and intensity normalization to the 1004 cm^{-1} Raman vibrational band. The Raman spectra were then plotted as a

scaled image (Figure 2). Figure 2 highlights the increased intensity of Gram positive spectra in the 1200-1500cm^{-1} and 1500-1700 cm^{-1} Raman spectral regions compared to the Gram negative spectra.

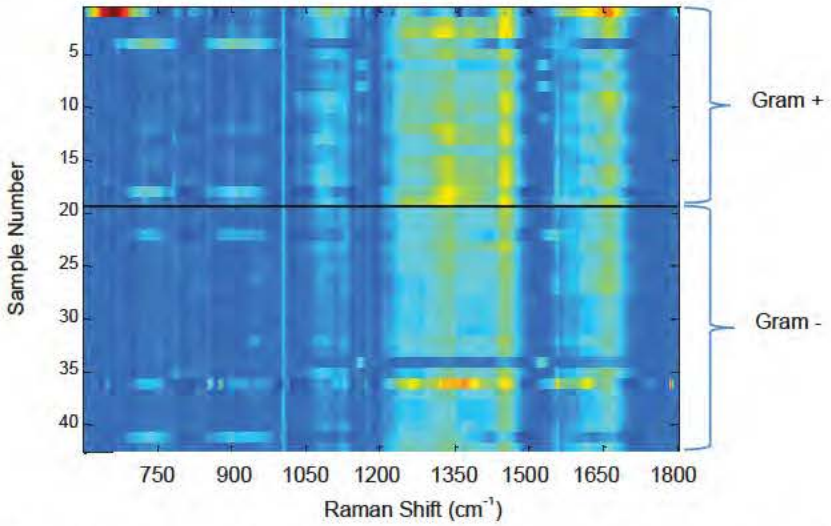

Figure 2. Scaled color map image of preprocessed spectra representing Gram positive and Gram negative isolates.

For multivariate statistical analysis, including Partial Least Squares Discriminant Analysis (PLSDA) and Hierarchical Cluster Analysis (HCA), both were performed using PLS Toolbox (Eigenvector Research, Inc., Wenatchee, WA, USA). PLSDA is a multivariate inverse least squares discrimination method used to classify samples. It calculates a prediction probability and classification threshold for each class modeled[31]. HCA is a common unsupervised pattern recognition method which generally functions by calculating the distance between samples in the original independent variable space [32].HCA was performed using Ward's linkage and Euclidean distance. Spectra were preprocessed by selecting the spectral window from 1200-1700 cm^{-1}, applying polynomial baseline correction, intensity normalization, and mean centering. To avoid overtraining of data, the least number of latent variables with the lowest root mean square error of cross validation results of training data were selected.

The remaining datasets of biochemistries, antimicrobial resistances, and HRM data were analyzed by autoscaling and performing HCA using Ward's linkage and Euclidean distance. DNA Sequences were analyzed using multiple sequence alignment of a 1250 base pair region, which was performed using MUSCLE (multiple sequence comparison by log-expectation) method and curated using G-blocks[33]. Each base was coded with a numerical value prior to performing HCA with Ward's linkage and Euclidean distance. Note that there are two missing data points in the HRM data, as data was not acquired for these two samples (*Enterococcus faecalis and Escherichia coli*).

3. Results

First, a PLSDA model was developed to discriminate between Gram positive and Gram negative bacteria using the 28 calibration bacterial samples (a total of 252 spectra), and the remaining 14 bacterial samples (126 spectra) were used for validation of the PLSDA model. The resulting PLSDA latent variables and prediction values of the model for each sample were then averaged and fed into the HCA algorithm (Figure 3A). Similarly a second and third PLSDA models were developed to discriminate between *Acinetobacter, Citrobacter, Enterobacter, Escherichia, Klebsiella, Morganella, Pseudomonas* and *Stenotrophomonas* (Gram negative bacteria, Figure 3B) and *Staphylococcaceae* and *Enterococcaceae* (Gram positive bacteria, Figure 3C), and then presented as HCA dendrograms. Additionally, HCA dendrograms are presented for biochemistries (Figure 4A), antimicrobial resistances (Figure 4B), High Resolution melt data (Figure 4C) and DNA sequencing (Figure 4D).

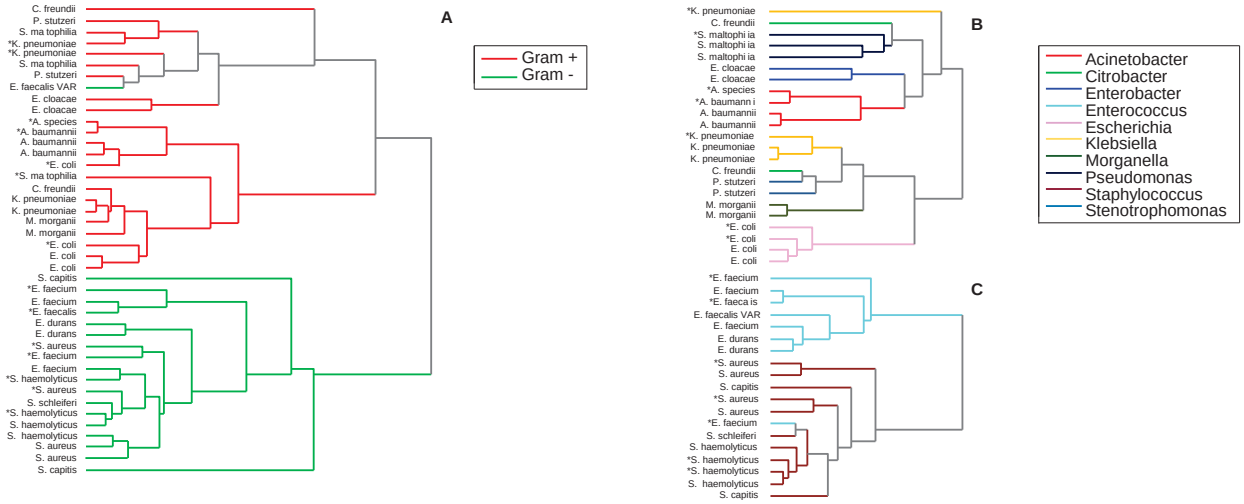

Figure 3. Hierarchical Clusters of Raman spectra data of all isolates modeled at the gram level (A) and at the genus level representing gram negative (B) and gram positive (C) isolates. Validation samples are marked with '*'.

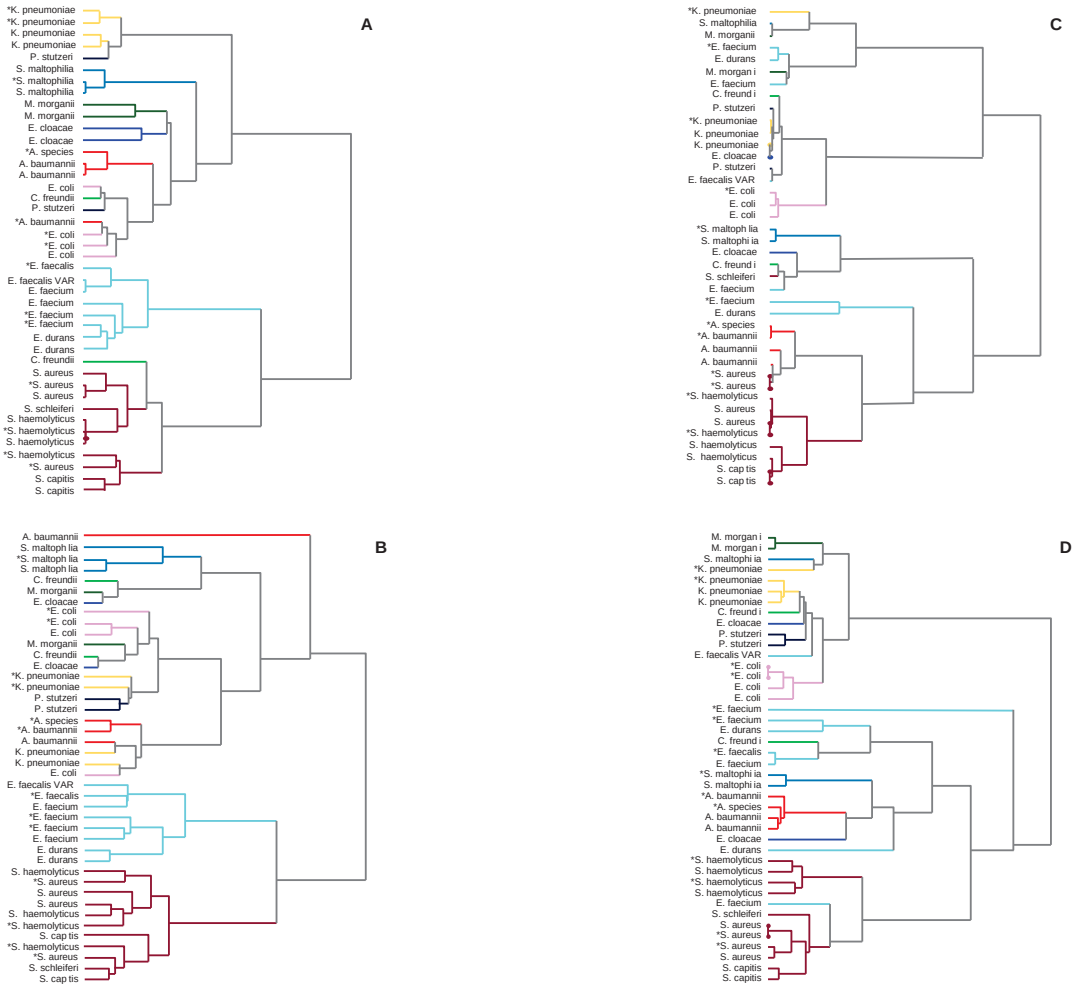

Figure 4. Hierarchical Clusters of Biochemical (A), Antimicrobial resistance (B), High Resolution Melt (C) and DNA sequencing (D) datasets of all bacterial isolates. Validation samples are marked with '*'.

In order to compare the performance of the Raman spectral hierarchical clustering to the hierarchical clustering of the other data types, external criteria of Rand index and purity were calculated using the *a priori* knowledge at the Gram and genus taxonomic levels for all hierarchical trees of the datasets. The Rand index is defined as the number of pairs of objects that are either in the same groups in both partitions or in different groups in both partitions, divided by the total number of pairs of objects [(34)]. Purity or 'cluster accuracy' is computed by assigning each cluster to the class which is the most frequent in the cluster and then taking the weighted sum of the number of correctly assigned documents in each cluster. In both Rand index and purity, bad clustering result in values close to 0 and perfect clustering gives a score of 1.

Given that we have several different types of datasets, it is expected that the resulting hierarchical trees will have variation in the structure of the resulting clusters. For this reason, the Rand index and purity values were calculated by using a widely known method described by Milligan and Cooper[(35)] called 'cutting the dendrogram'. In this method, the hierarchical tree is scanned to detect the level possessing the optimal recovery of the desired clusters. Each of the dendrograms displayed in Figures 3 and 4 were individually evaluated and a 'cutoff' point was determined to reveal the inherent groupings of the datasets at the different taxonomic levels. The Rand index and purity values for the various datasets are presented in Table 2.

		Rand Index			Purity		
		Gram +/-	Family	Genus	Gram +/-	Family	Genus
Raman Spectra	Gram -	0.952	0.668	0.881	0.976	0.87	0.869
	Gram +		0.933	0.933		0.947	0.947
Biochemistries		0.952	0.868	0.942	0.976	0.833	0.905
MIC and SIR		1.0	0.901	0.929	1.0	0.952	0.714
DNA Sequences		0.655	0.86	0.806	0.786	0.833	0.69
HRM		0.569	0.806	0.877	0.7	0.775	0.675

Table 2. Rand Index and Purity values of the five datatypes at gram, family and genus taxonomic levels.

The resulting Rand index and purity values of Raman spectra give comparable results with the other data types, particularly with biochemical data and antimicrobial resistance data at both the Gram and genus levels. In viewing the resulting dendrograms, Figure 3A shows the correct separation of the gram negative and gram positive isolates with the exception of one sample, giving a Rand index value of 0.952. Additionally, genus level clustering demonstrates accurate clustering of most isolates, as evidenced by high Rand indexes (0.881 for Gram negative species and 0.933 for Gram positive species). Based on these results, it is apparent that Raman spectroscopy has the ability to discriminate bacteria species with high specificity. Furthermore, classification accuracy values for the three PLSDA models generated from Raman spectra of the bacterial isolates were 88.1%, 66.68% and 90.48% for Gram status and genus (Gram negative and Gram positive, respectively).

4. DISCUSSION

After applying the validation set to our initial model formed by 28 samples, it became apparent that clustering on the gram level first was necessary before attempting to cluster by family or genus. Many studies have sought to cluster sets of closely-related bacterial strains and species. The clearest downside to such an approach is that in a clinical setting, there are countless possibilities for sources of bacterial infection. The most important questions to be answered are whether bacterial infection is present and which drugs should be administered to fight the infection. Knowing this, we can continue to create and improve our models by first starting with the broad question (Is there infection? Is this infection from a gram-positive or gram-negative bacteria?), and move towards more specific classifications (family, genus, species and strain). While such an approach will surely require developing and testing of multiple models, it may be the most practical technique to identifying bacterial infections outside of the lab and in a clinical setting.

As this study was preliminary in nature, there are many more methods to be explored and modifications to be made. For example, it is apparent that both the PLSDA and HCA models performed optimal at the gram level (Figure 3A) and genus level for the gram positive isolates (Figure 3 C). This could be due to the fact that there are 8 different genera modeled under the gram negative sub-group (Figure 3B), thereby making it more challenging for a higher model performance. This can be improved by enlarging our number of training and testing samples.

Many other data analysis approaches have been explored and found useful by researchers. In Rosch and Harz [36], 20 different strains of 9 gram-positive bacterial species typical of clean-room contaminants were successfully clustered using a SVM model (support vector machine). Rather than the traditional approach of training and testing a model, the SVM model automatically determined which peaks are relevant for discrimination between the spectra and a leave-one-out method was used to determine recognition rate for each strain and species. Such an approach could be useful in our case, given that our bacteria are highly diverse and it is difficult to determine which spectral regions are relevant for classification at the lower taxonomic levels. In addition, the fluorescence background that plagued many of the Raman spectra turned out to be useful. While several attempts were made to reduce fluorescence such as sample rinsing and photobleaching, the residual differences in the level of fluorescence between species may have contributed to better discrimination between bacterial isolates when applied to the models presented. In the future, other excitation wavelengths and methods for signal enhancement (surface enhanced Raman spectroscopy) will be used to determine if identification and classification of bacteria is possible in a complex biological milieu such as wound effluent.

5. CONCLUSIONS

Raman spectroscopy has proven to be a powerful tool for 'whole-organism' fingerprinting due to its ability to reveal both the chemical composition and structural formation of biological molecules [37]. By creating and validating PLSDA and HCA models using Raman spectroscopic data of a wide range of bacterial isolates, this study has demonstrated the capability of Raman spectroscopy in discriminating between bacterial isolates with high specificity. Moreover, the fact that the clustering of the Raman data was comparable to that of current bacterial identification tools such as antimicrobial susceptibility testing and biochemical testing, promotes the idea that this technology could be used to reliably identify bacterial isolates. Such a notion could revolutionize routine pathogenic identification approaches by providing a rapid and noninvasive method making Raman spectroscopy a powerful point-of-care tool in clinical settings.

6. ACKNOWLEDGEMENTS

The authors would like to thank LT Rebecca Pavlicek, Dr. Bradley Clay, Kristina Sault-Thomas and Rajiv Luthra for their contributions to this project. Bacterial isolates were provided by LT Rebecca Pavlicek and Dr. Bradley Clay. BD Phoenix™ data was collected by Kristina Sault-Thomas and Rajiv Luthra.

This work was prepared as part of the authors' official duties. Title 17 U.S.C. §105 provides that 'Copyright protection under this title is not available for any work of the United States Government.' Title 17 U.S.C. §101 defines a U.S. Government work as a work prepared by a military service member or employee of the U.S. Government as part of that person's official duties. The views expressed in this article are those of the author and do not necessarily reflect the official policy or position of the Department of the Navy, Department of Defense, nor the U.S. Government. This effort was supported (in part) by the U.S. Navy Bureau of Medicine and Surgery under the Medical Development Program and Office of Naval Research work unit number (602115HP.3720.001.A1015), USAMRMC Military Medical Research and Development award OR090136, as well as by The Geneva Foundation, funding number HU0001-10-1-0003. This study was performed under MUA 228 with the Walter Reed Army Institute of Research. I/We certify that all individuals who qualify as authors have been listed; each has participated in the conception and design of this work, the analysis of data (when applicable), the writing of the document, and the approval of the submission of this version; that the document represents valid work; that if we used information derived from another source, we obtained all necessary approvals to use it and made appropriate acknowledgements in the document; and that each takes public responsibility for it.

7. REFERENCES

1. C. K. Murray, M. K. Hinkle and H. C. Yun, "History of infections associated with combat-related injuries," *J Trauma* 64(3 Suppl), S221-231 (2008)
2. D. R. Hospenthal and H. K. Crouch, "Infection control challenges in deployed US military treatment facilities," *J Trauma* 66(4 Suppl), S120-128 (2009)
3. H. Wills, R. Kast, C. Stewart, R. Rabah, A. Pandya, J. Poulik, G. Auner and M. D. Klein, "Raman spectroscopy detects and distinguishes neuroblastoma and related tissues in fresh and (banked) frozen specimens," *J Pediatr Surg* 44(2), 386-391 (2009)
4. T. J. Harvey, E. C. Faria, A. Henderson, E. Gazi, A. D. Ward, N. W. Clarke, M. D. Brown, R. D. Snook and P. Gardner, "Spectral discrimination of live prostate and bladder cancer cell lines using Raman optical tweezers," *J Biomed Opt* 13(6), 064004 (2008)
5. P. O. Andrade, R. A. Bitar, K. Yassoyama, H. Martinho, A. M. Santo, P. M. Bruno and A. A. Martin, "Study of normal colorectal tissue by FT-Raman spectroscopy," *Anal Bioanal Chem* 387(5), 1643-1648 (2007)
6. H. P. Buschman, G. Deinum, J. T. Motz, M. Fitzmaurice, J. R. Kramer, A. van der Laarse, A. V. Bruschke and M. S. Feld, "Raman microspectroscopy of human coronary atherosclerosis: biochemical assessment of cellular and extracellular morphologic structures in situ," *Cardiovascular Pathology* 10(69-82 (2001)
7. A. Carden, R. M. Rajachar, M. D. Morris and D. H. Kohn, "Ultrastructural changes accompanying the mechanical deformation of bone tissue: a Raman imaging study," *Calcified Tissue International* 72(166-175 (2003)
8. K. L. Chan, G. Zhang, M. Tomic-Canic, O. Stojadinovic, B. Lee, C. R. Flach and R. Mendelsohn, "A Coordinated Approach to Cutaneous Wound Healing: Vibrational Microscopy and Molecular Biology," *J Cell Mol Med* (2008)
9. M. V. Chowdary, K. K. Kumar, K. Thakur, A. Anand, J. Kurien, C. M. Krishna and S. Mathew, "Discrimination of normal and malignant mucosal tissues of the colon by Raman spectroscopy," *Photomed Laser Surg* 25(4), 269-274 (2007)
10. N. J. Crane, V. Popescu, M. D. Morris, P. Steenhuis and M. A. Ignelzi Jr., "Raman spectroscopic evidence for octacalcium phosphate and other transient mineral species deposited during intramembraneous mineralization," *Bone* 39(434-442 (2006)
11. A. S. Haka, Z. Volynskaya, J. A. Gardecki, J. Nazemi, J. Lyons, D. Hicks, M. Fitzmaurice, R. R. Dasari, J. P. Crowe and M. S. Feld, "In vivo margin assessment during partial mastectomy breast surgery using raman spectroscopy," *Cancer Res* 66(6), 3317-3322 (2006)
12. P. R. Jess, D. D. Smith, M. Mazilu, K. Dholakia, A. C. Riches and C. S. Herrington, "Early detection of cervical neoplasia by Raman spectroscopy," *Int J Cancer* 121(12), 2723-2728 (2007)
13. S. Koljenovic, T. C. Schut, R. Wolthuis, A. J. Vincent, G. Hendriks-Hagevi, L. Santos, J. M. Kros and G. J. Puppels, "Raman spectroscopic characterization of porcine brain tissue using a single fiber-optic probe," *Anal Chem* 79(2), 557-564 (2007)
14. G. Leroy, G. Penel, N. Leroy and E. Brès, "Human tooth ename: a Raman polarized approach," *Applied Spectroscopy* 56(8), 1030-1034 (2002)
15. N. McGill, P. A. Dieppe, M. Bowden, D. J. Gardiner and M. Hall, "Identification of pathological mineral deposits by Raman microscopy," *The Lancet* 337(77-78 (1991)
16. A. Robichaux-Viehoever, E. Kanter, H. Shappell, D. Billheimer, H. Jones, 3rd and A. Mahadevan-Jansen, "Characterization of Raman spectra measured in vivo for the detection of cervical dysplasia," *Appl Spectrosc* 61(9), 986-993 (2007)
17. G. Shetty, C. Kendall, N. Shepherd, N. Stone and H. Barr, "Raman spectroscopy: elucidation of biochemical changes in carcinogenesis of oesophagus," *Br J Cancer* 94(10), 1460-1464 (2006)
18. M. G. Shim, B. C. Wilson, E. Marple and M. Wach, "Study of fiber-optic orobes for *in vivo* medical Raman spectroscopy," *Applied Spectroscopy* 53(6), 619-627 (1999)

19. T. D. Wang and J. Van Dam, "Optical biopsy: a new frontier in endoscopic detection and diagnosis," *Clin Gastroenterol Hepatol* 2(9), 744-753 (2004)
20. P. C. Buijtels, H. F. Willemse-Erix, P. L. Petit, H. P. Endtz, G. J. Puppels, H. A. Verbrugh, A. van Belkum, D. van Soolingen and K. Maquelin, "Rapid identification of mycobacteria by Raman spectroscopy," *J Clin Microbiol* 46(3), 961-965 (2008)
21. M. F. Escoriza, J. M. VanBriesen, S. Stewart, J. Maier and P. J. Treado, "Raman spectroscopy and chemical imaging for quantification of filtered waterborne bacteria," *J Microbiol Methods* 66(1), 63-72 (2006)
22. K. Maquelin, C. Kirschner, L. P. Choo-Smith, N. van den Braak, H. P. Endtz, D. Naumann and G. J. Puppels, "Identification of medically relevant microorganisms by vibrational spectroscopy," *J Microbiol Methods* 51(3), 255-271 (2002)
23. Q. Wu, W. H. Nelson, S. Elliot, J. F. Sperry, M. Feld, R. Dasari and R. Manoharan, "Intensities of E. coli nucleic acid Raman spectra excited selectively from whole cells with 251-nm light," *Anal Chem* 72(13), 2981-2986 (2000)
24. L. Zeiri, B. V. Bronk, Y. Shabtai, J. Eichler and S. Efrima, "Surface-enhanced Raman spectroscopy as a tool for probing specific biochemical components in bacteria," *Appl Spectrosc* 58(1), 33-40 (2004)
25. K. Maquelin, L. Dijkshoorn, T. J. van der Reijden and G. J. Puppels, "Rapid epidemiological analysis of Acinetobacter strains by Raman spectroscopy," *J Microbiol Methods* 64(1), 126-131 (2006)
26. K. Maquelin, L. P. Choo-Smith, T. van Vreeswijk, H. P. Endtz, B. Smith, R. Bennett, H. A. Bruining and G. J. Puppels, "Raman spectroscopic method for identification of clinically relevant microorganisms growing on solid culture medium," *Anal Chem* 72(1), 12-19 (2000)
27. K. S. Kalasinsky, T. Hadfield, A. A. Shea, V. F. Kalasinsky, M. P. Nelson, J. Neiss, A. J. Drauch, G. S. Vanni and P. J. Treado, "Raman chemical imaging spectroscopy reagentless detection and identification of pathogens: signature development and evaluation," *Anal Chem* 79(7), 2658-2673 (2007)
28. L. Zeiri, B. V. Bronk, Y. Shabtai, J. Czege and S. Efrima, "Silver metal induced surface enhanced Raman of bacteria," *Colloids and Surfaces A: Physicochemical and Engineering Aspects* 208(357-362 (2002)
29. G. Funke and P. Funke-Kissling, "Use of the BD PHOENIX automated identification and susceptibility testing positive blood cultures in a microbiology system for direct of gram-negative rods from three-phase trial," *J Clin Microbiol* 42(4), 1466-1470 (2004)
30. J. M. Andrews, "Determination of minimum inhibitory concentrations," *J Antimicrob Chemoth* 48(5-16 (2001)
31. "PLSDA," Eigenvector Research Inc, Eigenvector Documentation Wiki (2014).
32. J. S. N. K. M. Pierce, R. E. Synovec "Data Analysis Methods," in *Gas Chromatography* C. F. Poole, Ed., pp. 415-434, Elsevier Inc., 225 Wyman Street, Waltham, MA 02451, USA (2012).
33. A. Dereeper, V. Guignon, G. Blanc, S. Audic, S. Buffet, F. Chevenet, J. F. Dufayard, S. Guindon, V. Lefort, M. Lescot, J. M. Claverie and O. Gascuel, "Phylogeny.fr: robust phylogenetic analysis for the non-specialist," *Nucleic Acids Res* 36(W465-W469 (2008)
34. K. Y. Yeung, M. Medvedovic and R. E. Bumgarner, "Clustering gene-expression data with repeated measurements," *Genome Biol* 4(5), (2003)
35. G. W. Milligan and M. C. Cooper, "A Study of the Comparability of External Criteria for Hierarchical Cluster-Analysis," *Multivar Behav Res* 21(4), 441-458 (1986)
36. P. Rosch, M. Harz, M. Schmitt, K. D. Peschke, O. Ronneberger, H. Burkhardt, H. W. Motzkus, M. Lankers, S. Hofer, H. Thiele and J. Popp, "Chemotaxonomic identification of single bacteria by micro-Raman spectroscopy: Application to clean-room-relevant biological contaminations," *Appl Environ Microb* 71(3), 1626-1637 (2005)

37. E. Kastanos, Kyriakides, A., Hadjigeorgiou, K., and Pitris, C., "A Novel Method for Bacterial UTI Diagnosis Using Raman Spectroscopy," *International Journal of Spectroscopy* 2012(13 (2012)

Raman spectroscopy of non-penetrating peripheral nerve damage in swine: a tool for spectral pathology of nerves

Katherine E. Cilwa[*a,e], Tiffani Slaughter[b], Eric A. Elster[b,c], Jonathan A. Forsberg[a,b,d], Nicole J. Crane[a,b,e]

[a]Regenerative Medicine Department, Naval Medical Research Center, 503 Robert Grant Avenue, Silver Spring, MD, USA 20910; [b]Uniformed Services University of the Health Sciences, 4301 Jones Bridge Road, Bethesda, MD, USA, 20814; [c]Department of Surgery, Walter Reed National Military Medical Center, 8901 Rockville Pike, Bethesda, MD, USA 20889; [d]Department of Orthopaedic Oncology, Walter Reed National Military Medical Center, 8901 Rockville Pike, Bethesda, MD, USA 20889; [e]Henry M. Jackson Foundation for the Advancement of Military Medicine, 6720-A Rockledge Drive, Bethesda, MD, USA 20817

ABSTRACT

Over 30% of combat injuries involve peripheral nerve injury [1] compared to only 3% in civilian trauma [2]. In fact, nerve dysfunction is the second leading cause of long-term disability in injured service members [3] and is present in 37% of upper limb injuries with disability [4]. Identification and assessment of non-penetrating nerve injury in trauma patients could improve outcome and aid in therapeutic monitoring. We report the use of Raman spectroscopy as a non-invasive, non-destructive method for detection of nerve degeneration in intact nerves due to non-penetrating trauma. Nerve trauma was induced via compression and ischemia/reperfusion injury using a combat relevant swine tourniquet model (>3 hours ischemia). Control animals did not undergo compression/ischemia. Seven days post-operatively, sciatic and femoral nerves were harvested and fixed in formalin. Raman spectra of intact, peripheral nerves were collected using a fiber-optic probe with 3 mm diameter spot size and 785 nm excitation. Data was preprocessed, including fluorescence background subtraction, and Raman spectroscopic metrics were determined using custom peak fitting MATLAB® scripts. The abilities of bivariate and multivariate analysis methods to predict tissue state based on Raman spectroscopic metrics are compared. Injured nerves exhibited changes in Raman metrics indicative of 45% decreased myelin content and structural damage ($p<<0.01$). Axonal and myelin degeneration, cell death and digestion, and inflammation of nerve tissue samples were confirmed via histology. This study demonstrates the non-invasive ability of Raman spectroscopy to detect nerve degeneration associated with non-penetrating injury, relevant to neurapraxic and axonotmetic injuries; future experiments will further explore the clinical utility of Raman spectroscopy to recognize neural injury.

Keywords: Raman spectroscopy, Nerve, Ischemia/Reperfusion Injury, War Wounds, Trauma, Extremity Wounds

1. INTRODUCTION

Nerve injury is a serious consequence of both civilian and military trauma. Historically, war time injuries have served as the predominant clinical informant of nerve injury and repair. A survey of 5000 civilian traumas found only 3% involved peripheral nerve injury [2]. This is in stark contrast to modern combat-related injuries, which are most frequently due to high energy insults and characterized by multi-zonal, severe tissue damage to all types of tissue. A survey of US combat injuries sustained in a nine month period of Operation Desert Shield and Desert Storm indicated nerve injury accompanied 30% of limb traumas [1]. In a cohort of 450 medically retired, wounded soldiers (injured between October 2001 and January 2005) loss of nerve function was the second leading cause of disability both in frequency and impact severity [3]; and 37% of upper limb injuries within this cohort exhibited nerve dysfunction [4]. Within open tibial fractures resulting from conflicts occurring between 2003 and 2007, 22% involved nerve injury [5]. Most recently, the 2013 Extremity War Injury Symposium named major peripheral nerve injury as one of the greatest current challenges to surgical management of upper extremity war injuries [6]. Not only do peripheral nerve injuries lead in frequency within combat wounded service members, extremity wounds total nearly two-thirds of initial hospitalization and approximate disability costs [7]. Excision of non-viable tissue and repair are paramount to proper treatment, recovery, and reduction in disability. Therefore, the identification, localization, and prognostication of peripheral nerve injury are necessary to

both improve patient outcomes, quality of life, and potential for return to active duty or occupational responsibilities. In addition, these advancements would serve to reduce medical and support costs of combat casualties and civilian traumas.

Nerve dysfunction may be identified via physical exam and patient reported alteration in sensory and or motor function or by electromyography and nerve conduction studies prior to surgery if injury severity allows. However, superimposed traumatic brain injuries and other central nervous system trauma cloud recognition of peripheral nerve injury as the source of altered function; and electromyography and conduction studies merely illustrate dysfunction somewhere between the brain and nerve innervating the muscles tested. Both methods provide limited information on the location of and source of dysfunction. Localization of nerve damage is conventionally made during surgery and relies upon some visual cue of abnormal tissue. The decision to excise and undergo reconstruction or graft, or simply wait and observe, depends heavily upon the experience of the surgeon. Peripheral nerve injury may be classified using either Seddon [8] or Sunderland [9] systems, based upon the increasing level of connective tissue disruption and concomitant, decreasing outcome. Such systems provide guidance as to the necessary level of surgical intervention but rely on a system of description that requires information not readily available without time consuming and destructive, histopathological examination. Non-penetrating nerve injury ruptures and scars tissue beneath the external epineurium and may not be visible. Without removal or treatment, patients are at risk of continued motor and sensory loss, abnormal function, muscle atrophy, and neuroma formation. Retention of healthy tissue and nerve length are important factors in repairing penetrating nerve injury to preserve and restore function. Removal of damaged nerve at the borders of penetrating nerve trauma is also vital for reinnervation and avoidance of scar tissue and neuroma formation. Without a real-time, objective metric of nerve tissue injury, clinical treatment is limited. Raman spectroscopy is a non-destructive, noninvasive optical technique that can provide detailed compositional information about tissue, both *ex vivo* and *in vivo* [10-15]. Raman spectroscopy has the potential to guide surgical decision making to excise or not to excise tissue at all levels of nerve tissue disruption. It may also be combined with other biomarkers to build risk assessment models. Previous Raman studies of peripheral nerve tissue have examined only normal sectioned tissue [16, 17], sectioned tissue with minor ligation injury [18], or the histomorphometry of intact, non-injured tissue [19] all via microscopy. We present the first report to detect nerve damage in intact peripheral nerves using a Raman fiber-optic probe and tourniquet induced injury, with potential for translation as a hand-held tool to aid in surgical decision making.

2. METHODOLOGY

2.1 Nerve Injury Model

In an IRB approved protocol (USUHS protocol 11-SUR-816; NMRC protocol 11-OUMD-13), ten adolescent female swine (*sus scrofa*) were anesthetized and randomized to sham (n=5) and 4.7 hour tourniquet (n=5) experiment arms. Tourniquetion was accomplished via pneumatic tourniquet inflated to 250mm Hg placed on the proximal left lower extremity. The sham study group had catheters placed but no induced ischemia by tourniquet application. Following ischemia, the limb was allowed to reperfuse for 30 minutes after which animals were awoken from anesthesia and observed for a period of seven days, prior to euthanasia. At one week post procedure, animals were euthanized and sciatic and femoral nerves harvested and formalin fixed. (Sham: 5 Sciatic and 3 Femoral, Tourniquet: 5 Sciatic and 1 Femoral).

2.2 Raman Spectroscopy of Nerves

Fingerprint Region (600-1800 cm^{-1}): Nerve samples were examined *ex vivo* via Raman Spectroscopy using a Kaiser Rxn1 PhAT probe 785 nm system (Kaiser Optical Systems, Inc., Ann Arbor, MI, USA) with 3 mm diameter excitation spot size. Dark subtracted and intensity-corrected spectra were acquired at four locations within each intact nerve using 5 second acquisitions and 20 accumulations each (Figure 1A). Preprocessing of spectra was conducted using in-house MATLAB® scripts. Spectra were truncated to 600-1800 cm^{-1} and baseline subtracted using a fourth-order polynomial fitting routine described in Cao and Freeman [20]. Finally, spectra were intensity normalized to the phenylalanine band at 1004 cm^{-1}. Following preprocessing, spectra were curve fit using mixed Gaussian and Lorentzian functions of known Raman spectral bands based on the algorithms of GRAMS/AI software fitting features (Thermo Fisher Scientific, Madison, WI, USA). Raman spectral band assignments of nerve tissue are found in Table 1. An example of peak fitting of nerve tissue spectra is shown in Figure 1B. Band area ratios (BARs) were calculated using curve fit derived band areas of peaks of interest. BARs calculated include sphingomyelin content [(719+760)/1004 cm^{-1}]; cholesterol content

[(608+700)/1004 cm^{-1}]; lipid/protein content (1439/1455 cm^{-1}); protein-lipid disorder, or PLD (1240/1270 cm^{-1}), a measure of β-sheet and disordered protein over α-helix, ordered protein and lipids; protein disorder I (1240/1455 cm^{-1}), a measure of β-sheet and disordered protein over total protein; and protein disorder II (1240/1340 cm^{-1}), a measure of β-sheet and disordered protein over total protein.

Table 1. Raman spectral band assignments of nerve tissue [21], [22].

ν (cm^{-1})	Band Assignment	Component
608	OH out of plane bend	Cholesterol
702		Cholesterol
719	$N^+(CH_3)_3$ symmetric stretch	Choline
760	OPO diester sym. str.	Phosphocholine
1004	CC aromatic ring stretch	Phenylalanine
1240	Amide III β-sheet/ disordered	β-sheet, disordered protein
1270	Amide III α-helix, C=C stretch	ordered protein, lipid
1298	CH_2 twist	Fatty acid, protein
1340	γ(CH2, CH3) wag	Protein
1439	CH_2 deformation	Fatty acid, cholesterol, protein
2850	CH_2 symmetric stretch	Fatty acid, protein
2930	CH_3 symmetric stretch	Protein, fatty acid

C-H Stretch Region (2700-3100 cm^{-1}): Nerve samples were examined *ex vivo* via Raman Spectroscopy using a Perkin Elmer RamanStation 400F, which utilizes 785 nm laser excitation and 100 micron diameter excitation spot. Dark subtracted and intensity-corrected spectra were acquired at eight locations within each intact nerve using 10 second acquisitions and 20 accumulations each. Spectra were truncated to 2700-3100 cm^{-1}. Spectra were curve fit using mixed Gaussian and Lorentzian bands using GRAMS/AI software fitting features (Thermo Fisher Scientific, Madison, WI, USA). BARs calculated include symmetric CH_2/CH_3 stretches (2850/2930 cm^{-1}) indicative of lipid/protein content and myelination [16].

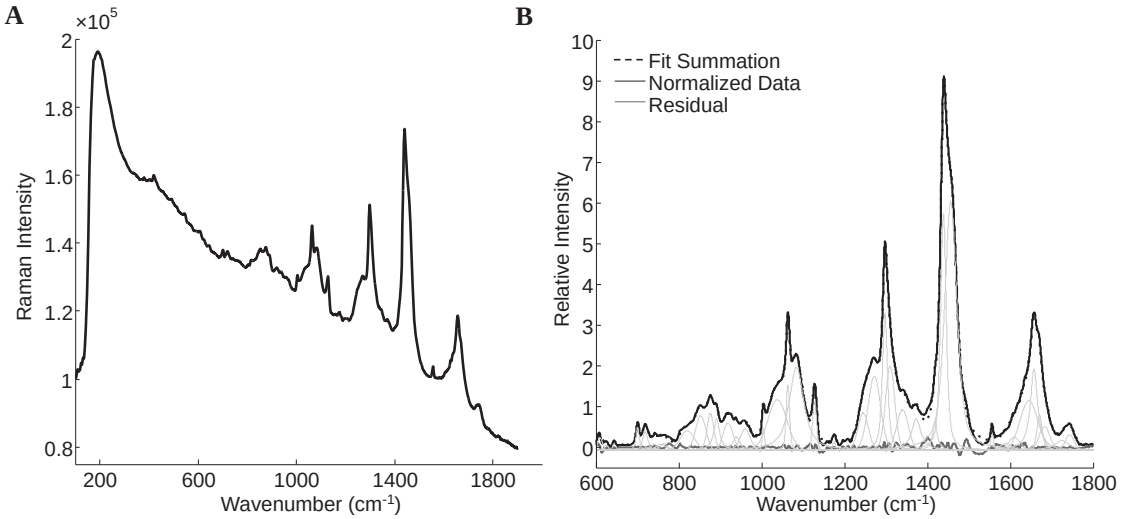

Figure 1. A) Raw Raman spectrum of porcine, peripheral nerve tissue using hand-held fiber-optic probe B) Mixed Gaussian and Lorentzian peak fitting.

2.3 Tissue Histology

Following Raman collection, nerve samples were paraffin embedded and H&E sections and Luxol blue/Cresyl violet sections stained. Under 100× magnification, H&E and Luxol blue/Cresyl violet stained sections were examined by a veterinary pathologist and given a histological score. Histological scoring assessed the levels of degeneration, infiltrate, and hemorrhage in each tissue section of nerve. Signs of degeneration include the presence of axonal swelling, dilated

myelin sheaths, cellular debris, macrophages, and digestion chambers. Infiltrate is characterized as the presence of lymphocytes and plasma cells indicate hemorrhage. Separate scores were assigned for degeneration, infiltrate, and hemorrhage using the following system: NSF: No significant findings, 1. Minimal: < 5%, 2. Slight: 5-25%, 3. Moderate: 25-50%, 4. Marked: 50-75%, and 5. Severe: > 75% of the nerve affected. Degeneration, infiltrate, and hemorrhage scores were added together to obtain an overall combined histological score of nerve damage for each nerve.

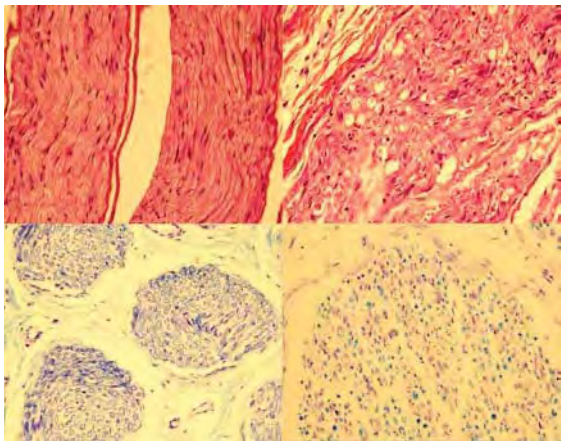

Figure 2: H&E (top) and Luxol Blue/Cresyl Violet (bottom) stained histological section of sham (left) and tourniqueted nerves (right), 20x magnification.

2.4 Statistical Analysis

Raman metrics between sham and tourniquet samples were compared using a two-tailed Student's t-test; *p*-values less than 0.05 are considered statistically significant. Scatter plot comparison of univariate metrics was examined for differences across treatment groups. Correlation of each Raman metric with combined histological scores of nerve damage was determined by calculating Pearson's correlation coefficients. Principal component analysis (PCA) of raw Raman spectral data between 600-1800 cm^{-1} was executed using PLS Toolbox (Eigenvector Research, Inc., Seattle, WA, USA) with automatic Whittaker filter baselining, band area normalization, and mean centering preprocessing prior to model building. Outliers outside of the 95% confidence interval were identified by a Hotelling/T^2 plot and removed.

3. RESULTS

Histological findings both confirmed and characterized Wallerian degeneration in tourniquet treated animals. Swollen axons and dilated myelin sheaths, digestion chambers containing macrophages and cellular debris, and increased lymphplasmacytic infiltrate were evident in longitudinal sections of H&E stained peripheral nerve tissue from tourniquet animals (Figure 2, top right) when compared to sham (Figure 2, top left). Luxol blue and Creysl violet stained, transverse nerve sections of tourniquet samples (Figure 2, bottom right) reveal reduced myelin and increased nuclei content indicative of degeneration and infiltration when compared to sham (Figure 2, bottom left). Combined histological scores of nerve damage indicated slight to moderate damage according to cellular findings with some variation in the level of damage produced by tourniquet injury. Visual and histological inspection verified that the injuries examined were non-penetrating, as indicated by the preservation of external epineurium layers and disruption of internal epineurium and endoneurium layers (characteristic of neurapraxic and axonotmetic, non-penetrating injuries).

Raman metrics in the fingerprint region (Figure 3) showed significantly decreased sphingomyelin ([(719+760)/1004 cm^{-1}], *p=0.004*), cholesterol ([(608+700)/1004 cm^{-1}], *p=0.005*), and overall lipid content (1439/1455 cm^{-1}, *p=0.02*); and significantly increased PLD (1240/1270 cm^{-1}, *p=0.007*), protein disorder I (1240/1455 cm^{-1}, *p=0.001*), and protein disorder II (1240/1340 cm^{-1}, *p=0.001*) in tourniquet treated samples indicative of demyelination and nerve fibrosis. Raman spectra obtained in the C-H stretching region (2700-3100 cm^{-1}) are shown in Figure 4A. CH_2/CH_3 stretches (2850/2930 cm^{-1}, *p=0.00002*) were significantly decreased in tourniquet treated samples (Figure 4A, inset) indicative of decreased lipid/protein content and demyelination.

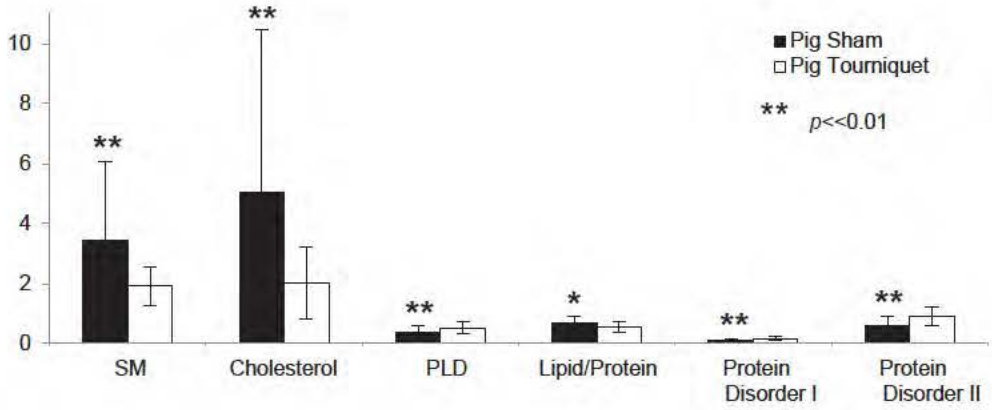

Figure 3. Mean Raman metrics of sham and tourniqueted nerves exhibit distinct differences. Sphingomyelin (SM), Protein-Lipid Disorder (PLD).

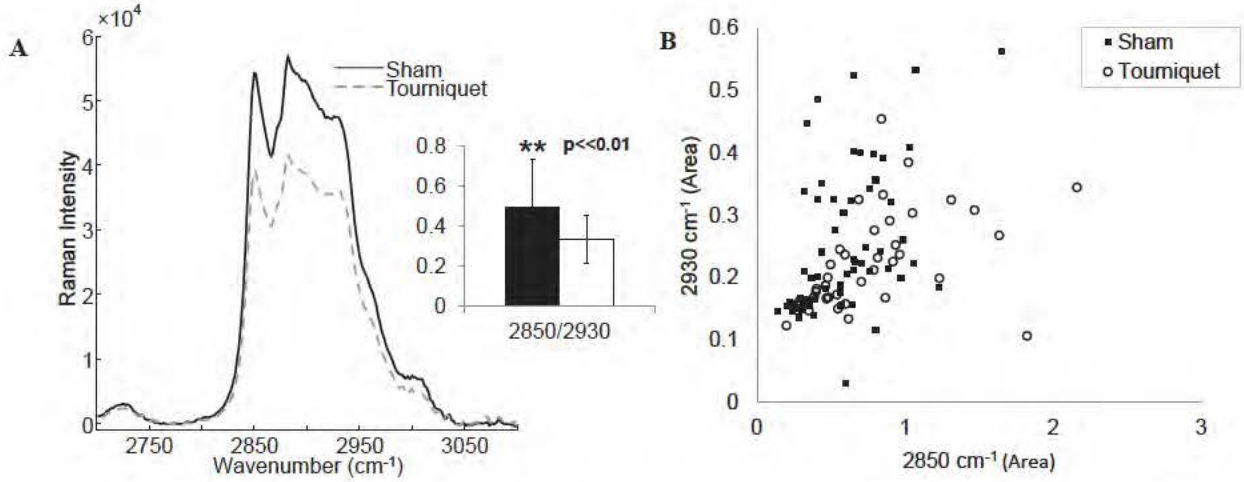

Figure 4. A) Mean nerve spectra, C-H stretch region. Lipid/protein or symmetric CH_2/CH_3 stretches, sham (black) and tourniqueted samples (white) (inset). B) Scatter plot of C-H stretch Raman band areas.

Bivariate scatter plotting of Raman metrics and multivariate methods of Raman BARs were examined to determine suitable metrics for distinguishing between injured and non-injured nerves. These groups are not distinguishable in the scatter plot of C-H stretch region band areas (Figure 4B) which describes demyelination alone. A scatter plot of protein lipid disorder (1240/1270 cm^{-1}) vs. protein disorder II (1240/1340 cm^{-1}) demonstrate the potential to distinguish tissue type (sham and tourniqueted peripheral nerve) using fingerprint region Raman band area ratios representative of lipid/myelin loss and structural damage (Figure 5A). PCA of the raw fingerprint region spectra resulted in three principal components with >99.9% variation explained by PC 1 and PC 2. PCA analysis shows less separation between sham and tourniqueted nerves (scores, Figure 5B) than with bivariate analysis.

Correlation of Raman metrics with combined histology scores was not significantly high, however analysis revealed higher correlation for fingerprint region Raman metrics than more commonly reported C-H region metrics (fingerprint region metrics: 0.6 Pearson's correlation coefficient, C-H stretch region metrics: 0.4 Pearson's correlation coefficients). This suggests that Raman fiber-optic probes, most commonly sold with gratings only out to 1800 cm^{-1} may perform better at differentiating damaged nerve than commercial Raman microscopes due possibly to both larger tissue volume sampled and more sensitive metrics using fingerprint region Raman fiber-probes.

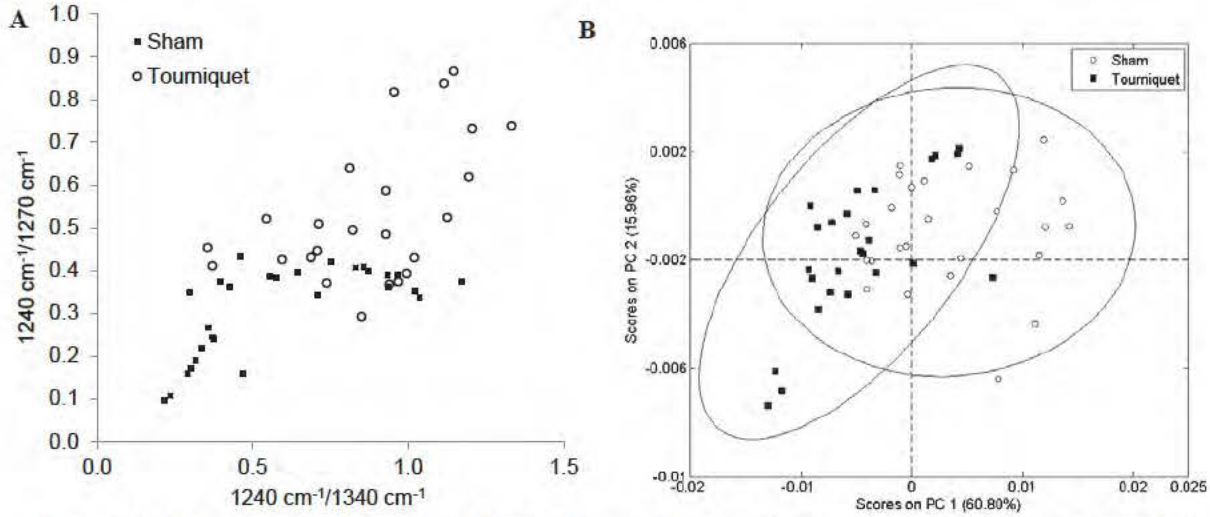

Figure 5. A) Scatter plot of PLD and protein disorder II Raman BARs and B) Principal component analysis of nerve injury Raman data.

4. DISCUSSION

Nerve injury involves an initial phase of cell death at and around the injury site due to mechanical trauma triggering cellular and excitatory molecular infiltration. Damage progresses by scar tissue formation around the lesion and distal demyelination and continued necrosis. In this study, we report changes in fingerprint region of Raman spectra indicative of demyelination and structural damage in peripheral nerves, damaged by tourniquet application. Significant decreases in the Raman spectral band areas of choline and phosphocholine bands [(719+760)/1004 cm^{-1}], free form and cholesterol ester band areas [(608+700)/1004 cm^{-1}], and lipid band areas are evidence of myelin loss. Minamikawa et al. first associated changes in 2850/2930 cm^{-1} CH_2/CH_3 stretches with myelination in efforts to distinguish between healthy myelinated and unmyelinated peripheral nerves using Raman microscopy with visible light excitation but reported no differences between the types of nerve in the fingerprint region [16]. Morisaki et al. examined sciatic rat nerves injured by short term ligation also using visible light excitation Raman microscopy and similarly noted a decrease in the CH_2/CH_3 stretch band ratio as a metric of myelination; these changes were then correlated to a decrease in myelin/axon turnover using immunohistochemical staining for myelin basic protein and NF200 [18]. Saxena et al., using Raman spectroscopy with near infrared excitation to examine both hemisected and contused rat spinal cord, demonstrated significant decreases in band areas in the fingerprint region of the Raman spectrum, attributed to cholesterol and lipid [23]. To the authors' knowledge, results herein are the first report of changes in the fingerprint region of the Raman spectrum that can be associated with myelin loss in peripheral nerve injury. A significant decrease in the 2850/2930 cm^{-1} metric herein corroborates changes in fingerprint metrics with previous literature measures of demyelination. Additionally, we report changes in Raman spectral bands indicative of the relative disorder of protein within nerve tissue: significantly increased PLD (1240/1270 cm^{-1}), protein disorder I (1240/1455 cm^{-1}), and protein disorder II (1240/1340 cm^{-1}) metrics were observed. An increase in these BARs may also be described as a decrease in α–helix content relative to total protein and may be markers of axonal death, structural damage, and nerve fibrosis; and are particularly important when examining intact nerve in a clinical setting as outcome is not determined solely by *initial* myelin loss following trauma. Previously mentioned studies examined sectioned nerve fibers via Raman microscopy without examining the surrounding layers of connective tissue. Real-time monitoring of nerve health within the surgical suite requires the ability to assess whole nerve health to determine patient risk. Fiber-optic probes with millimeter scale excitation spot sizes and penetration depths, low laser light exposure, and sensitivity of near-infrared excitation are more practical within a clinical setting than visible excitation and microscopy techniques, which have been previously used [16-19], and have the potential to provide real-time optical biopsies.

The qualitative changes Raman spectroscopy demonstrates in nerve tissue composition following injury illustrate the utility of Raman as vital tool in basic research. For translation into a clinical tool, Raman spectroscopy may be used alone to decipher between healthy and injured tissue and subsequently combined with other objective biomarkers to

determine outcome and assess risk. A scatter plot of PLD (1240/1270 cm^{-1}) vs. protein disorder II (1240/1340 cm^{-1}) demonstrates the potential to distinguish tissue type (sham and tourniqueted peripheral nerve) using fingerprint region Raman band area ratios representative of lipid/myelin loss and structural damage. Bivariate analysis of C-H stretch band areas, indicative of myelin loss alone, are not suitable for identifying traumatically injured, peripheral nerves. Multivariate analysis is currently en vogue, yet powerful when applied appropriately. It often more accurately identifies variables that separate groups than simple univariate or bivariate analyses in which the importance of variables are pre-selected based on descriptive metrics such as BARs. This is particularly true as the complexity of the data increases. Raman data contain a large number of variables (~4,000 Raman shift data per spectrum), therefore, there is potential for multivariate spectroscopic analysis to be more sensitive than univariate/bivariate methods even with a small sample size. We employed PCA as a conservative method for identifying injury groupings in our data. PCA corroborates the bivariate simplicity of the data with >99.9% variance explained by the first two components; but shows less separation between sham and tourniqueted nerve types compared to bivariate scatter plots of fingerprint region Raman metrics. PCA and other complex analyses of variance are often overused in pilot studies with small sample sizes without examination of simpler analytical techniques or the use of conceptually based metrics. Multivariate analysis of peripheral nerve spectral data may perform better than results shown herein in a larger data set by increasing sample size or when combined with non-spectroscopic data. However, the performance of bivariate description of data should not be overlooked. Multivariate methods may not be advantageous or Raman metrics (instead of raw spectra) may perform better in a larger model. Decreased complexity of analytical methods and data processing reduces computational time between spectral collection and tissue categorization, and the use of pre-selected Raman BARs may aid in standardization of analysis for clinical use.

5. CONCLUSIONS

Injured nerves exhibited changes in Raman metrics ($p<<0.01$) indicative of: decreased sphingomyelin, cholesterol, and lipid content; and increased protein disorder. Axonal and myelin degeneration, cell death and digestion, cellular infiltration, hemorrhage, and inflammation of tourniqueted samples were confirmed via histology. Raman spectroscopy using fiber-optic probes with near infrared excitation detects myelin degeneration and structural damage within intact nerves. Scatter plot comparison of Raman metrics indicative of both lipid/myelin loss and protein disorder demonstrates the potential for identification and isolation of injured peripheral nerve tissue in a more robust and simplified manner than PCA multivariate analysis or than when using C-H stretch region myelination metrics. Raman spectral BARs in the fingerprint region may also correlate with histological markers of nerve injury better than Raman spectral BARs in the C-H stretching region. Additionally, fingerprint region differences between injured and non-injured nerves may not be easily detectible using visible light excitation. This study is limited by the number of samples and serves as a demonstration of the potential and non-invasive ability of Raman spectroscopic fiber-optic probes with near infrared excitation to detect nerve damage associated with non-penetrating injury relevant to neurapraxic and axonotmetic injuries in peripheral nerve tissue and the importance of whole-tissue measurements for clinical use. The use of histological scoring in future studies would be aided by the incorporation of fibrosis measures into the combined scoring system used within this study. In the future, Raman data may be combined with other biomarkers indicative of nerve injury and outcome for prediction of risk stratification in the clinic in a larger scale study.

ACKNOWLEDGMENTS

The authors would like to thank Major Leonora Dickson, the consulting veterinary pathologist at the Walter Reed Army Institute of Research. The views expressed in this presentation are those of the authors and do not necessarily reflect the official policy or position of the Department of the Navy, the Department of Defense, nor the U.S. Government. This work was supported/funded by work unit number 602115HP.3720.001.A1015. Funding Support includes USAMRMC Military Medical Research and Development award OR090136. The study protocol (11-SUR-816; 11-OUMD-13) was reviewed and approved by the Uniformed Services University of Health Sciences and by the Walter Reed Army Institute of Research's/Naval Medical Research Center's Institutional Animal Care and Use Committees in compliance with all applicable Federal regulations governing the protection of animals in research. We are military service members or employees of the U.S. Government. This work was prepared as part of our official duties. Title 17 U.S.C. 105 provides the "Copyright protection under this title is not available for any work of the United States Government." Title 17 U.S.C. 101 defines a U.S. Government work as a work prepared by a military service member or employee of the U.S. Government as part of that person's official duties. We certify that the document represents valid work; that if we used

information derived from another source, we obtained all necessary approvals to use it and made appropriate acknowledgements in the document; and we take public responsibility for it.

REFERENCES

[1] M. O. Hansen, D. W. Polly, K. A. McHale *et al.*, "A prospective evaluation of orthopedic patients evacuated from Operations Desert Shield and Desert Storm: the Walter Reed experience," Mil Med, 159(5), 376-80 (1994).

[2] J. Noble, C. A. Munro, V. S. Prasad *et al.*, "Analysis of upper and lower extremity peripheral nerve injuries in a population of patients with multiple injuries," J Trauma, 45(1), 116-22 (1998).

[3] J. D. Cross, J. R. Ficke, J. R. Hsu *et al.*, "Battlefield orthopaedic injuries cause the majority of long-term disabilities," J Am Acad Orthop Surg, 19 Suppl 1, S1-7 (2011).

[4] J. C. Rivera, G. P. Glebus, and M. S. Cho, "Disability following combat-sustained nerve injury of the upper limb," Bone Joint J, 96-b(2), 254-8 (2014).

[5] M. J. Beltran, T. C. Burns, T. T. Eckel *et al.*, "Fate of combat nerve injury," J Orthop Trauma, 26(11), e198-203 (2012).

[6] R. C. Andersen, J. C. D'Alleyrand, M. F. Swiontkowski *et al.*, "Extremity War Injuries VIII: sequelae of combat injuries," J Am Acad Orthop Surg, 22(1), 57-62 (2014).

[7] B. D. Masini, S. M. Waterman, J. C. Wenke *et al.*, "Resource utilization and disability outcome assessment of combat casualties from Operation Iraqi Freedom and Operation Enduring Freedom," J Orthop Trauma, 23(4), 261-6 (2009).

[8] S. H. Seddon, [Surgical Disorders of the Peripheral Nerves] Churchill Livingstone, (1975).

[9] S. Sunderland, [Nerves and Nerve Injuries] Churchill Livingstone, (1978).

[10] S. Wachsmann-Hogiu, T. Weeks, and T. Huser, "Chemical analysis in vivo and in vitro by Raman spectroscopy--from single cells to humans," Curr Opin Biotechnol, 20(1), 63-73 (2009).

[11] D. I. Ellis, and R. Goodacre, "Metabolic fingerprinting in disease diagnosis: biomedical applications of infrared and Raman spectroscopy," Analyst, 131(8), 875-85 (2006).

[12] M. Diem, M. Romeo, S. Boydston-White *et al.*, "A decade of vibrational micro-spectroscopy of human cells and tissue (1994-2004)," Analyst, 129(10), 880-5 (2004).

[13] L. P. Choo-Smith, H. G. Edwards, H. P. Endtz *et al.*, "Medical applications of Raman spectroscopy: from proof of principle to clinical implementation," Biopolymers, 67(1), 1-9 (2002).

[14] K. Esmonde-White, "Raman Spectroscopy of Soft Musculoskeletal Tissues," (2014).

[15] M. D. Morris, and G. S. Mandair, "Raman assessment of bone quality," Clin Orthop Relat Res, 469(8), 2160-9 (2011).

[16] T. Minamikawa, Y. Harada, N. Koizumi *et al.*, "Label-free detection of peripheral nerve tissues against adjacent tissues by spontaneous Raman microspectroscopy," Histochem Cell Biol, 139(1), 181-93 (2013).

[17] H. Wang, F. Ma, F. Wang *et al.*, "Identification of motor and sensory fascicles in peripheral nerve trunk using immunohistochemistry and micro-Raman spectroscopy," J Trauma, 71(5), 1246-51 (2011).

[18] S. Morisaki, C. Ota, K.-i. Matsuda *et al.*, "Application of Raman spectroscopy for visualizing biochemical changes during peripheral nerve injury in vitro and in vivo," Journal of Biomedical Optics, 18(11), 116011-116011 (2013).

[19] T. B. Huff, and J. X. Cheng, "In vivo coherent anti-Stokes Raman scattering imaging of sciatic nerve tissue," J Microsc, 225(Pt 2), 175-82 (2007).

[20] A. Cao, A. K. Pandya, G. K. Serhatkulu *et al.*, "A robust method for automated background subtraction of tissue fluorescence," Jornal of Raman Spectroscopy, 38, 1199-1205 (2007).

[21] C. Krafft, L. Neudert, T. Simat *et al.*, "Near infrared Raman spectra of human brain lipids," Spectrochim Acta A Mol Biomol Spectrosc, 61(7), 1529-35 (2005).

[22] R. C. Spiker, Jr., and I. W. Levin, "Raman spectra and vibrational assignments for dipalmitoyl phosphatidylcholine and structurally related molecules," Biochim Biophys Acta, 388(3), 361-73 (1975).

[23] T. Saxena, B. Deng, D. Stelzner *et al.*, "Raman spectroscopic investigation of spinal cord injury in a rat model," J Biomed Opt, 16(2), 027003 (2011).

The Spectroscopist: An Unexpected Journey

Nicole Crane, Ph.D.

Advanced Surgical Imaging Program
Department of Regenerative Medicine
Naval Medical Research Center
Silver Spring, MD

Department of Surgery
Uniformed Services University of Health Sciences
Bethesda, MD

Career Path

Lucent Technologies
Bell Labs Innovations

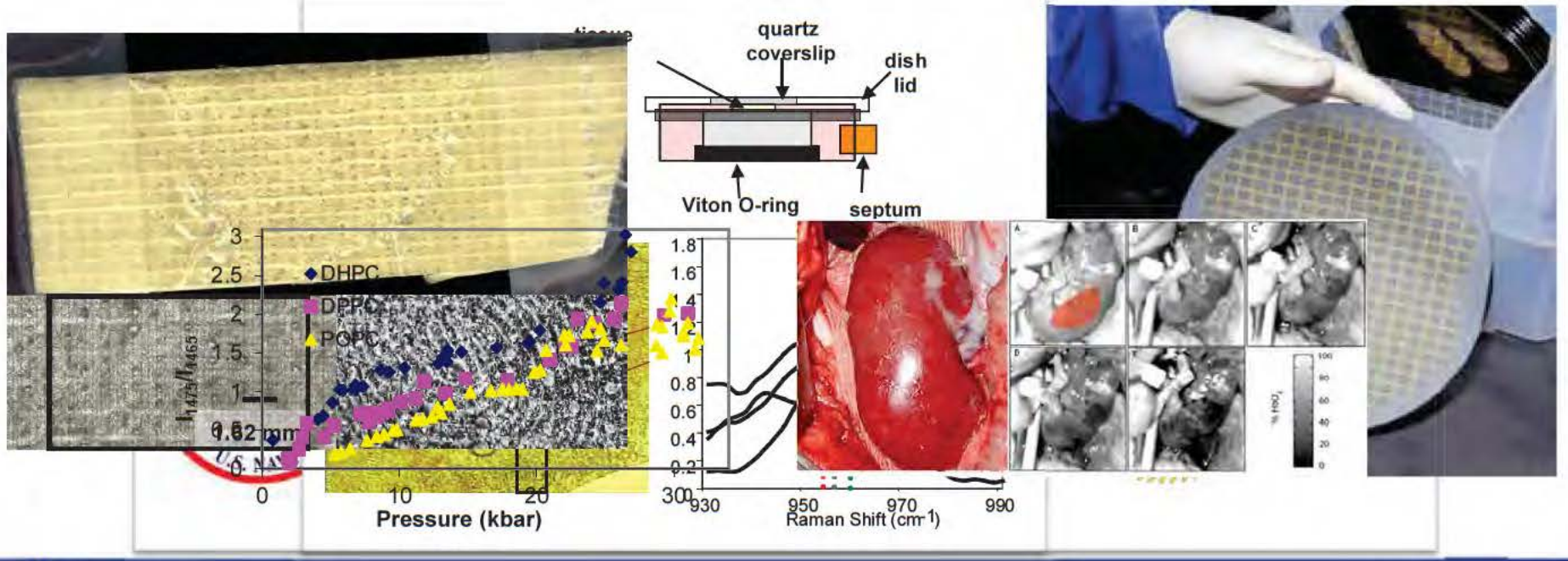

REGMED

Military Medicine - NMRC

Our team leverages real-world experience in combat casualty care: heterotopic ossification, wound healing, advanced surgical imaging, transplant tolerance, and stem cells.

In addition, we develop novel and dynamic bioinformatic approaches to deliver point-of-care personalized medicine.

- *3-CCD Imaging*
- *IR Imaging*
- *Raman Spectroscopy*

Technologies that can non-invasively and objectively assess the wound microenvironment are critical for understanding and evaluating the wound healing process.

Accurate assessment of extremity injuries and wounds is necessary for appropriate treatment in the operating room.

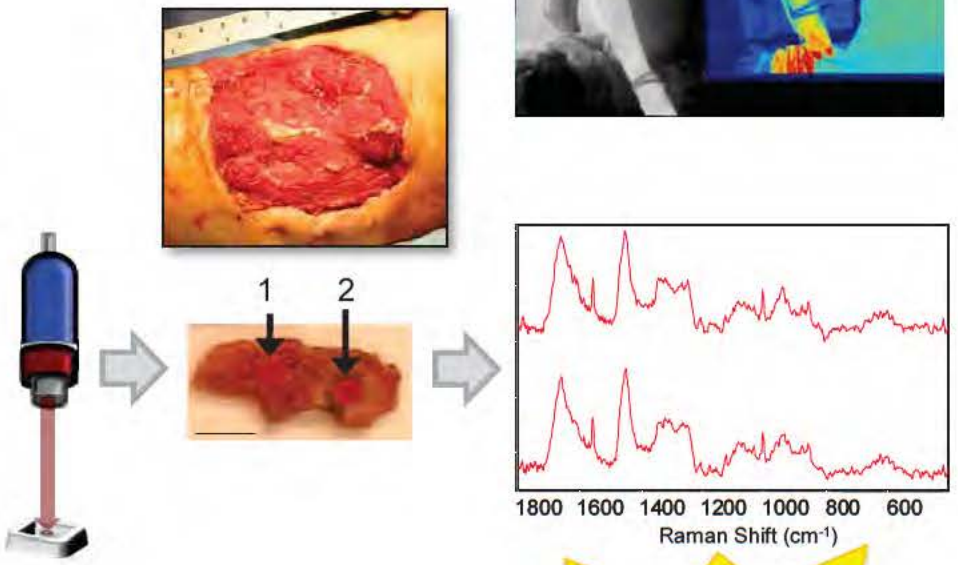

Wound Repair Regen. 2010 Jul-Aug;18(4):409-16.
J Urol. 2010 Oct;184(4):1279-85.
J Bone Joint Surg Am. 2010 Dec;92 Suppl 2:74-89.
J Pediatr Surg. 2012 Jan;47(1):142-7.
J Biomed Opt. 2012 Jan;17(1):010902.
Bone. 2013 Sep 5;57(2):335-342.

Graphic pictures next slide!

Acute Combat Wounds

Modern war ballistics inflict devastating extremity injuries, violating soft tissue, bone, and neurovascular structures.

Complex war wounds require aggressive surgical care. Serial debridements are performed to remove devitalized tissue and decrease bacterial load.

High-pressure irrigation and vacuum-assisted closure device (VAC) application have improved wound management.

The ensuing inflammatory response ultimately dictates the pace of wound healing and tissue regeneration.

Despite these technological advances, the basic surgical decision regarding appropriate timing of war wound closure remains subjective, and some wounds dehisce.

REGMED

Current Treatment and Challenges

Surgical debridements are performed every 2-3 days to remove devitalized tissue and reduce the bacterial load.

- Negative pressure wound therapy (NPWT) is applied between debridements - promote wound closure.

Wound assessment involves: patient's general condition, injury location, adequacy of perfusion, and gross appearance of the wound.

Our goal is to **monitor wound healing *in vivo***, i.e. monitor wound healing during surgical debridements.

- *Is it the best time to close the wound?*
- *Is the wound developing HO?*
- *Is the wound infected? With what?*

Develop an **objective and predictive model for wound healing**.

Raman Spectroscopy

Raman Spectroscopy

Raman spectroscopy can be utilized non-invasively and provide real-time feedback.

Raman spectra of biological materials are not affected by spectral interference of water.

Raman spectroscopy is sensitive to both organic and inorganic components.

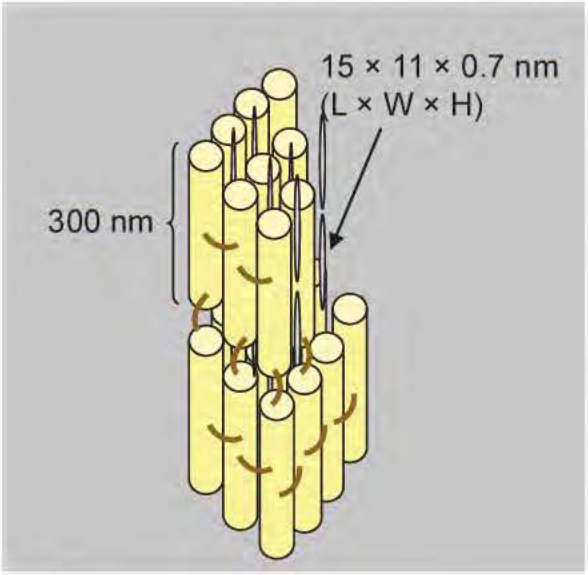

Bone is 35% organic material and 65% inorganic material.

For organic material: 90% of organic material is type I collagen, 10% noncollagenous proteins.

For inorganic material: commonly assumed to be some form of hydroxyapatite - $Ca_{10}(PO_4)_2(OH)_6$ but more closely resembles a B-type carbonated apatite $Ca_{8.3}\square_{1.7}(PO_4)_{4.3}(CO_3)_1(HPO_4)_{0.7}(OH)_{0.3}$.

Raman Fiber Probe Data Collection

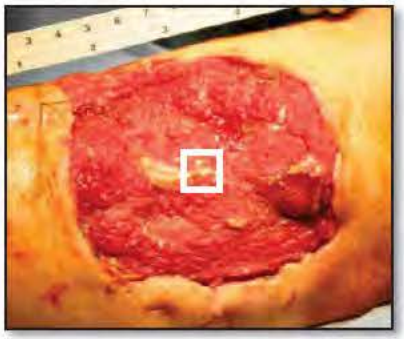

Approximately 1 cm^2 tissue biopsy is excised from the center of the wound bed.

Tissue is fixed in 10% neutral buffered formalin for storage.

Prior to spectral acquisition, samples are rinsed in 0.9% NaCl saline solution.

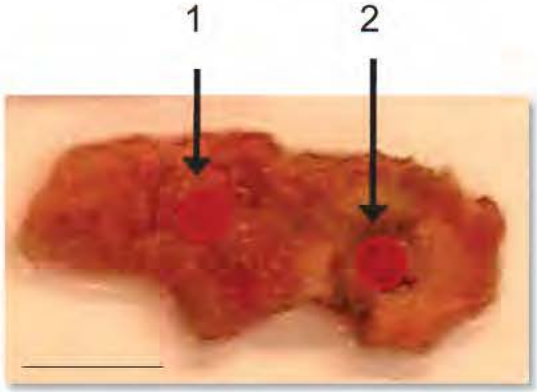

Examine multiple spots across the tissue.

14 accumulations, 5s spectrum
7 accumulations, 10s spectrum

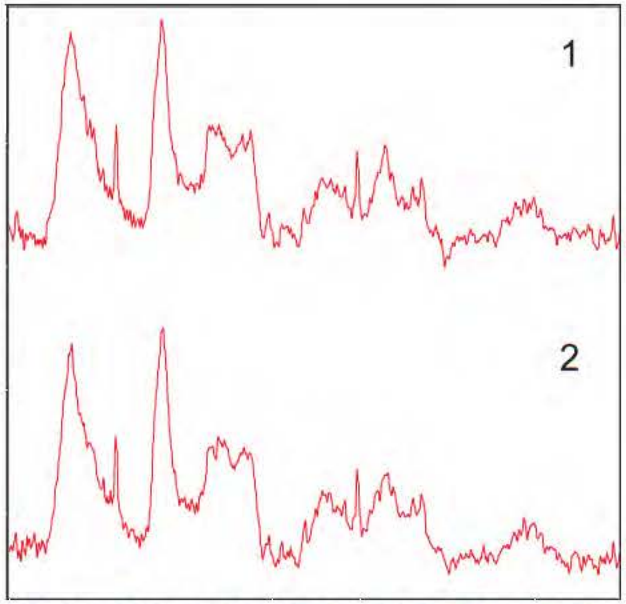

REGMED

Peakfitting for Spectral Deconvolution

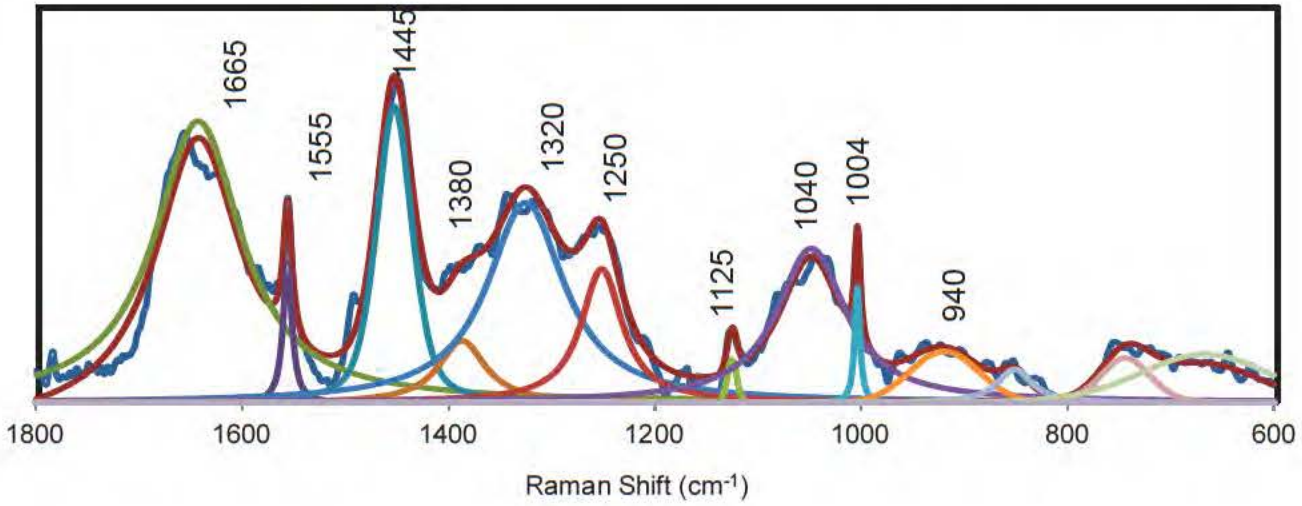

Raman Shift (cm^{-1})	Vibrational Band Assignment	Component
860	ν(C-C)	nucleic acids
920,940	ν(C-N), ν(C-C)	nucleic acids, keratin
1004	ν(C-C) ring	phenylalanine
1040	ν(C-C) skeletal	nucleic acids, protein
1125	ν(C-C), ν(C-N)	nucleic acids, protein
1250	ν (C-N) and δ(N-H); Amide III	protein
1320	$\delta(CH_2)$ twisting	nucleic acids, protein
1445	$\delta(CH_3)$ and $\delta(CH_{2})$ scissoring	protein
1555		aromatic amino acids, heme
1665	ν(C=O); Amide I	protein

REGMED

Heterotopic Ossification

Heterotopic Ossification (HO)

Heterotopic ossification (HO) refers to the aberrant formation of mature, lamellar bone in non-osseous tissues.

Currently, orthopaedic surgeons faced with treating mature, refractory, symptomatic HO are left with few options other than operative excision.

Potter et al. J Bone Joint Surg Am. 2007;89:476-486.

Following most civilian trauma, HO formation is relatively rare in the absence of head injury. Even following traumatic brain or spinal cord injury, it develops in only 20% and 11% of patients. Rates of HO formation exceed 50% only in the setting of femoral shaft fractures with concomitant head injury and severe burns.

Potter et al. J Bone Joint Surg Am. 2010; 92, Suppl2: 74-89.

USA Today, February 12, 2006.

ORTHOPEDICS 2008;31(12):1237.

UPOJ 1998;11:59-66.

REGMED

What is needed is a technology can risk stratify the development of HO and identify tissue that *may* become HO – Raman spectroscopy.

Muscle Histopathology

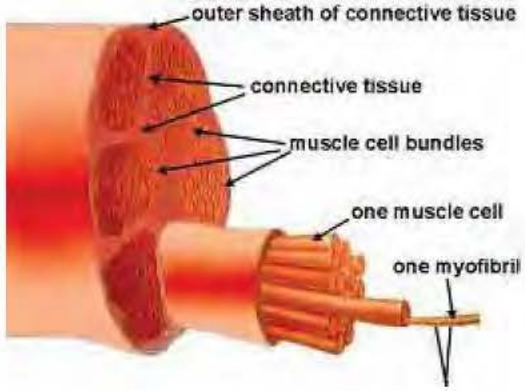

Myofibrils are composed of actin and myosin filaments and form muscle cells. Muscle cells are myofibers and bundle to form fascicles, which form muscle.

Normal muscle myofibers are relatively uniform.

Injured muscle myofibers are surrounded by fibrous connective tissue.

Closer examination demonstrates inflammation (evidenced by lymphocytes), myofiber degradation, necrosis, and hemorrhage in injured muscle tissue.

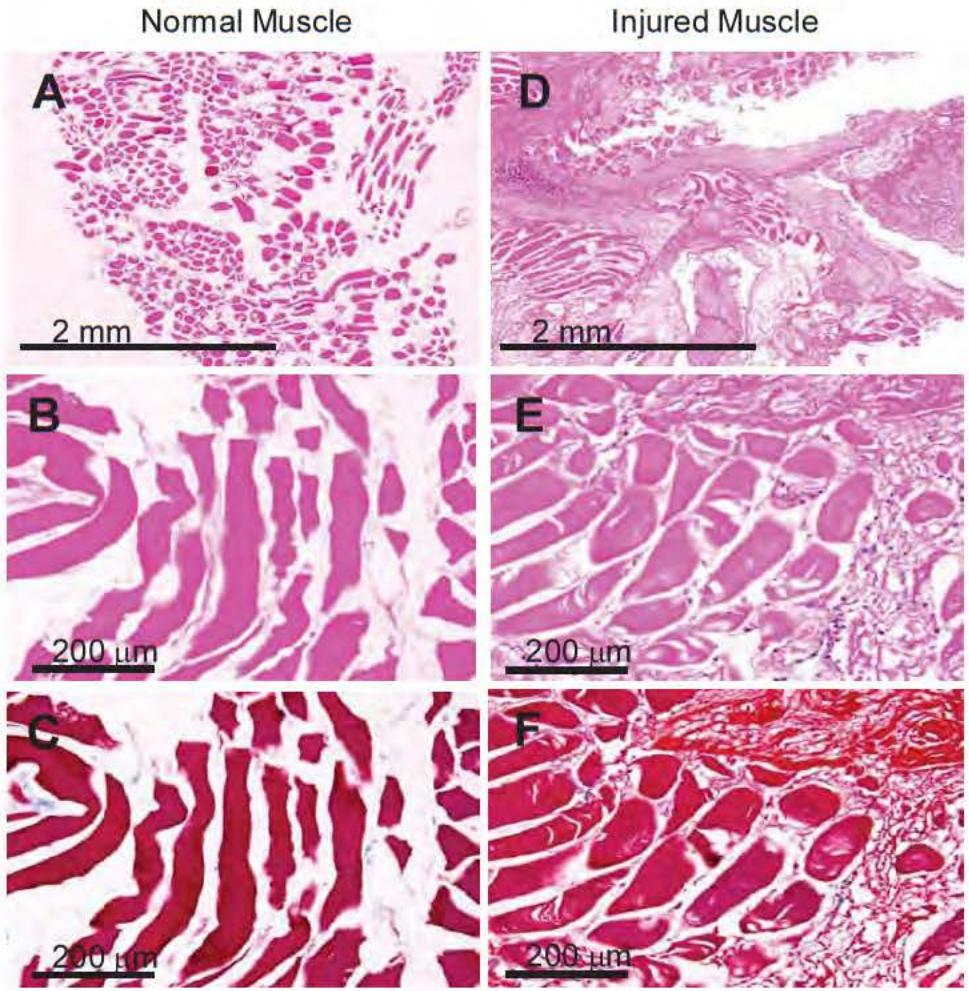

http://www.tutorvista.com/content/biology/biology-iii/animal-histology/muscular-tissue.php

HO Osteoid Histopathology

Osteoid is the unmineralized, organic portion of the bone matrix that forms prior to the maturation of bone. Bone forming cells, or osteoblasts, begin the process of forming bone tissue by secreting osteoid. When the osteoid becomes mineralized, it and adjacent osteoblasts develop into new bone tissue.

Immature osteoid (early HO) on H&E stained slides appears more eosinophilic than mature bone and only stains blue with Masson's trichrome.

As the osteoid matures (mature HO), Masson's trichrome reveals osteoid that stains both blue and red.

Von Kossa staining corroborates these results by demonstrating a greater degree of mineralization (darker stain) in the mature osteoid.

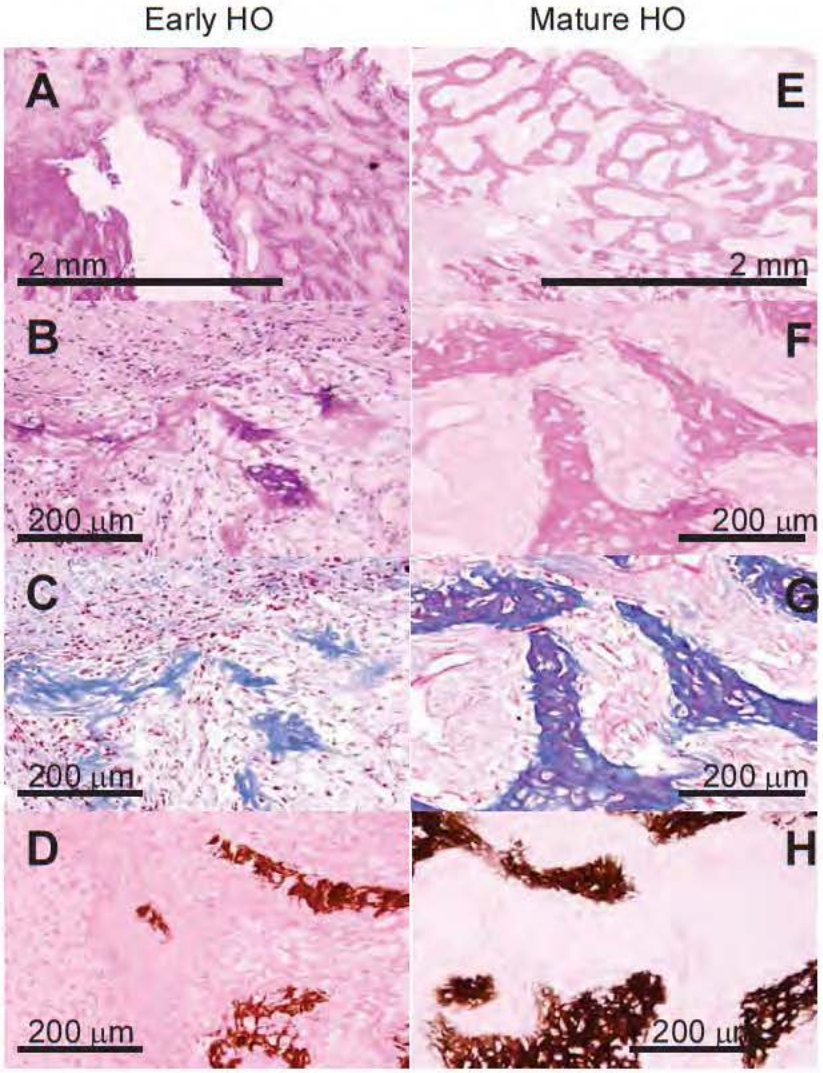

Heterotopic Ossification Histopathology

In this particular patient, the HO developed directly adjacent to the femur, beneath a skin grafted area which had been treated with INTEGRA® bioartificial dermal replacement (Integra Life Sciences; Plainsboro, NJ) application pre-skin graft.

The HO lesion was excised over 160 days post-injury, after ulcerating and becoming persistently symptomatic.

Mature HO demonstrates cortical and trabecular bone – osteons with clear and organized cement lines, Haversian canals, and bone marrow elements.

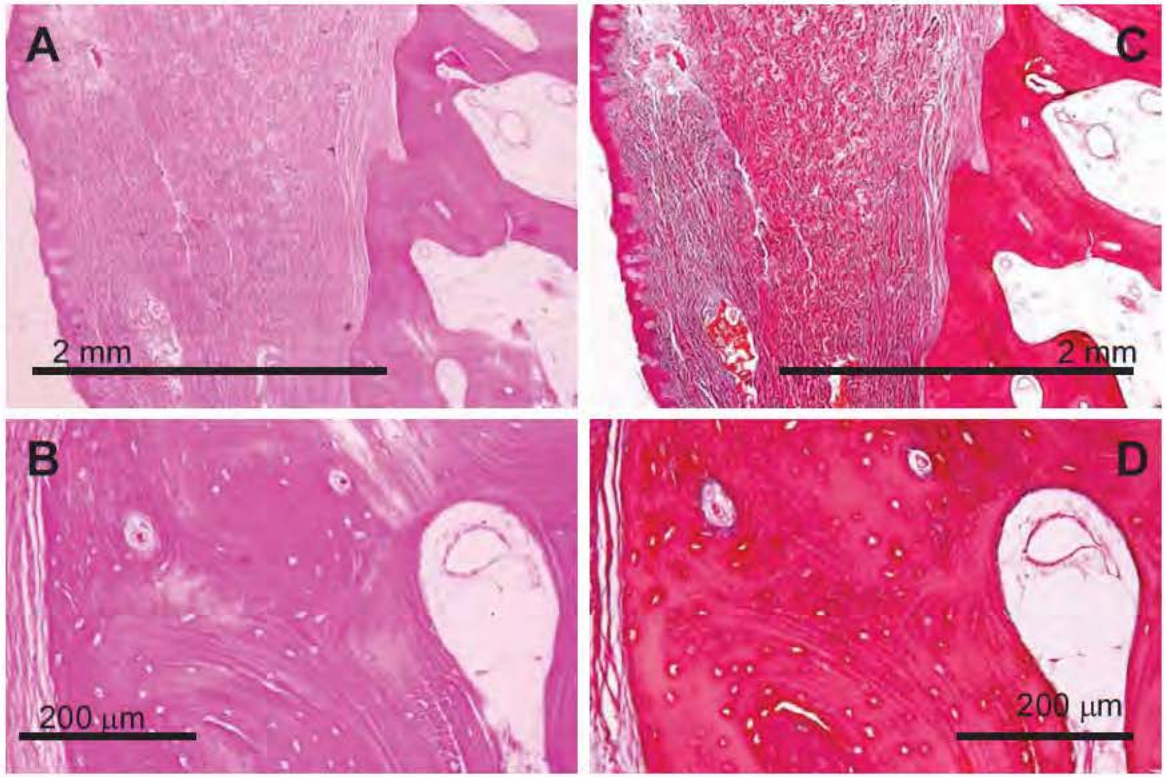

Comparison of Histology for Patients with and without HO

H&E stained slides made from wound biopsies from10 combat wounded patients were graded by a pathologist for : regeneration, degeneration (muscle atrophy), acute inflammation (presence of neutrophils), chronic inflammation (presence of lymphocytes and macrophages), necrosis, and hemorrhage.

Additionally, slides were evaluated for presence of nerve bundles (S-100) and brown fat (UCP-1).

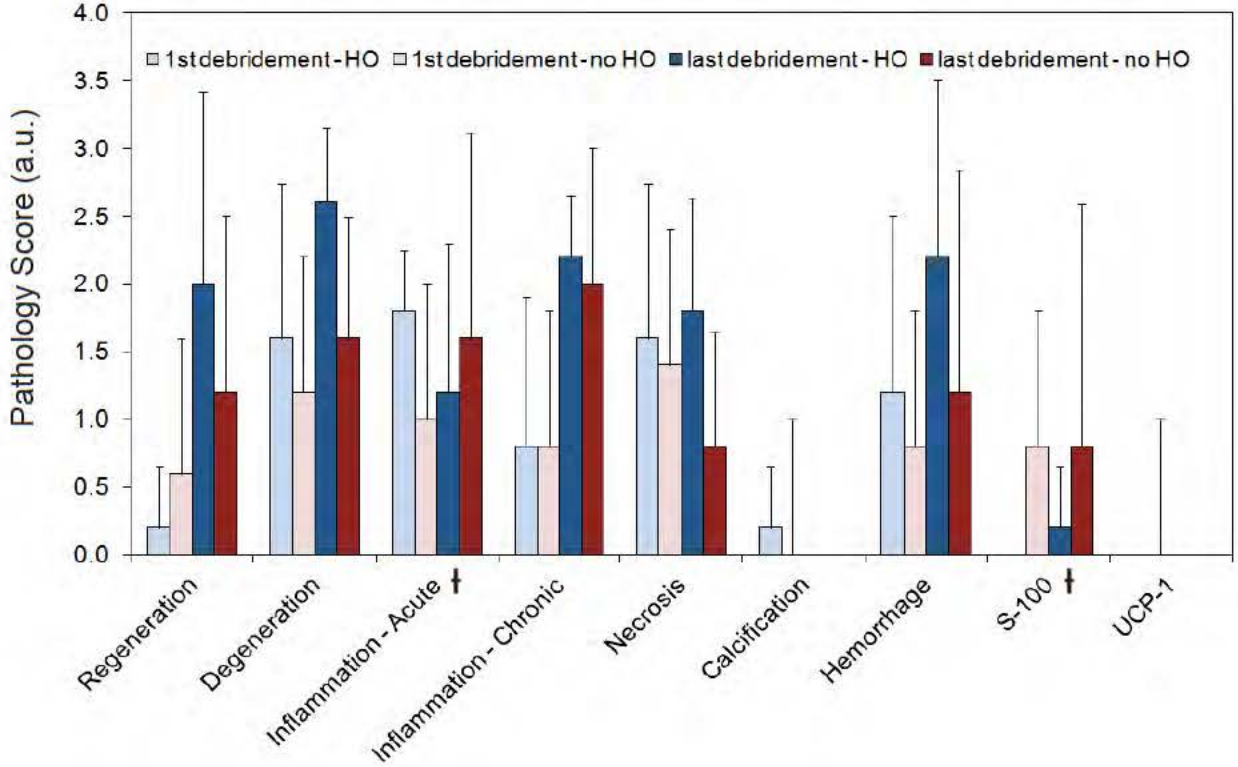

Scoring used to grade tissue sections:

0 – not present

1 – mild (present in 1-25% of tissue)

2 - moderate (present in 26-75% of tissue)

3 – severe (present in 76-100% of tissue)

REGMED

Osteogenic Gene Expression Correlates with Development of HO

Biopsy specimens from 54 high-energy penetrating extremity wounds obtained at the initial and final surgical debridements were evaluated. The levels of selected osteogenic-related gene transcripts from RNA extracts were assessed by quantitative reverse transcriptase-polymerase chain reaction (RT-PCR) analysis.

Gene	Initial debridement			Final debridement		
	Fold change (normalized to GAPDH)	95% CI	p-value	Fold change (normalized to GAPDH)	95% CI	p-value
ALPL	4.1	3.5–4.8	***0.006***	6.2	5.7–6.8	0.054
BMP-2	4.8	4.3–5.4	***0.001***	8.2	7.7–8.8	***0.001***
BMP-3	2.1	1.6–2.5	0.060	2.9	2.4–3.3	0.083
COL2A1	4.7	4.2–5.3	***0.001***	8.4	8.1–8.9	***0.004***
COL10A1	4.3	3.6–5.0	***0.001***	8.5	7.8–9.1	***0.001***
COL11A1	6	5.1–6.8	***0.006***	10.8	9.2–10.4	***0.010***
COMP	4.2	3.8–4.6	***0.020***	7.9	7.3–8.4	***0.032***
CSF2	4.8	4.2–5.3	***0.003***	8.7	8.2–9.5	***0.003***
CSF3	5.8	5.2–6.3	***0.012***	9.2	8.5–9.9	***0.024***
MMP8	5.8	5.4–6.5	***0.001***	9.3	8.7–9.6	***0.001***
MMP9	4.5	4.1–5.1	***0.014***	9.1	8.8–9.5	***0.030***
SMAD1	4.4	3.9–5.2	***0.024***	8.1	7.5–9.0	***0.028***
VEGF-A	4.2	3.6–4.8	***0.017***	8.3	7.8–8.9	***0.001***

As a result of its key role in osteogenesis, the concentration of BMP-2 in the effluent of 29 wounds also was determined.

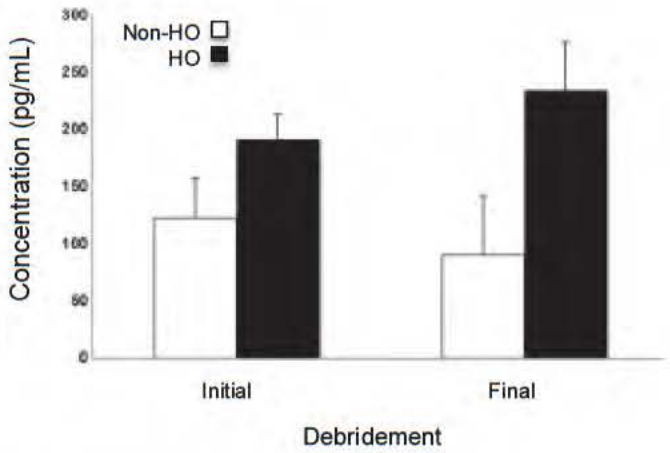

The expression of transcripts necessary for synthesis of cartilaginous matrix (COL2A1, COL10A1, COL11A1, COMP) and tissue remodeling (MMP8, MMP9) were upregulated in wounds in which HO developed.

Raman Spectroscopic Pilot Study of HO

HO/Raman Spectroscopy Pilot Study

Tissue biopsies, approximately 1cm^3, were obtained during surgical procedures and immediately snap frozen.

Normal Muscle (n=10)	Injured Muscle (n=10)	Early HO (n=10)	Mature HO (n=10)	Normal Bone (n=4)

Samples were thawed no more than 15 minutes unfixed and were immediately refrozen after spectral collection.

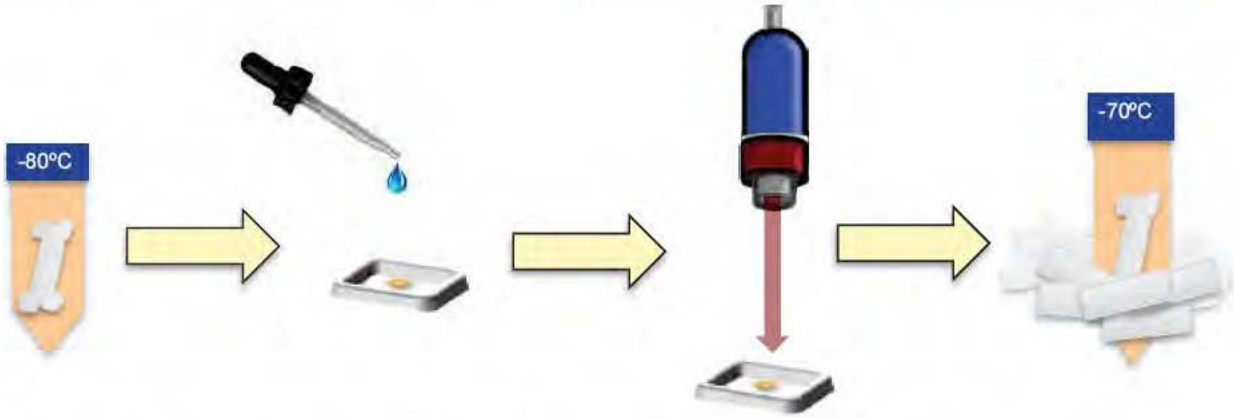

Muscle and early HO tissue biopsies were paraffin-embedded and stained with hematoxylin and eosin (H&E), Masson's trichrome, and Alcian blue.

Mature HO tissue was embedded in glycolmethacrylate (GMA) and stained with H&E and Von Kossa stains.

Raman Spectrum of Bone

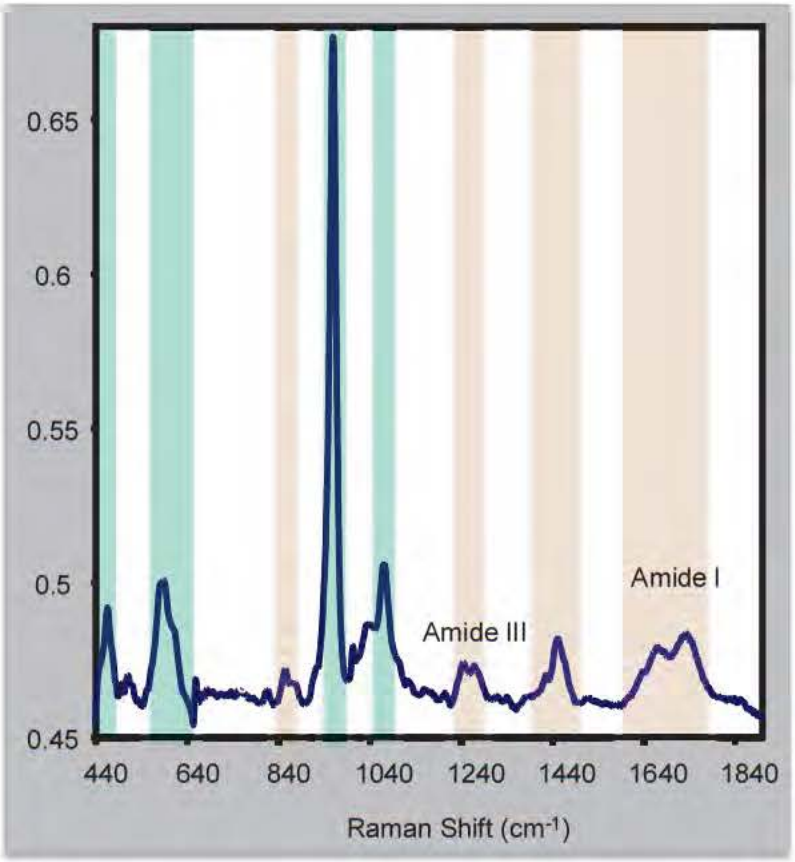

ν (cm^{-1})	Band Assignment	Component
593	ν_4 PO_4^{3-} bending	hydroxyapatite
821	ν(CC) of backbone	collagen; muscle
856	ν(CC) of hydroxyproline ring	collagen; muscle
873	ν_3 P-OH stretching	bone
876	ν(CC) of ˙ y ˙roxypro¨ne ring	collagen; protein
921	ν(CC) of proline ring	collagen; protein
938	ν¸CC¸ of ¸rotein backbone	collagen¸ muscle¸ protein
945-952	ν_1 PO_4^{3-} stretch	amorphous calcium phosphate
959	ν_1 PO_4^{3-} stretch	hydroxyapatite
1004	ν(CC) aromatic ring	Phe; collagen; muscle
1032	ν_3 PO_4^{3-} ; ν(CC) skeletal; C-O stretch	bone; collagen; muscle
1071	$\nu_1(CO_3^{2-})$	bone
1075	ν_3 PO_4^{3-} stretch	hydroxyapatite
1080	ν(CC) and ν(CN) skeletal	collagen; muscle
1159	ν(CC) and ν(CN) skeletal	carotenoid
1178	ν(CC) and ν(CN) skeletal	collagen; muscle
1244	$\delta(CH_2)$ wagging; ν(CN) amide III disordered/β-sheet	collagen; muscle
1274	ν(CN) and δ(NH) amide III α-helix	collagen; muscle
1297	$\delta(CH_2)$ twisting	collagen; muscle
1343	$\gamma(CH_2, CH_3)$ wagging	collagen; muscle
1385	$\delta(CH_3)$ symmetric	collagen
1448	$\delta(CH_2)$ scissoring	collagen; muscle
1524	caro˙eno¨	collagen; muscle
1552	ν(CC) ring stretch	collagen; muscle; Trp
1665	ν(CO) amide I	collagen; muscle

Using Raman spectroscopy, can we identify early changes in tissue that correspond to the development of HO?

REGMED

Raman Comparison of Muscle and HO

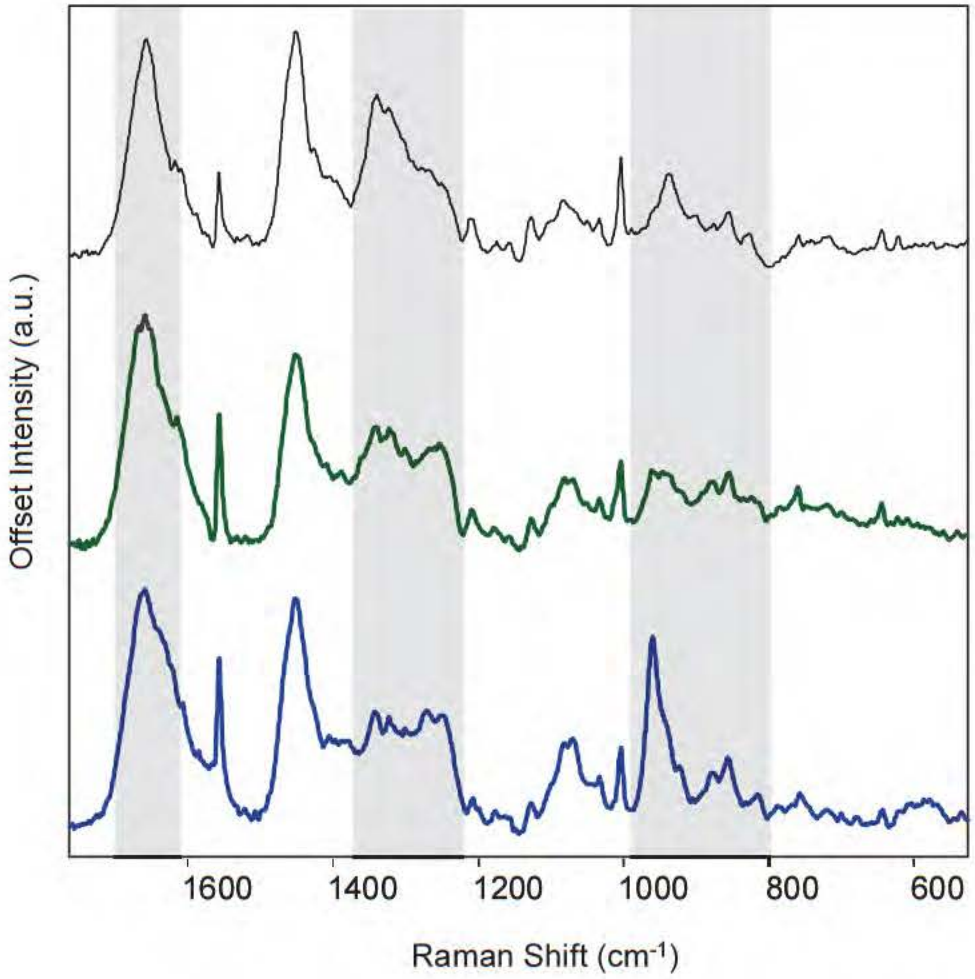

For the HO tissue, whether early or mature, the Amide I band shifts to a higher frequency and is centered at 1660 cm^{-1}.

The intensity of the 1340 cm^{-1} Raman vibrational band is decreased in the spectra of the HO tissue compared to the uninjured muscle tissue.

The 1270 cm^{-1} and 1240 cm^{-1} Raman vibrational bands are increased in the spectra of the HO tissue compared to the uninjured muscle.

The most notable difference in the spectrum of the mineralized HO tissue is the presence of the 960 cm^{-1} band, a ν_1 P-O stretching mode.

Finally, the intensities of the 921 cm^{-1}, 876 cm^{-1}, and 855 cm^{-1} bands are more intense in the spectra of the HO tissue than in the spectrum of the uninjured or injured muscle.

J Bone Joint Surg Am. 2010 Dec;92 Suppl 2:74-89.

REGMED

Raman Spectral Band Area Ratios (BARs)

Band area ratios (BARs), a pseudoquantitative measure, were calculated by dividing the band area of a Raman band of interest (for example 1070 cm^{-1}) by another band area (for example 1445 cm^{-1}).

Compositional trends in related samples can be explored using BARs, such as:

- an increase in mineral carbonation (1070/960 cm^{-1})
- a decrease in reducible collagen crosslinking (1680/1660 cm^{-1})
- mineral carbonation (1070/960 cm^{-1} and 1070/1445 cm^{-1})
- mineral maturity (945/960 cm^{-1})
- collagen order/disorder (1240/1270 cm^{-1})
- Protein α-helical structure (1240/1300 cm^{-1})
- mineral crystallinity is determined by the full width at half maximum of the 960 cm^{-1} ν_1 phosphate band

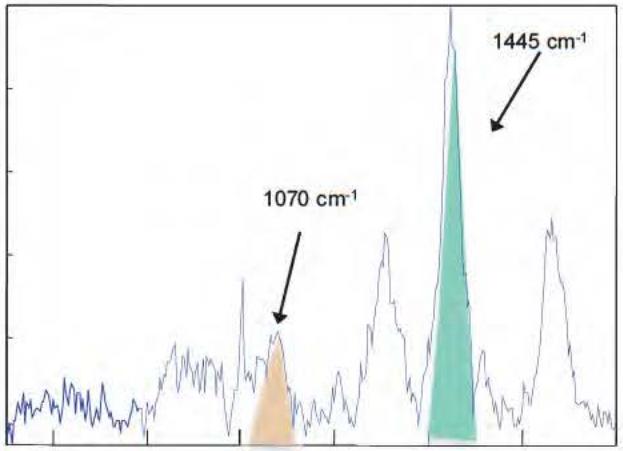

Comparison of Raman Spectral BARs

In general, when comparing muscle (normal or injured) to HO tissue (early or mature), we note a decrease in the 1660/1445 cm^{-1} ($p<0.03$), 1680/1445 cm^{-1} ($p=0.28$), and 1340/1270 cm^{-1} ($p<0.01$) BARs.

There is also an increase in the 1640/1445 cm^{-1} BAR ($p<0.1$), the 1240/1270 cm^{-1} (collagen order/disorder) BAR ($p<0.03$), and the 1240/1300 cm^{-1} (protein α-helical structure, $p<0.001$). These changes in BARs can also be examined as a progression of normal tissue to diseased tissue.

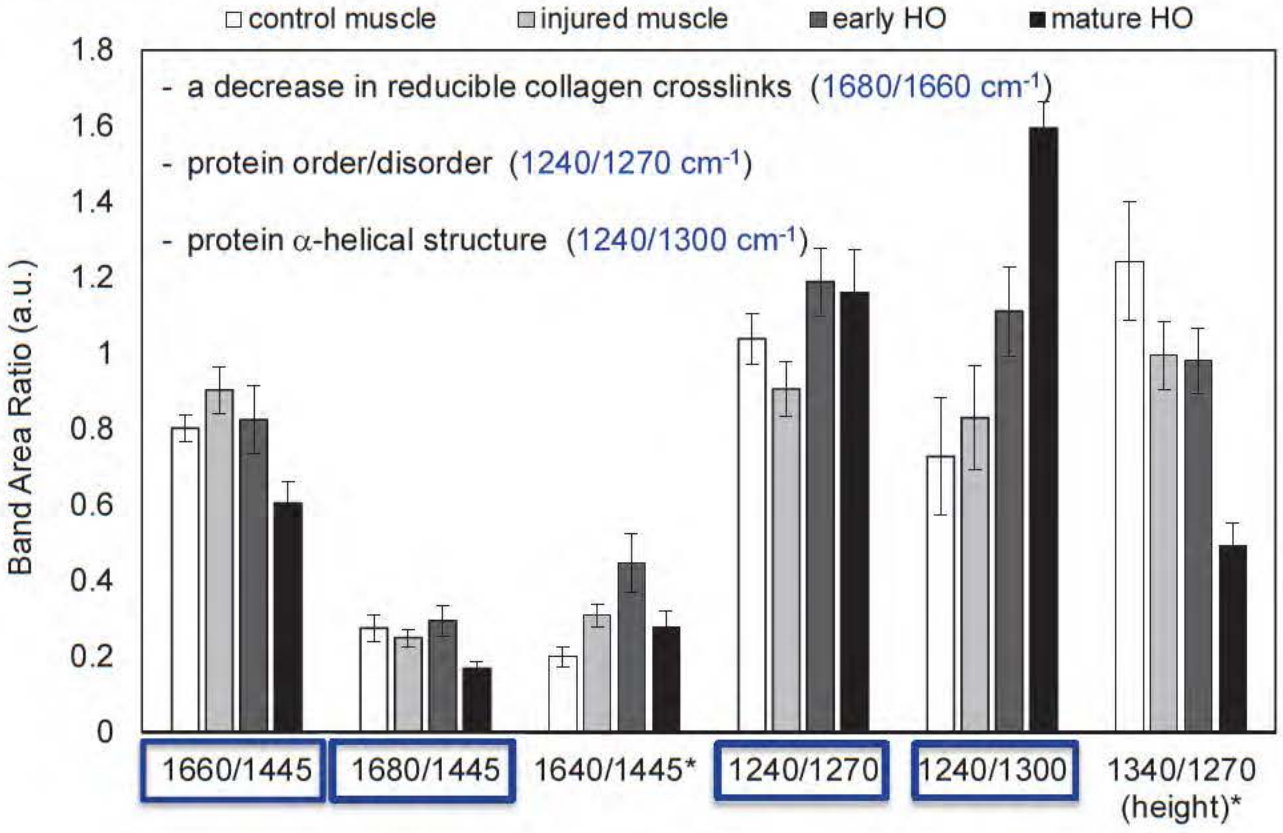

Transition from normal to injured muscle –

↑ 1660/1445 cm^{-1} and 1640/1445 cm^{-1}, collagen order/disorder, and 1340/1270 cm^{-1} BRs.

Transition from injured muscle to HO tissue -

↓1660/1445 cm^{-1} and 1680/1445 cm^{-1} BAR

↑ in the collagen order/disorder BAR and the protein α-helical structure BAR.

Bone. 2013 Sep 5;57(2):335-342.

REGMED

** Statistically significant differences ($p<0.05$) with a Bonferroni correction.*

Bone. 2013 Sep 5;57(2):335-342.

Normal Bone versus HO

Early HO tissue was surgically removed within 165 days post-injury (mean) while mature HO was excised on average over 600 days post-injury.

- mineral carbonation (1070/960 cm^{-1} and 1070/1445 cm^{-1})
- mineral immaturity (945/960 cm^{-1})
- mineral crystallinity is determined by the full width at half maximum of the 960 cm^{-1} ν_1 phosphate band

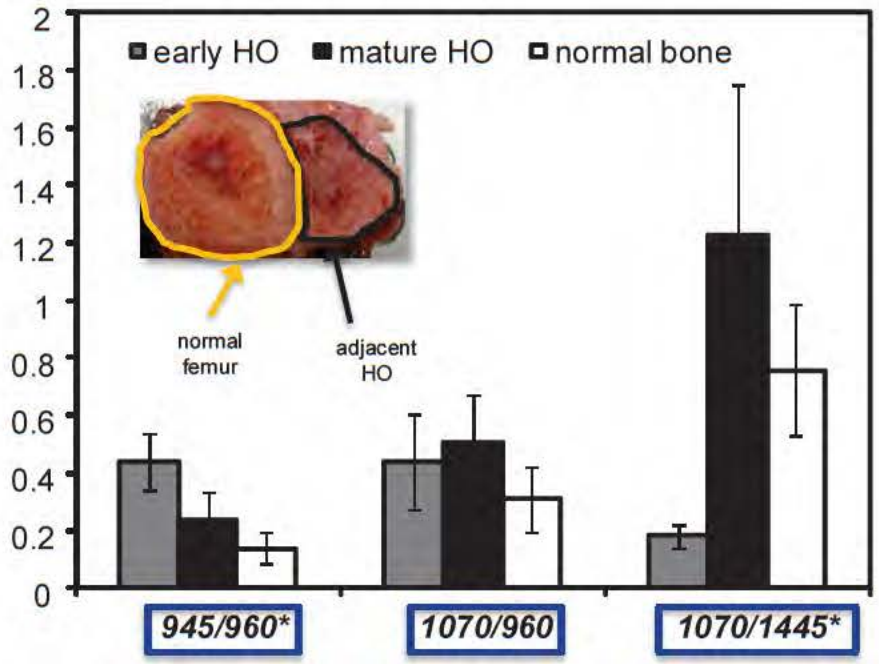

As bone matures –

↓945/960 cm^{-1} BAR and ↑1070/1445 cm^{-1} BAR

Early HO has the highest mineral immaturity BARs and the lowest mineral carbonation BARs.

This trend is reversed for mature HO –

- the mineral immaturity BARs are lower than early HO
- mineral carbonation BARs are higher than early HO tissue.

Mineral crystallinity is higher in mature HO samples than in normal bone or early HO samples.

REGMED

** Statistically significant differences ($p<0.05$) with a Bonferroni correction.*

Bone. 2013 Sep 5;57(2):335-342.

Discrimination of HO Tissue by Raman Metrics

PLS-DA – supervised machine learning that uses classical PLS regression to regress a categorical variable, i.e. development of HO.

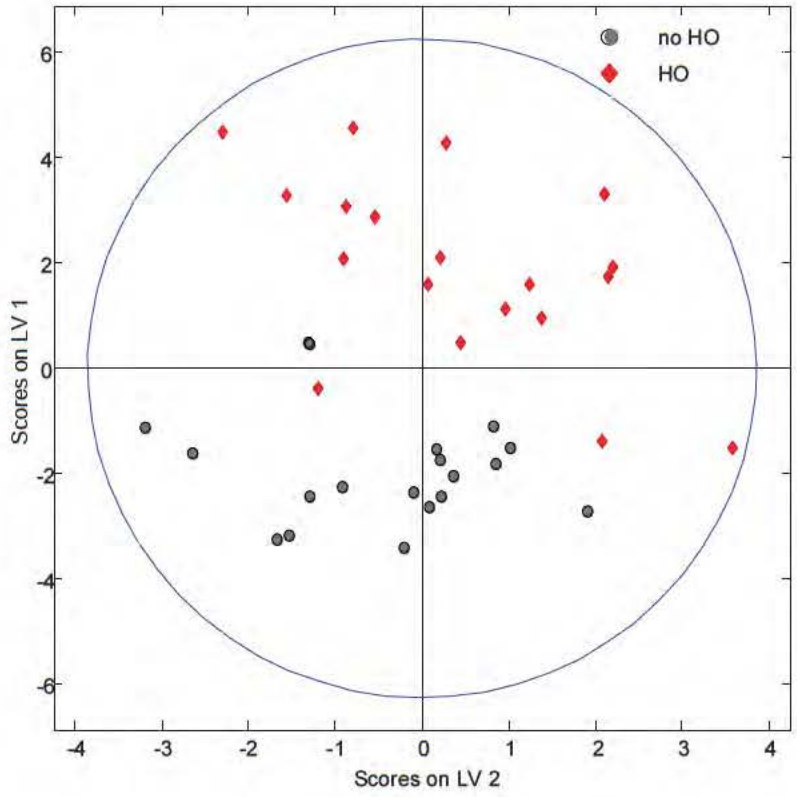

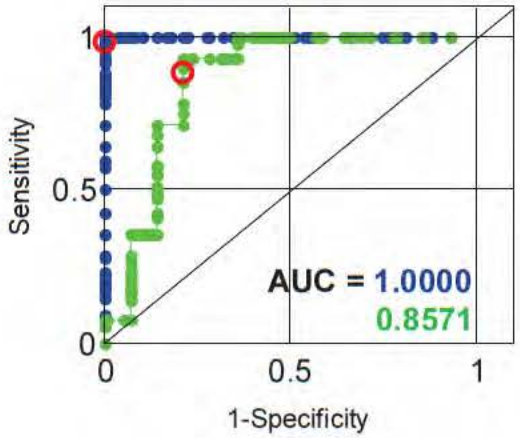

No HO

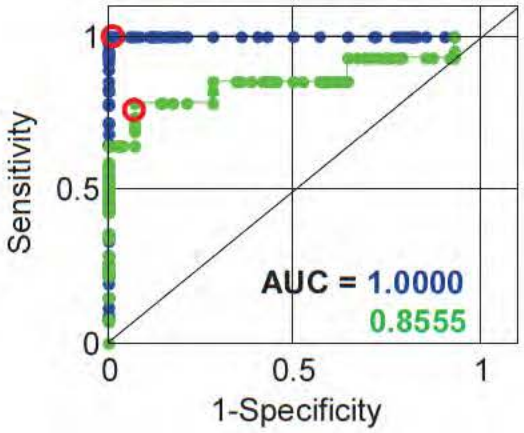

HO

Discrimination of HO Tissue by Raman Metrics

Cross-validation	Actual no HO	Actual HO
Predicted no HO	13	3
Predicted HO	1	11

Prediction	Actual no HO	Actual HO
Predicted no HO	4	0
Predicted HO	1	5

Sensitivity = 100%
Specificity = 80%

Positive predictive value = 83.3%
Negative predictive value = 100%

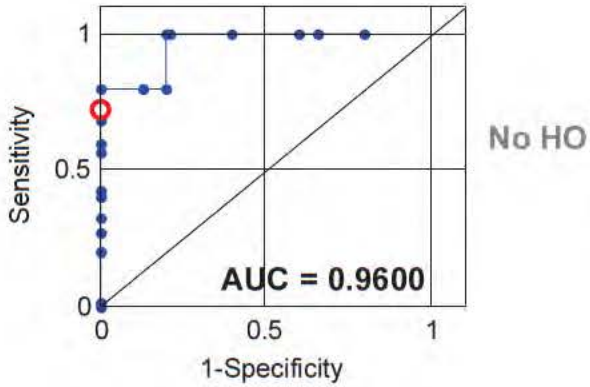

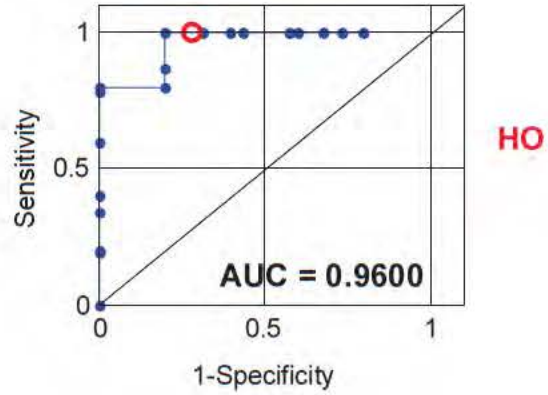

Heterotopic Ossification

In this preliminary study, we used Raman spectroscopy to discern molecular changes that that occur prior to and during the formation of HO.

While mature HO tissue is generally apparent upon physical examination and/or radiologic examination, immature and largely unmineralized HO tissue is not as clinically obvious.

The Raman spectra of various tissues demonstrate that there are clear differences in the Amide I and Amide III spectral regions of HO tissue compared to normal muscle tissue, which may indicate whether or not muscle tissue will develop HO.

Raman spectroscopy also provides insight into the actual mineralization of the soft tissue.

Raman spectroscopy can be adapted as an **objective, intraoperative, non-invasive** means by which to risk stratify wounds, and can be **performed in real-time**.

Preliminary prediction models for “detection” of HO are promising, with **greater than 80% sensitivity and specificity**.

If Raman spectroscopy demonstrates that a wound has Raman spectral features associated with the formation of HO, prophylaxis could be employed in select cases.

Alternatively, in areas that appear prone to HO development the clinician can consider early preferential excision of pre-HO tissue while the patient is undergoing debridement and/or amputation revision for final closure.

Overall Concept

1) Apply best of breed technologies in

   - *biomarker analysis*
   - *informatics*
   - *medical technology*

2) Clinical Decision Support tools can be developed that can optimize and personalize treatment using *patient-specific clinical variables combined with local and systemic biomarkers.*

3) Goal: <u>maximize patient outcomes while minimizing complications</u>.

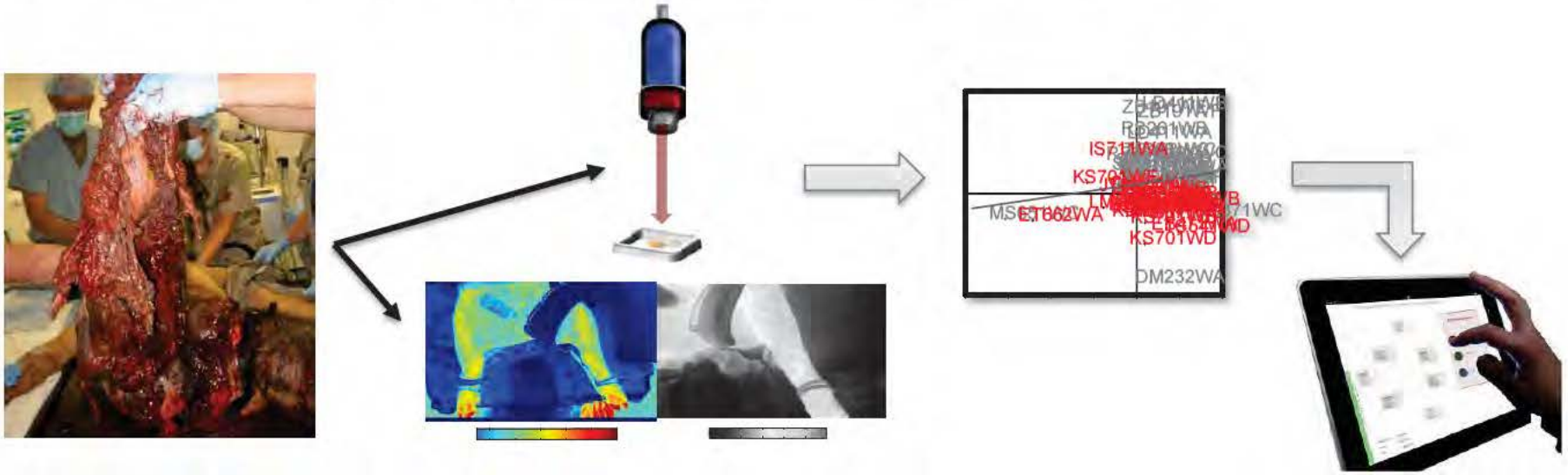

Acknowledgements

Regenerative Medicine Dept, NMRC

Jonathan Forsberg, MD
Thomas Davis, PhD
Nicole Crane, PhD
Trevor Brown, PhD
Matthew Wagner, PhD
Richard Barth, MS
Ying Cao, MS
Felipe Lisboa, MD
Khairul Anam, PhD
Anthony Foster, PhD
Ammar Qureshi, PhD
Michael Wiley, MBA
Mihret Amare, MS
Yelena Lazdun, MS
Chioma Aglibe, MS
Alison Tomasino, BS
Nick Clark, BS
Crystal Leonhardt
Stacia Moreno, BS
Fred Gage
Toby Perkins

Orthopaedics Dept, WRNMMCB

Romney Andersen, MD
B. Kyle Potter, MD
Wade Gordon, MD
Jean Claude D'Allyrand, MD
Robert Beer, MD
Mark Fleming, MD
Susan Foster, RN

Department of Surgery, USUHS

Eric Elster, MD FACS
Leon Nesti, MD, PhD
Arnaud Belard, MBA
Tiffani Slaughter, BS

Disclaimer

The views expressed in this presentation are those of the author and do not necessarily reflect the official policy or position of the Department of the Navy, the Department of Defense, nor the U.S. Government.

This work was supported/funded by work unit number 602115HP.3720.001.A1015. Funding Support includes DoD BUMED Advance Medical Development 0604771N; USAMRMC Military Medical Research and Development OR090136**;** Defense Medical Research and Development Plan D10_I_AR_J2_501.

The study protocol (WRNMMC 374863) was approved by the Walter Reed National Military Medical Center Institutional Review Board in compliance with all applicable Federal regulations governing the protection of human subjects.

I am a military service member (or employee of the U.S. Government). This work was prepared as part of my official duties. Title 17 U.S.C. 105 provides the “Copyright protection under this title is not available for any work of the United States Government.” Title 17 U.S.C. 101 defines a U.S. Government work as a work prepared by a military service member or employee of the U.S. Government as part of that person’s official duties.

I certify that the document represents valid work; that if I used information derived from another source, I obtained all necessary approvals to use it and made appropriate acknowledgements in the document; and I take public responsibility for it.

REGMED
Shaping the Future of Casualty Care

THANK YOU!

Surveying Tourniquet Induced Nerve Damage in Swine using Raman Spectroscopy

Katherine E. Cilwa, PhD
Tiffani Slaughter
Eric A. Elster, MD
Jonathan A. Forsberg, MD
Nicole J. Crane, PhD

Disclaimer

The views expressed in this presentation are those of the author and do not necessarily reflect the official policy or position of the Department of the Navy, the Department of Defense, nor the U.S. Government.

This work was supported/funded by work unit number 602115HP.3720.001.A1015. Funding Support includes USAMRMC Military Medical Research and Development OR090136; Defense Medical Research and Development Plan D10_I_AR_J2_501.

The study protocol (11-SUR-816) was approved by the Uniformed Services University of Health Sciences Institutional Animal Care and Use Committee in compliance with all applicable Federal regulations.

I am a military service member (or employee of the U.S. Government). This work was prepared as part of my official duties. Title 17 U.S.C. 105 provides the "Copyright protection under this title is not available for any work of the United States Government." Title 17 U.S.C. 101 defines a U.S. Government work as a work prepared by a military service member or employee of the U.S. Government as part of that person's official duties.

I certify that the document represents valid work; that if I used information derived from another source, I obtained all necessary approvals to use it and made appropriate acknowledgements in the document; and I take public responsibility for it.

Peripheral Nerves & Injury

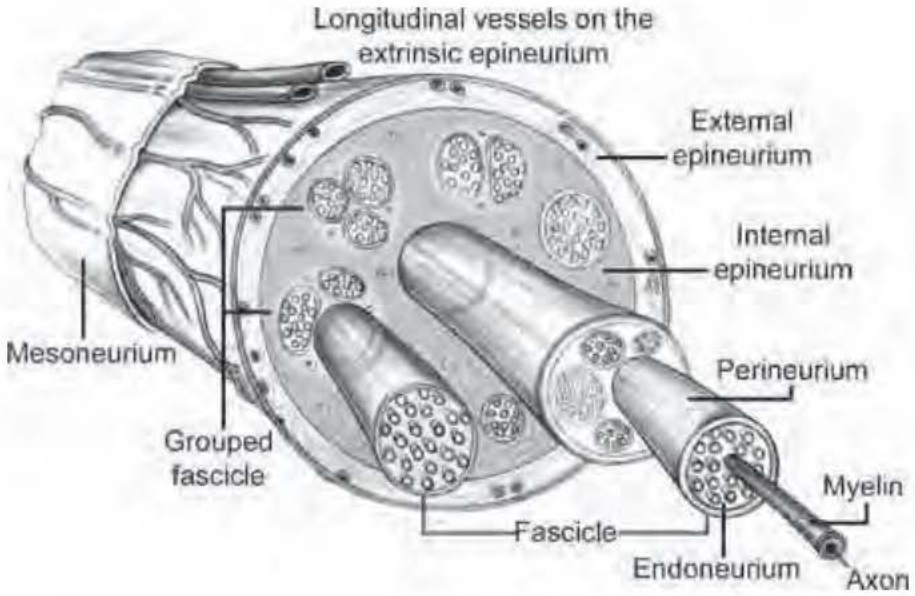

Ref. 1

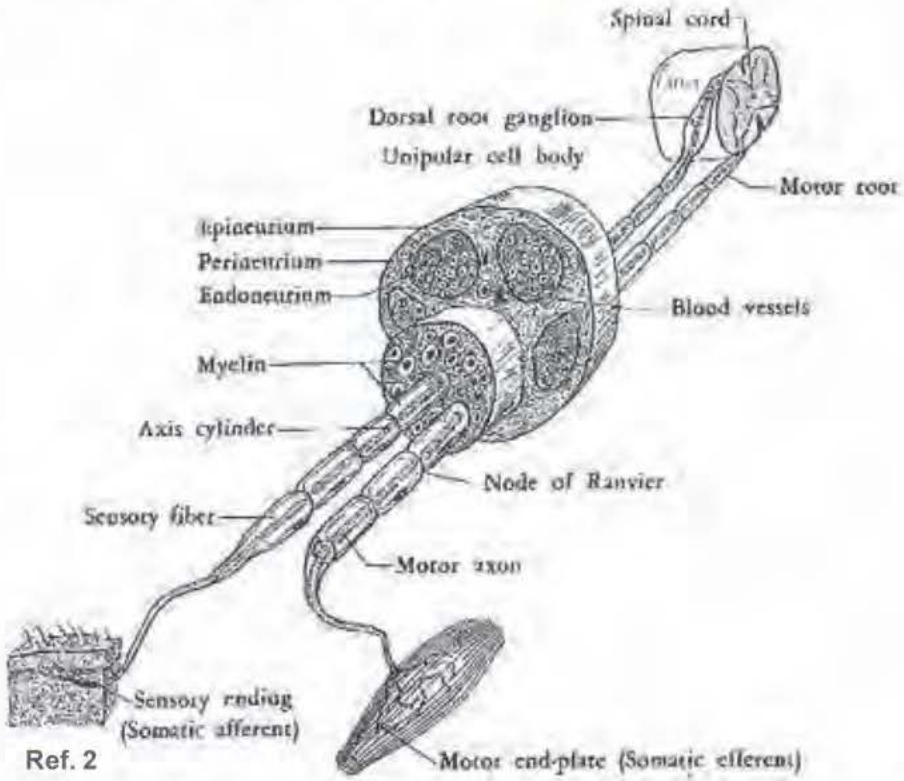

Ref. 2

Classification	Tissue Disruption	Recovery	Potential Raman Application
Neuropraxia	Demyelination	Complete	*Monitoring repair*
Axonotmesis	Axon	Good to Poor, 1 mm/day	*Detection of damage*
	Endoneurium	Poor, Surgery may be required	*Detection of damage*
	Perineurium	Poor, Surgery may be required	*Detection of damage*
Neurotmesis	Epineurium	Surgery Required	*Triage of nerve tissue*

1. Weber RA. *et al.*"Nerve Lacerations: Repair of Acute Injuries" in Hand Surgery 2004
2. Jenkins TW. Functional Mammalian Neuroanatomy, 1978.

REGMED

Nerve Injury in Combat Wounded

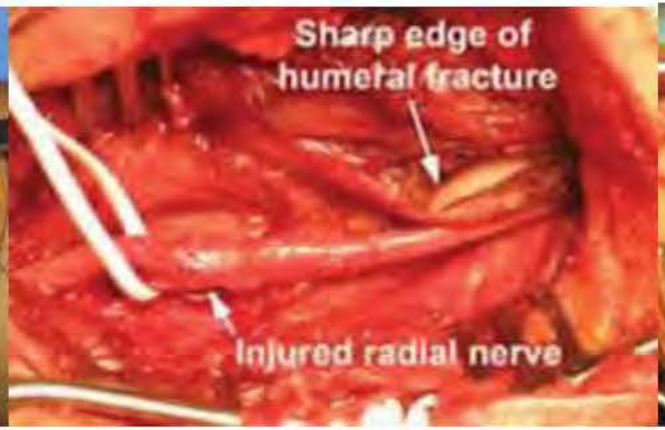

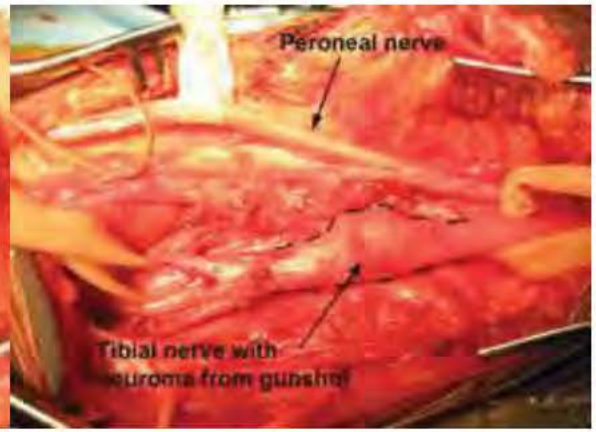

- Over 30% of combat injuries involve peripheral nerve injury[3,4] compared to only 3% in civilian trauma.[5]
- Nerve dysfunction is the second leading cause of long-term disability in injured service members[6] and is present in 37% of upper limb injuries with disability.[7]
- Identification and assessment of non-penetrating nerve injury would improve outcome and aid in therapeutic monitoring.
- Previous Raman studies of nerve tissue have assessed only normal sectioned tissue,[8,9] sectioned tissue with penetrating trauma,[10] intact non-injured tissue,[11,12] or intact chemically demyelinated tissue[13] all via microscopy.
- To our knowledge, this is the first report to detect nerve degeneration using a Raman spectroscopy fiber optic probe.

3. Hansen MO, *et al.* Mil Med. 1994
4. Roganovic Z, *et al.* Vojnosanit Pregl. 1995
5. Nobel J, J Trauma. 1998
6. Cross JD *et al.* J Am Acad Orthop Surg . 2011
7. Rivera JC *et al.* Bone and Joint J. 2014
8. Minamikawa T, *et al.* Histochem Cell Biol. 2013
9. Wang H, *et al.* J Trauma. 2011
10. Morisaki S, *et al.* J Biomed Opt. 2013
11. Huff TB, *et al.* J Microscopy. 2007
12. Bélanger E, *et al.* J Biomed Opt. 2012
13. Shi Y, *et al.* J Biomed Opt. 2011
14. Kan JS, *et al.* J Am Acad Orthop Surg. 2011

REGMED

Peripheral Nerve Crush Injury

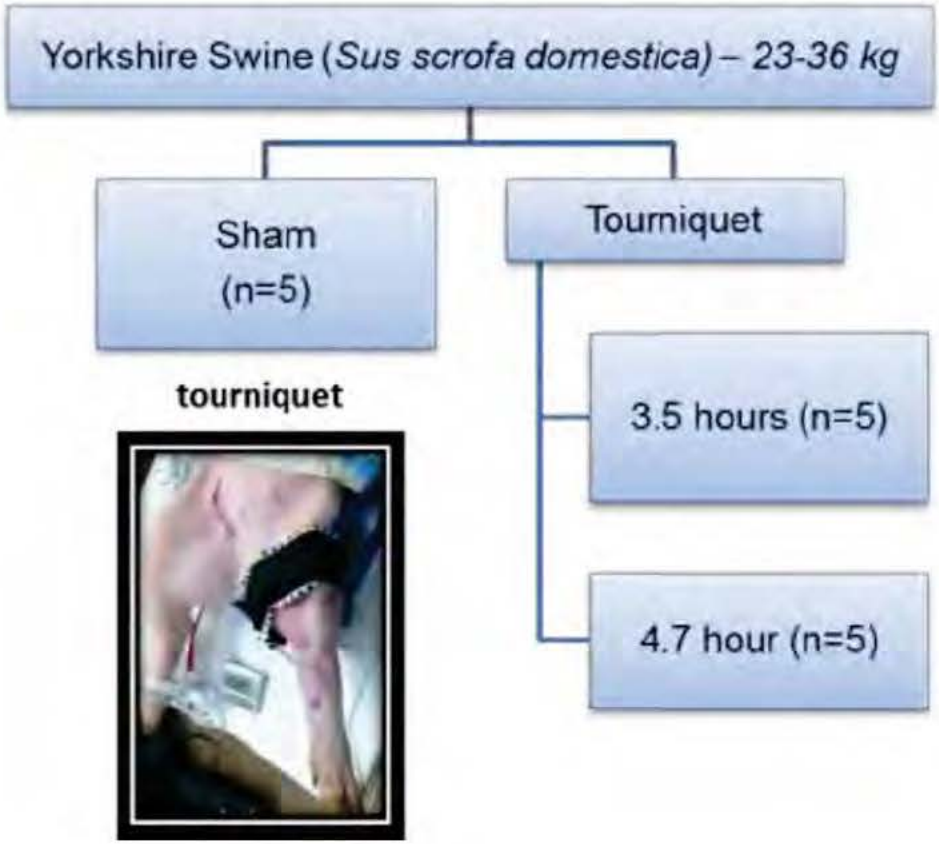

- A pneumatic tourniquet is applied to the limb (250 mm Hg) for 3.5 or 4.7 hours.
- After the limb is reperfused, the animal is survived for 1 week.
- At necropsy, sciatic and femoral nerves are harvested, formalin fixed

ex vivo samples for analysis

Tissue Analysis

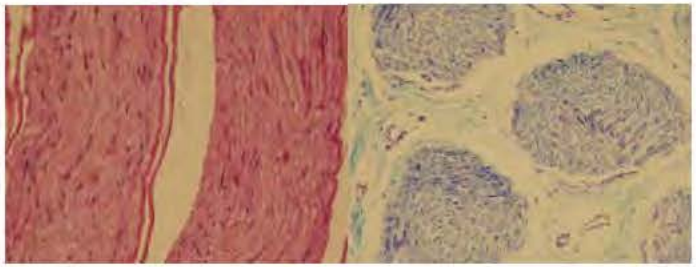

Raman Spectroscopy: Kaiser Rxn1, 785 nm excitation, PhAT probe with 3mm spot size, 4 spectra per sample.

Histology: paraffin embedded, H&E and Luxol blue/Cresyl violet.

Statistical Analysis: Raman metrics are compared using a two-tailed Student's t-test; p-values <0.05 are considered statistically significant.

Sample Size

Sham: 5 Sciatic and 3 Femoral

Tourniquet: 5 Sciatic and 1 Femoral

Raw Data & Preprocessing

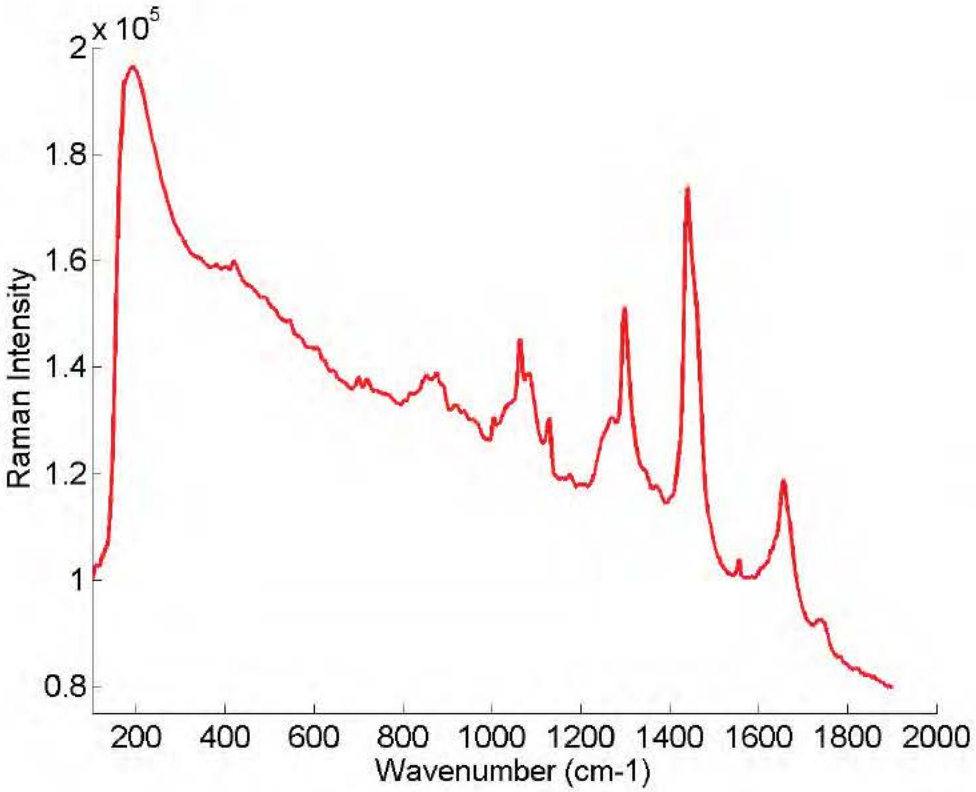

Raw spectra: 5 sec acquisitions, 20 accumulations

Backround Subtraction: automated 4th order polynomial fit

Based on "A robust method for automated background subtraction of tissue fluorescence." Alex Cao, 2007, JRS.

1004 cm-1 normalization

Mean Nerve Spectra

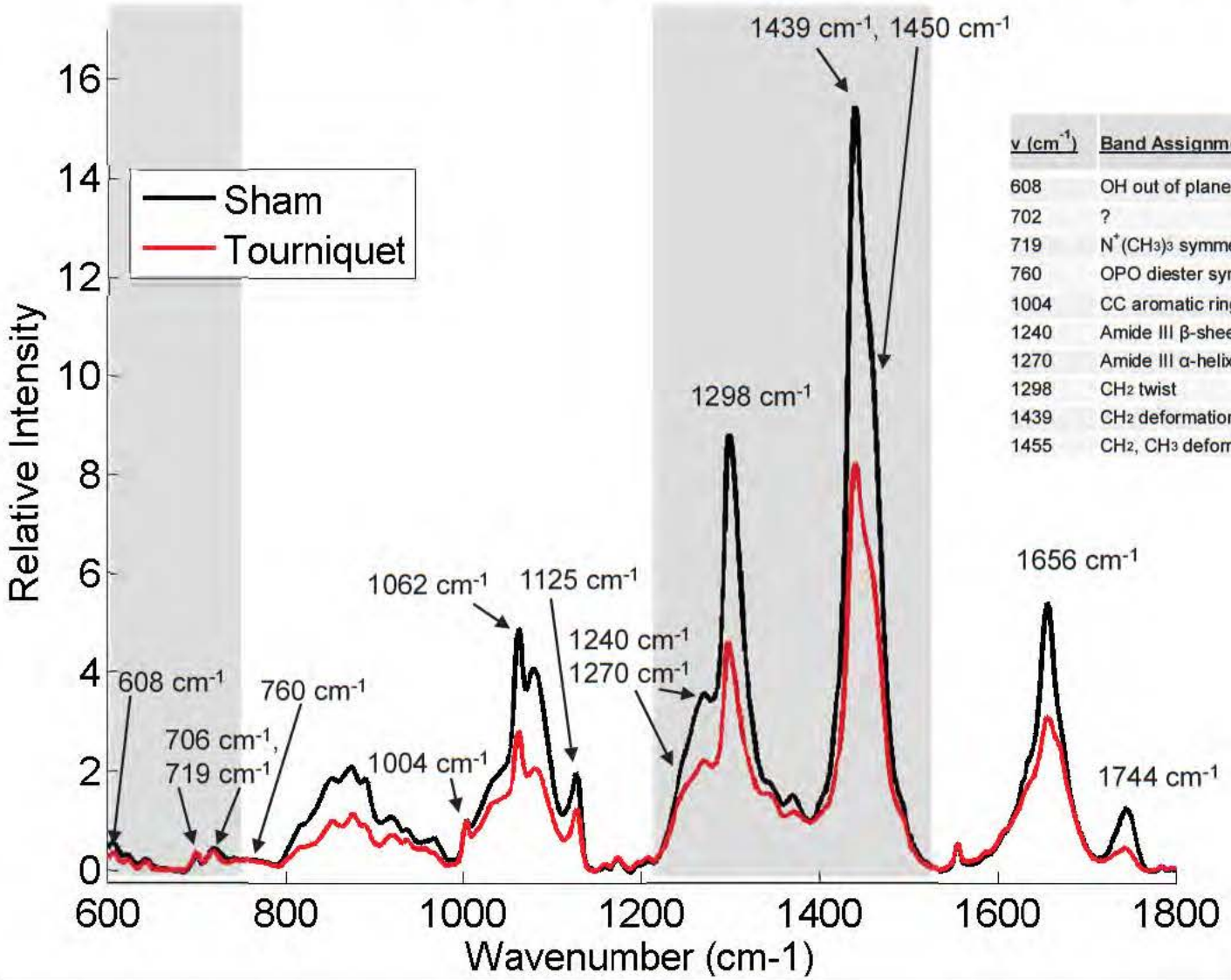

ν (cm^{-1})	Band Assignment[15,16]	Component
608	OH out of plane bend?	cholesterol
702	?	cholesterol
719	$N^+(CH_3)_3$ symmetric stretch	choline
760	OPO diester sym. str.	phosphocholine
1004	CC aromatic ring stretch	phenylalanine
1240	Amide III β-sheet/ disordered	β-sheet, disordered protein
1270	Amide III α-helix, C=C stretch	ordered protein, lipid
1298	CH_2 twist	fatty acid, protein
1439	CH_2 deformation	fatty acid, cholesterol, protein
1455	CH_2, CH_3 deformation	protein, fatty acid

15. Krafft, C, et al. Spectrochim Acta A. 2005
16. Spiker RC, et al. Biochim Biophys Acta. 1975

REGMED

Band Area Ratios: Peaking Fitting

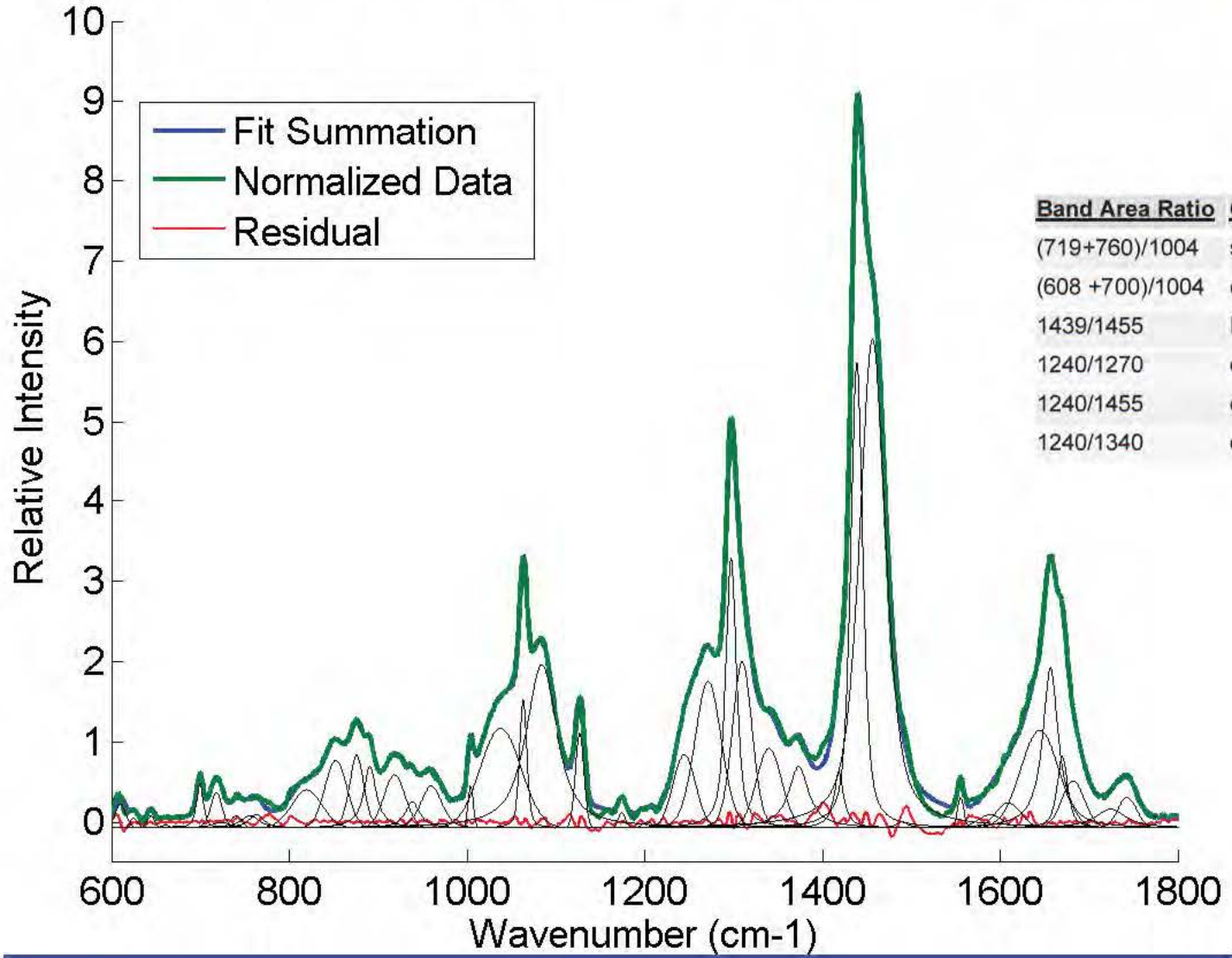

Band Area Ratio	Content
(719+760)/1004	sphingomyelin
(608 +700)/1004	cholesterol
1439/1455	Lipid/protein
1240/1270	disordered/(ordered protein+ lipid)
1240/1455	disordered protein/total protein I
1240/1340	disordered protein/total protein II

Fingerprint Region BARs

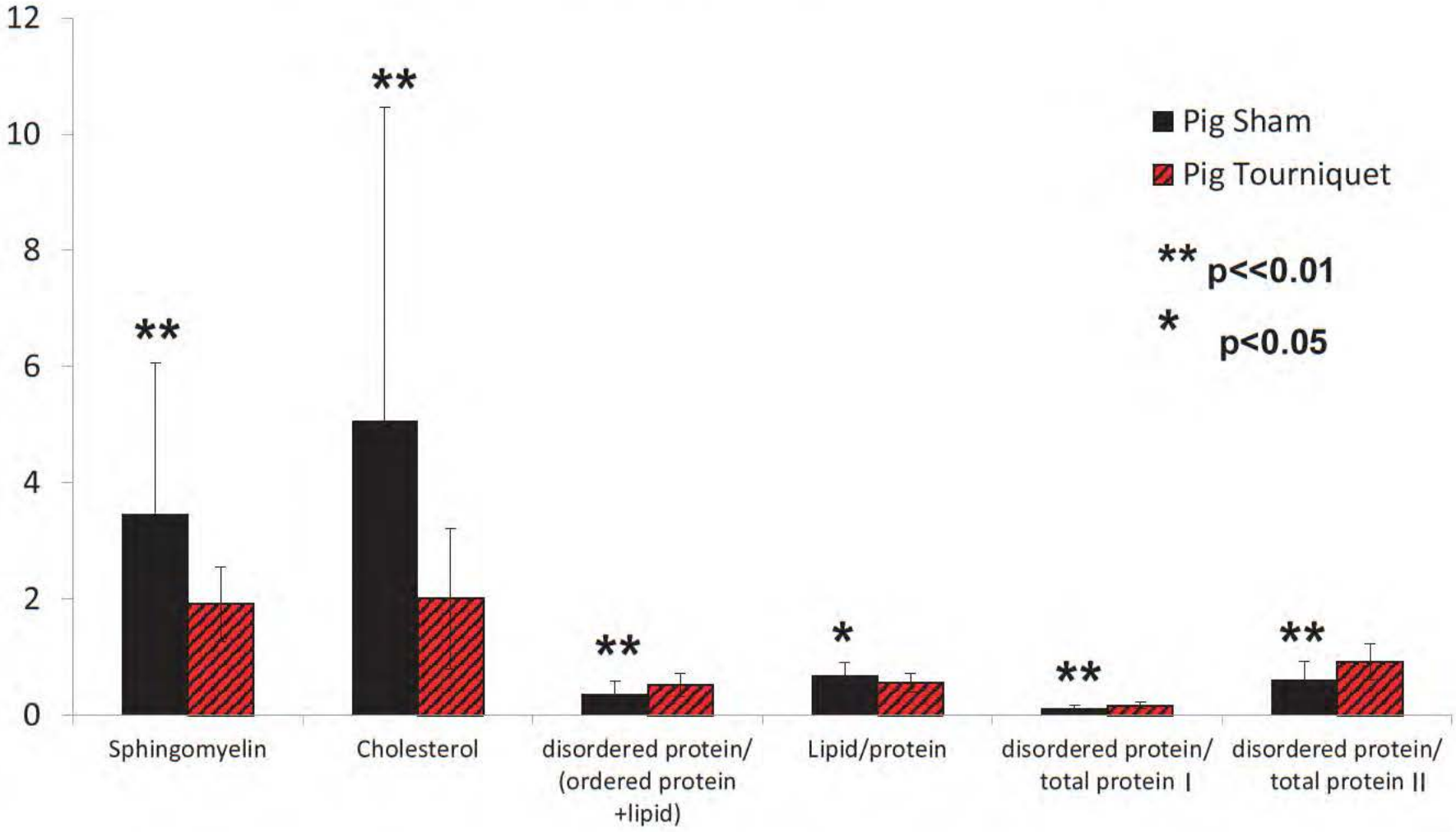

Comparison to Literature: C-H Stretch Region

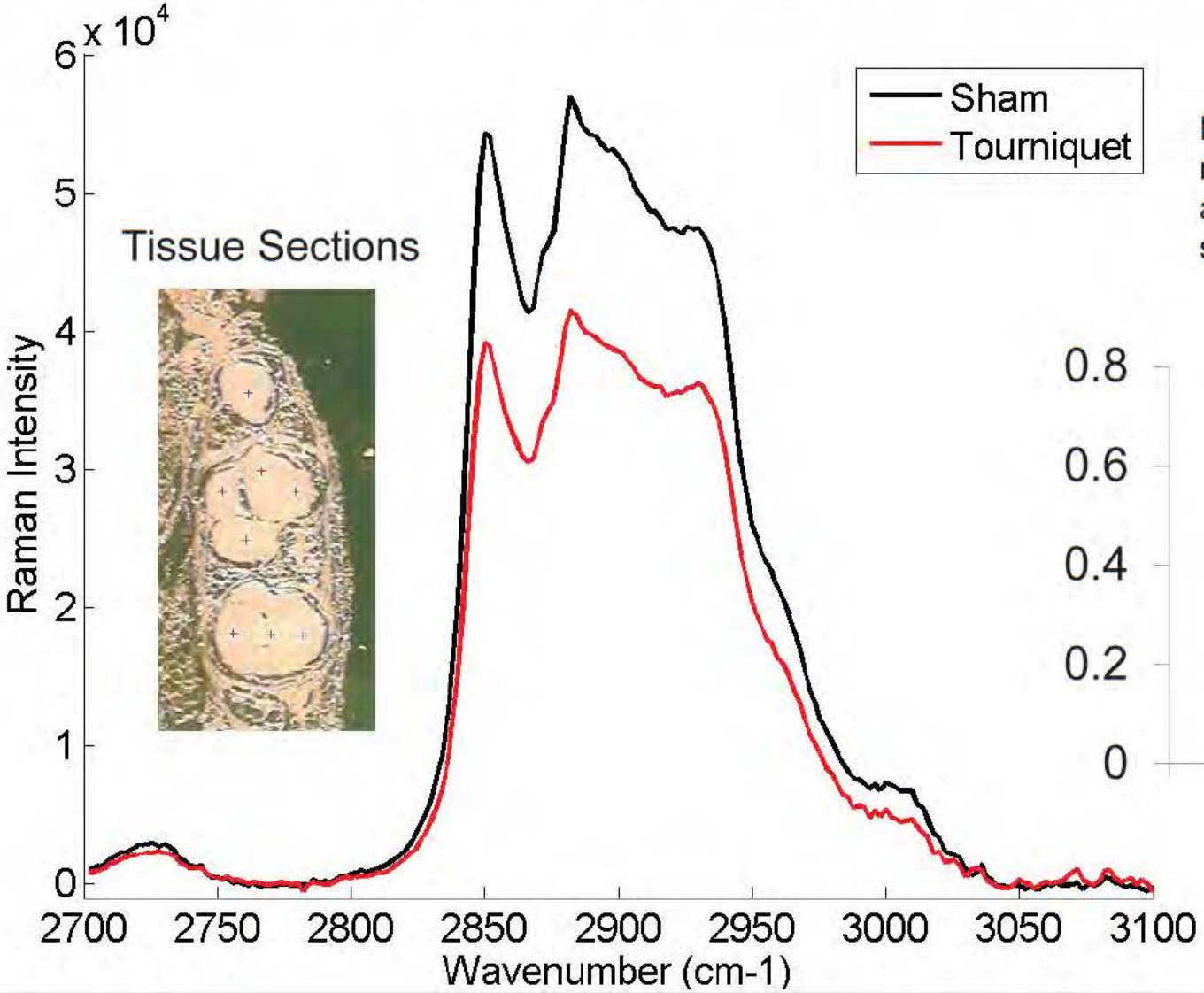

Perkin Elmer Raman microscope, 10 sec, 20 accumulations, 8 spectra per specimen

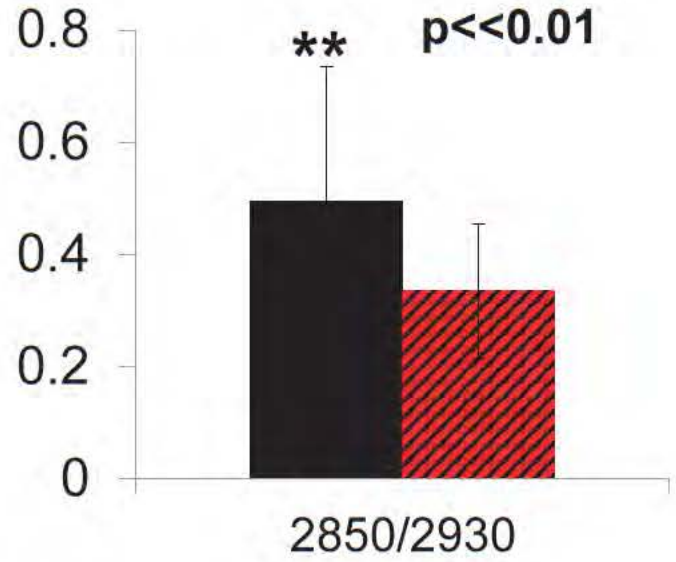

Univariate Analysis

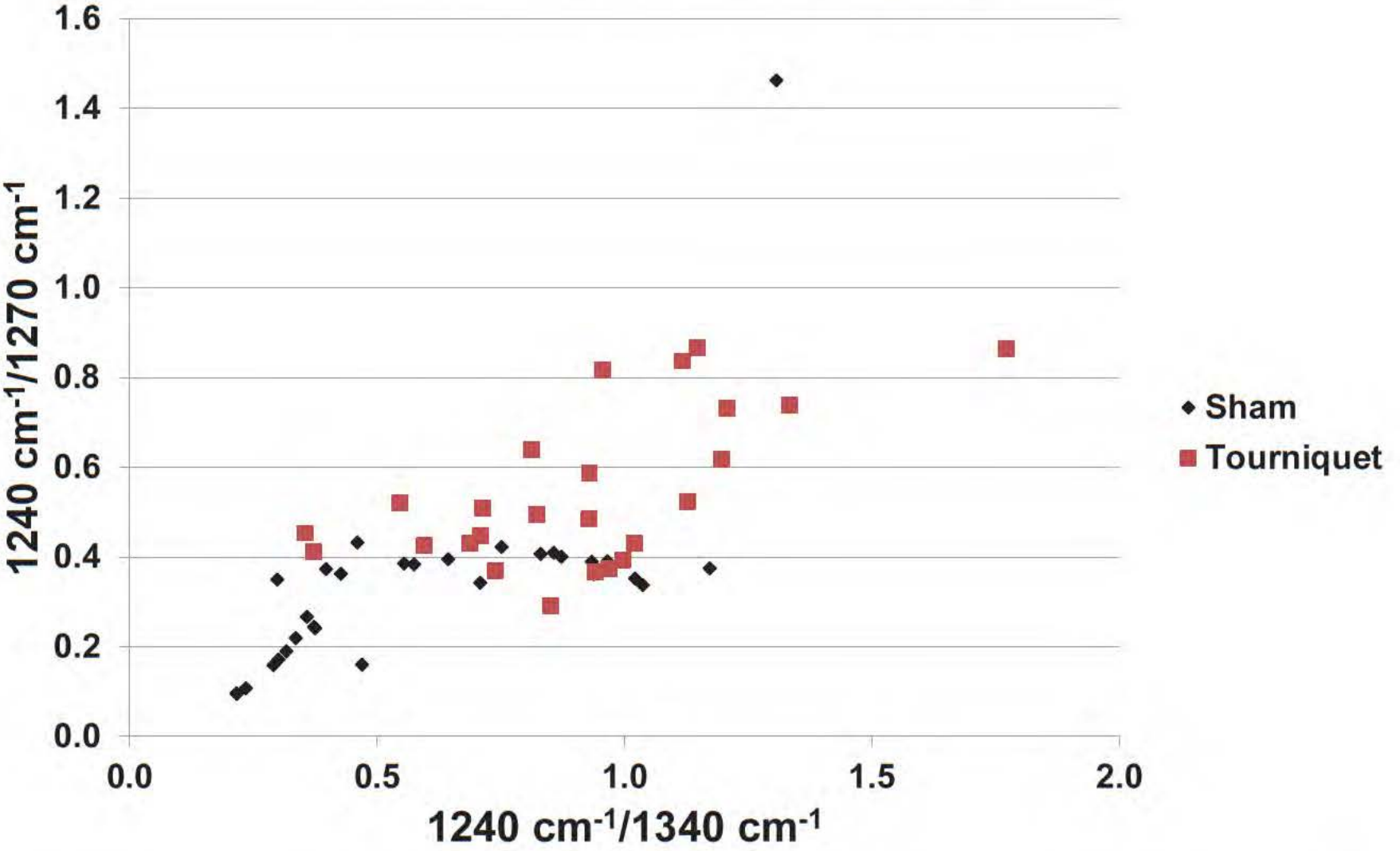

Combined Histology Scoring Confirms Nerve Injury: Degeneration and Infiltrate

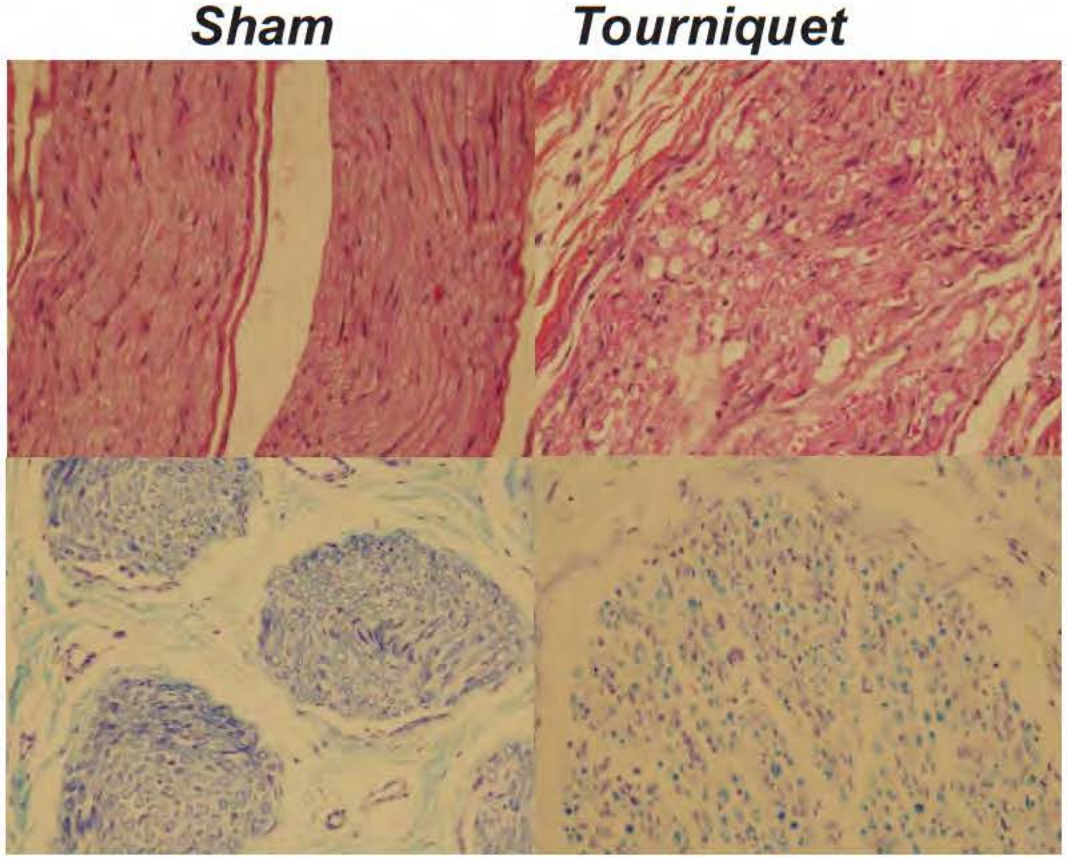

Correlation Score

	Histology
2850/2930	-0.4
(719+760)/1004	-0.6
1439/1340	-0.6
1240/1455	0.6

Fingerprint region metrics may correlate with tissue changes better than C-H stretch metric

Summary

Injured nerves exhibited changes in Raman metrics, $p<<0.01$, indicative of:

- 45% decreased sphingomyelin
- 60% decreased cholesterol
- 18% decreased lipid
- 50% decreased α-helix content versus total protein

Axonal and myelin degeneration, cell death and digestion, and inflammation of tourniquet samples were confirmed via histology.

Raman spectroscopy detects myelin degeneration and structural damage within intact nerves.
Univariate comparison of metrics identifies tissue type.

Fingerprint region BARs may correlate with histology better than C-H stretch BAR

This study demonstrates the noninvasive ability of Raman spectroscopy to detect nerve degeneration associated with non-penetrating injury relevant to neurapraxic and axonotmetic injuries

Current & Future Directions

animals models: peripheral nerve & spinal nerve *human tissue*: peripheral & diabetic nerve

Acknowledgements

NMRC Regenerative Medicine Dept.

- Jonathan Forsberg, MD
- Douglas Tadaki, PhD
- Thomas Davis, PhD
- Nicole Crane, PhD
- Khairul Anam, PhD
- Anthony Foster, PhD
- Lydia Rosenbaum, MS
- Mihret Amare, MS
- Yelena Lazdun, MS
- Rajiv Luthra, BS
- Darren Fryer BS
- Crystal Leonhardt BS
- Emily F. Ludwig, BS
- Dana Golden, BS
- Aileen Mooney, BS
- Fred Gage
- Toby Perkins
- Kyle Brunette, BS
- Maricela Rodriguez
- Jeffrey Hyde

WRAIR Pathology

- Major Leonora Dickson

Orthopaedics Dept, WRNMMCB

- Romney Andersen, MD
- B. Kyle Potter, MD
- Wade Gordon, MD
- Jean Claude D'Allyrand, MD
- Robert Beer, MD
- Mark Fleming, MD
- Susan Foster, RN

USUHS Department of Surgery

- Eric Elster, MD FACS
- Leon Nesti, MD, PhD

DecisionQ Inc. Washington D

- Todd Radano
- Liz Silvius
- Benjamin Petersen

DecisionQ

Turning Data Into Decisions.

REGMED
Shaping the Future of Casualty Care

Thank you

Evaluation of Raman Spectroscopic Discrimination between Bacterial Strains and Species using Hierarchical Cluster Analysis

Nicole Crane[1], Meron Ghebremedhin[1], Shubha Yesupriya[1]

[1]Naval Medical Research Center (NMRC), Silver Spring, MD

Abstract

There has been a great deal of interest in the use of Raman spectroscopy in the biomedical field due to its rapidity and noninvasive nature. In this study, we aim to evaluate the reliability of Raman spectroscopy for the purpose of bacterial species differentiation. Using a sample set of 28 unique bacterial samples associated with clinical infections, we performed cluster analyses of Raman spectra, biochemical tests, high resolution melting data (HRM), DNA sequences and antimicrobial susceptibility tests of minimum inhibitory concentration (MIC) and a measure of degree of resistance (SIR) data sets. Clustering was performed in MATLAB using multivariate statistical techniques - hierarchical cluster analysis with various distances and linkages. DNA sequences were evaluated using Multiple Sequence Comparison by Log-Expectation (MUSCLE) software as well as in MATLAB. In order to quantify the validity of these clusters, F-measures were calculated for the hierarchical clustering of Raman spectra, biochemistries, HRM, DNA sequence, MIC and SIR data sets. In addition, we compared the resulting dendrograms of each clustering to known classification of the bacteria using a taxonomic chart as a point of reference. In evaluating the F-measure values of the Raman spectral clustering in comparison to the clustering of other data types, we observe consistent correct clustering of bacteria. This study clearly demonstrates reliability of Raman analysis for bacterial identification down to the species level. Our ultimate goal is to produce a model for evaluating wound bioburden using Raman spectroscopy as a faster, more efficient way to detect the presence of bacterial infection.

Background

Reliable application of Raman spectroscopy in a clinical setting could revolutionize routine identification of pathogenic organisms. Many studies have been conducted on Raman identification of microbial organisms over the years, but none have targeted the identification of microbial infection in combat-related injuries specifically. Current methods of identifying bacterial infection rely on culturing microbes from patient material and performing biochemical tests, which together can take 2-3 days to complete. If Raman spectroscopy could recognize bacterial infection from patient material directly, physicians would be able to determine course of treatment and drug administration in a matter of hours. In this preliminary study, a number of bacteria known to cause clinical infections are grown on solid culture media and Raman spectra are obtained. Additionally, various types of data are analyzed for comparison, including biochemical arrays, high resolution melting points, DNA sequences, antimicrobial susceptibility tests, and degree of resistance tests. Next, we plan on taking spectra of effluent samples from combat-related wounds and perform a similar cluster analysis based on our current findings.

Materials & Methods

High Resolution Melting (HRM) :
- Exact temperature at which double stranded DNA separates was determined using HRM analysis of each isolate

Biochemical data :
- BD Phoenix ™ panels give results (+ or -) for an array of enzymatic and biochemical substrates

DNA sequences: *analyzed using www.phylogeny.fr*[1]
- MUSCLE method of multiple sequence alignment
- GBlocks curation

Antimicrobial resistance : BD Phoenix™ Antimicrobial Susceptibility Test (AST) results
- Susceptible, Intermediate or Resistant (SIR)
- Minimum Inhibitory Concentration (MIC)
- any resistance markers found

Raman Spectra :
- Reference bacterial isolates grown on LBA and blood agar plates for 48 hours.
- 9 spectra taken from plated samples (4 from blood agar, 5 from LBA) using 785-nm laser with spot size of 3 mm
- Preprocessing of spectra
- Partial Lease Squares Discriminant Analyses (PLSDA) method used to develop classification model[2]

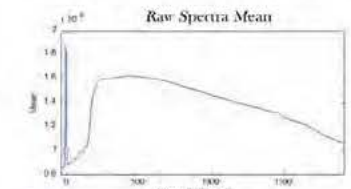

Results

Step 1: Preprocessing of Spectra

Sample Averaging → Region Selection → Baseline Removal → Intensity normalization → Mean Centering

Figure 1a

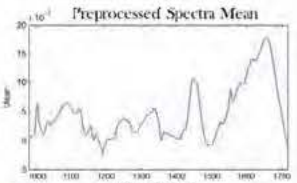

Figure 1b

Figure 1: Figure 1b represents Figure 1a after preprocessing (but before mean centering)

Step 2: Model Development

Partial Lease Squares Discriminant Analyses (PLSDA) is a multivariate inverse least squares discrimination method used to classify samples. It calculates a prediction probability and a classification threshold for each class modeled.[2]

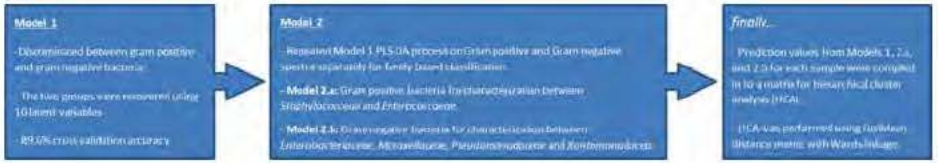

Step 3: Model Analysis
- Raman Spectra clustering was compared to clustering of other data types and taxonomic classification of bacteria.
- In order to compare and measure cluster validity, F-measures were calculated for each data type on the genus, family, and gram+/- levels. F-measure is the harmonic mean of precision and recall:[3]

$$Precision = \frac{tp}{tp+fp} \qquad Recall = \frac{tp}{tp+fn} \qquad F = 2\,\frac{precision \cdot recall}{precision+recall}$$

Figure 2: Taxonomic classification including kingdom phylum class order family genus and species of all isolates.

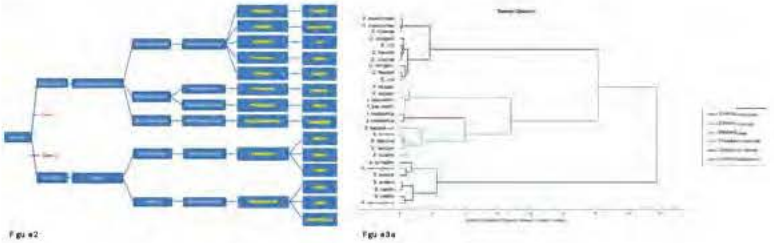

Figu e2

Figu e3a

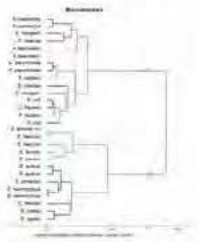

Figu e3b

Figu e3c

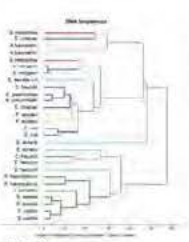

Figu e3d

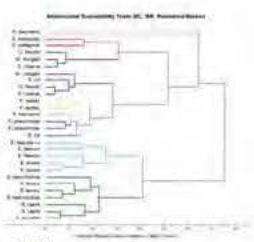

Figu e3e

Summary of Results & Conclusions

As visualized in comparison of known taxonomic classification with our model for Raman classification, (Figs. 2 and 3a) the model is successful in correctly classifying a majority of the isolates into exclusive family groups. This demonstrates the ability of Raman spectra data to differentiate between bacteria using PLS-DA and hierarchical cluster analysis.

	F-Measure		
	Family	Genus	Gram
Biochemistries	0.825	0.893	0.973
Antimicrobial Resistance	0.914	0.914	0.973
DNA Sequences	0.822	0.826	0.973
HRM	0.826	0.882	0.973
Spectra	0.856	0.926	0.973

Figure 4

It should be noted that while clustering of Raman spectra is clearly not perfect, neither are any of the other data types (Figs. 3b-3e). F-measures demonstrate similar precision and recall for dendrograms of each data type (Fig. 4).

Challenges
- There was concern that many samples gave highly fluorescent spectra. However, this may have actually contributed to better discrimination between bacterial isolates when applied to our model.
- Occasionally, spectra from blood agar plates would appear distinctly different than those of LBA plates for the same isolate. We decided that in the future we use only LBA plates.

Future Plans
- Test HCA model with a validation set of bacterial isolates.
- Collect spectra using SERS and using an 830-nm laser and repeat experiment
- Collect spectra of wound effluent samples directly to determine if identification and classification of bacterial infection is possible using our model.

References

1. Dereeper A., Guignon V., Blanc G., Audic S., Buffet S., Chevenet F., Dufayard J.-F., Guindon S., Lefort V., Lescot M., Claverie J.-M., Gascuel O. *Phylogeny.fr: robust phylogenetic analysis for the non-specialist* Nucleic Acids Research. 2008 Jul 1;36 (Web Server Issue) W465-9. Epub 2008 Apr 19.

2. "Plsda." - *Eigenvector Documentation Wiki*. Eigenvector Research Inc., 09 June 2014. Web. 19 Sept. 2014.<http //wiki.eigenvector.com/index.php?title Plsda>.

3. E. Rendon, I. Abandez, A. Arizmendi and E. M. Quiroz. Internal Versus External Cluster Validation Indexes. *International Journal of computers and communications*. 2011 27-34.

Acknowledgements

Multivariate Approaches to Predicting Wound Outcome Using Multimodal Data

Nicole Crane, Ph.D.

Advanced Surgical Imaging Program
Department of Regenerative Medicine
Naval Medical Research Center
Silver Spring, MD

Department of Surgery
Uniformed Services University of Health Sciences
Bethesda, MD

Disclaimer

The views expressed in this presentation are those of the author and do not necessarily reflect the official policy or position of the Department of the Navy, the Department of Defense, nor the U.S. Government.

This work was supported/funded by work unit number 602115HP.3720.001.A1015. Funding Support includes DoD BUMED Advance Medical Development 0604771N; USAMRMC Military Medical Research and Development OR090136**;** Defense Medical Research and Development Plan D10_I_AR_J2_501.

The study protocols were approved by the Walter Reed National Military Medical Center and Naval Medical Research Center Institutional Review Boards in compliance with all applicable Federal regulations governing the protection of human subjects.

I am a military service member (or employee of the U.S. Government). This work was prepared as part of my official duties. Title 17 U.S.C. 105 provides the “Copyright protection under this title is not available for any work of the United States Government.” Title 17 U.S.C. 101 defines a U.S. Government work as a work prepared by a military service member or employee of the U.S. Government as part of that person’s official duties.

I certify that the document represents valid work; that if I used information derived from another source, I obtained all necessary approvals to use it and made appropriate acknowledgements in the document; and I take public responsibility for it.

Military Medicine - NMRC

Our team leverages real-world experience in combat casualty care: heterotopic ossification, wound healing, advanced surgical imaging, transplant tolerance, and stem cells.

In addition, we develop novel and dynamic bioinformatic approaches to deliver point-of-care personalized medicine.

- *3-CCD Imaging*
- *IR Imaging*
- *Raman Spectroscopy*

Technologies that can non-invasively and objectively assess the wound microenvironment are critical for understanding and evaluating the wound healing process.

Accurate assessment of extremity injuries and wounds is necessary for appropriate treatment in the operating room.

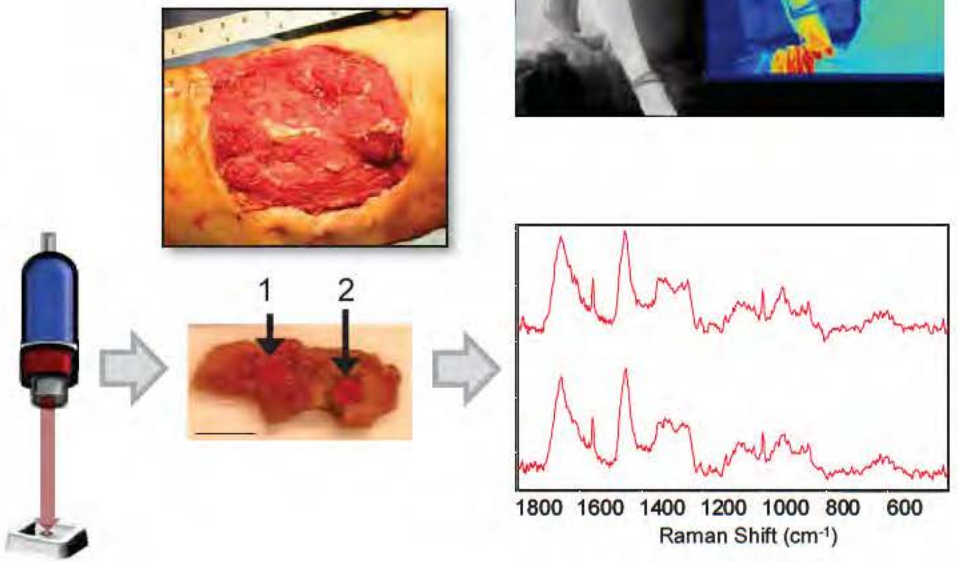

Wound Repair Regen. 2010 Jul-Aug;18(4):409-16.
J Urol. 2010 Oct;184(4):1279-85.
J Bone Joint Surg Am. 2010 Dec;92 Suppl 2:74-89.
J Pediatr Surg. 2012 Jan;47(1):142-7.
J Biomed Opt. 2012 Jan;17(1):010902.
Bone. 2013 Sep 5;57(2):335-342.

Acute Combat Wounds

Modern war ballistics inflict devastating extremity injuries, violating soft tissue, bone, and neurovascular structures.

Complex war wounds require aggressive surgical care. Serial debridements are performed to remove devitalized tissue and decrease bacterial load.

High-pressure irrigation and vacuum-assisted closure device (VAC) application have improved wound management.

The ensuing inflammatory response ultimately dictates the pace of wound healing and tissue regeneration.

Despite these technological advances, the basic surgical decision regarding appropriate timing of war wound closure remains subjective, and some wounds dehisce.

REGMED

Current Treatment and Challenges

Surgical debridements are performed every 2-3 days to remove devitalized tissue and reduce the bacterial load.

- Negative pressure wound therapy (NPWT) is applied between debridements - promote wound closure.

Wound assessment involves: patient's general condition, injury location, adequacy of perfusion, and gross appearance of the wound.

Our goal is to **monitor wound healing *in vivo***, i.e. monitor wound healing during surgical debridements.

- *Is it the best time to close the wound?*
- *Is the wound developing HO?*
- *Is the wound infected? With what?*

Develop an **objective and predictive model for wound healing**.

Our Toolbox

Multiplex Protein Assay (Luminex)

Raman Spectroscopy

Gene Expression (RT-PCR)

Clinical Data

Serum Chemistry

Clinical Data

Clinical data includes mostly observational variables.

ID	ISS head	Blood products	Antibiotic beads	Antibiotics (19 types)
Age	ISS face	Type of closure	Wound outcome	Neurontin
BMI	ISS chest	Wound type	HO wound and grade	Ambien
Tobacco use	ISS abdomen	Amputation	Days post injury	Valium
Mechanism of injury	ISS extremity	Surface Area	Days until closure	Nortriptyline
OIF/OEF	ISS skin	Vascular injury	APACHEII	Amitriptyline
TBI	ISS total	Neurologic injury	Albumin	Seroquel

Identifiers were removed from the analysis.

Outcome related data points were removed.

Data points with too many missing values were excluded – VTE, detailed blood product information.

Luminex (Multiplex Protein Assay)

The Luminex 100/200 System is a flexible analyzer based on the principles of flow cytometry.

The system enables you to multiplex (simultaneously measure) up to 100 analytes in a single microplate well, using very small sample volumes.

- family of 100 fluorescently dyed 5.6 micron-sized polystyrene microspheres that act as both the identifier and the solid surface to build the assay
- flow cytometry-based instrument
- Company software which is designed for protocol-based data acquisition with robust data regression analysis

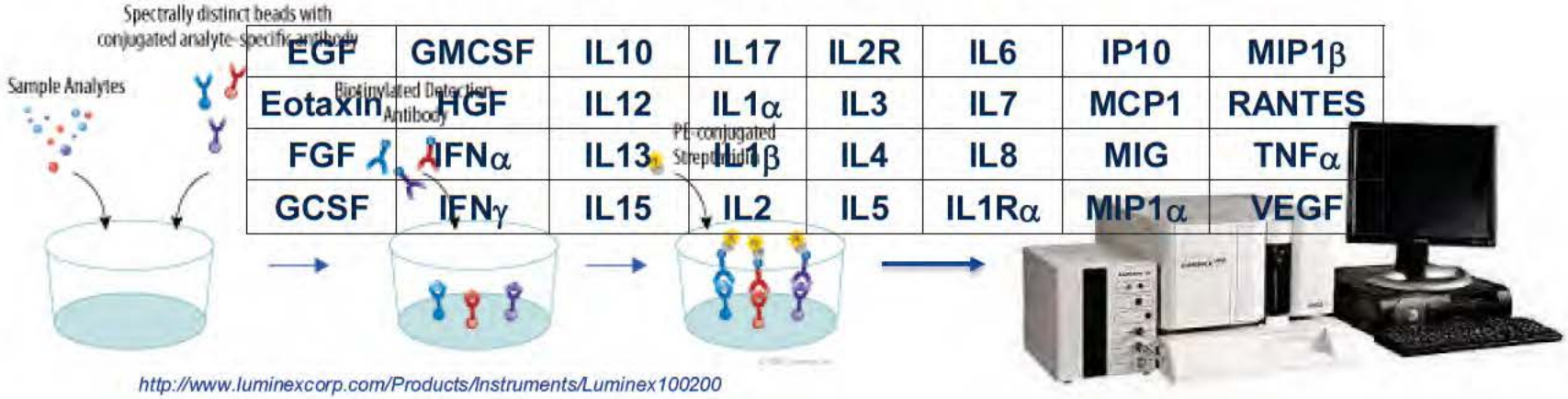

EGF	GMCSF	IL10	IL17	IL2R	IL6	IP10	MIP1β
Eotaxin	HGF	IL12	IL1α	IL3	IL7	MCP1	RANTES
FGF	IFNα	IL13	IL1β	IL4	IL8	MIG	TNFα
GCSF	IFNγ	IL15	IL2	IL5	IL1Rα	MIP1α	VEGF

http://www.luminexcorp.com/Products/Instruments/Luminex100200

Raman Spectroscopy

Raman spectroscopy can be utilized non-invasively and provide real-time feedback.

Raman spectra of biological materials are not affected by spectral interference of water.

Raman spectroscopy is sensitive to both organic and inorganic components.

USA Today, February 12, 2006.

Some biopsies may contain both soft tissue (muscle, fat, vessel, nerve) and mineralized tissue (cartilage and bone).

Heterotopic ossification (HO) refers to the aberrant formation of mature, lamellar bone in non-osseous tissues and is a complication in over 60% of OIF/OEF combat wounds.

Raman Spectroscopy for Wound Healing

Approximately 1 cm^3 of tissue is collected from the center of the debrided wound bed.

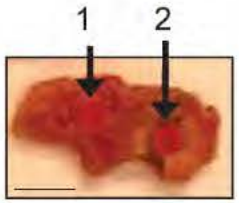

Several spots are examined on the biopsy.

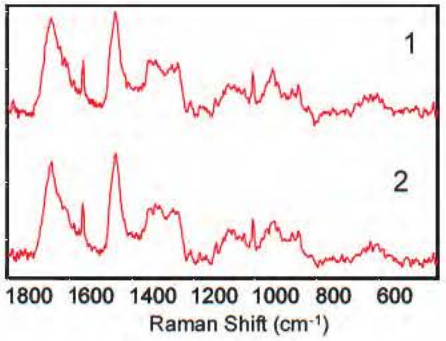

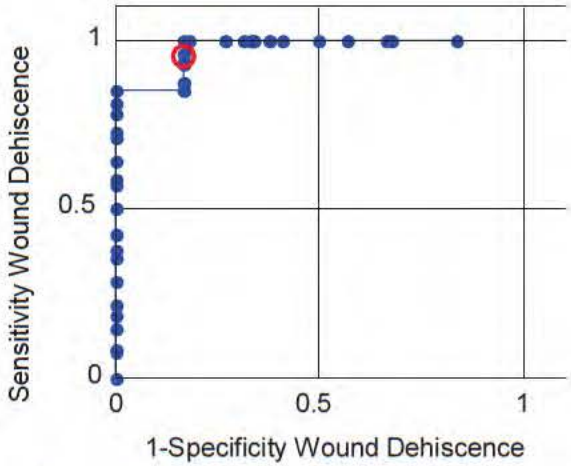

Confusion	Actual	*Healed*	*Dehisced*
Predicted	*Healed*	25	1
	Dehisced	6	26

A prediction model (PLSDA) can be created and validated.

92.9% Sensitivity, **83.3%** Specificity for wound dehiscence

REGMED

Calibration and Validation Data Sets

Preliminary Data Analysis – 58 Calibration samples, 23 Validation Samples

- 53% Healed, 47% Dehisced, 60% HO, 40% no HO

189 Calibration Samples -

- 72% Healed, 28% Dehisced, 60% HO, 40% no HO

65 Validation Samples -

- 72% Healed, 28% Dehisced, 60% HO, 40% no HO

Clinical Data – 61 variables (everything), 45 variables (point of care only)

Luminex Data – 96 variables (everything), 32 variables (serum), 64 variables (effluent, 2 dilutions)

Raman Spectroscopic Data – 785nm spectra have 6484 variables

Clinical Data - PCA

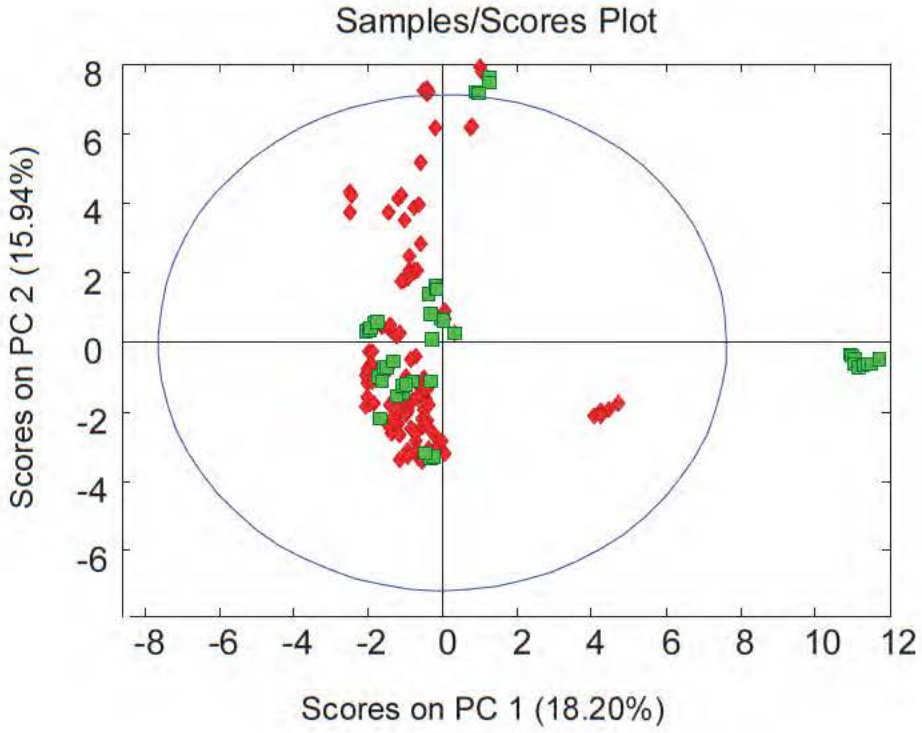

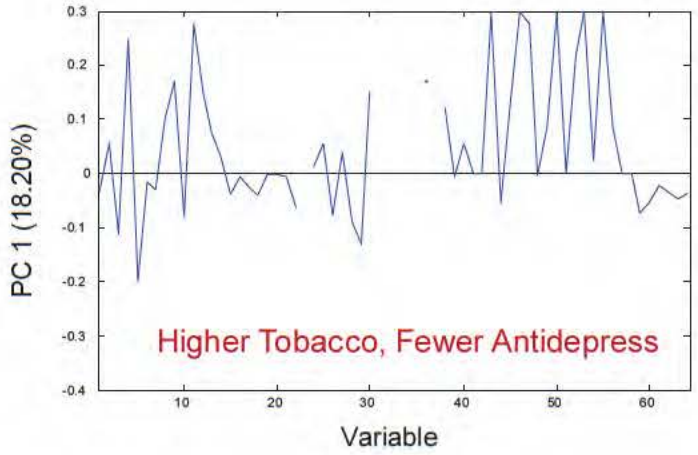

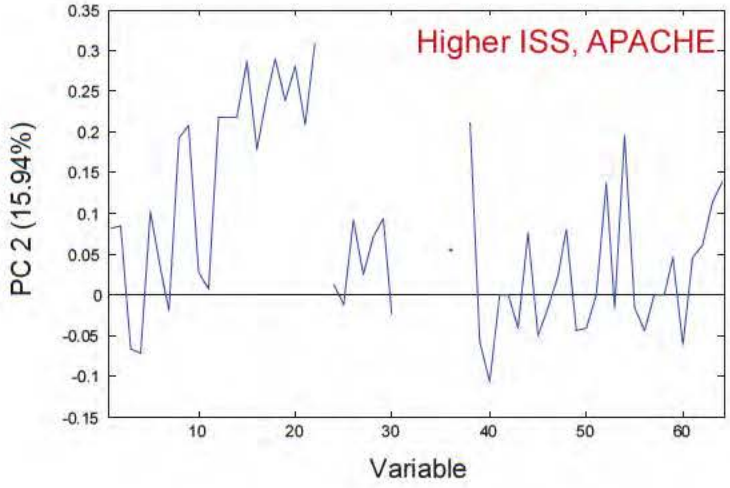

8 LVs, autoscale, (random subsets – 16 splits, 10 iterations)

REGMED

Luminex Data - PCA

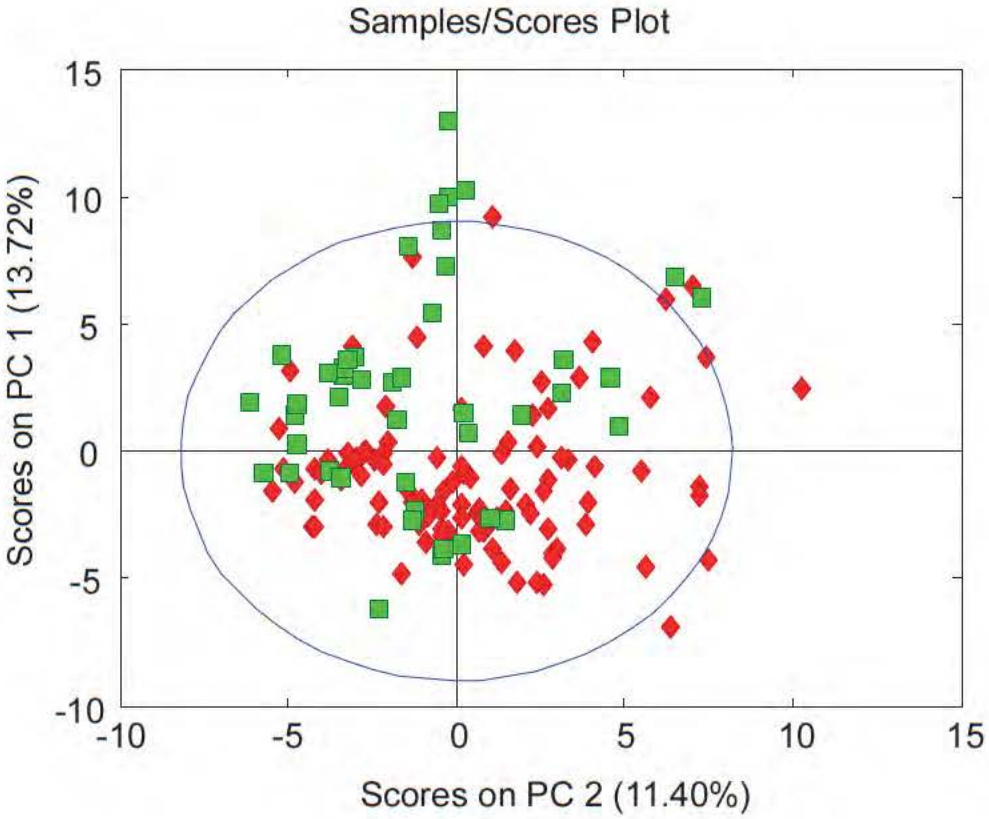

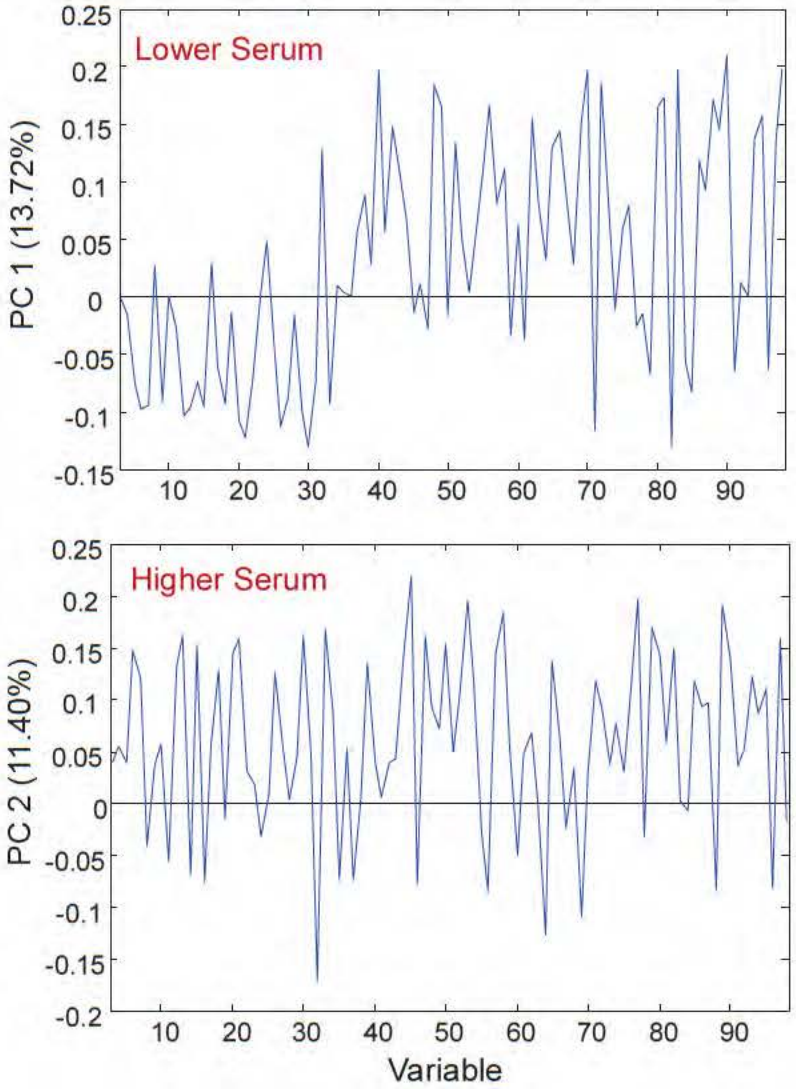

8 LVs, autoscale, (random subsets – 16 splits, 10 iterations)

REG MED

Raman Spectra (785nm) - PCA

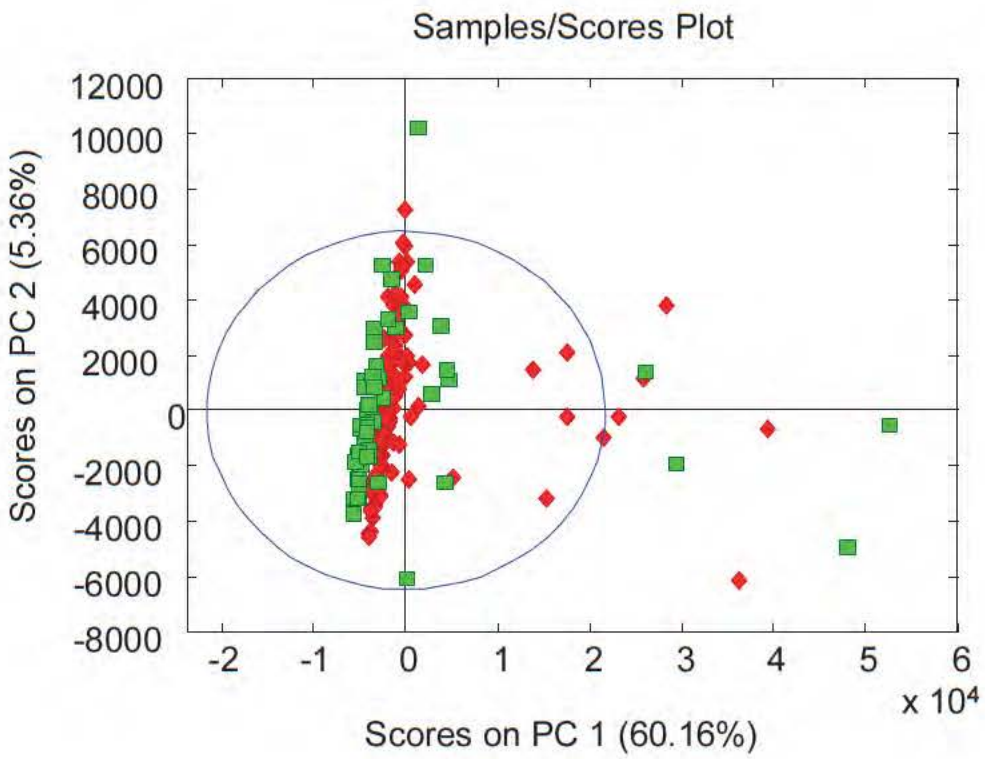

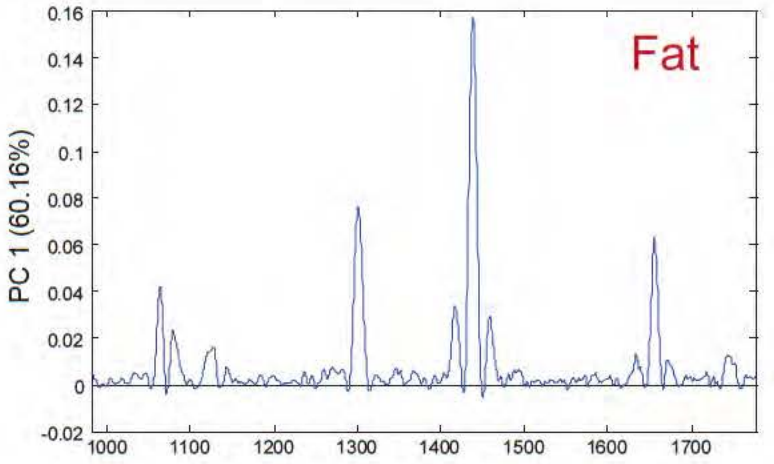

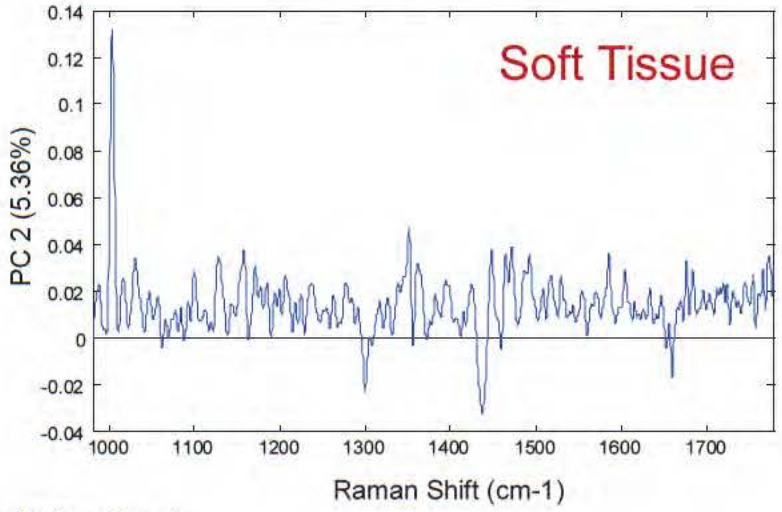

4 LVs, class center, automatic Whittaker baseline, (random subsets – 16 splits, 10 iterations)

Clinical Variables - PLSDA

Predicted ROCs – all variables except outcome

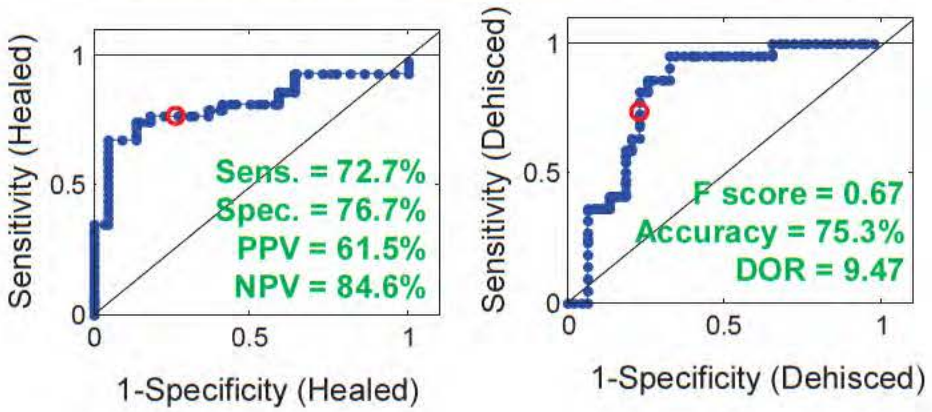

Confusion	Actual	*Healed*	*Dehisced*
Predicted	*Healed*	33	6
	Dehisced	10	16

AUC = 0.8118

Predicted ROCs – POC variables only

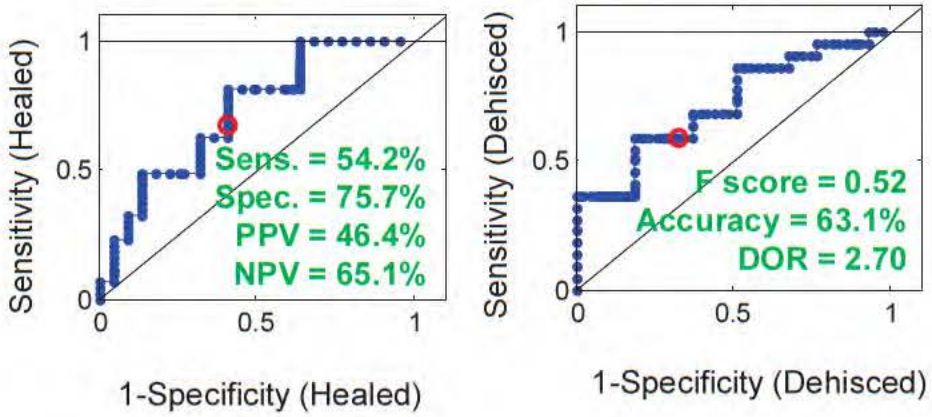

Confusion	Actual	*Healed*	*Dehisced*
Predicted	*Healed*	28	9
	Dehisced	15	13

AUC = 0.7230

8 LVs, autoscale preprocessing, (random subsets – 16 splits, 10 iterations)

Clinical Variables - KNN

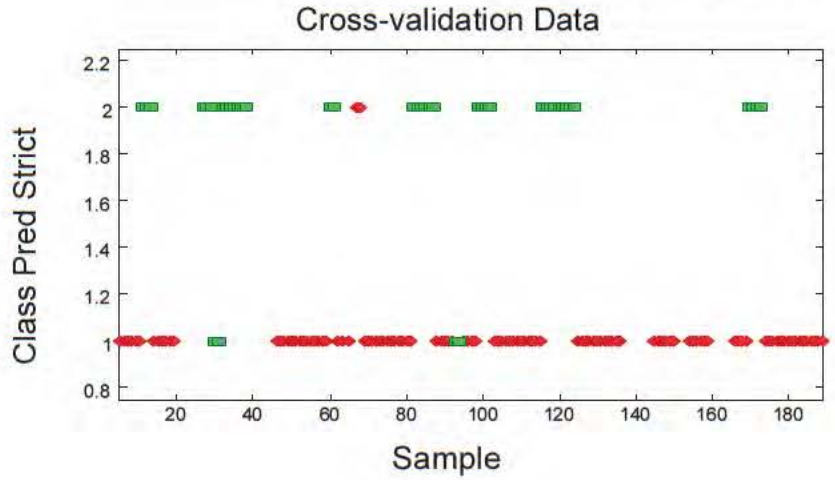

Confusion	Actual	*Healed*	*Dehisced*
Predicted	*Healed*	97	0
	Dehisced	0	31

Sens. = 0%
Spec. = 77.5%
PPV = 0%
NPV = 72.1%

F score = 0
Accuracy = 59.0%
DOR = 0

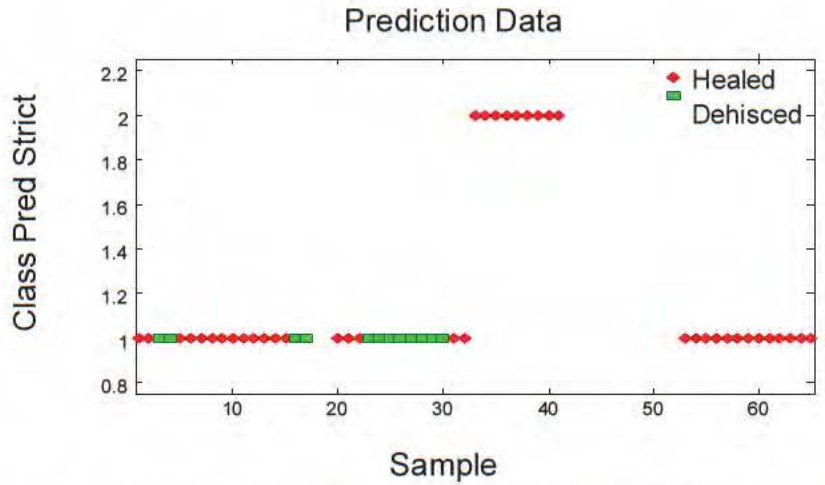

Confusion	Actual	*Healed*	*Dehisced*
Predicted	*Healed*	31	12
	Dehisced	9	0

k=3, excluded 37 samples for calibration, 13 samples for prediction (random subsets – 16 splits, 10 iterations)

Luminex Variables - PLSDA

Predicted ROCs – all variables except outcome

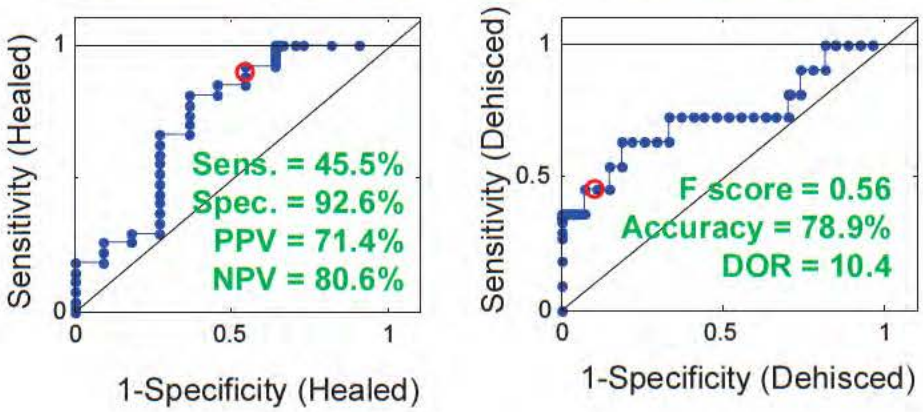

Confusion	Actual	*Healed*	*Dehisced*
Predicted	*Healed*	25	6
	Dehisced	2	5

AUC = 0.7273

Predicted ROCs – Effluent variables only

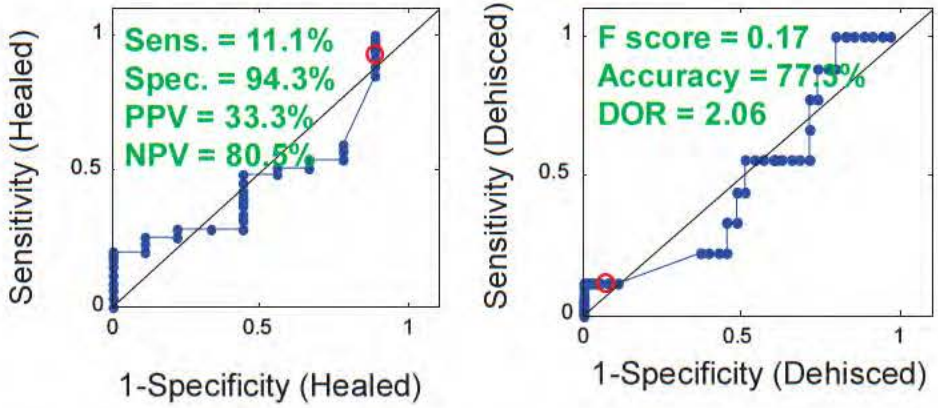

Confusion	Actual	*Healed*	*Dehisced*
Predicted	*Healed*	33	8
	Dehisced	2	1

AUC = 0.4810

3 LVs, autoscale preprocessing, 27 and 21 samples excluded (random subsets – 16 splits, 10 iterations)

Luminex Variables - KNN

All Luminex variables – serum and effluent

Sensitivity = 100%
Specificity = 100%
PPV = 100%
NPV = 100%
F score = 1.0
Accuracy = 100%

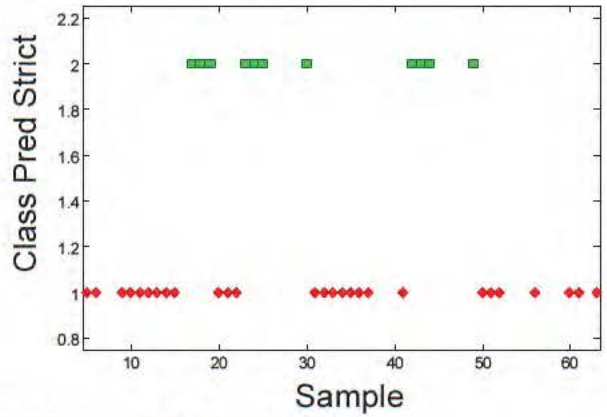

Confusion	Actual	*Healed*	*Dehisced*
Predicted	*Healed*	27	0
	Dehisced	0	11

Luminex variables – effluent only

Sensitivity = 91.7%
Specificity = 100%
PPV = 100%
NPV = 97.6%
F score = 0.96
Accuracy = 98.1%

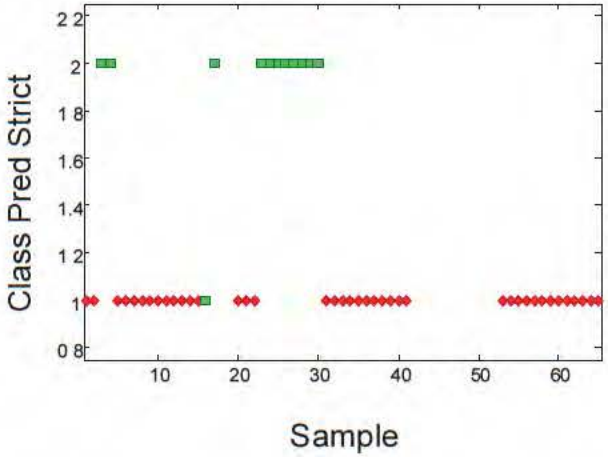

Confusion	Actual	*Healed*	*Dehisced*
Predicted	*Healed*	28	9
	Dehisced	15	13

k=3/8, class center, excluded 29/54 samples for calibration, 27/13 samples for prediction (random subsets – 16 splits, 10 iterations)

REGMED

Raman Spectra (785nm) Only

PLSDA Predicted ROCs

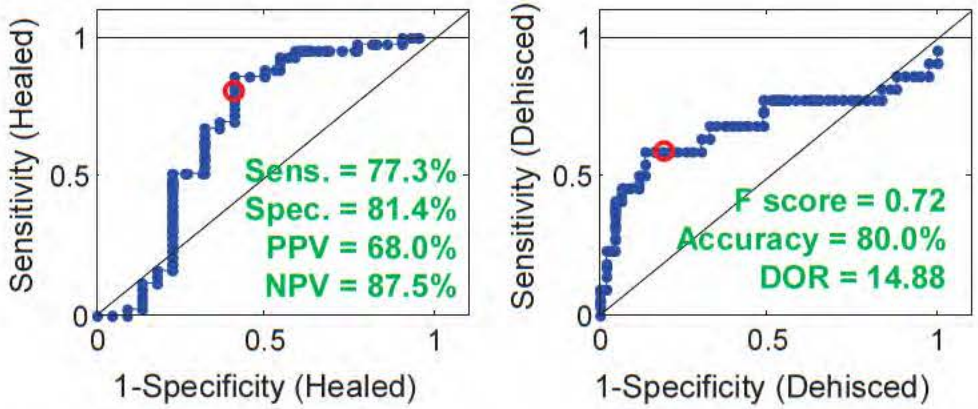

Confusion	Actual	*Healed*	*Dehisced*
Predicted	*Healed*	35	7
	Dehisced	8	15

AUC = 0.6808

3 LVs, class center, automatic Whittaker baseline, truncated 980-1746 cm^{-1}, random subsets – 16 splits, 10 iterations

KNN

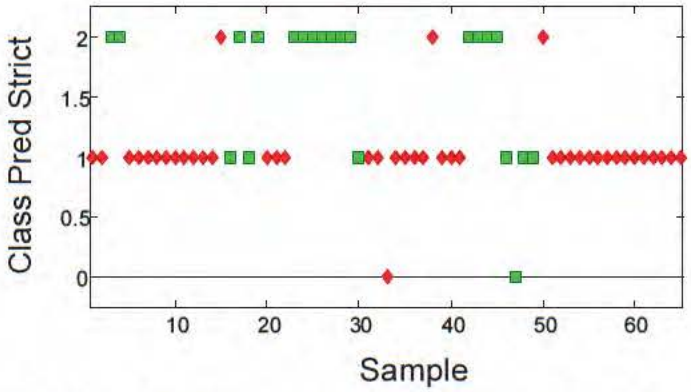

Confusion	Actual	*Healed*	*Dehisced*
Predicted	*Healed*	40	7
	Dehisced	3	15

Sensitivity = 68.2%
Specificity = 93%
PPV = 83.3%
NPV = 85.1%
F score = 0.75
Accuracy = 84.6%
DOR = 28.6

k=8, class center, automatic Whittaker baseline, truncated 980-1746 cm^{-1}, random subsets – 16 splits, 10 iterations

REGMED

Clinical and Luminex Variables

PLSDA Predicted ROCs – clinical and serum

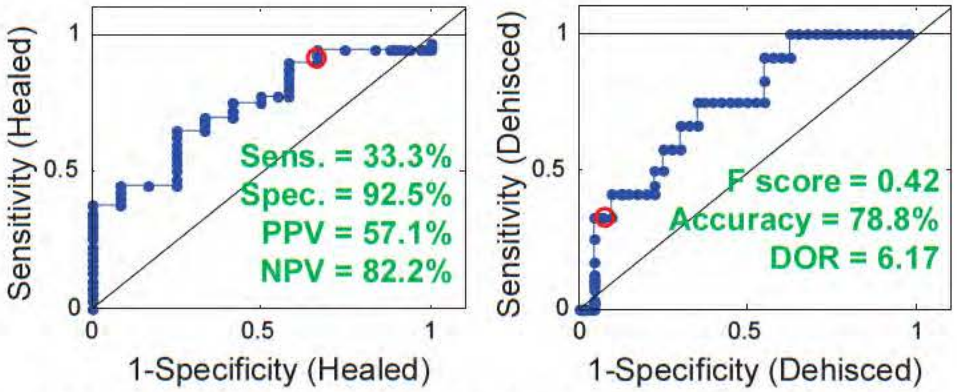

Confusion	Actual	*Healed*	*Dehisced*
Predicted	*Healed*	37	8
	Dehisced	3	4

AUC = 0.7375

4 LVs, autoscale preprocessing, 37 and 13 samples excluded (random subsets – 16 splits, 10 iterations)

KNN – clinical and effluent

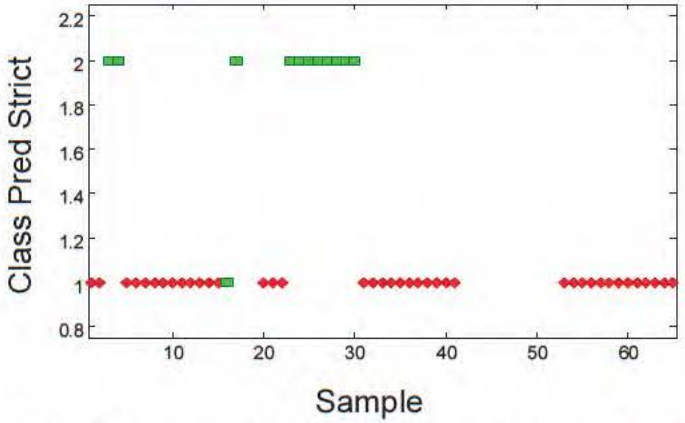

Confusion	Actual	*Healed*	*Dehisced*
Predicted	*Healed*	40	1
	Dehisced	0	11

Sensitivity = 91.7%
Specificity = 100%
PPV = 100%
NPV = 97.6%
F score = 0.96
Accuracy = 98.1%

k=8, class center, excluded 54 samples for calibration, 13 samples for prediction

REGMED

Clinical, Luminex, and Raman Variables

PLSDA Predicted ROCs – clinical, Luminex and Raman

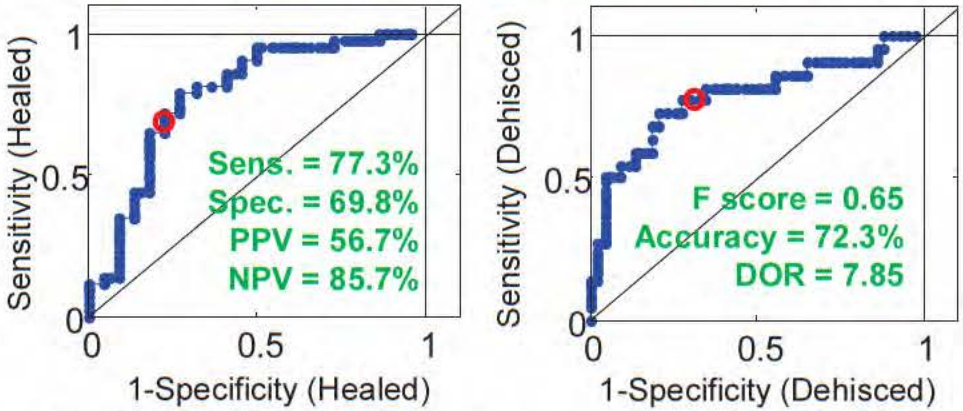

Confusion	Actual	*Healed*	*Dehisced*
Predicted	*Healed*	30	5
	Dehisced	13	17

AUC = 0.7865

6 LVs, class center, automatic Whittaker baseline preprocessing, truncated 980-1746 cm^{-1}, (random subsets – 16 splits, 10 iterations)

KNN – clinical, Luminex, and Raman

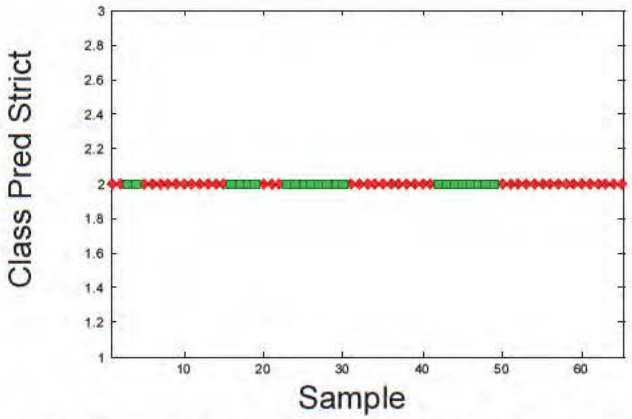

Confusion	Actual	*Healed*	*Dehisced*
Predicted	*Healed*	0	0
	Dehisced	43	22

Sensitivity = 100%
Specificity = 0%
PPV = 33.8%
NPV =
F score = 0.51
Accuracy = 33.8

k=8, class center, automatic Whittaker baseline, truncated 980-1746 cm^{-1}, (random subsets – 16 splits, 10 iterations)

REGMED

Summary of Results

Classification	Data Sets	Sensitivity	Specificity	PPV	NPV	F score	Accuracy	DOR
PLSDA	C (≠O)	72.7	76.7	61.5	84.6	0.67	75.3	9.5
PLSDA	C (≠O), POC	54.2	75.7	46.4	65.1	0.52	63.1	2.7
KNN	C (≠O)	0.0	77.5	0.0	72.1	0.00	59.0	0.0
PLSDA	L, all	45.5	92.6	71.4	80.6	0.56	78.9	10.4
PLSDA	L, eff	11.1	94.3	33.3	80.5	0.17	77.3	2.1
KNN	L, all	100.0	100.0	100.0	100.0	1.00	100.0	
KNN	L, eff	[illegible]	[illegible]	[illegible]	[illegible]	[illegible]	[illegible]	
PLSDA	R	[illegible]	[illegible]	[illegible]	[illegible]	[illegible]	[illegible]	[illegible]
KNN	R	68.2	93.0	83.3	85.1	0.75	84.6	28.6
PLSDA	C, L serum	[illegible]	[illegible]	[illegible]	[illegible]	[illegible]	[illegible]	[illegible]
KNN	C, L eff	91.7	100.0	100.0	97.6	0.96	98.1	
PLSDA	all	[illegible]	[illegible]	[illegible]	[illegible]	[illegible]	[illegible]	[illegible]
KNN	all	100.0	0.0	33.8		0.51	33.8	

The diagnostic odds ratio is a measure of the effectiveness of a diagnostic test – the ratio of the odds of the test being positive if the subject has a disease relative to the odds of the test being positive if the subject does not have the disease.

F-score is the harmonic mean of precision and recall.

Conclusions

Luminex data, particularly the effluent data, show the highest sensitivity, specificity, accuracy and F score, but the results are suspicious.

The Raman data provides the next best sensitivity, specificity, accuracy, F scores, and the highest overall Diagnostic Odds Ratio (DOR).

Luminex data requires at least two hours for processing along with significant cost for consumables, in addition to instrumentation and assays.

Raman spectroscopy can be performed intraoperatively, with little to no consumable cost and no additional assay cost. Instrument cost is comparable.

Additional modelling techniques need to be explored.

This preliminary study demonstrates the promise of multimodal data sets, particularly multimodal data sets with spectroscopic components.

We need to further explore outcome modelling – healed vs. delayed healing vs. dehisced; develops HO versus does not develop HO.

Overall Concept

1) Apply best of breed technologies in

   - *biomarker analysis*
   - *informatics*
   - *medical technology*

2) Clinical Decision Support tools can be developed that can optimize and personalize treatment using *patient-specific clinical variables combined with local and systemic biomarkers.*

3) Goal: <u>maximize patient outcomes while minimizing complications</u>.

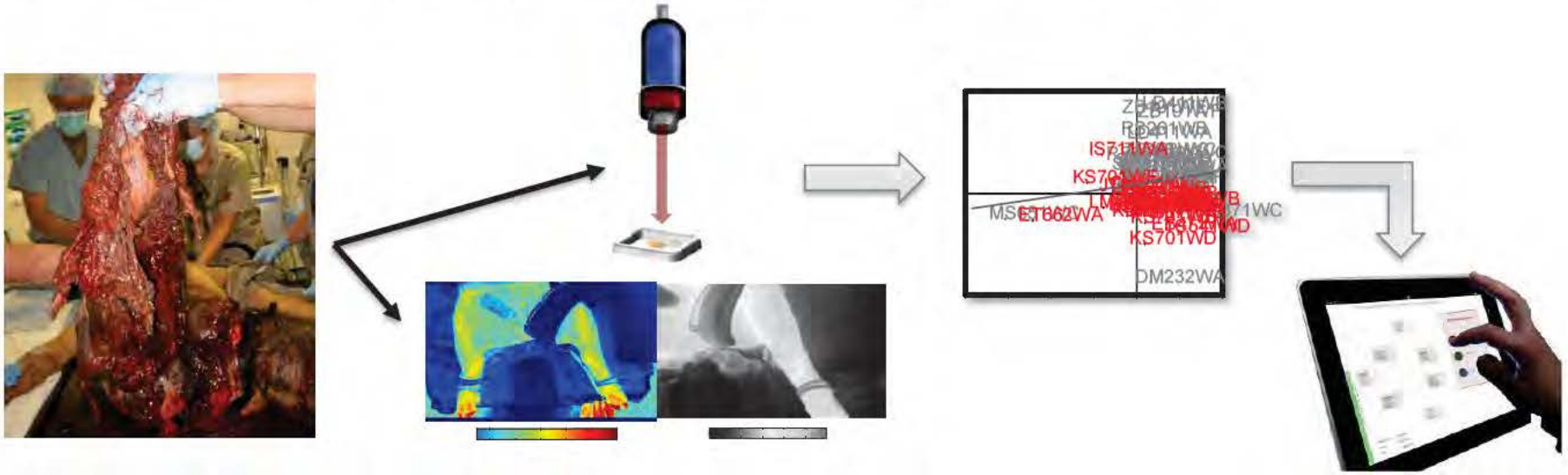

Acknowledgements

Regenerative Medicine Dept, NMRC

Jonathan Forsberg, MD
Thomas Davis, PhD
Nicole Crane, PhD
Trevor Brown, PhD
Matthew Wagner, PhD
Richard Barth, MS
Ying Cao, MS
Felipe Lisboa, MD
Khairul Anam, PhD
Anthony Foster, PhD
Ammar Qureshi, PhD
Michael Wiley, MBA
Mihret Amare, MS
Yelena Lazdun, MS
Chioma Aglibe, MS
Alison Tomasino, BS
Nick Clark, BS
Crystal Leonhardt
Stacia Moreno, BS
Fred Gage
Toby Perkins

Orthopaedics Dept, WRNMMCB

Romney Andersen, MD
B. Kyle Potter, MD
Wade Gordon, MD
Jean Claude D'Allyrand, MD
Robert Beer, MD
Mark Fleming, MD
Susan Foster, RN

Department of Surgery, USUHS

Eric Elster, MD FACS
Leon Nesti, MD, PhD
Arnaud Belard, MBA
Tiffani Slaughter, BS

REGMED
Shaping the Future of Casualty Care

THANK YOU!

Raman Spectroscopic Analysis of Combat Wounds

Nicole Crane, Ph.D.

Advanced Surgical Imaging Program
Regenerative Medicine Department
Naval Medical Research Center
Silver Spring, MD

Department of Surgery
Uniformed Services University of Health Sciences
Bethesda, MD

Disclaimer

The views expressed in this presentation are those of the author and do not necessarily reflect the official policy or position of the Department of the Navy, the Department of Defense, nor the U.S. Government.

This work was supported/funded by work unit number 602115HP.3720.001.A1015. Funding Support includes DoD BUMED Advance Medical Development 0604771N; USAMRMC Military Medical Research and Development OR090136; Defense Medical Research and Development Plan D10_I_AR_J2_501.

The study protocol (WRNMMC 374863) was approved by the Walter Reed National Military Medical Center Institutional Review Board in compliance with all applicable Federal regulations governing the protection of human subjects.

I am a military service member (or employee of the U.S. Government). This work was prepared as part of my official duties. Title 17 U.S.C. 105 provides the "Copyright protection under this title is not available for any work of the United States Government." Title 17 U.S.C. 101 defines a U.S. Government work as a work prepared by a military service member or employee of the U.S. Government as part of that person's official duties.

I certify that the document represents valid work; that if I used information derived from another source, I obtained all necessary approvals to use it and made appropriate acknowledgements in the document; and I take public responsibility for it.

Military Medicine - NMRC

Our team leverages real-world experience in combat casualty care: heterotopic ossification, wound healing, advanced surgical imaging, transplant tolerance, and stem cells.

In addition, we develop novel and dynamic bioinformatic approaches to deliver point-of-care personalized medicine.

- *3-CCD Imaging*
- *IR Imaging*
- *Raman Spectroscopy*

Technologies that can non-invasively and objectively assess the wound microenvironment are critical for understanding and evaluating the wound healing process.

Accurate assessment of extremity injuries and wounds is necessary for appropriate treatment in the operating room.

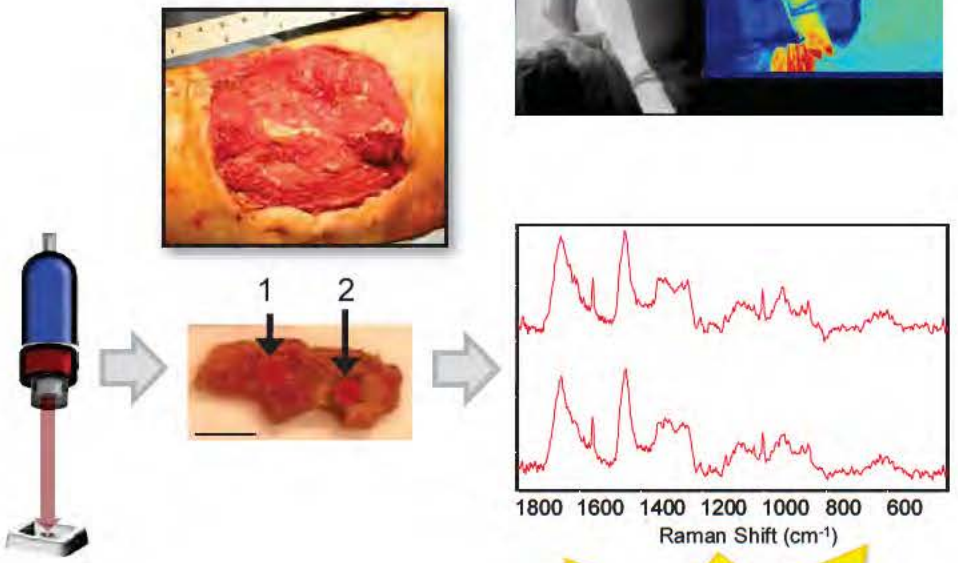

Wound Repair Regen. 2010 Jul-Aug;18(4):409-16.
J Urol. 2010 Oct;184(4):1279-85.
J Bone Joint Surg Am. 2010 Dec;92 Suppl 2:74-89.
J Pediatr Surg. 2012 Jan;47(1):142-7.
J Biomed Opt. 2012 Jan;17(1):010902.
Bone. 2013 Sep 5;57(2):335-342.

Graphic pictures next slide!

Acute Combat Wounds

Modern war ballistics inflict devastating extremity injuries, violating soft tissue, bone, and neurovascular structures.

Complex war wounds require aggressive surgical care. Serial debridements are performed to remove devitalized tissue and decrease bacterial load.

The ensuing inflammatory response ultimately dictates the pace of wound healing and tissue regeneration.

Despite these technological advances, the basic surgical decision regarding appropriate timing of war wound closure remains subjective, and some wounds dehisce.

REGMED

Current Treatment and Challenges

Surgical debridements are performed every 2-3 days to remove devitalized tissue and reduce the bacterial load.

- Negative pressure wound therapy (NPWT) is applied between debridements - promote wound closure.

Wound assessment involves: patient's general condition, injury location, adequacy of perfusion, and gross appearance of the wound.

Our goal is to **monitor wound healing *in vivo***, i.e. monitor wound healing during surgical debridements.

- *Is it the best time to close the wound?*
- *Is the wound developing HO?*
- *Is the wound infected? With what?*

Develop an **objective and predictive model for wound healing**.

Sample Collection

Wound is surgically cleaned

Collect 1 cm^3 tissue biopsy from center of wound bed

RT-PCR
Raman spectroscopy
Micro culture

NPWT is applied

Serum is collected

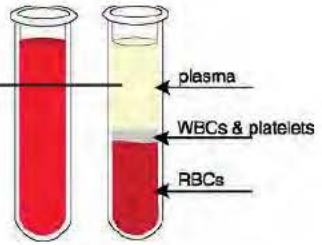

Protein assay

Effluent is collected

Protein assay

Raman spectroscopy
Micro culture

REGMED

Our Toolbox

Multiplex Protein Assay (Luminex)

Raman Spectroscopy

Gene Expression (RT-PCR)

Clinical Data

Serum Chemistry

Raman Spectroscopy

Raman Spectroscopy

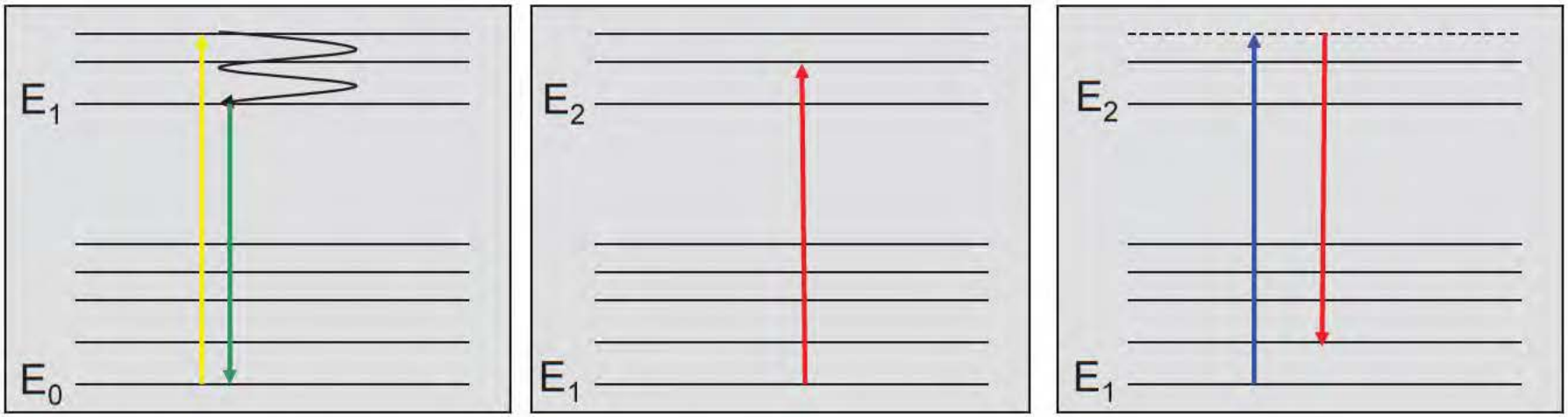

Fluorescence

Incident radiation (photon) excites the material to a vibrational state, where some energy is dissipated, and then emitted as photon so that the molecule relaxes back to the ground state.

Infrared

Radiation (energy from a photon) is absorbed by the material, exciting a vibrational mode.

Raman

Radiation (energy from a photon) interacts with the material, exciting it to a "virtual" vibrational state before emitting a photon (longer wavelength) to return to the ground state.

Peak Fitting for Spectral Deconvolution

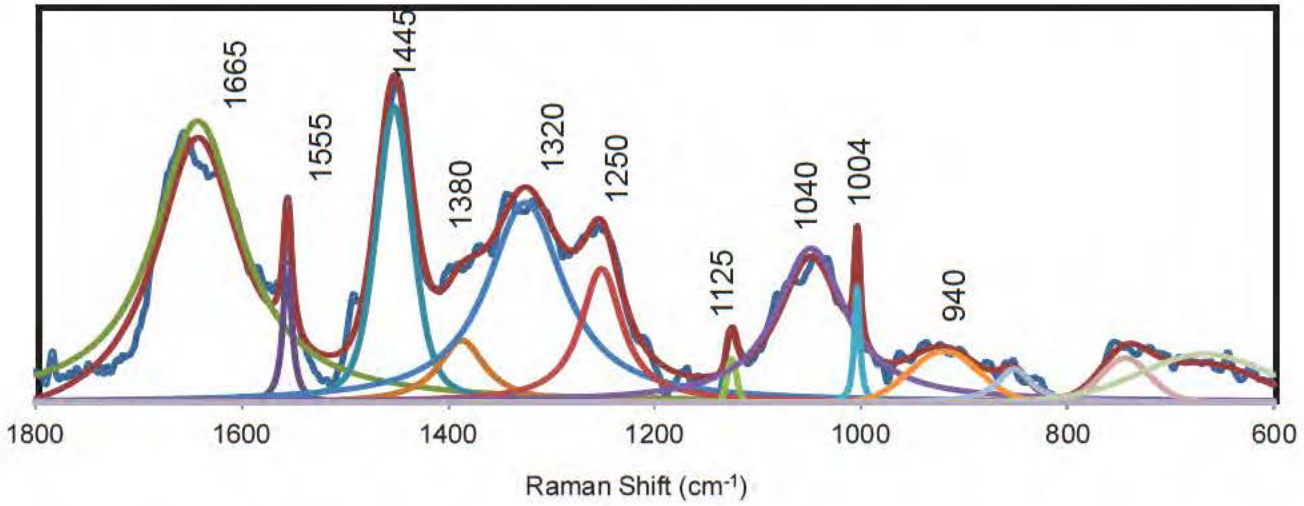

Raman Shift (cm^{-1})	Vibrational Band Assignment	Component
860	ν(C-C)	nucleic acids
920,940	ν(C-N), ν(C-C)	nucleic acids, keratin
1004	ν(C-C) ring	phenylalanine
1040	ν(C-C) skeletal	nucleic acids, protein
1125	ν(C-C), ν(C-N)	nucleic acids, protein
1250	ν (C-N) and δ(N-H); Amide III	protein
1320	$\delta(CH_2)$ twisting	nucleic acids, protein
1445	$\delta(CH_3)$ and $\delta(CH_{2})$ scissoring	protein
1555		aromatic amino acids, heme
1665	ν(C=O); Amide I	protein

REGMED

Wound Healing and Dehiscence

Clinical Data

Clinical data includes mostly observational variables.

ID	ISS head	Blood products	Antibiotic beads	Antibiotics (19 types)
Age	ISS face	Type of closure	Wound outcome	Neurontin
BMI	ISS chest	Wound type	HO wound and grade	Ambien
Tobacco use	ISS abdomen	Amputation	Days post injury	Valium
Mechanism of injury	ISS extremity	Surface Area	Days until closure	Nortriptyline
OIF/OEF	ISS skin	Vascular injury	APACHEII	Amitriptyline
TBI	ISS total	Neurologic injury	Albumin	Seroquel

Identifiers were removed from the analysis.

Outcome related data points were removed.

Data points with too many missing values were excluded – VTE, detailed blood product information.

Luminex (Multiplex Protein Assay)

The Luminex 100/200 System is a flexible analyzer based on the principles of flow cytometry.

The system enables you to multiplex (simultaneously measure) up to 100 analytes in a single microplate well, using very small sample volumes.

- family of 100 fluorescently dyed 5.6 micron-sized polystyrene microspheres that act as both the identifier and the solid surface to build the assay
- flow cytometry-based instrument

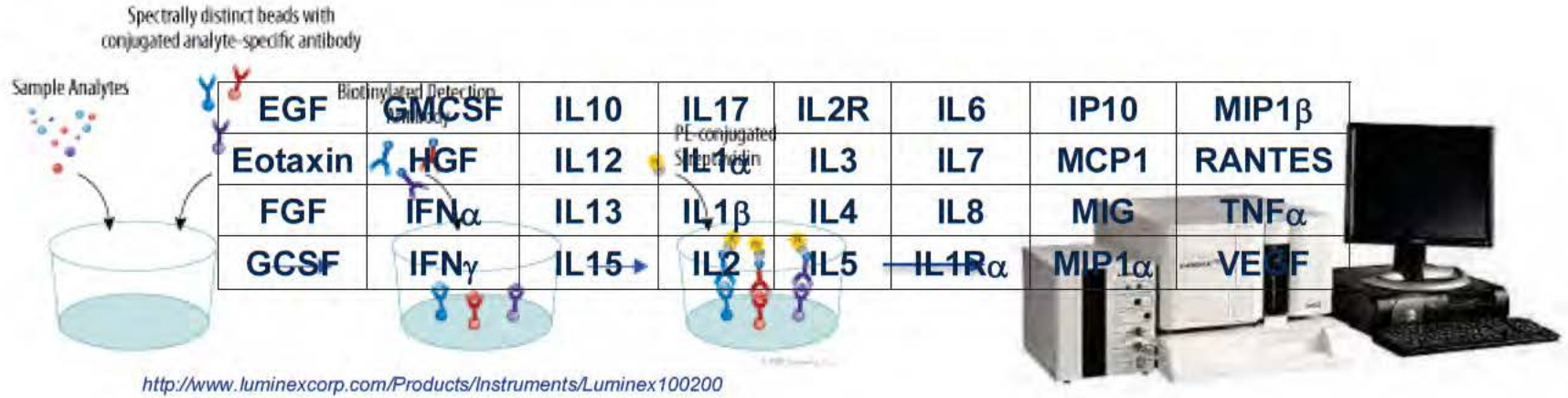

http://www.luminexcorp.com/Products/Instruments/Luminex100200

Raman Spectroscopy

Raman spectroscopy can be utilized non-invasively and provide real-time feedback.

Raman spectra of biological materials are not affected by spectral interference of water.

Raman spectroscopy is sensitive to both organic and inorganic components.

USA Today, February 12, 2006.

Some biopsies may contain both soft tissue (muscle, fat, vessel, nerve) and mineralized tissue (cartilage and bone).

Heterotopic ossification (HO) refers to the aberrant formation of mature, lamellar bone in non-osseous tissues and is a complication in over 60% of OIF/OEF combat wounds.

Raman Spectroscopy for Wound Healing

Approximately 1 cm^3 of tissue is collected from the center of the debrided wound bed.

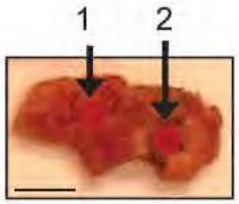

Several spots are examined on the biopsy.

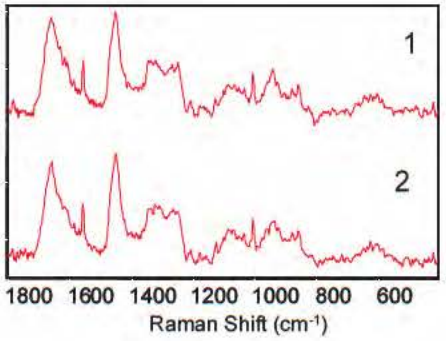

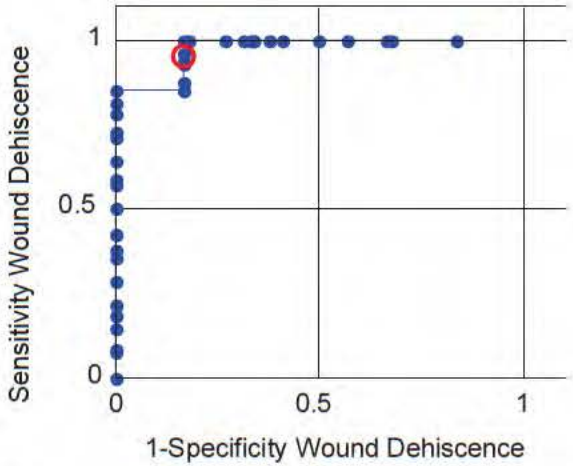

Confusion	Actual	*Healed*	*Dehisced*
Predicted	*Healed*	25	1
	Dehisced	6	26

A prediction model (PLSDA) can be created and validated.

92.9% Sensitivity, **83.3%** Specificity for wound dehiscence

REGMED

Calibration and Validation Data Sets

Preliminary Data Analysis – 58 Calibration samples, 23 Validation Samples

- 53% Healed, 47% Dehisced, 60% HO, 40% no HO

189 Calibration Samples -

- 72% Healed, 28% Dehisced, 60% HO, 40% no HO

65 Validation Samples -

- 72% Healed, 28% Dehisced, 60% HO, 40% no HO

Clinical Data – 61 variables (everything), 45 variables (point of care only)

Luminex Data – 96 variables (everything), 32 variables (serum), 64 variables (effluent, 2 dilutions)

Raman Spectroscopic Data – 785nm spectra have 6484 variables

Principal Component Analysis

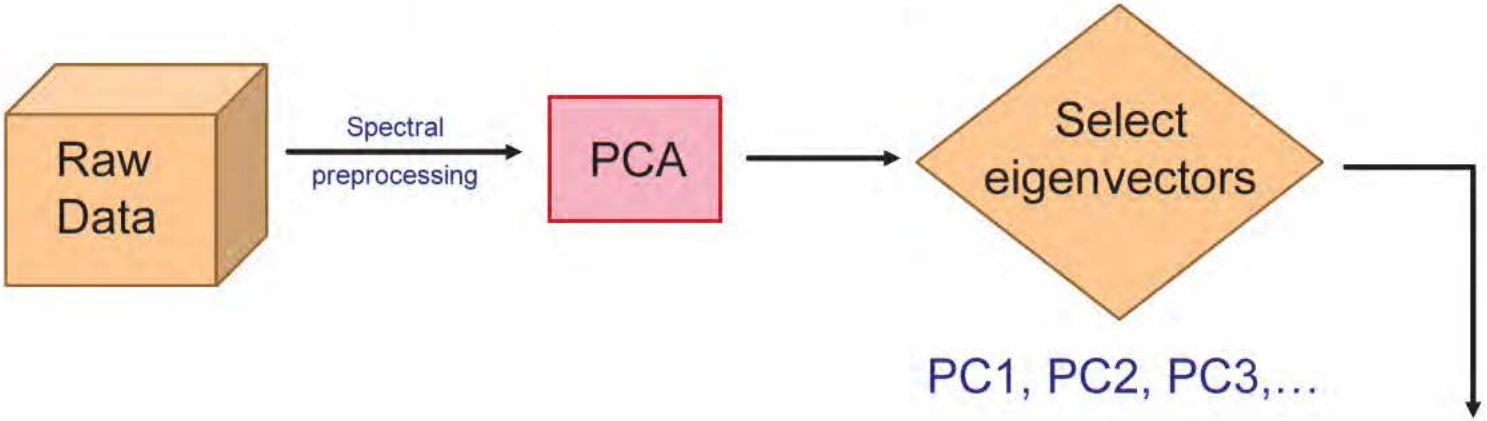

Orthogonal transformation to convert a set of spectra of possibly correlated variables (Raman shifts and/or bands) into a set of values of linearly uncorrelated variables called principal components (PCs).

The first PC is orthogonal to the other PCs.

This can be used to reduce dimensionality of the data set and to visualize the variance in the data – often a first step in PLSDA.

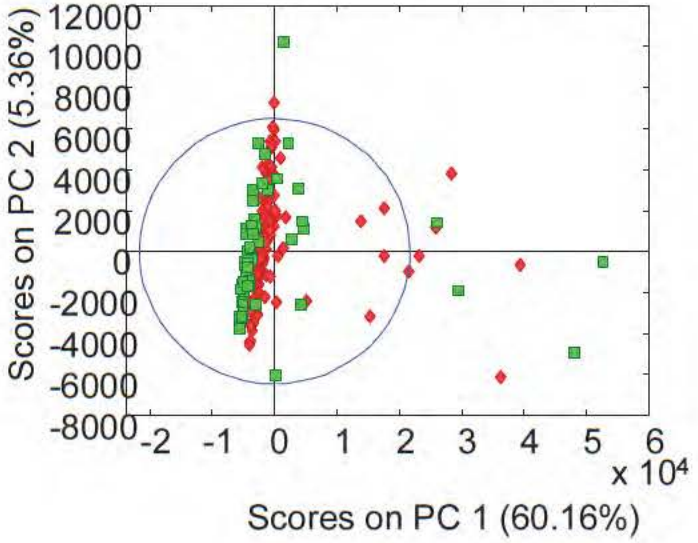

Clinical Data - PCA

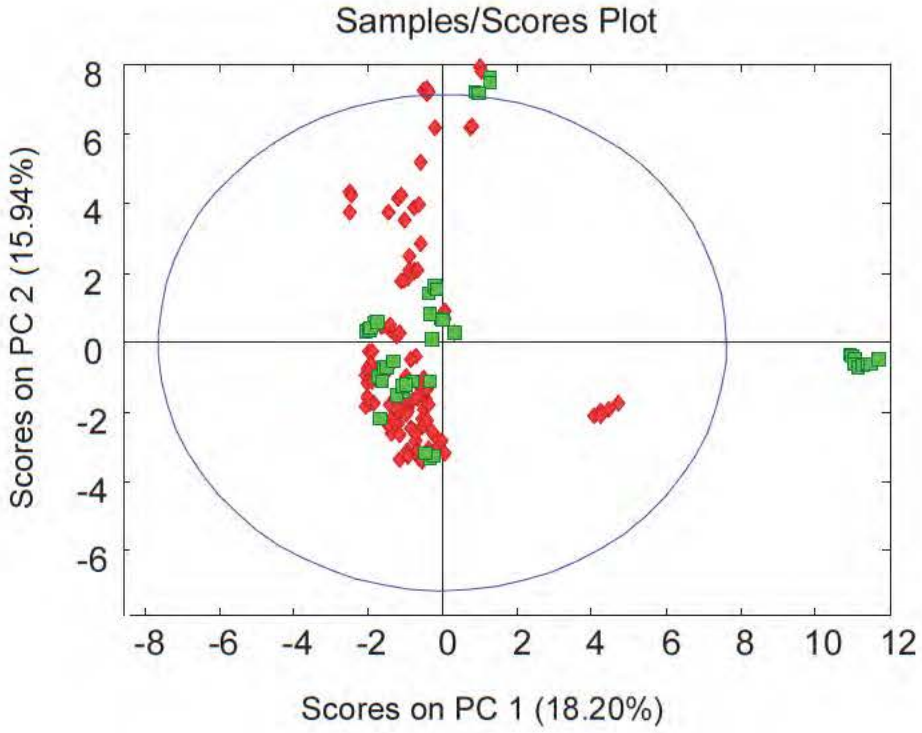

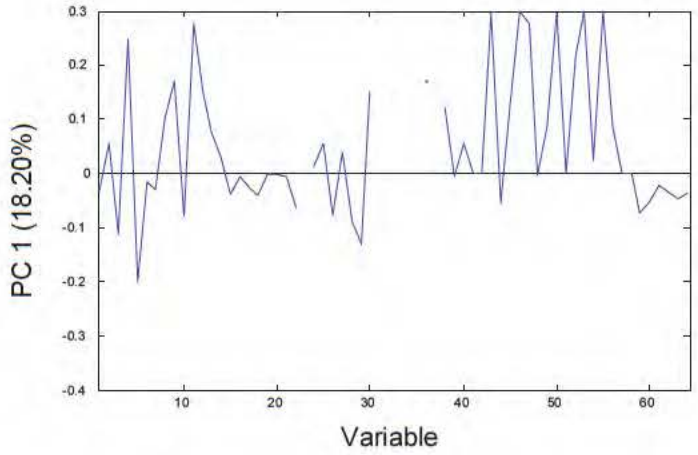

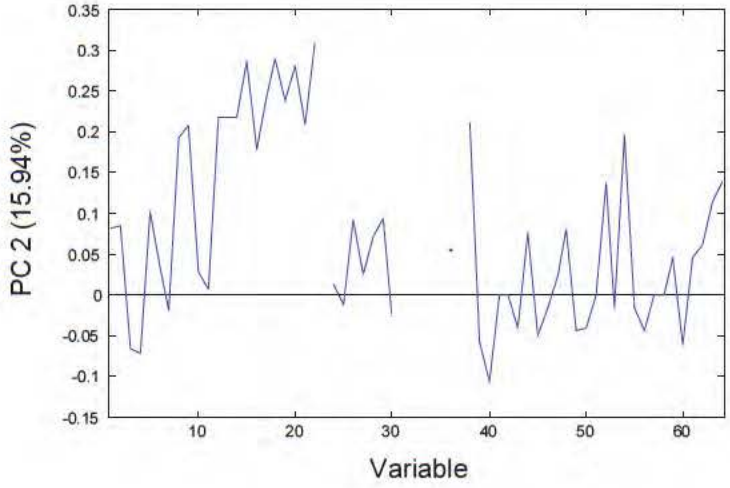

8 LVs, autoscale, (random subsets – 16 splits, 10 iterations)

REGMED

Luminex Data - PCA

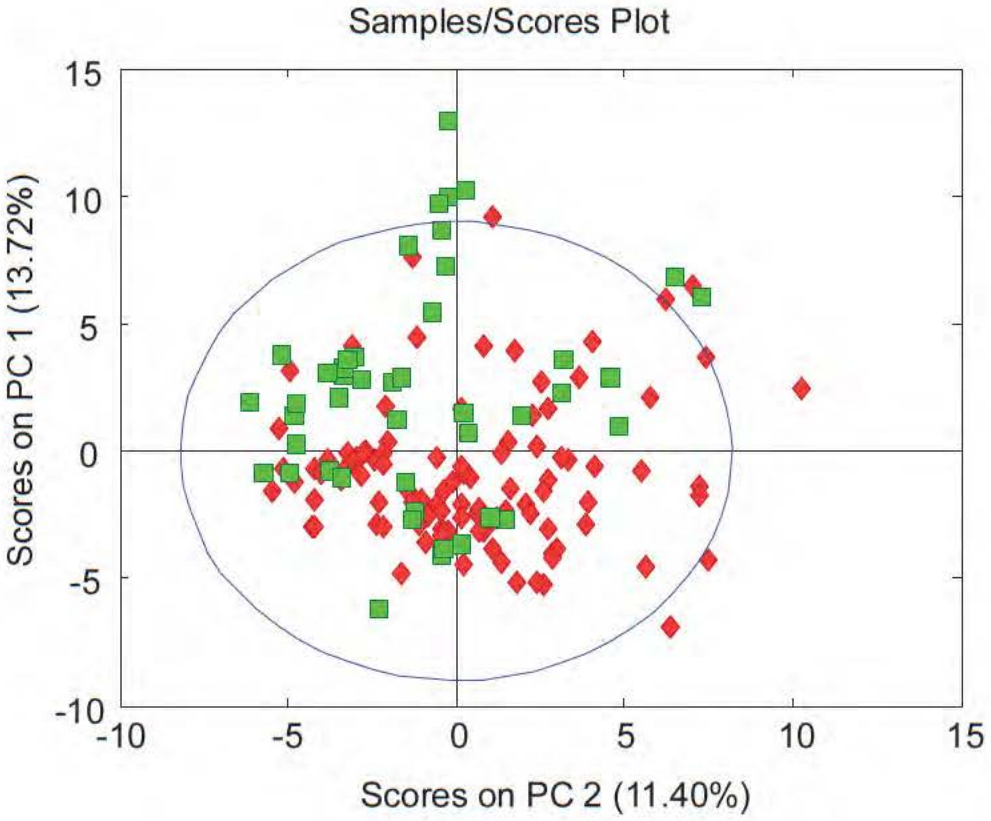

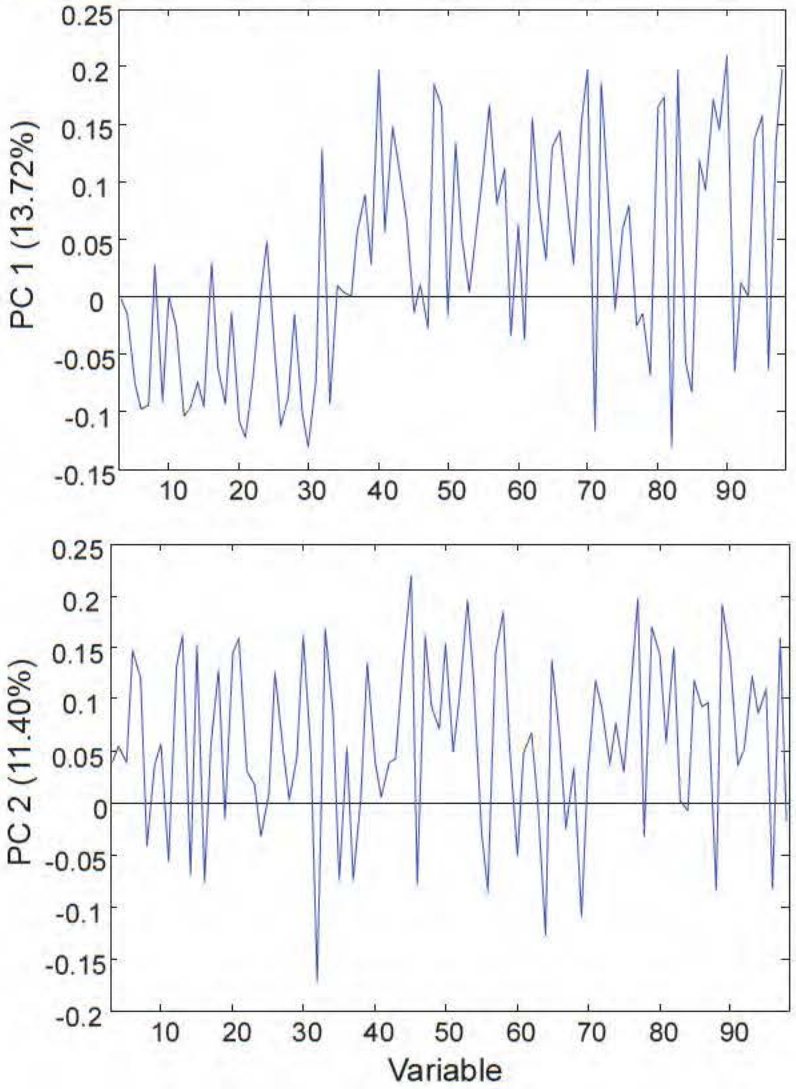

8 LVs, autoscale, (random subsets – 16 splits, 10 iterations)

REGMED

Raman Spectra (785nm) - PCA

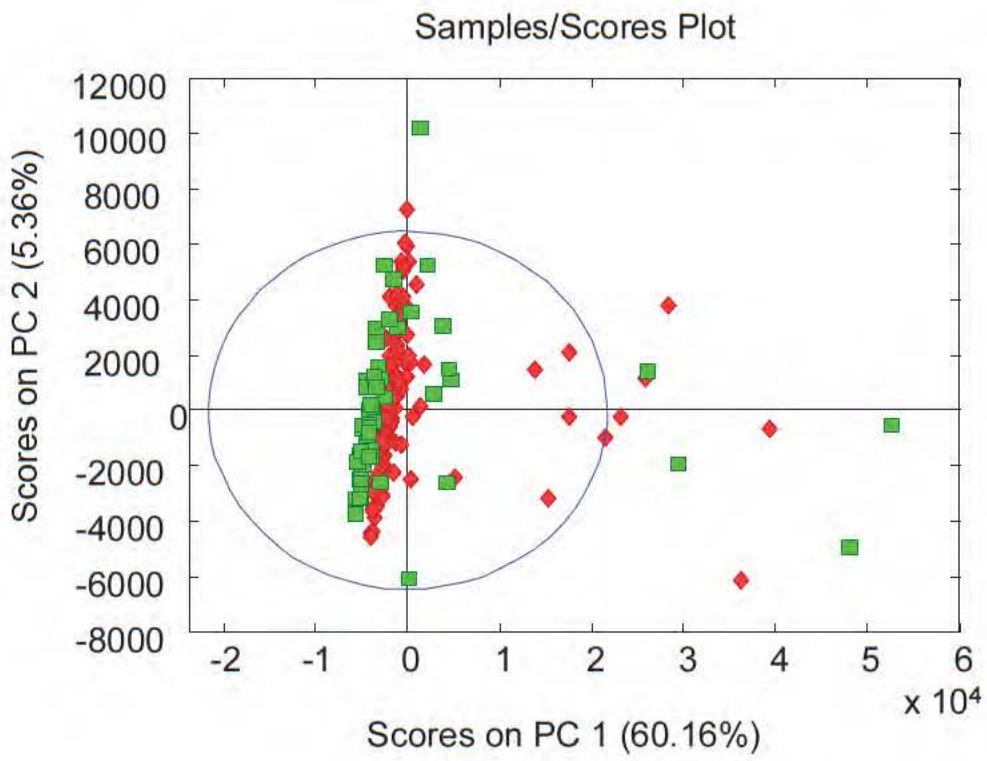

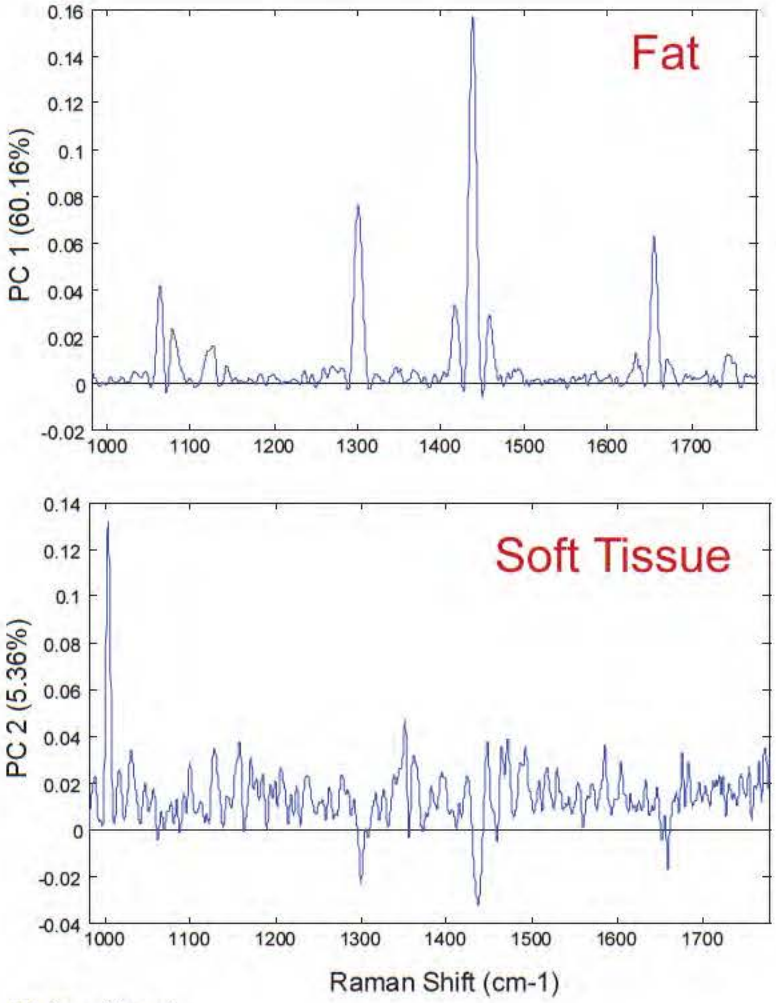

4 LVs, class center, automatic Whittaker baseline, (random subsets – 16 splits, 10 iterations)

REGMED

Partial Least Squares Discriminant Analysis

What's being measured -

CALIBRATION

Regression Model

What's unknown -

PREDICTION

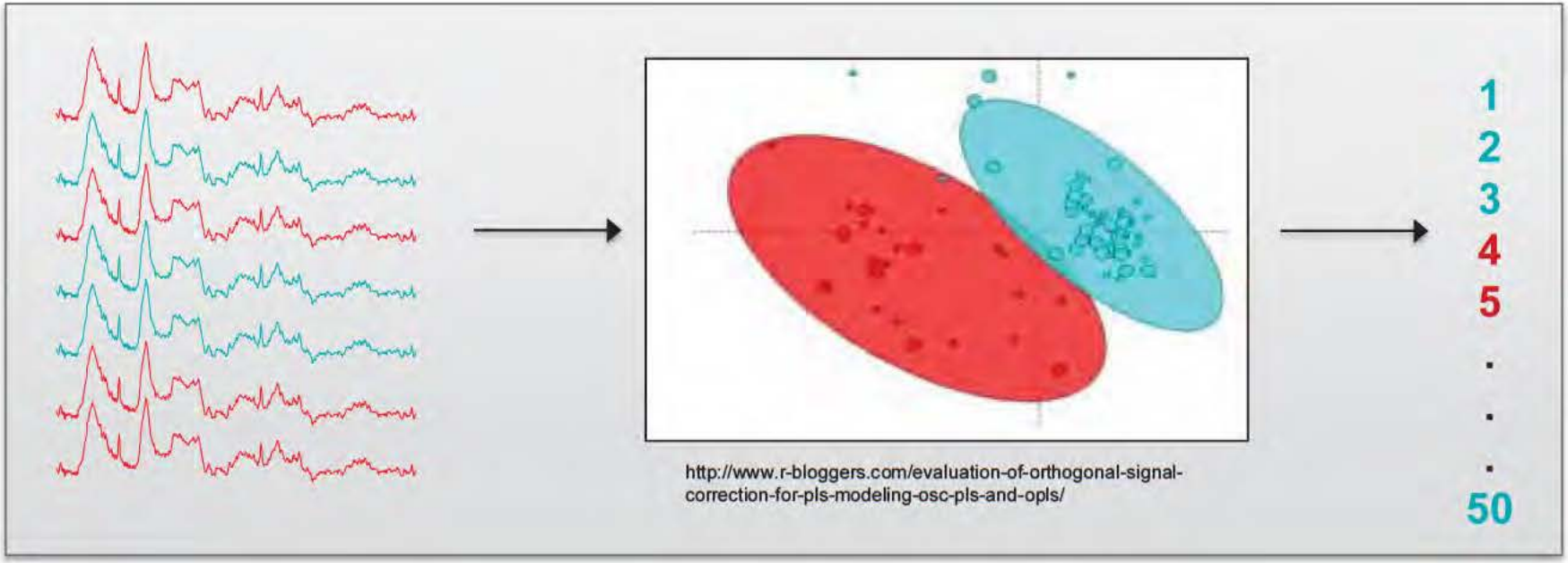

http://www.r-bloggers.com/evaluation-of-orthogonal-signal-correction-for-pls-modeling-osc-pls-and-opls/

REGMED

Clinical Variables - PLSDA

Predicted ROCs – All variables except outcome

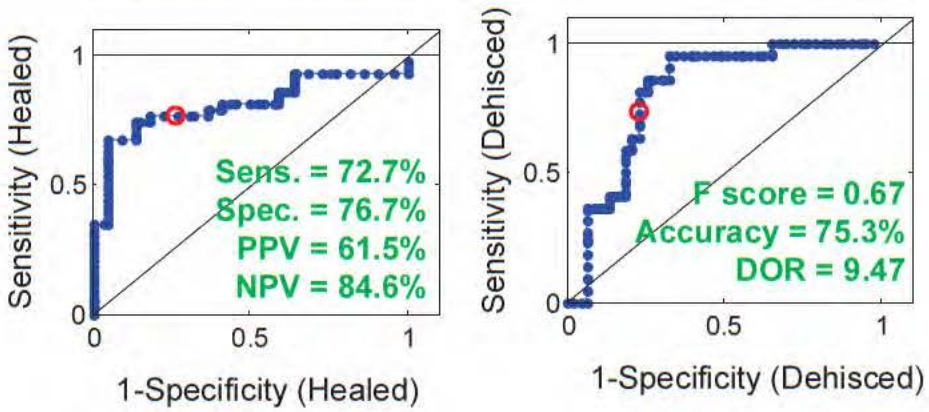

Confusion	Actual	*Healed*	*Dehisced*
Predicted	*Healed*	33	6
	Dehisced	10	16

AUC = 0.8118

Predicted ROCs – POC variables only

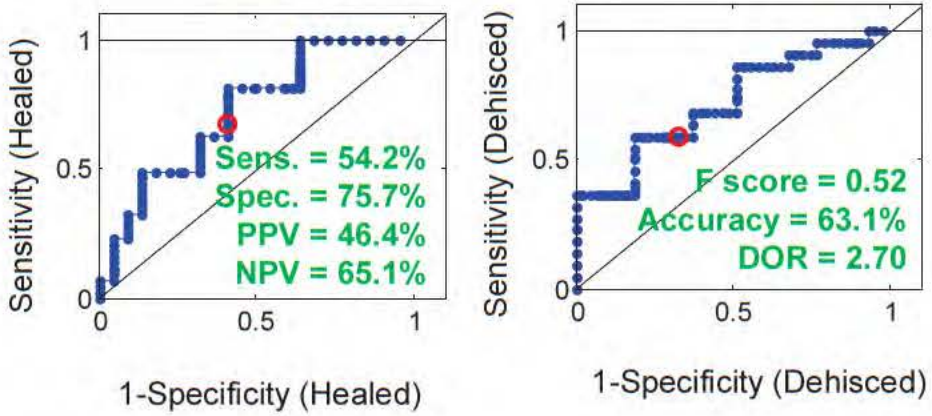

Confusion	Actual	*Healed*	*Dehisced*
Predicted	*Healed*	28	9
	Dehisced	15	13

AUC = 0.7230

8 LVs, autoscale preprocessing, (random subsets – 16 splits, 10 iterations)

REGMED

Luminex Variables - PLSDA

Predicted ROCs – All variables (serum and effluent)

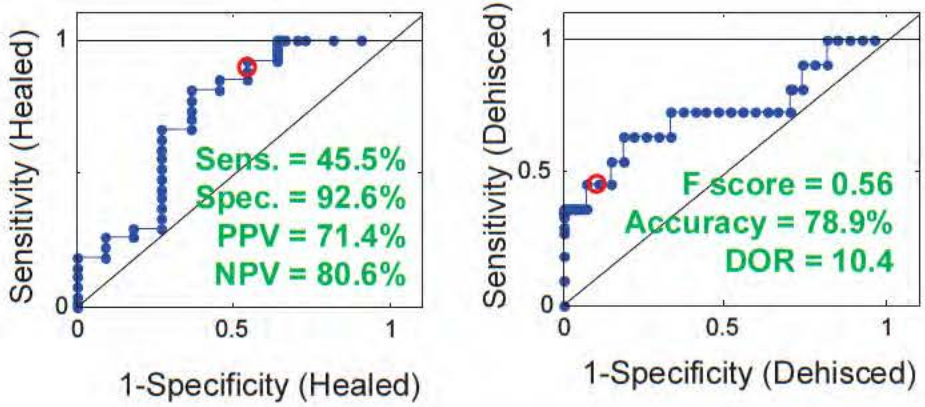

Confusion	Actual	*Healed*	*Dehisced*
Predicted	*Healed*	25	6
	Dehisced	2	5

AUC = 0.7273

Predicted ROCs – Effluent variables only

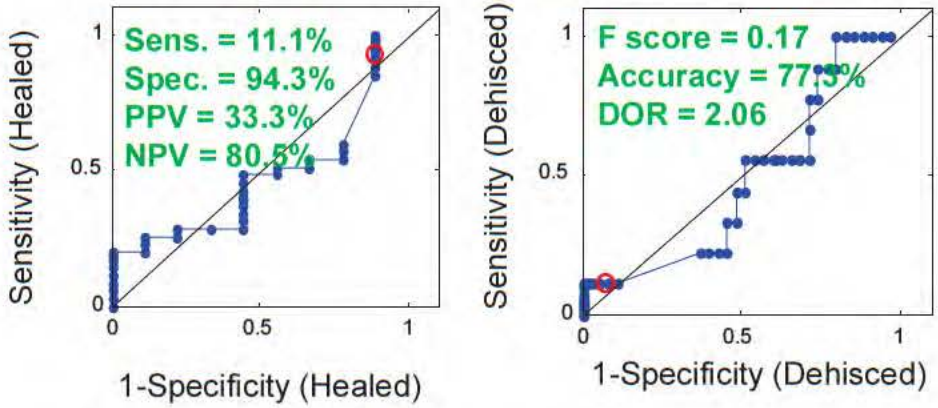

Confusion	Actual	*Healed*	*Dehisced*
Predicted	*Healed*	33	8
	Dehisced	2	1

AUC = 0.4810

3 LVs, autoscale preprocessing, 27 and 21 samples excluded (random subsets – 16 splits, 10 iterations)

REGMED

Raman Spectra (785nm) Only

PLSDA Predicted ROCs

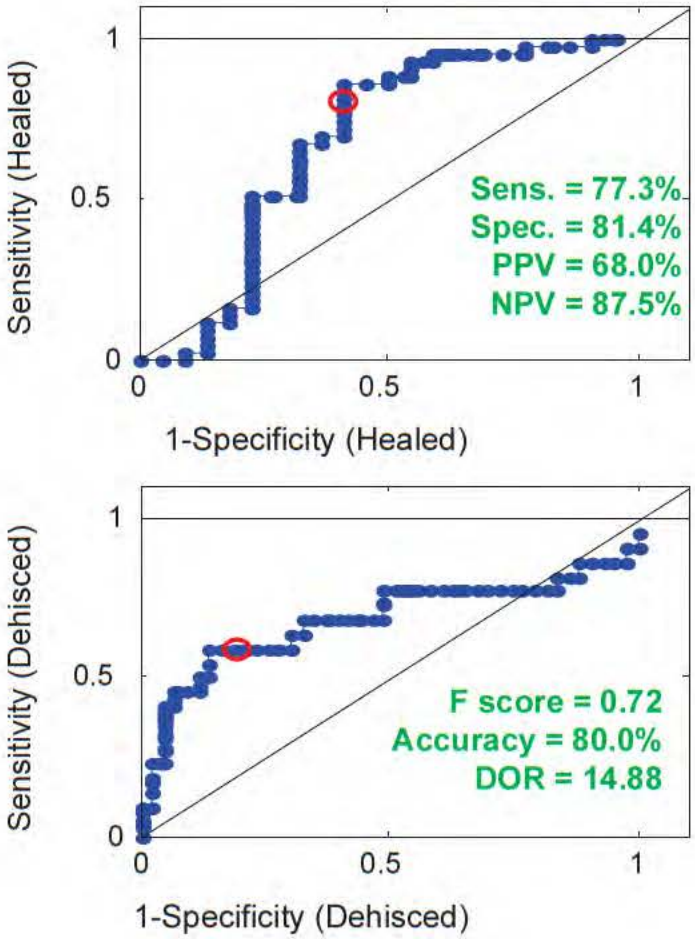

Confusion	Actual	*Healed*	*Dehisced*
Predicted	*Healed*	35	7
	Dehisced	8	15

AUC = 0.6808

3 LVs, class center, automatic Whittaker baseline, truncated 980-1746 cm^{-1}, random subsets – 16 splits, 10 iterations

REGMED

Summary of Results

Classification	Data Sets	Sensitivity	Specificity	PPV	NPV	F score	Accuracy	DOR
PLSDA	C (≠O)	72.7	76.7	61.5	84.6	0.67	75.3	9.5
PLSDA	C (≠O), POC	54.2	75.7	46.4	65.1	0.52	63.1	2.7
KNN	C (≠O)	0.0	77.5	0.0	72.1	0.00	59.0	0.0
PLSDA	L, all	45.5	92.6	71.4	80.6	0.56	78.9	10.4
PLSDA	L, eff	11.1	94.3	33.3	80.5	0.17	77.3	2.1
KNN	L, all	100.0	100.0	100.0	100.0	1.00	100.0	
KNN	L, eff							
PLSDA	R							
KNN	R	68.[illegible]	93.0	83.3	85.[illegible]	0.[illegible]5	8[illegible].6	28.6
PLSDA	C, L serum							
KNN	C, L eff	91.7	100.0	100.0	97.6	0.96	98.1	
PLSDA	all							
KNN	all	100.0	0.0	33.8		0.51	33.8	

The diagnostic odds ratio is a measure of the effectiveness of a diagnostic test – the ratio of the odds of the test being positive if the subject has a disease (positive likelihood ratio) relative to the odds of the test being positive if the subject does not have the disease (negative likelihood ratio).

F-score is a measure of a test's accuracy; weighted mean of precision and recall.

Wound Healing Conclusions

Luminex data, particularly the effluent data, show the highest sensitivity, specificity, accuracy and F score, but the results are suspicious.

The Raman data provides the next best sensitivity, specificity, accuracy, F scores, and the highest overall Diagnostic Odds Ratio (DOR).

Luminex data requires at least two hours for processing along with significant cost for consumables, in addition to instrumentation and assays.

Raman spectroscopy can be performed intraoperatively, with little to no consumable cost and no additional assay cost. Instrument cost is comparable.

Additional modelling techniques need to be explored.

This preliminary study demonstrates the promise of multimodal data sets, particularly multimodal data sets with spectroscopic components.

We need to further explore outcome modelling – healed vs. delayed healing vs. dehisced; 830nm spectra versus 785nm spectra.

Heterotopic Ossification

Heterotopic Ossification (HO)

Heterotopic ossification (HO) refers to the aberrant formation of mature, lamellar bone in non-osseous tissues.

Currently, orthopaedic surgeons faced with treating mature, refractory, symptomatic HO are left with few options other than operative excision.

Potter et al. J Bone Joint Surg Am. 2007;89:476-486.

Following most civilian trauma, HO formation is relatively rare in the absence of head injury. Even following traumatic brain or spinal cord injury, it develops in only 20% and 11% of patients. Rates of HO formation exceed 50% only in the setting of femoral shaft fractures with concomitant head injury and severe burns.

Potter et al. J Bone Joint Surg Am. 2010; 92, Suppl2: 74-89.

USA Today, February 12, 2006.

ORTHOPEDICS 2008;31(12):1237.

UPOJ 1998;11:59-66.

REGMED

What is needed is a technology can risk stratify the development of HO and identify tissue that *may* become HO – Raman spectroscopy.

Muscle Histopathology

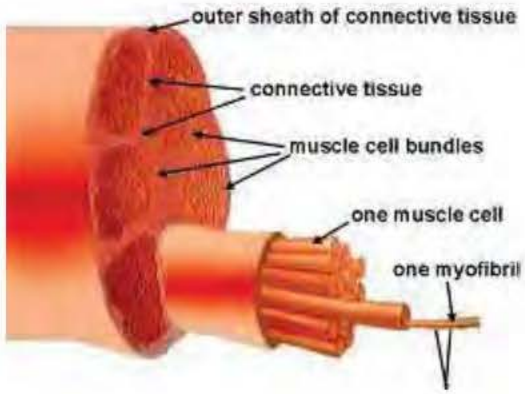

Myofibrils are composed of actin and myosin filaments and form muscle cells. Muscle cells are myofibers and bundle to form fascicles, which form muscle.

Normal muscle myofibers are relatively uniform.

Injured muscle myofibers are surrounded by fibrous connective tissue.

Closer examination demonstrates inflammation (evidenced by lymphocytes), myofiber degradation, necrosis, and hemorrhage in injured muscle tissue.

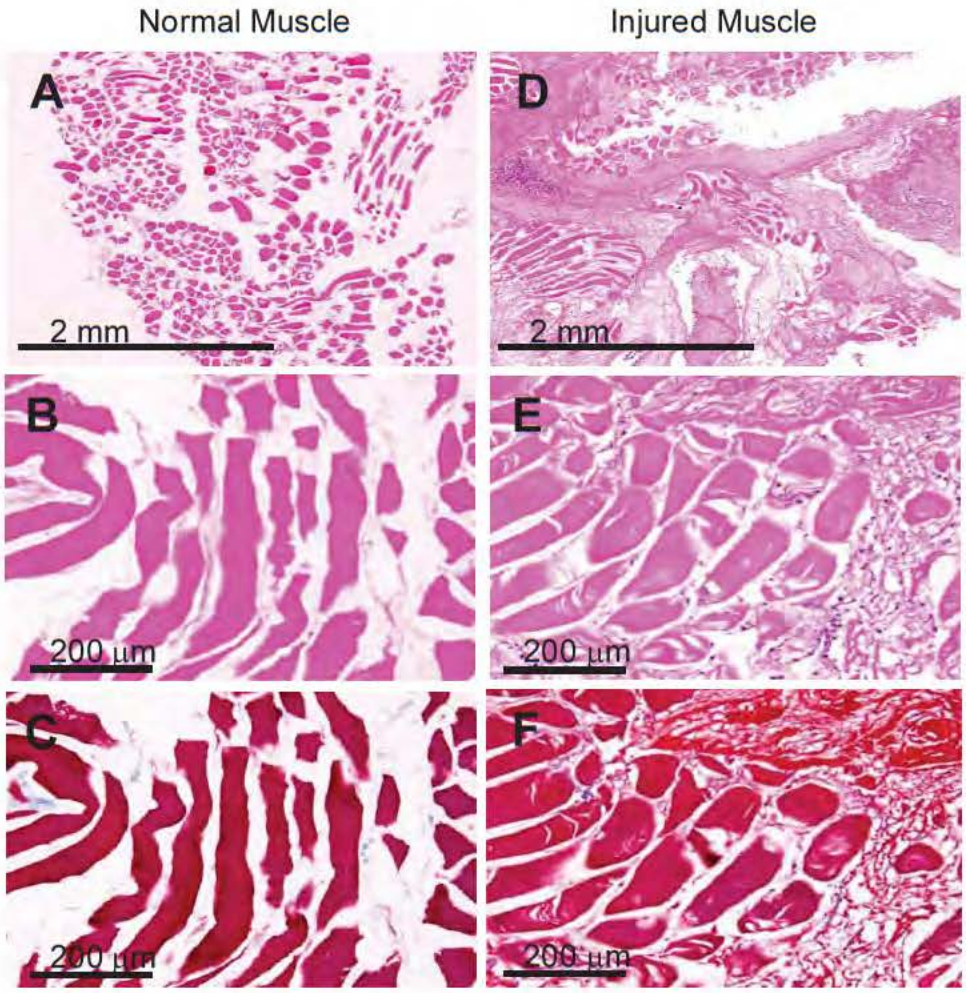

http://www.tutorvista.com/content/biology/biology-iii/animal-histology/muscular-tissue.php

HO Osteoid Histopathology

Osteoid is the unmineralized, organic portion of the bone matrix that forms prior to the maturation of bone. Bone forming cells, or osteoblasts, begin the process of forming bone tissue by secreting osteoid. When the osteoid becomes mineralized, it and adjacent osteoblasts develop into new bone tissue.

Immature osteoid (early HO) on H&E stained slides appears more eosinophilic than mature bone and only stains blue with Masson's trichrome.

As the osteoid matures (mature HO), Masson's trichrome reveals osteoid that stains both blue and red.

Von Kossa staining corroborates these results by demonstrating a greater degree of mineralization (darker stain) in the mature osteoid.

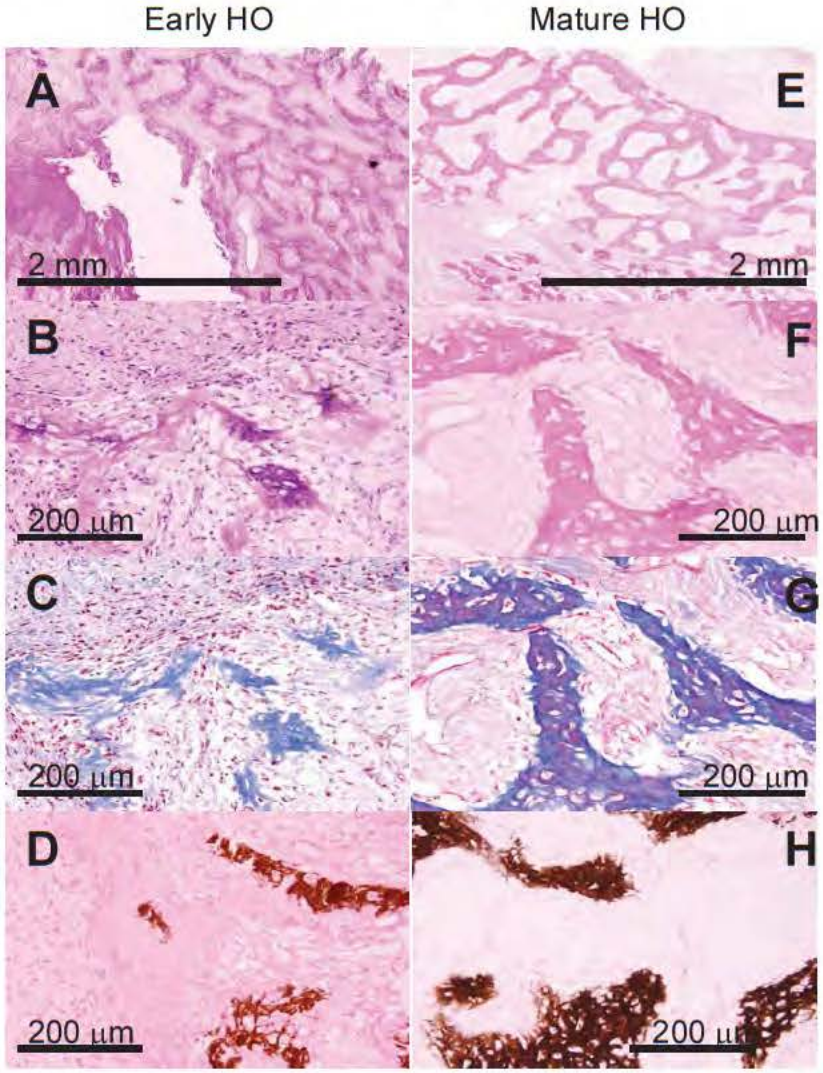

REGMED

Heterotopic Ossification Histopathology

In this particular patient, the HO developed directly adjacent to the femur, beneath a skin grafted area which had been treated with INTEGRA® bioartificial dermal replacement (Integra Life Sciences; Plainsboro, NJ) application pre-skin graft.

The HO lesion was excised over 160 days post-injury, after ulcerating and becoming persistently symptomatic.

Mature HO demonstrates cortical and trabecular bone – osteons with clear and organized cement lines, Haversian canals, and bone marrow elements.

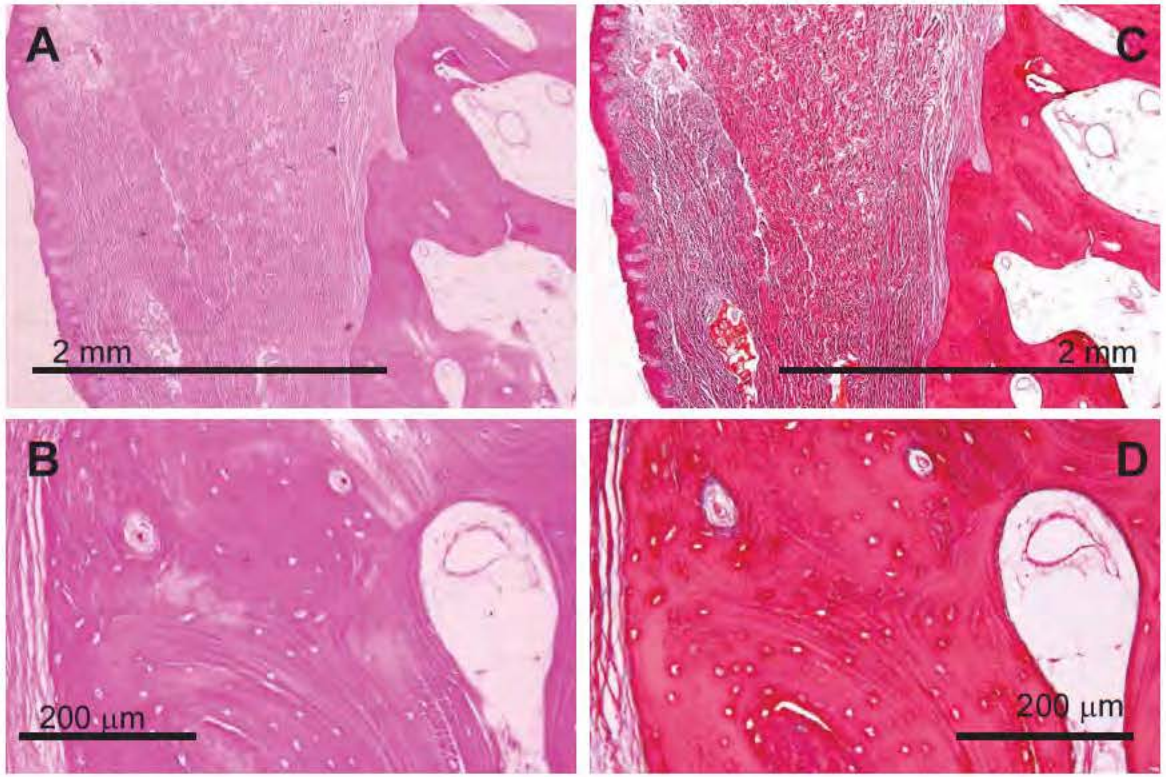

Comparison of Histology

H&E stained slides made from wound biopsies from10 combat wounded patients were graded by a pathologist for : regeneration, degeneration (muscle atrophy), acute inflammation (presence of neutrophils), chronic inflammation (presence of lymphocytes and macrophages), necrosis, and hemorrhage.

Additionally, slides were evaluated for presence of nerve bundles (S-100) and brown fat (UCP-1).

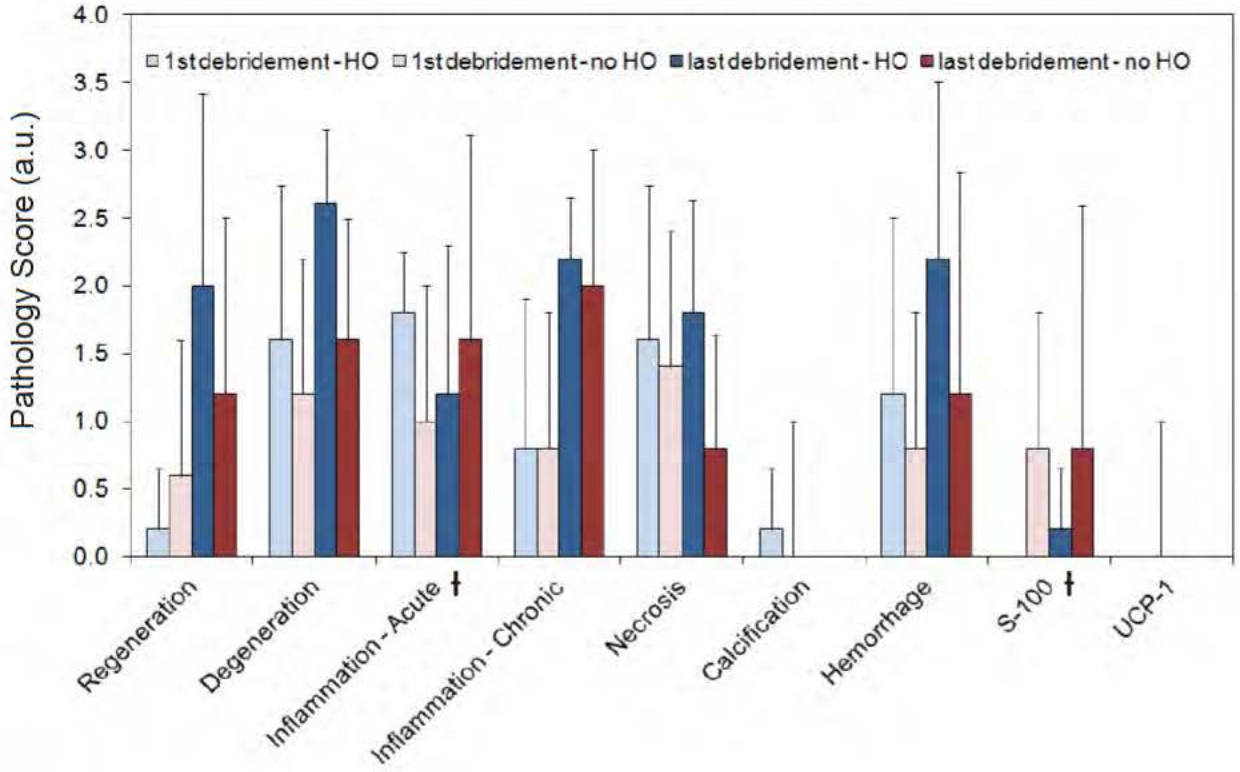

Scoring used to grade tissue sections:

0 – not present

1 – mild (present in 1-25% of tissue)

2 - moderate (present in 26-75% of tissue)

3 – severe (present in 76-100% of tissue)

REGMED

Raman Spectroscopic Pilot Study of HO

HO/Raman Spectroscopy Pilot Study of HO

Tissue biopsies, approximately 1cm^3, were obtained during surgical procedures and immediately snap frozen.

Normal Muscle (n=10)	Injured Muscle (n=10)	Early HO (n=10)	Mature HO (n=10)	Normal Bone (n=4)

Samples were thawed no more than 15 minutes unfixed and were immediately refrozen after spectral collection.

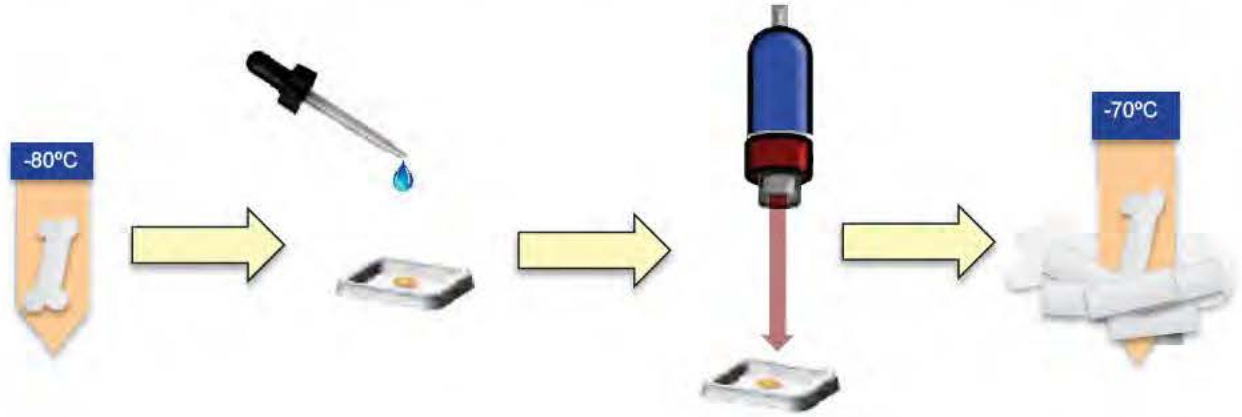

Raman Spectrum of Bone

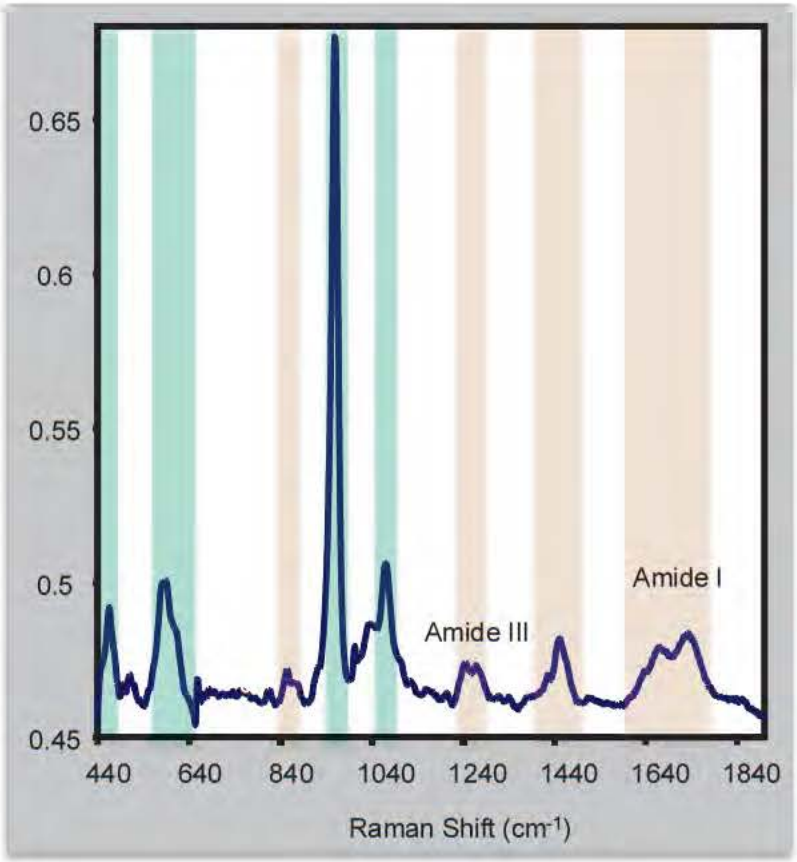

ν (cm^{-1})	Band Assignment	Component
593	ν_4 PO_4^{3-} bending	hydroxyapatite
821	ν(CC) o[illegible] ackbone	collagen; muscle
856	ν(CC) of hydroxyproline ring	collagen; muscle
873	ν_3 P-OH stretching	bone
876	ν(CC) of [illegible] y [illegible]roxypro[illegible]ne ring	collagen; protein
921	ν(CC) of proline ring	collagen; protein
938	ν(CC) of protein backbone	co lagen; muscle; protein
945-952	ν_1 PO_4^{3-} stretch	amorphous calcium phosphate
959	ν_1 PO_4^{3-} stretch	hydroxyapatite
1004	ν(CC) aromatic ring	Phe; collagen; muscle
1032	ν_3 PO_4^{3-} ; ν(CC) skeletal; C-O stretch	bone; collagen; muscle
1071	$\nu_1(CO_3^{2-})$	bone
1075	ν_3 PO_4^{3-} stretch	[illegible] y [illegible]roxyapatite
1080	ν(CC) and ν(CN) skeletal	collagen; muscle
1159	ν(CC) and ν(CN) skeletal	carotenoid
1178	ν(CC) and ν(CN) skeletal	collagen; muscle
1244	δ(CH_2) wagging; ν(CN) amide III disordered/β-sheet	collagen; muscle
1274	ν(CN) and δ(NH) amide III α-helix	collagen; muscle
1297	δ(CH_2) twisting	collagen; muscle
1343	γ(CH_2, CH_3) wagging	collagen; muscle
1385	δ(CH_3) symmetric	collagen
1448	δ(CH_2) scissoring	collagen; muscle
1524	caro[illegible]enoi[illegible]	collagen; muscle
1552	ν(CC) ring stretch	collagen; muscle; Trp
1665	ν(CO) amide I	collagen; muscle

REGMED

Raman Comparison of Muscle and HO

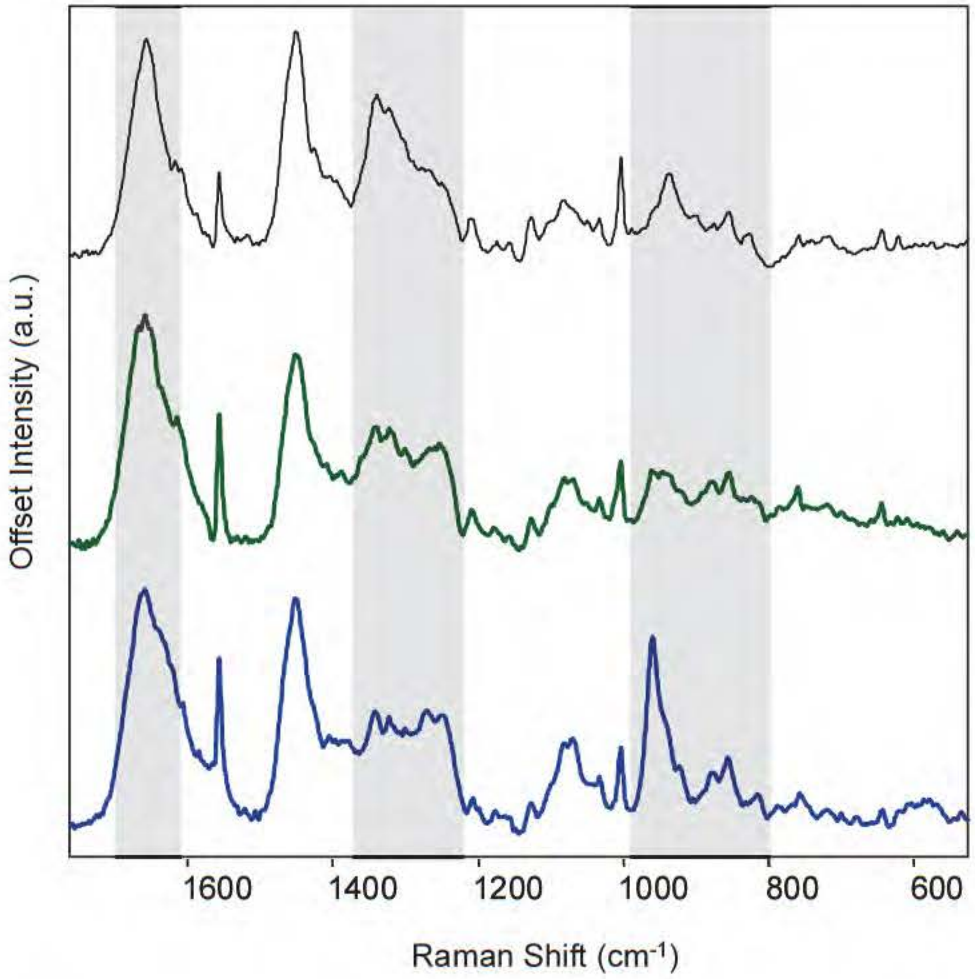

For the HO tissue, whether early or mature, the Amide I band shifts to a higher frequency and is centered at 1660 cm^{-1}.

The intensity of the 1340 cm^{-1} Raman vibrational band is decreased in the spectra of the HO tissue compared to the uninjured muscle tissue.

The 1270 cm^{-1} and 1240 cm^{-1} Raman vibrational bands are increased in the spectra of the HO tissue compared to the uninjured muscle.

The most notable difference in the spectrum of the mineralized HO tissue is the presence of the 960 cm^{-1} band, a ν_1 P-O stretching mode.

Finally, the intensities of the 921 cm^{-1}, 876 cm^{-1}, and 855 cm^{-1} bands are more intense in the spectra of the HO tissue than in the spectrum of the uninjured or injured muscle.

J Bone Joint Surg Am. 2010 Dec;92 Suppl 2:74-89.

REGMED

Raman Spectral Band Area Ratios (BARs)

Band area ratios (BARs), a pseudoquantitative measure, were calculated by dividing the band area of a Raman band of interest (for example 1070 cm^{-1}) by another band area (for example 1445 cm^{-1}).

Compositional trends in related samples can be explored using BARs, such as:

- a decrease in reducible collagen crosslinking (1680/1660 cm^{-1})
- mineral carbonation (1070/960 cm^{-1} and 1070/1445 cm^{-1})
- mineral maturity (945/960 cm^{-1})
- collagen order/disorder (1240/1270 cm^{-1})
- Protein α-helical structure (1240/1300 cm^{-1})
- mineral crystallinity is determined by the full width at half maximum of the 960 cm^{-1} ν_1 phosphate band

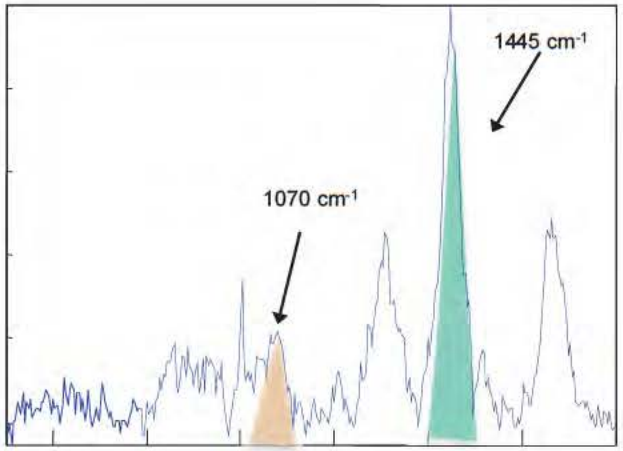

Comparison of Raman Spectral BARs

In general, when comparing muscle (normal or injured) to HO tissue (early or mature), we note a decrease in the 1660/1445 cm^{-1} ($p<0.03$), 1680/1445 cm^{-1} ($p=0.28$), and 1340/1270 cm^{-1} ($p<0.01$) BARs.

There is also an increase in the 1640/1445 cm^{-1} BAR ($p<0.1$), the 1240/1270 cm^{-1} (collagen order/disorder) BAR ($p<0.03$), and the 1240/1300 cm^{-1} (protein α-helical structure, $p<0.001$). These changes in BARs can also be examined as a progression of normal tissue to diseased tissue.

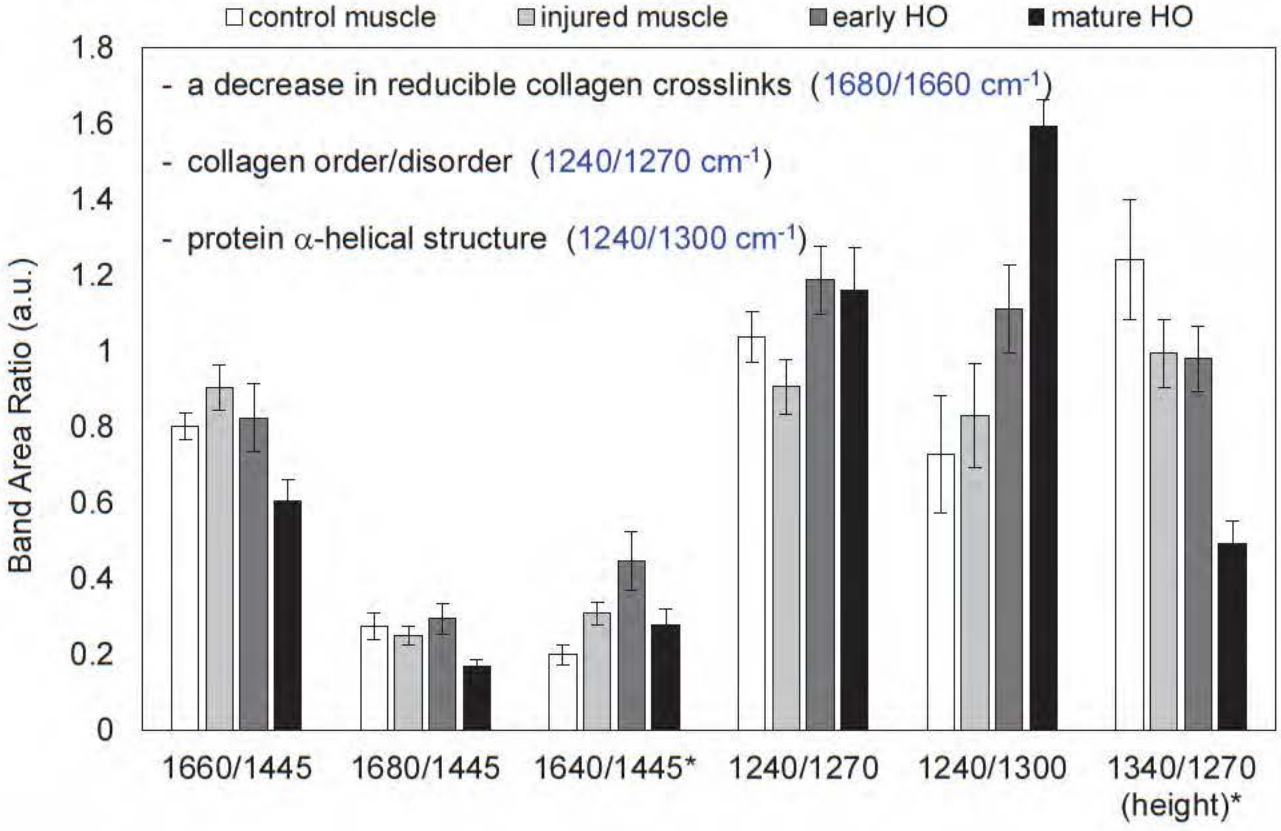

Transition from normal to injured muscle –

↑ 1660/1445 cm^{-1} and 1640/1445 cm^{-1}

↓ collagen order/disorder, and 1340/1270 cm^{-1}

Transition from injured muscle to HO tissue -

↓1660/1445 cm^{-1} and 1680/1445 cm^{-1} BAR

↑ in the collagen order/disorder BAR and the protein α-helical structure BAR

Bone. 2013 Sep 5;57(2):335-342.

REGMED

** Statistically significant differences ($p<0.05$) with a Bonferroni correction.*

Bone. 2013 Sep 5;57(2):335-342.

Normal Bone versus HO

Early HO tissue was surgically removed within 165 days post-injury (mean) while mature HO was excised on average over 600 days post-injury.

- mineral carbonation (1070/960 cm^{-1} and 1070/1445 cm^{-1})
- mineral immaturity (945/960 cm^{-1})
- mineral crystallinity is determined by the full width at half maximum of the 960 cm^{-1} ν_1 phosphate band

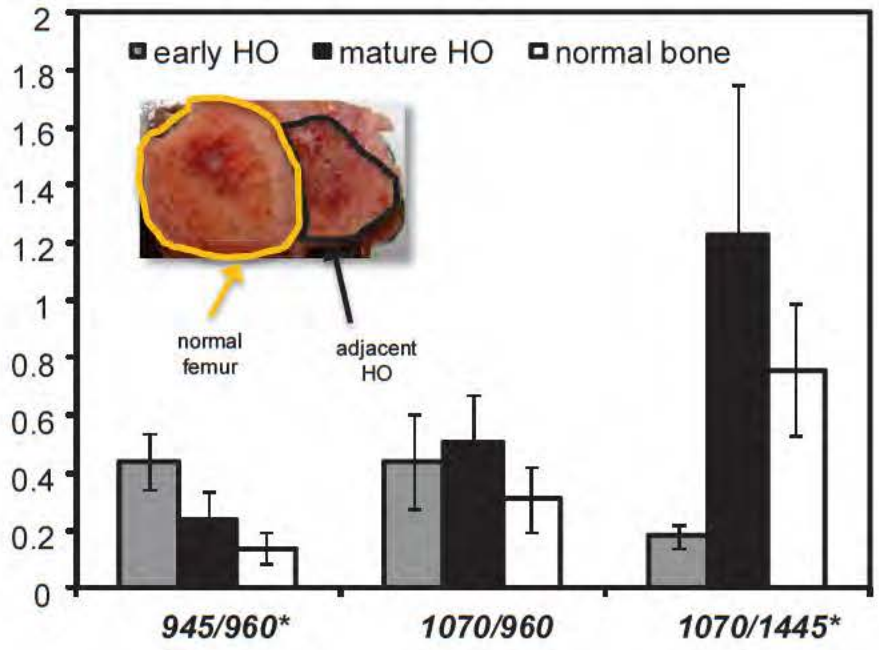

As bone matures –

↓945/960 cm^{-1} BAR and ↑1070/1445 cm^{-1} BAR

Early HO has the highest mineral immaturity BARs and the lowest mineral carbonation BARs.

This trend is reversed for mature HO –

- the mineral immaturity BARs are lower than early HO
- mineral carbonation BARs are higher than early HO tissue.

Mineral crystallinity is higher in mature HO samples than in normal bone or early HO samples.

REGMED

** Statistically significant differences ($p<0.05$) with a Bonferroni correction.*

Bone. 2013 Sep 5;57(2):335-342.

Discrimination of HO Tissue by Raman Metrics

PLS-DA – supervised machine learning that uses classical PLS regression to regress a categorical variable, i.e. development of HO.

Band Areas and Band Centers
29 variables, 40 samples

Cross-validation	Actual no HO	Actual HO
Predicted no HO	18	2
Predicted HO	2	18

Sensitivity = 90%
Specificity = 90%

Positive predictive value = 90%
Negative predictive value = 90%

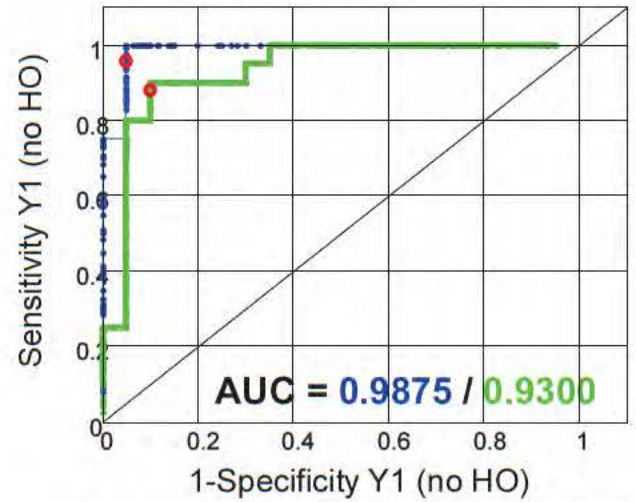

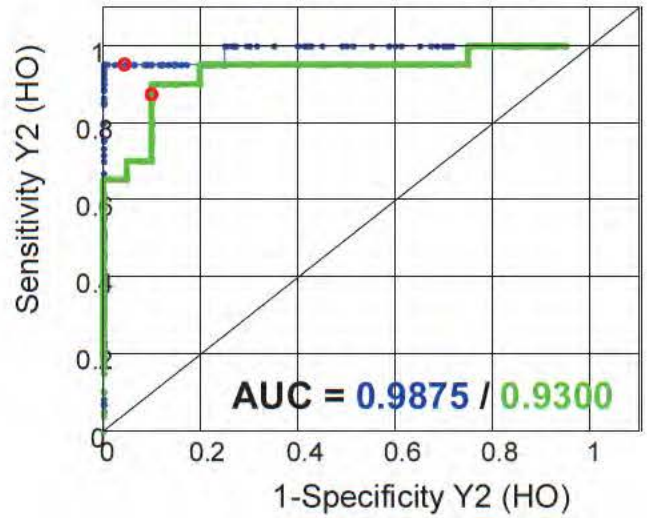

Discrimination of HO Tissue by Raman Spectroscopy

Raman Spectral Features
2027 variables, 40 samples

Cross-validation	Actual HO	Actual no HO
Predicted HO	17	2
Predicted no HO	3	18

Sensitivity = 85%
Specificity = 90%

Positive predictive value = 89.4%
Negative predictive value = 85.7%

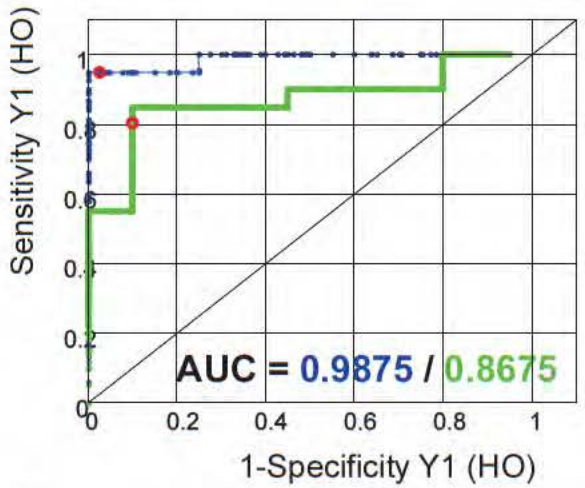

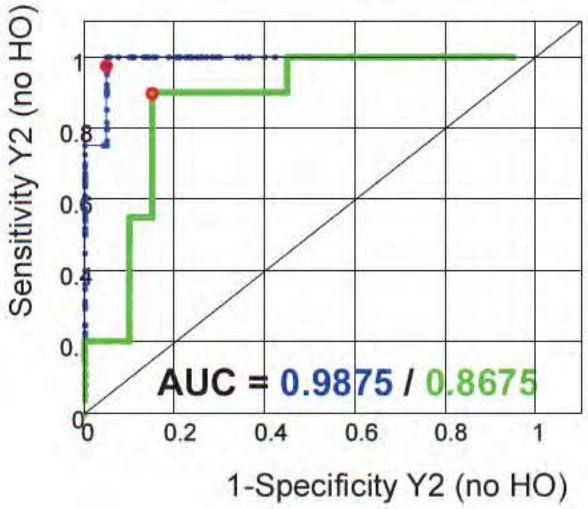

REGMED

Discrimination of HO Tissue by Raman Spectroscopy

Validation data set (external) consisting of 15 samples (53% HO, 47% no HO).

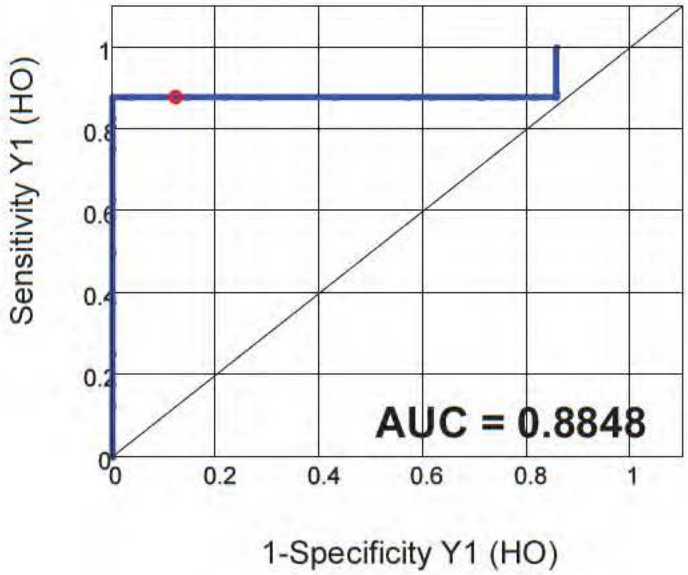

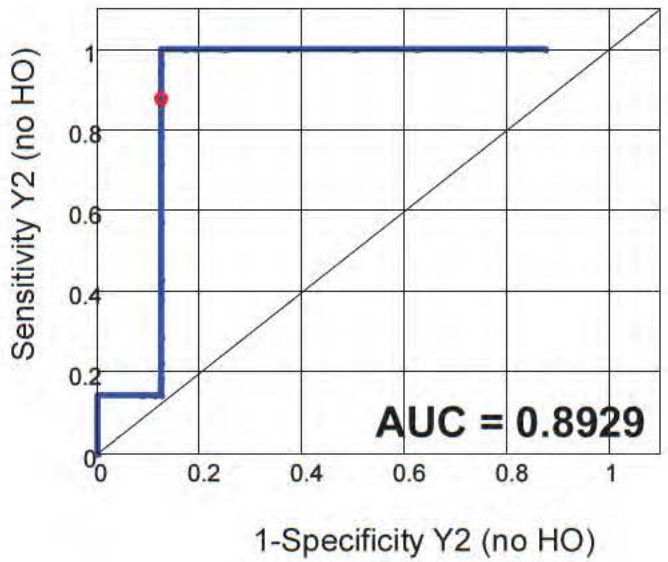

Sensitivity = 87.5%
Specificity = 85.7%

Positive predictive value = 87.5%
Negative predictive value = 85.7%

Prediction	Actual HO	Actual no HO
Predicted HO	7	1
Predicted no HO	1	6

REG MED

Heterotopic Ossification Conclusions

In this preliminary study, we used Raman spectroscopy to discern molecular changes that that occur prior to and during the formation of HO.

While mature HO tissue is generally apparent upon physical examination and/or radiologic examination, immature and largely unmineralized HO tissue is not as clinically obvious.

The Raman spectra of various tissues demonstrate that there are clear differences in the Amide I and Amide III spectral regions of HO tissue compared to normal muscle tissue, which may indicate whether or not muscle tissue will develop HO.

Raman spectroscopy also provides insight into the actual mineralization of the soft tissue.

Raman spectroscopy can be adapted as an **objective, intraoperative, non-invasive** means by which to risk stratify wounds, and can be **performed in real-time**.

If Raman spectroscopy demonstrates that a wound has Raman spectral features associated with the formation of HO, prophylaxis could be employed in select cases.

Alternatively, in areas that appear prone to HO development the clinician can consider early preferential excision of pre-HO tissue while the patient is undergoing debridement and/or amputation revision for final closure.

Overall Concept

1) Apply best of breed technologies in

   - *biomarker analysis*
   - *informatics*
   - *medical technology*

2) Clinical Decision Support tools can be developed that can optimize and personalize treatment using *patient-specific clinical variables combined with local and systemic biomarkers.*

3) Goal: <u>maximize patient outcomes while minimizing complications</u>.

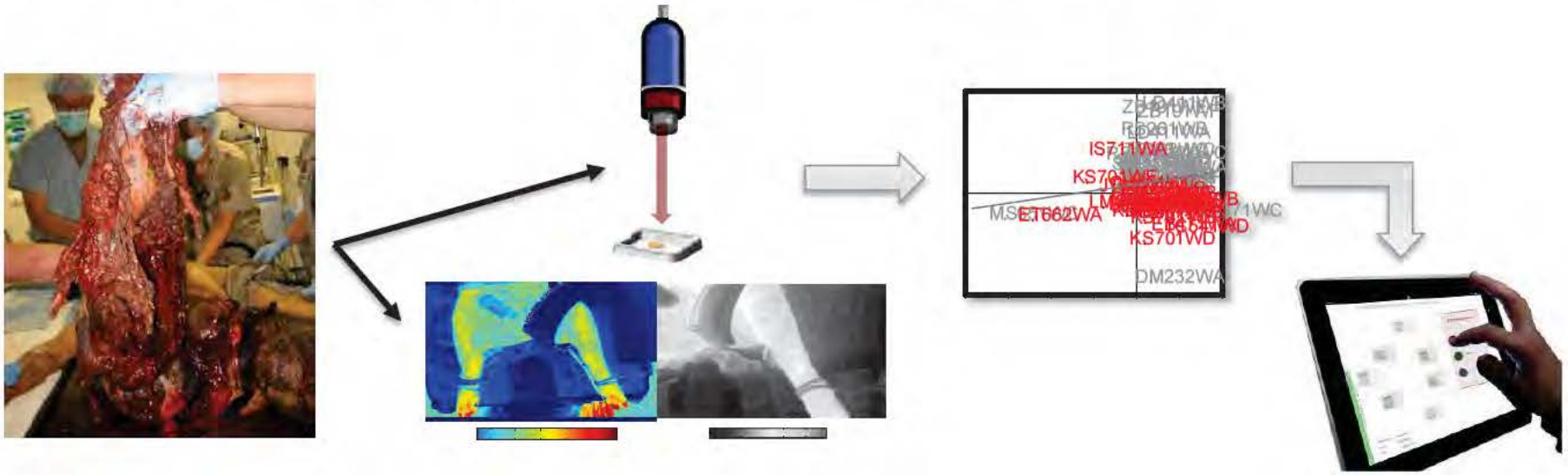

Acknowledgements

Regenerative Medicine Dept, NMRC

Jonathan Forsberg, MD
Thomas Davis, PhD
Nicole Crane, PhD
Trevor Brown, PhD
Matthew Wagner, PhD
Richard Barth, MS
Ying Cao, MS
Felipe Lisboa, MD
Khairul Anam, PhD
Anthony Foster, PhD
Ammar Qureshi, PhD
Michael Wiley, MBA
Mihret Amare, MS
Yelena Lazdun, MS
Chioma Aglibe, MS
Alison Tomasino, BS
Nick Clark, BS
Crystal Leonhardt
Stacia Moreno, BS
Fred Gage
Toby Perkins

Orthopaedics Dept, WRNMMCB

Romney Andersen, MD
B. Kyle Potter, MD
Wade Gordon, MD
Jean Claude D'Allyrand, MD
Robert Beer, MD
Mark Fleming, MD
Susan Foster, RN

Department of Surgery, USUHS

Eric Elster, MD FACS
Leon Nesti, MD, PhD
Arnaud Belard, MBA
Tiffani Slaughter, BS

REGMED
Shaping the Future of Casualty Care

THANK YOU!

Spectroscopy and Imaging for Combat-Related Medicine

Nicole Crane, Ph.D.

Advanced Surgical Imaging Program
Regenerative Medicine Department
Naval Medical Research Center
Silver Spring, MD

Department of Surgery
Uniformed Services University of Health Sciences
Bethesda, MD

Disclaimer

The views expressed in this presentation are those of the author and do not necessarily reflect the official policy or position of the Department of the Navy, the Department of Defense, nor the U.S. Government.

This work was supported/funded by work unit number 602115HP.3720.001.A1015. Funding Support includes DoD BUMED Advance Medical Development 0604771N; USAMRMC Military Medical Research and Development OR090136; Defense Medical Research and Development Plan D10_I_AR_J2_501.

The study protocols were approved by the Naval Medical Research Center and Walter Reed National Military Medical Center Institutional Review Boards in compliance with all applicable Federal regulations governing the protection of human subjects, and the Naval Medical Research Center and USUHS Institutional Animal Care and Use Committees in compliance with all applicable Federal regulations governing the protection of animals in research.

I am a military service member (or employee of the U.S. Government). This work was prepared as part of my official duties. Title 17 U.S.C. 105 provides the “Copyright protection under this title is not available for any work of the United States Government.” Title 17 U.S.C. 101 defines a U.S. Government work as a work prepared by a military service member or employee of the U.S. Government as part of that person’s official duties.

I certify that the document represents valid work; that if I used information derived from another source, I obtained all necessary approvals to use it and made appropriate acknowledgements in the document; and I take public responsibility for it.

Military Medicine

Our team leverages real-world experience in combat casualty care: heterotopic ossification, wound healing, advanced surgical imaging, transplant tolerance, and stem cells.

In addition, we develop novel and dynamic bioinformatic approaches to deliver point-of-care personalized medicine.

- *3-CCD Imaging*
- *IR Imaging*
- *Raman Spectroscopy*

Technologies that can non-invasively and objectively assess the wound microenvironment are critical for understanding and evaluating the wound healing process.

Accurate assessment of extremity injuries and wounds is necessary for appropriate treatment in the operating room.

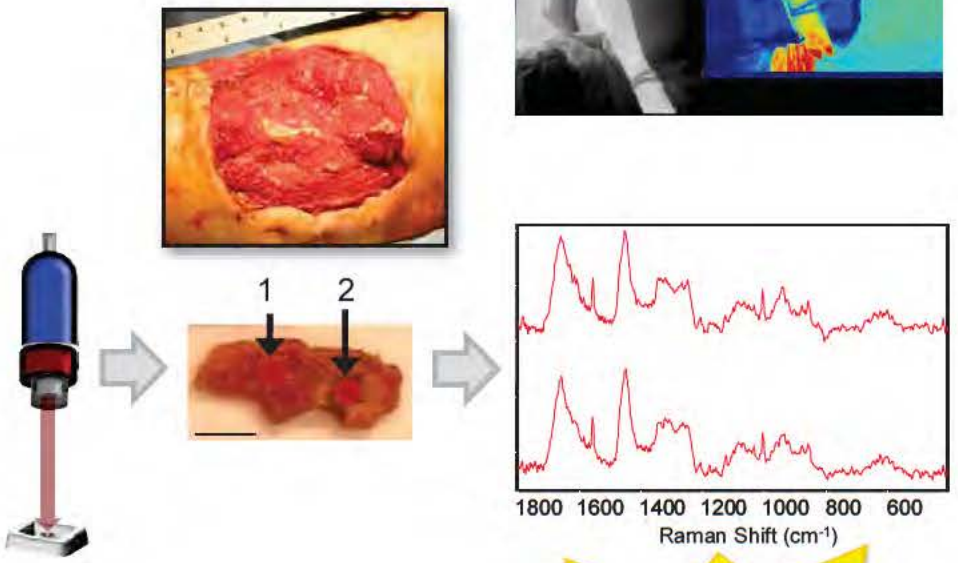

Wound Repair Regen. 2010 Jul-Aug;18(4):409-16.
J Urol. 2010 Oct;184(4):1279-85.
J Bone Joint Surg Am. 2010 Dec;92 Suppl 2:74-89.
J Pediatr Surg. 2012 Jan;47(1):142-7.
J Biomed Opt. 2012 Jan;17(1):010902.
Bone. 2013 Sep 5;57(2):335-342.

Graphic pictures next slide!

Acute Combat Wounds

Modern war ballistics inflict devastating extremity injuries, violating soft tissue, bone, and neurovascular structures.

Complex war wounds require aggressive surgical care. Serial debridements are performed to remove devitalized tissue and decrease bacterial load.

The ensuing inflammatory response ultimately dictates the pace of wound healing and tissue regeneration.

Despite these technological advances, the basic surgical decision regarding appropriate timing of war wound closure remains subjective, and some wounds dehisce or fail.

REGMED

Acute Combat Wound Outcome

An understanding of the molecular environment of acute wounds throughout the debridement process can provide valuable insight into the mechanisms associated with the eventual wound outcome.

- *wound dehiscence*
- *wound colonization*
- *heterotopic ossification (HO)*

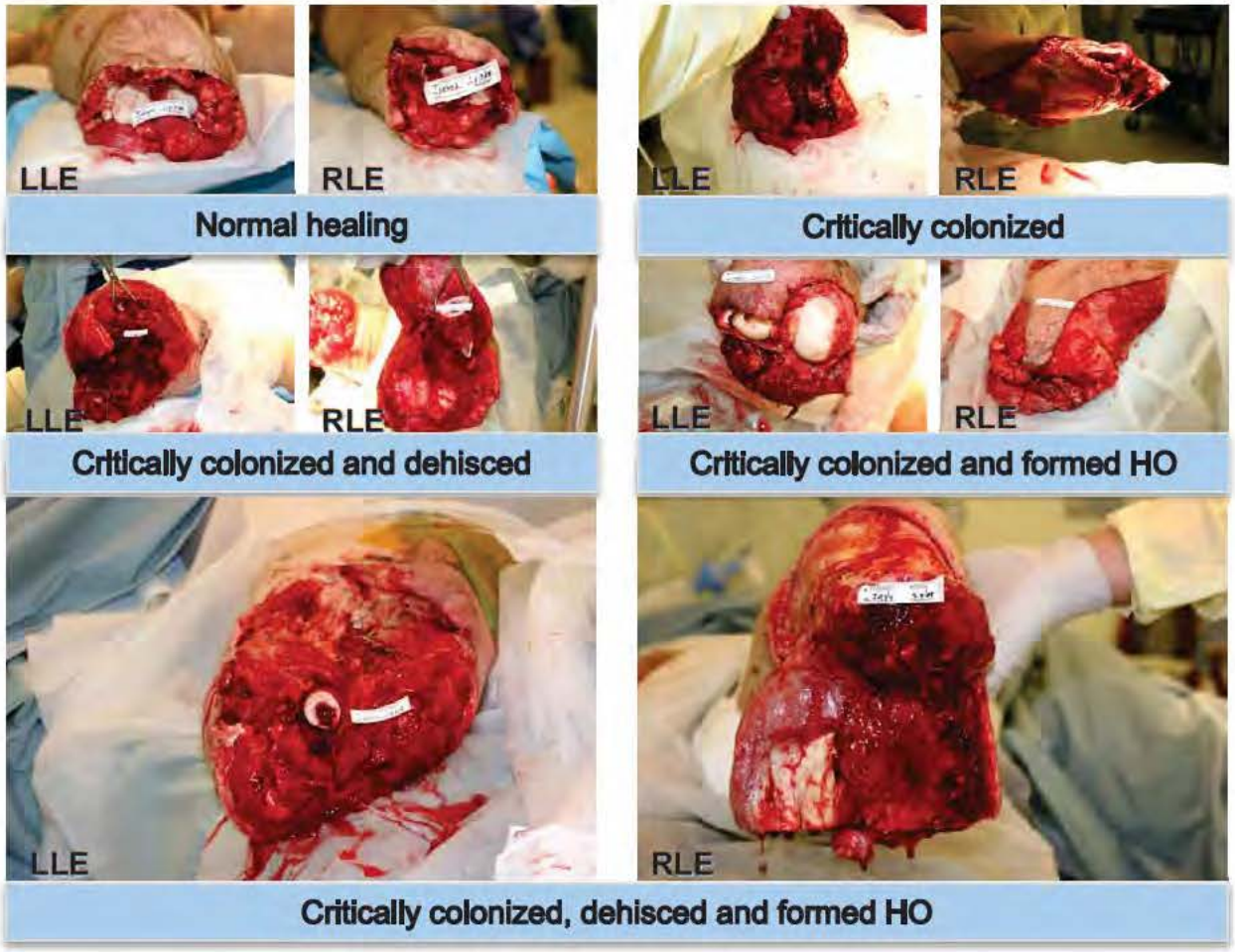

Current Treatment and Challenges

Surgical debridements are performed every 2-3 days to remove devitalized tissue and reduce the bacterial load.

- Negative pressure wound therapy (NPWT) is applied between debridements - promote wound closure.

Wound assessment involves: patient's general condition, injury location, adequacy of perfusion, and gross appearance of the wound.

Our goal is to **monitor wound healing *in vivo***, i.e. monitor wound healing during surgical debridements.

- *Is it the best time to close the wound?*
- *Is the wound developing HO?*
- *Is the wound infected? With what?*

We aim to develop an **objective and predictive model for wound healing**.

Sample Collection

Wound is surgically cleaned

Collect 1 cm³ tissue biopsy from center of wound bed

Gene expression
Raman spectroscopy
Bacterial Analysis

NPWT is applied

Serum is collected

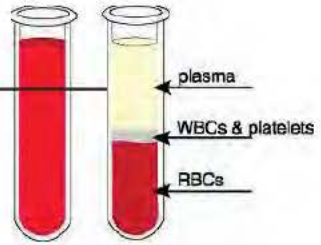

Cytokine and Chemokine Assays

Effluent is collected

Cytokine/Chemokine Assays

Raman spectroscopy
Bacterial Analysis

REGMED

Our Toolbox

Cytokine/Chemokine Assays

Gene Expression

Serum Chemistry

Clinical Data

Bacterial Analysis

Infrared Imaging

3CCD Imaging

Raman Spectroscopy

REGMED

Raman Spectroscopy

Commonly Used Optical Spectroscopies

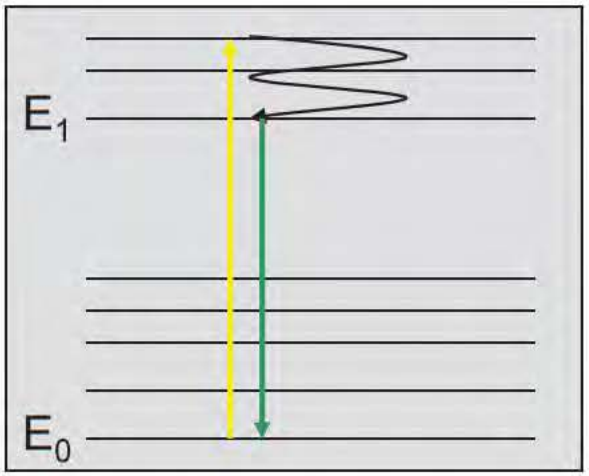

Fluorescence

Radiation (photon) excites the material to a vibrational state, where some energy is dissipated, and then emitted as photon so that the molecule relaxes back to the ground state.

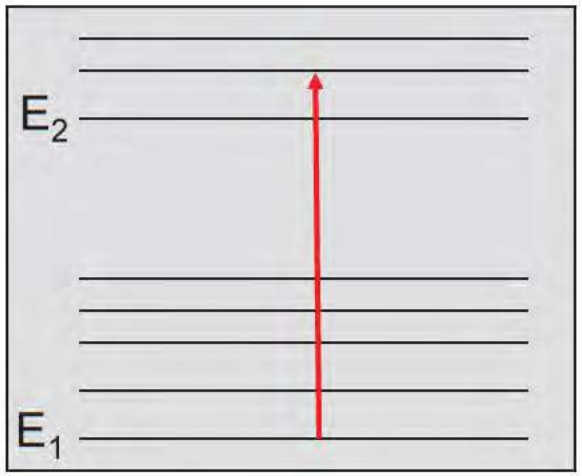

Infrared

Radiation (energy from a photon) is absorbed by the material, exciting a vibrational mode.

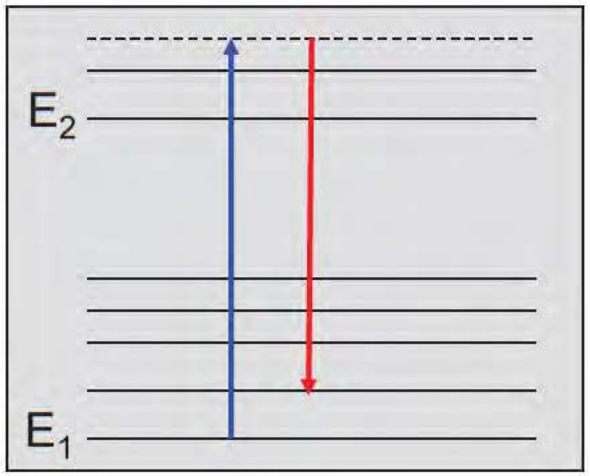

Raman

Radiation (energy from a photon) interacts with the material, exciting it to a "virtual" vibrational state before emitting a photon (longer wavelength) to return to the ground state.

Vibrational Spectroscopy

In infrared spectroscopy, the molecules absorb specific frequencies that matches the transition energy of the bond or group that vibrates.

For Raman scattering, the emitted photon's frequency is the difference in energy between the original state and this new state. This difference in energy is the frequency of the energy of the bond or group that vibrates.

The band positions of IR and Raman spectroscopy will lie at frequencies that correspond to the energy levels of different functional groups and their corresponding vibrations – i.e. a chemical fingerprint

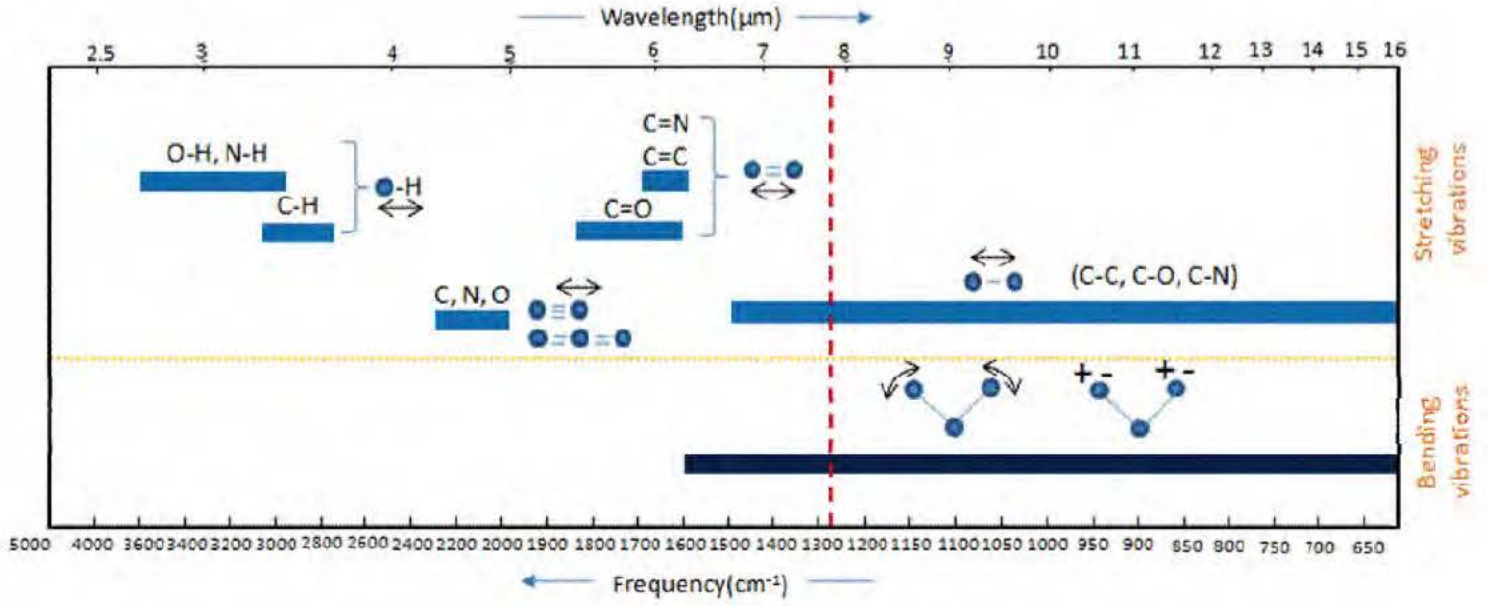

Raman Spectroscopy

Raman spectroscopy can be utilized non-invasively and provide real-time feedback.

Raman spectra of biological materials are not affected by spectral interference of water.

Raman spectroscopy is sensitive to both organic and inorganic components. Some biopsies may contain both soft tissue (muscle, fat, vessel, nerve) and mineralized tissue (cartilage and bone).

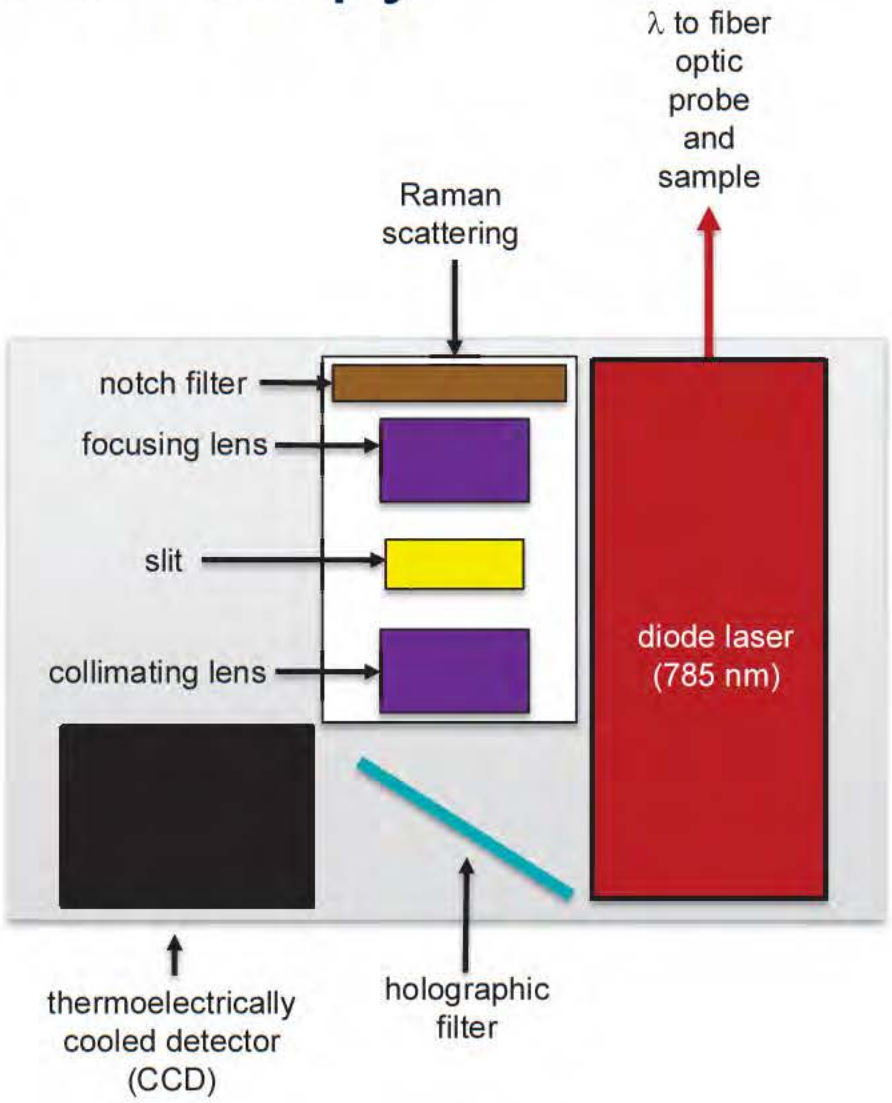

Interpreting a Raman Spectrum

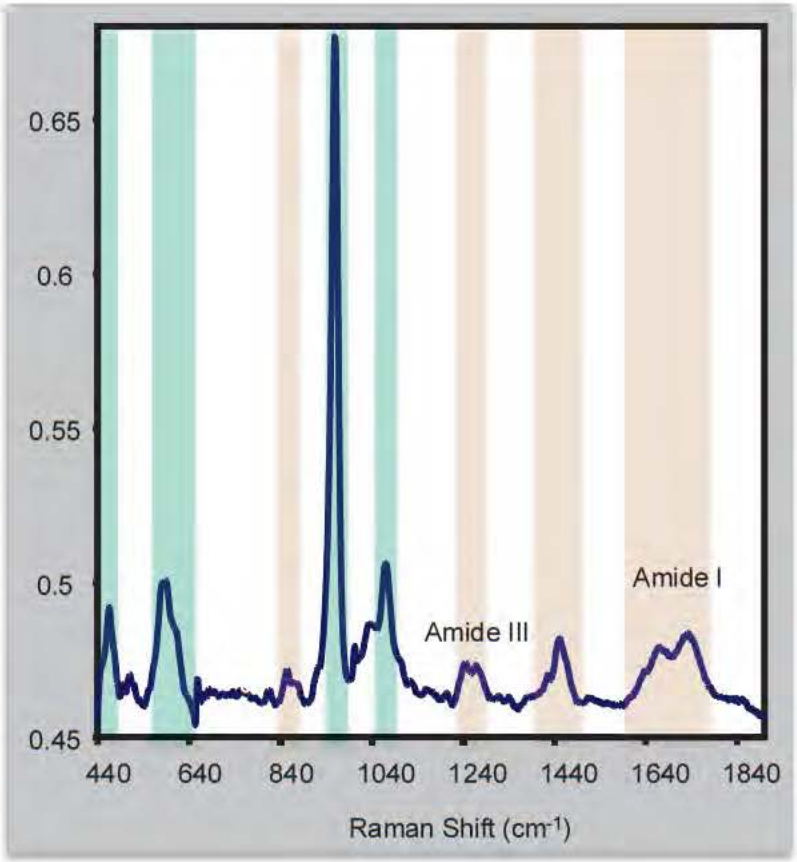

ν (cm^{-1})	Band Assignment	Component
593	ν_4 PO_4^{3-} bending	hydroxyapatite
821	ν(CC) o[illegible] ackbone	collagen; muscle
856	ν(CC) of hydroxyproline ring	collagen; muscle
873	ν_3 P-OH stretching	bone
876	ν(CC) of [illegible] y [illegible]roxypro[illegible]ne ring	collagen; protein
921	ν(CC) of proline ring	collagen; protein
938	ν(CC) of protein backbone	co lagen; muscle; protein
945-952	ν_1 PO_4^{3-} stretch	amorphous calcium phosphate
959	ν_1 PO_4^{3-} stretch	hydroxyapatite
1004	ν(CC) aromatic ring	Phe; collagen; muscle
1032	ν_3 PO_4^{3-} ; ν(CC) skeletal; C-O stretch	bone; collagen; muscle
1071	$\nu_1(CO_3^{2-})$	bone
1075	ν_3 PO_4^{3-} stretch	[illegible] y [illegible]roxyapatite
1080	ν(CC) and ν(CN) skeletal	collagen; muscle
1159	ν(CC) and ν(CN) skeletal	carotenoid
1178	ν(CC) and ν(CN) skeletal	collagen; muscle
1244	$\delta(CH_2)$ wagging; ν(CN) amide III disordered/β-sheet	collagen; muscle
1274	ν(CN) and δ(NH) amide III α-helix	collagen; muscle
1297	$\delta(CH_2)$ twisting	collagen; muscle
1343	$\gamma(CH_2, CH_3)$ wagging	collagen; muscle
1385	$\delta(CH_3)$ symmetric	collagen
1448	$\delta(CH_2)$ scissoring	collagen; muscle
1524	caro[illegible]enoi[illegible]	collagen; muscle
1552	ν(CC) ring stretch	collagen; muscle; Trp
1665	ν(CO) amide I	collagen; muscle

REGMED

Peak Fitting for Spectral Deconvolution

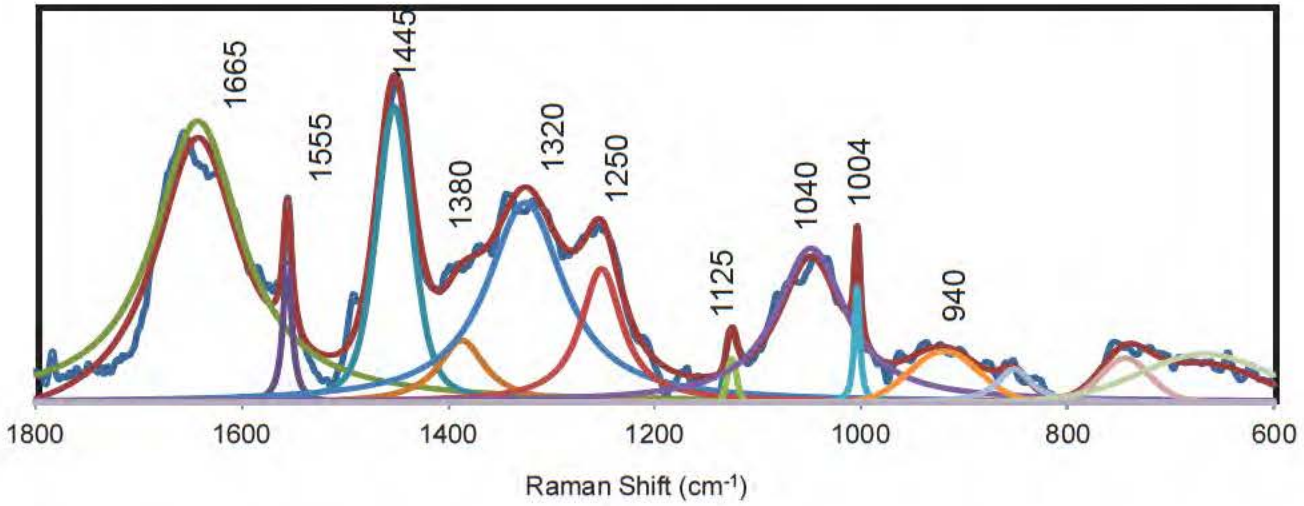

Raman Shift (cm^{-1})	Vibrational Band Assignment	Component
860	ν(C-C)	nucleic acids
920,940	ν(C-N), ν(C-C)	nucleic acids, keratin
1004	ν(C-C) ring	phenylalanine
1040	ν(C-C) skeletal	nucleic acids, protein
1125	ν(C-C), ν(C-N)	nucleic acids, protein
1250	ν (C-N) and δ(N-H); Amide III	protein
1320	$\delta(CH_2)$ twisting	nucleic acids, protein
1445	$\delta(CH_3)$ and $\delta(CH_{2})$ scissoring	protein
1555		aromatic amino acids, heme
1665	ν(C=O); Amide I	protein

REGMED

Information from Raman Vibrational Bands

Raman frequencies → composition of material

Changes in frequency → composition of material; stress/strain of state

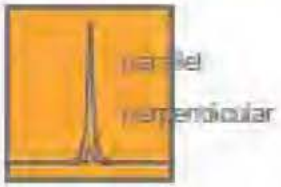

Polarization of band → crystal symmetry and orientation

Width of band → quality of structure, i.e. ordered vs. disorder

Intensity of band → amount of material

Raman Spectral Band Area Ratios (BARs)

Band area ratios (BARs), a pseudoquantitative measure, were calculated by dividing the band area of a Raman band of interest (for example 1070 cm^{-1}) by another band area (for example 1445 cm^{-1}).

Compositional trends in related samples can be explored using BARs, such as:

- a decrease in reducible collagen crosslinking (1680/1660 cm^{-1})
- mineral carbonation (1070/960 cm^{-1} and 1070/1445 cm^{-1})
- mineral maturity (945/960 cm^{-1})
- collagen order/disorder (1240/1270 cm^{-1})
- protein helical structure (1240/1300 cm^{-1})
- mineral crystallinity is determined by the full width at half maximum of the 960 cm^{-1} ν_1 phosphate band

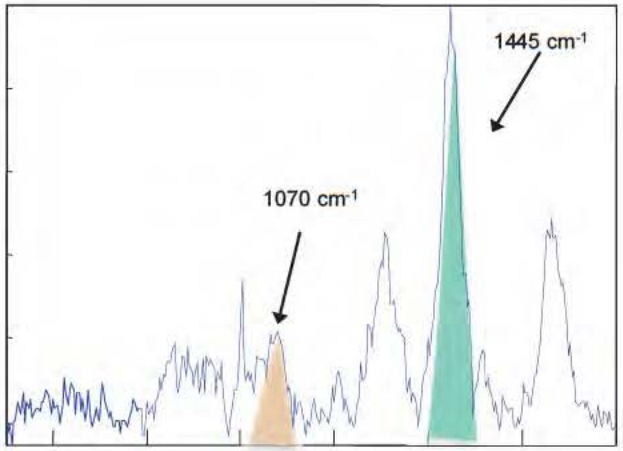

Wound Healing and Dehiscence

Data Collection – Wound Biopsies

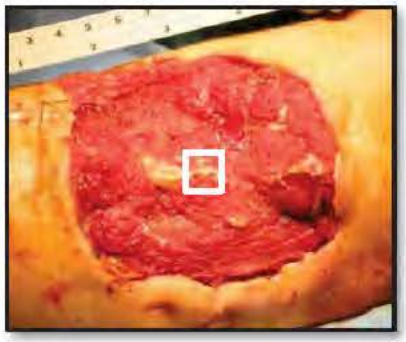

Approximately 1 cm^2 tissue biopsy is excised from the center of the wound bed.

Tissue is fixed in 10% neutral buffered formalin for storage.

Prior to spectral acquisition, samples are rinsed in 0.9% NaCl saline solution.

Examine multiple spots across the tissue.

20-40 accumulations, 5s spectrum

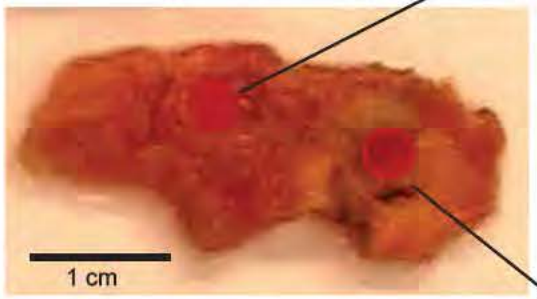

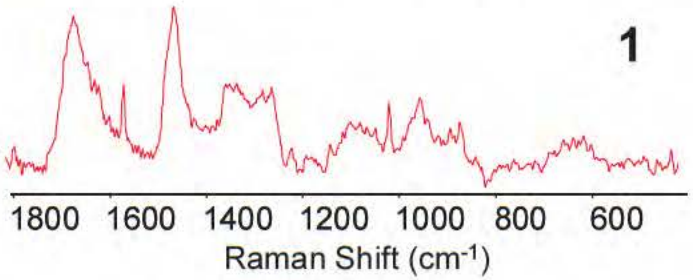

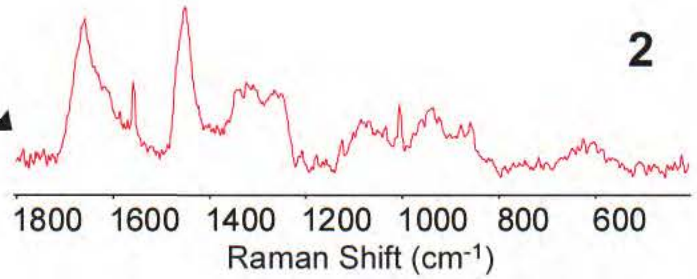

REGMED

Preliminary Study: Normal vs. Impaired Healing Wounds

Previous study demonstrated the potential of Raman spectroscopic analysis of wound biopsies for classification of wounds as normal or impaired healing from changes in the 1665 cm^{-1}/1445 cm^{-1} band area ratio.

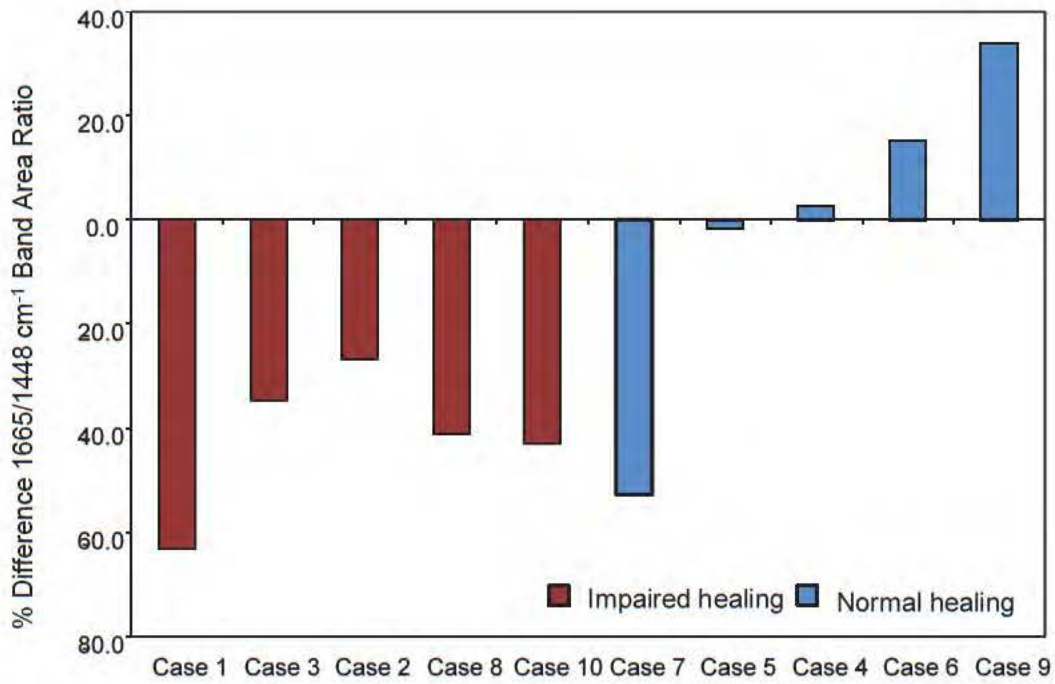

Impaired healing wounds demonstrate a significant decrease in the 1665/1448 cm^{-1} band area ratio compared to normal healing wounds, as demonstrated by Raman spectroscopic mapping.

REGMED

Wound Rep Regen. 18(4): 409-416, 2010.
Ann Surg. 250(6):1002-7, 2009.

Preliminary Study: Normal vs. Dehisced Wounds

Preliminary Data Analysis – 58 Calibration samples, 23 Validation Samples

- *53% healed normally , 47% dehisced*
- *60% developed HO, 40% did not develop HO*

Confusion	Actual	*Healed*	*Dehisced*
Predicted	*Healed*	25	1
	Dehisced	6	26

A prediction model can be created and validated.

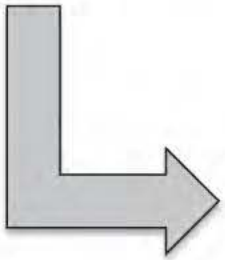

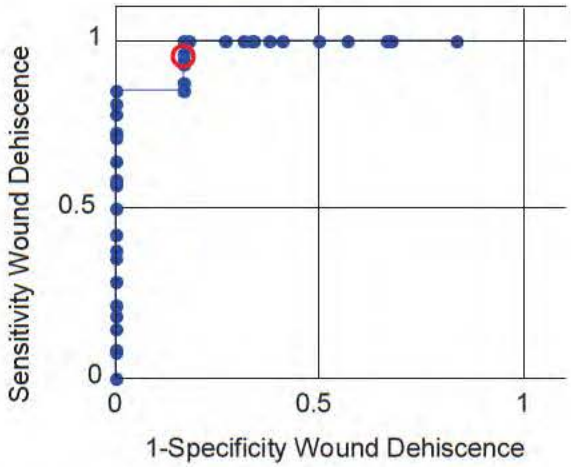

92.9% Sensitivity, **83.3%** Specificity for wound dehiscence

REGMED

Principal Component Analysis

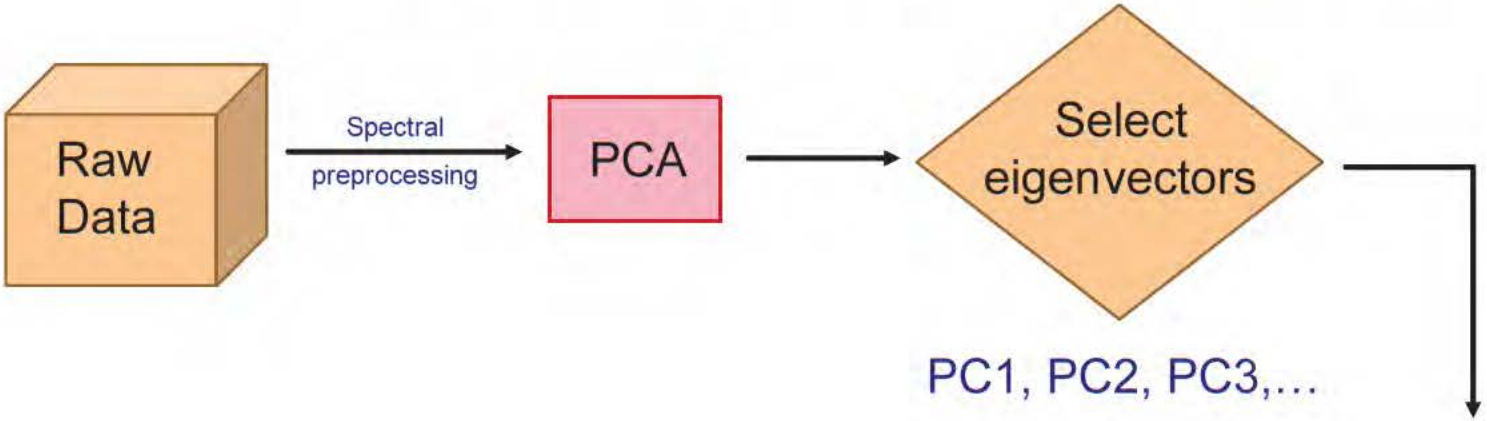

Orthogonal transformation to convert a set of spectra of possibly correlated variables (Raman shifts and/or bands) into a set of values of linearly uncorrelated variables called principal components (PCs).

The first PC is orthogonal to the other PCs.

This can be used to reduce dimensionality of the data set and to visualize the variance in the data – often a first step in PLSDA.

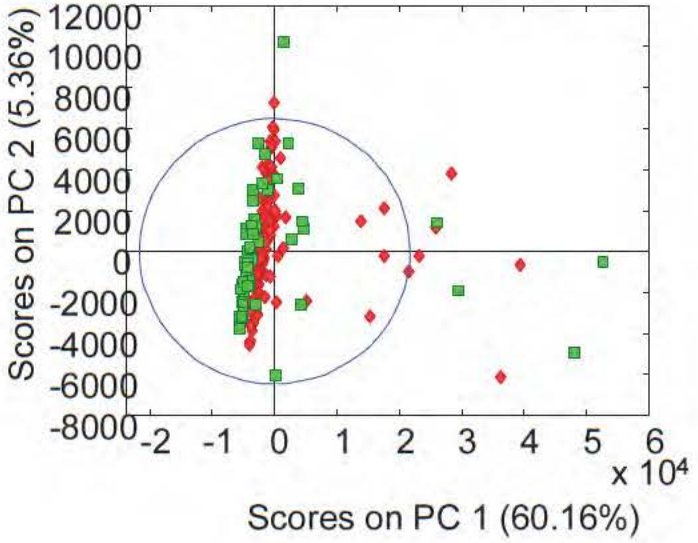

Raman Spectra of Wound Biopsies- PCA

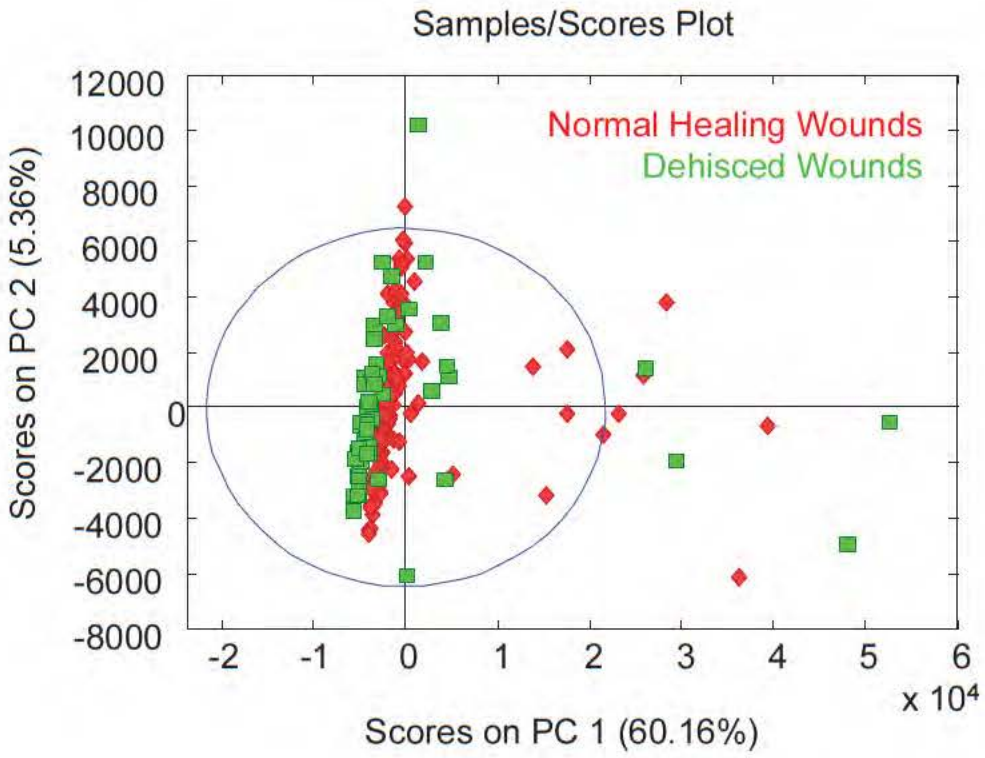

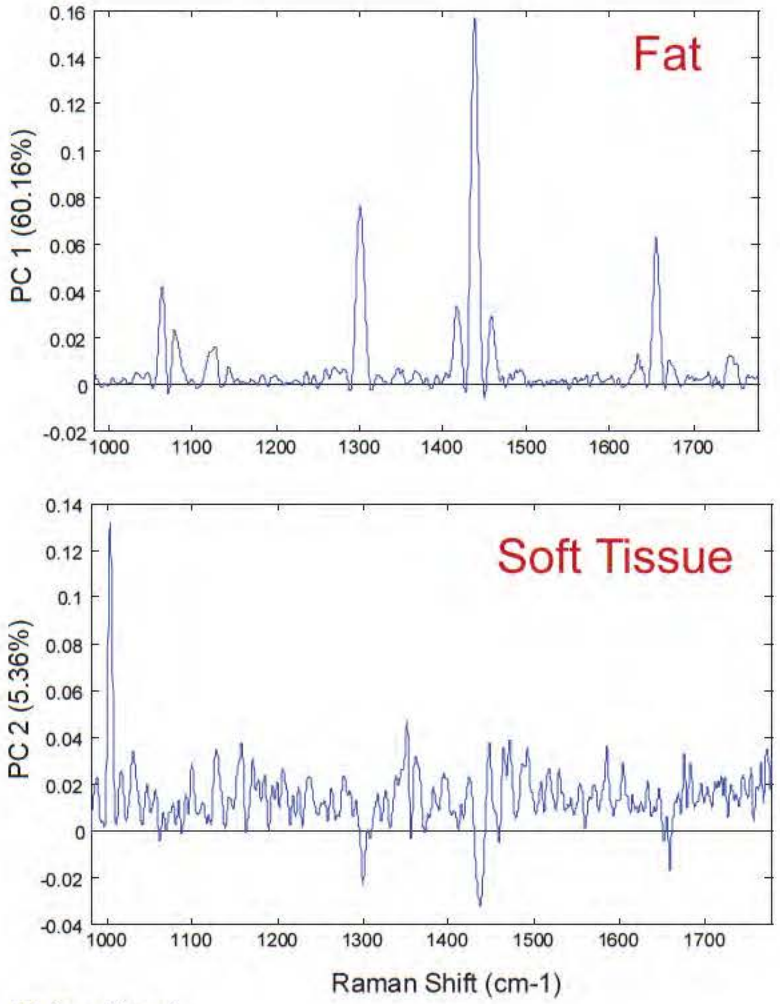

4 LVs, class center, automatic Whittaker baseline, (random subsets – 16 splits, 10 iterations)

Partial Least Squares Discriminant Analysis

What's being measured -

CALIBRATION

Regression Model

What's unknown -

PREDICTION

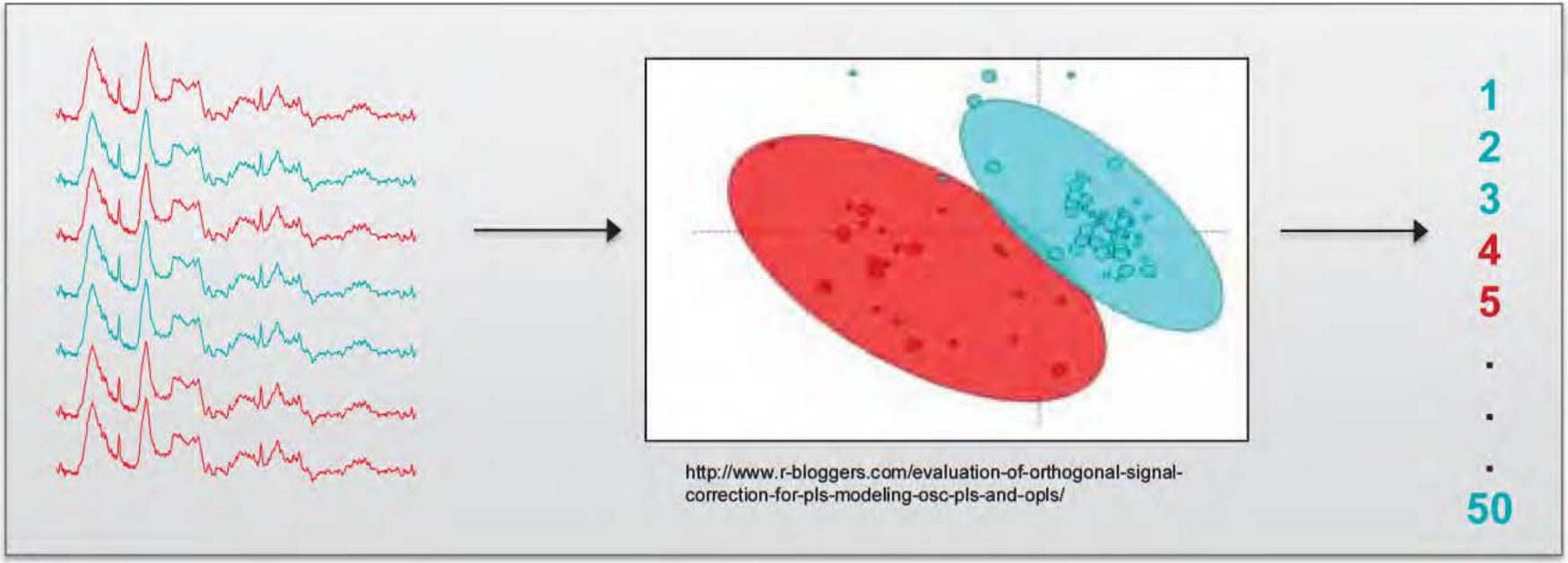

http://www.r-bloggers.com/evaluation-of-orthogonal-signal-correction-for-pls-modeling-osc-pls-and-opls/

REGMED

PLSDA of Raman Spectra for Wound Healing

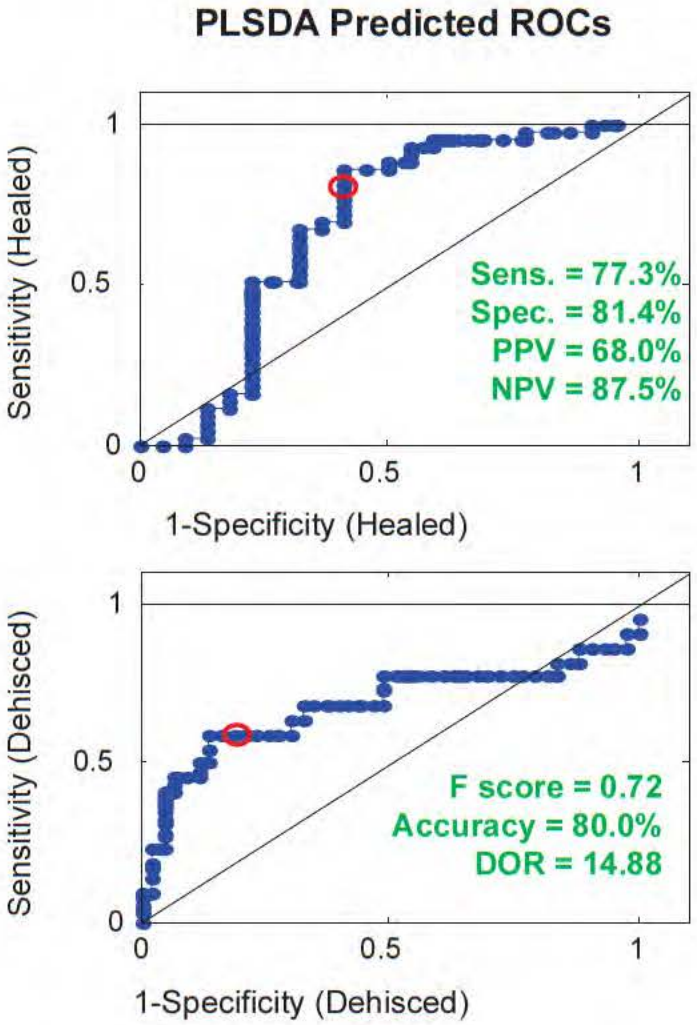

Confusion	Actual	*Healed*	*Dehisced*
Predicted	*Healed*	35	7
	Dehisced	8	15

AUC = 0.6808

3 LVs, class center, automatic Whittaker baseline, truncated 980-1746 cm^{-1}, random subsets – 16 splits, 10 iterations

REGMED

Wound Healing Conclusions

Preliminary studies demonstrate the promise of Raman spectroscopy for predicting wound outcome.

We need to further explore what might be contributing to the differences in outcome. Can we quantitate the amount of collagen in the wound via Raman spectroscopy?

We also need to test outcome modelling with additional outcome categories– healed vs. delayed healing vs. dehisced.

We propose applying the best of breed technologies in our toolbox, including:

- biomarker analysis
- informatics
- medical technology

Clinical Decision Support tools can be developed that can optimize and personalize treatment using patient-specific clinical variables combined with local and systemic biomarkers.

Goal: Maximize patient outcomes while minimizing complications.

Heterotopic Ossification

Heterotopic Ossification (HO)

Heterotopic ossification (HO) refers to the aberrant formation of mature, lamellar bone in non-osseous tissues.

Currently, orthopaedic surgeons faced with treating mature, refractory, symptomatic HO are left with few options other than operative excision.

Potter et al. J Bone Joint Surg Am. 2007;89:476-486.

Following most civilian trauma, HO formation is relatively rare in the absence of head injury. Even following traumatic brain or spinal cord injury, it develops in only 20% and 11% of patients. Rates of HO formation exceed 50% only in the setting of femoral shaft fractures with concomitant head injury and severe burns.

Potter et al. J Bone Joint Surg Am. 2010; 92, Suppl2: 74-89.

USA Today, February 12, 2006.

ORTHOPEDICS 2008;31(12):1237.

UPOJ 1998;11:59-66.

REGMED

What is needed is a technology can risk stratify the development of HO and identify tissue that *may* become HO – Raman spectroscopy.

Raman Spectroscopy Pilot Study of HO

Tissue biopsies, approximately 1cm^3, were obtained during surgical procedures and immediately snap frozen.

Normal Muscle (n=10)	Injured Muscle (n=10)	Early HO (n=10)	Mature HO (n=10)	Normal Bone (n=4)

Samples were thawed no more than 15 minutes unfixed and were immediately refrozen after spectral collection.

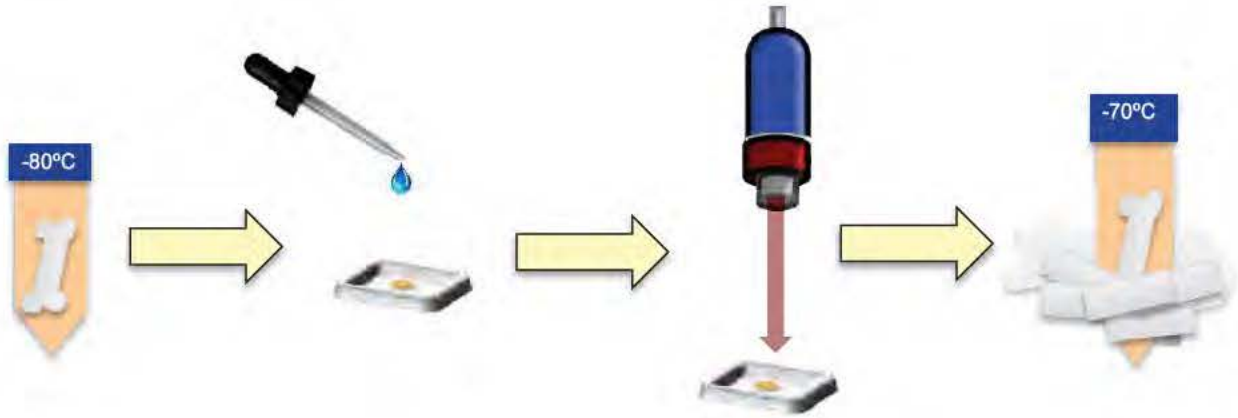

Raman Comparison of Muscle and HO

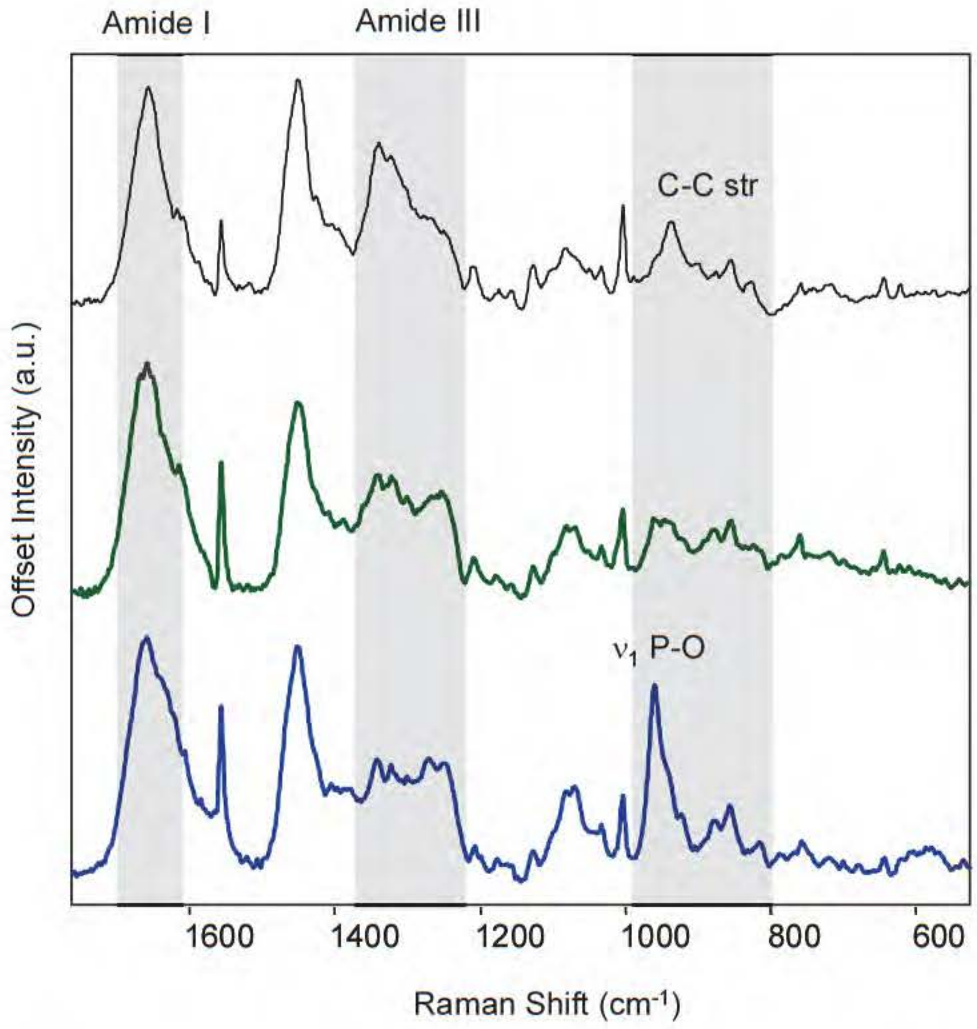

For the HO tissue, whether early or mature, the Amide I band shifts to a higher frequency and is centered at 1660 cm^{-1}.

The intensity of the 1340 cm^{-1} Raman vibrational band is decreased in the spectra of the HO tissue compared to the uninjured muscle tissue.

The 1270 cm^{-1} and 1240 cm^{-1} Raman vibrational bands are increased in the spectra of the HO tissue compared to the uninjured muscle.

The most notable difference in the spectrum of the mineralized HO tissue is the presence of the 960 cm^{-1} band, a ν_1 P-O stretching mode.

Finally, the intensities of the 921 cm^{-1}, 876 cm^{-1}, and 855 cm^{-1} bands are more intense in the spectra of the HO tissue than in the spectrum of the uninjured or injured muscle.

REGMED

J Bone Joint Surg Am. 2010 Dec;92 Suppl 2:74-89.

Comparison of Raman Spectral BARs

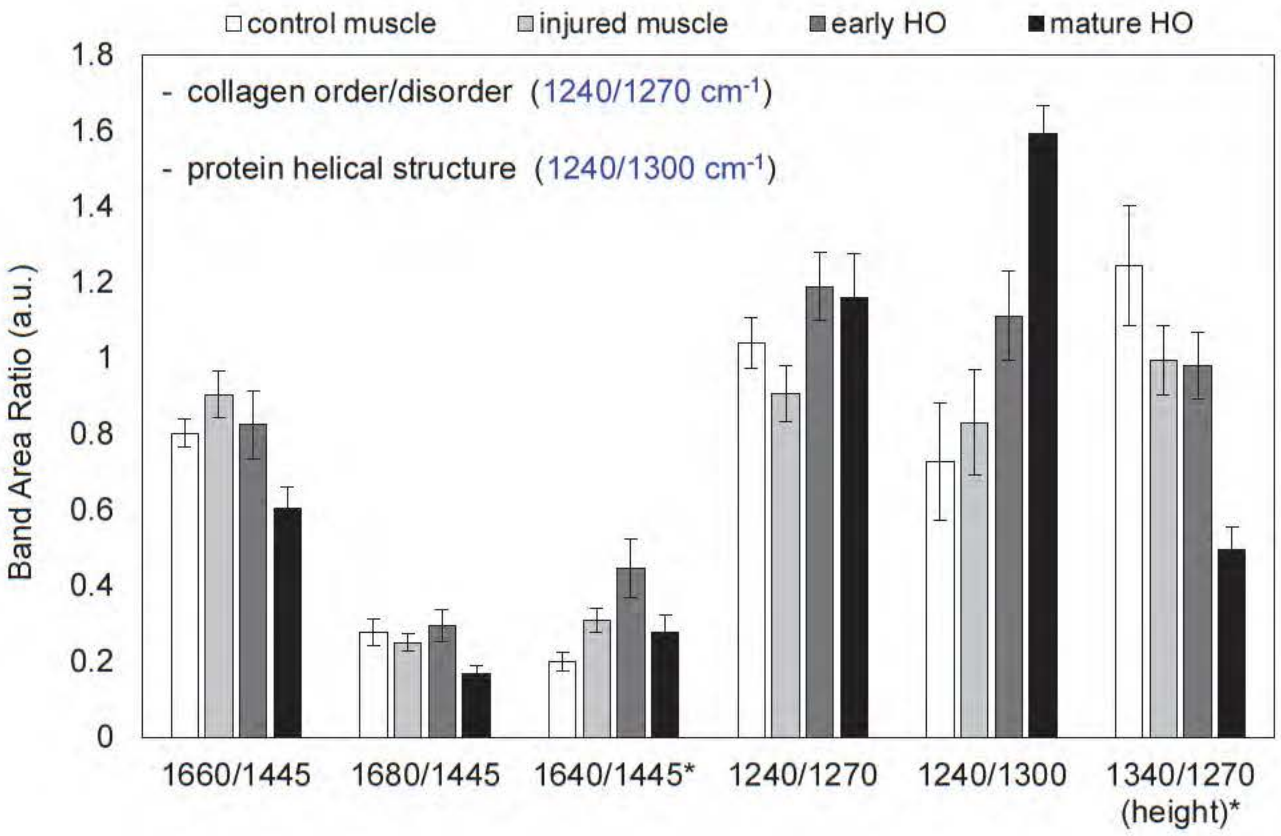

Transition from normal to injured muscle –

↑ 1660/1445 cm^{-1} and 1640/1445 cm^{-1}

↓ collagen order/disorder, and 1340/1270 cm^{-1}

Transition from injured muscle to HO tissue -

↓1660/1445 cm^{-1} and 1680/1445 cm^{-1} BAR

↑ in the collagen order/disorder BAR and the protein helical structure BAR

** Statistically significant differences ($p<0.05$) with a Bonferroni correction.*

REGMED

Bone. 2013 Sep 5;57(2):335-342.

Normal Bone versus Heterotopic Ossification

Early HO tissue was surgically removed within 165 days post-injury (mean) while mature HO was excised on average over 600 days post-injury.

- mineral carbonation (1070/960 cm^{-1} and 1070/1445 cm^{-1})
- mineral immaturity (945/960 cm^{-1})
- mineral crystallinity - FWHM of the 960 cm^{-1} ν_1 P-O band

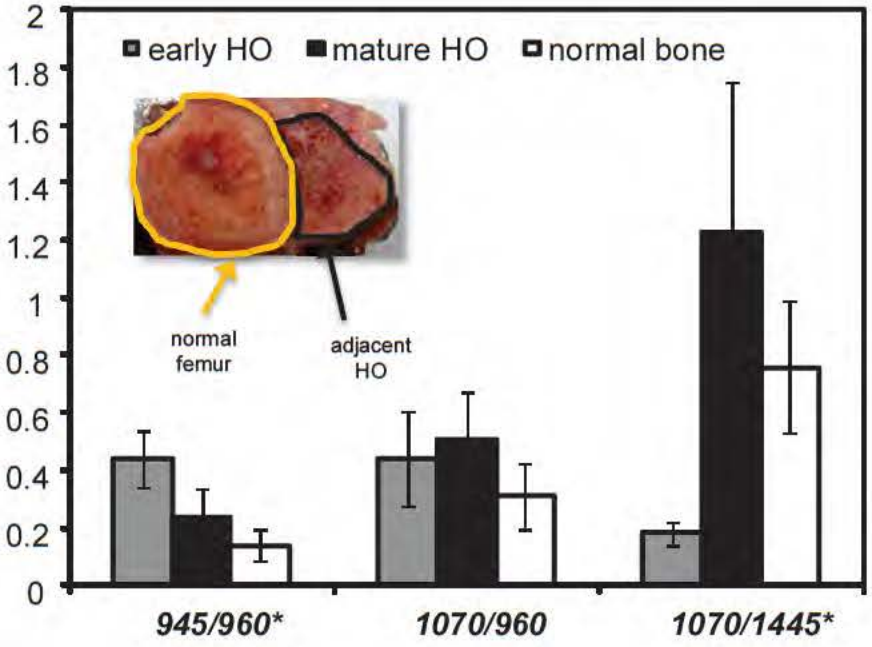

As bone matures –

↓945/960 cm^{-1} BAR and ↑1070/1445 cm^{-1} BAR

Early HO has the highest mineral immaturity BARs and the lowest mineral carbonation BARs.

This trend is reversed for mature HO –

- the mineral immaturity BARs are lower than early HO
- mineral carbonation BARs are higher than early HO tissue.

Mineral crystallinity is higher in mature HO samples than in normal bone or early HO samples.

REGMED

* *Statistically significant differences ($p<0.05$) with a Bonferroni correction.*

Bone. 2013 Sep 5;57(2):335-342.

Discrimination of HO Tissue by Raman Spectroscopy

Raman Spectral Features
2027 variables, 40 samples

Cross-validation	Actual HO	Actual no HO
Predicted HO	17	2
Predicted no HO	3	18

Sensitivity = 85%
Specificity = 90%

Positive predictive value = 89.4%
Negative predictive value = 85.7%

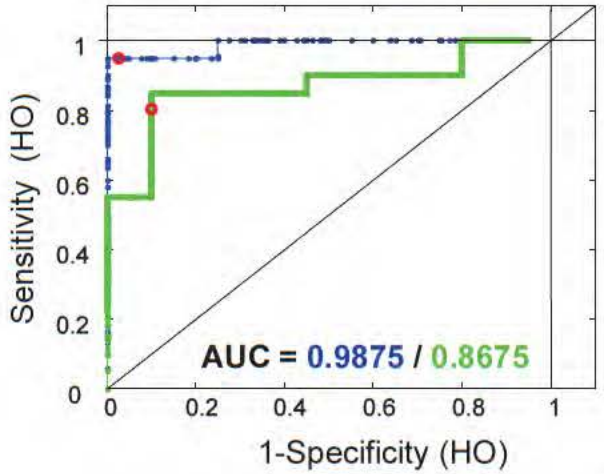

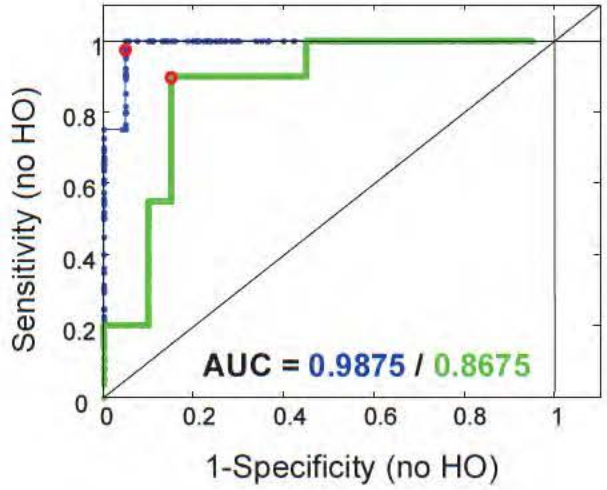

REGMED

Discrimination of HO Tissue by Raman Spectroscopy

Validation data set (external) consisting of 15 samples (53% HO, 47% no HO).

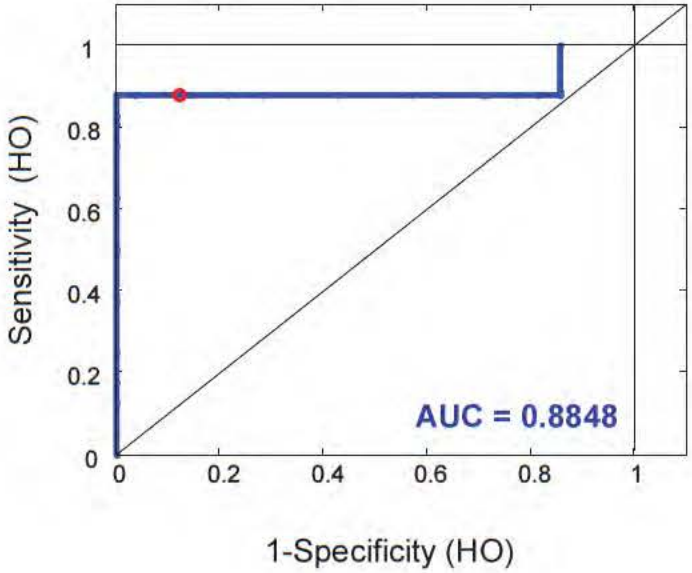

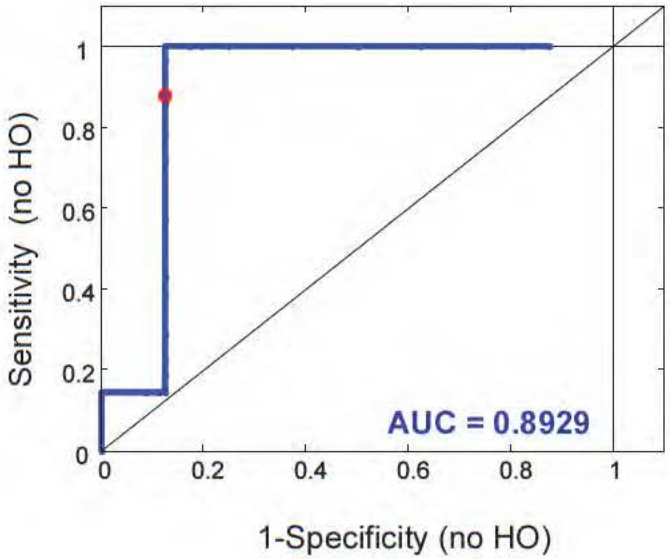

Sensitivity = 87.5%
Specificity = 85.7%

Positive predictive value = 87.5%
Negative predictive value = 85.7%

Prediction	Actual HO	Actual no HO
Predicted HO	7	1
Predicted no HO	1	6

Heterotopic Ossification Conclusions

In this preliminary study, we used Raman spectroscopy to discern molecular changes that that occur prior to and during the formation of HO.

While mature HO tissue is generally apparent upon physical examination and/or radiologic examination, immature and largely unmineralized HO tissue is not as clinically obvious.

The Raman spectra of various tissues demonstrate that there are clear differences in the Amide I and Amide III spectral regions of HO tissue compared to normal muscle tissue, which may indicate whether or not muscle tissue will develop HO.

Raman spectroscopy also provides insight into the actual mineralization of the soft tissue.

Raman spectroscopy can be adapted as an **objective, intraoperative, non-invasive** means by which to risk stratify wounds, and can be **performed in real-time**.

If Raman spectroscopy demonstrates that a wound has Raman spectral features associated with the formation of HO, prophylaxis could be employed in select cases.

Alternatively, in areas that appear prone to HO development the clinician can consider early preferential excision of pre-HO tissue while the patient is undergoing debridement and/or amputation revision for final closure.

Imaging Tissue Oxygenation and Perfusion

Extremity Injuries in Combat

Over 50% of military casualties from Operation Iraqi Freedom and Operation Enduring Freedom were recorded as involving major limb injury.

> Over 70% of vascular injuries in the Israeli-Lebanese conflict involved an injury to an artery in the extremity.

Tourniquets are appropriately applied in the field in 99.5% of extremity wounds to prevent hemorrhage.

Rapid restoration of blood flow to restore tissue perfusion is desirable, but not always possible.

Swine Model of Extremity I/R Injury

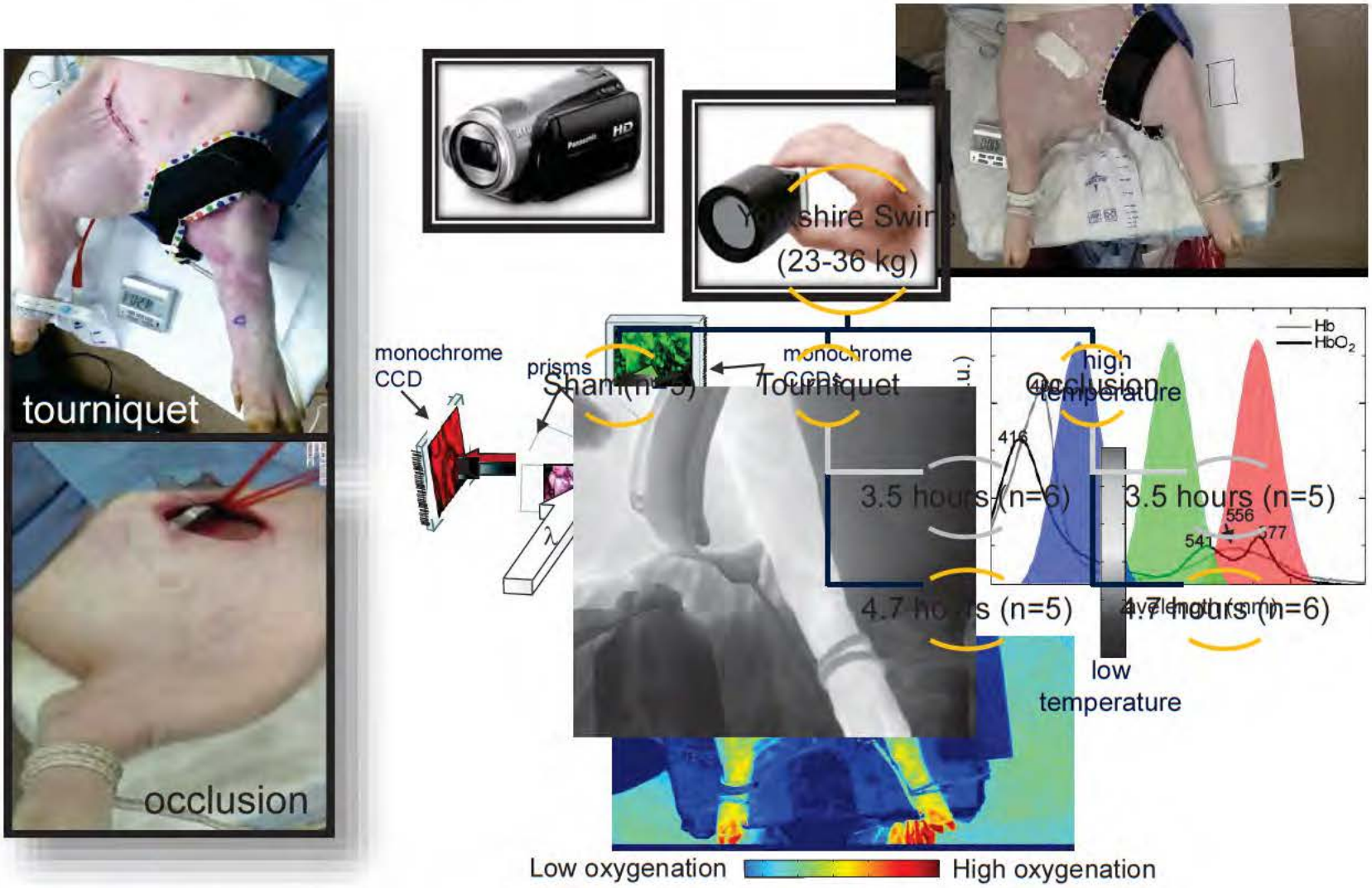

Visualizing Extremity I/R Injury

4.7 hour tourniquet case -

Images were extracted every 5 minutes for 282 minutes of ischemia and 30 minutes of reperfusion.

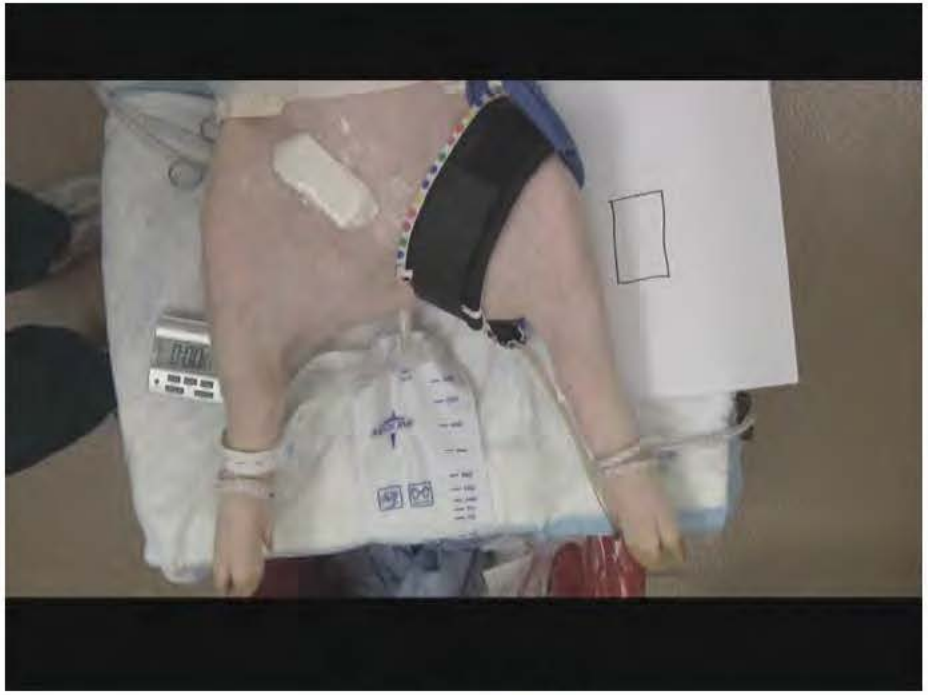

Raw 3CCD

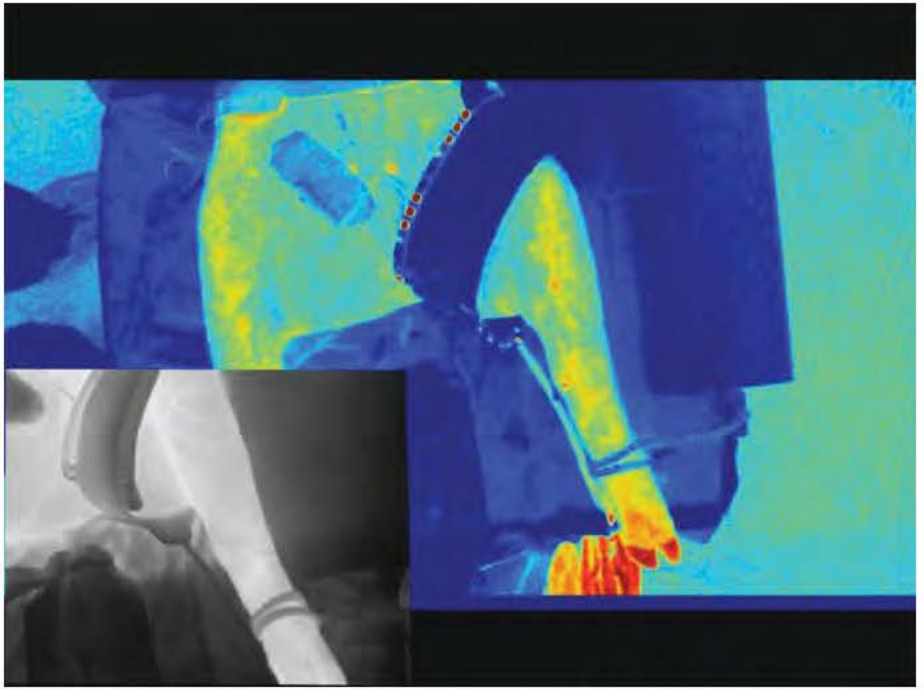

Composite Enhanced 3CCD/IR

REGMED

Visualizing Extremity I/R Injury - 2D

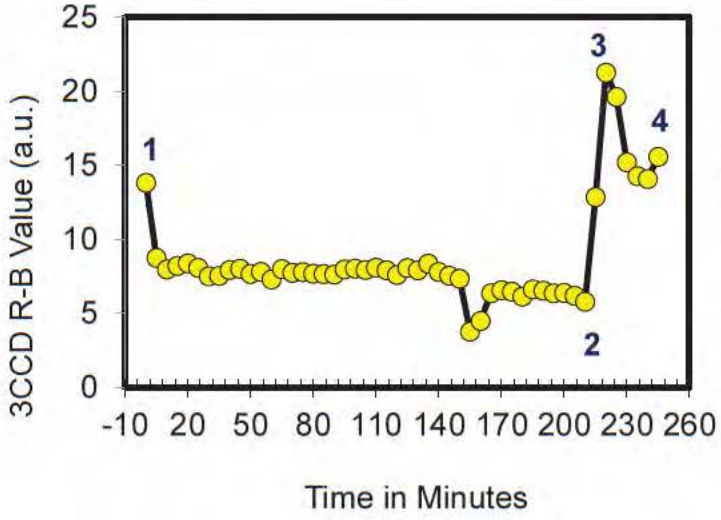

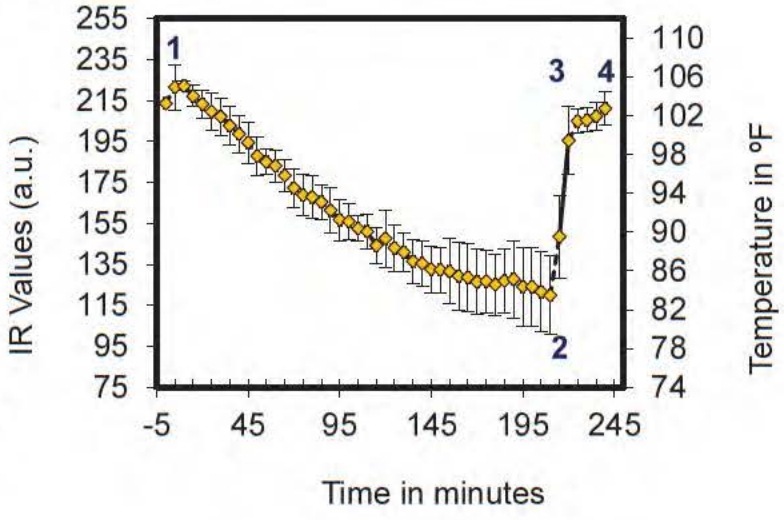

REGMED

Tissue Perfusion ≠ Tissue Oxygenation

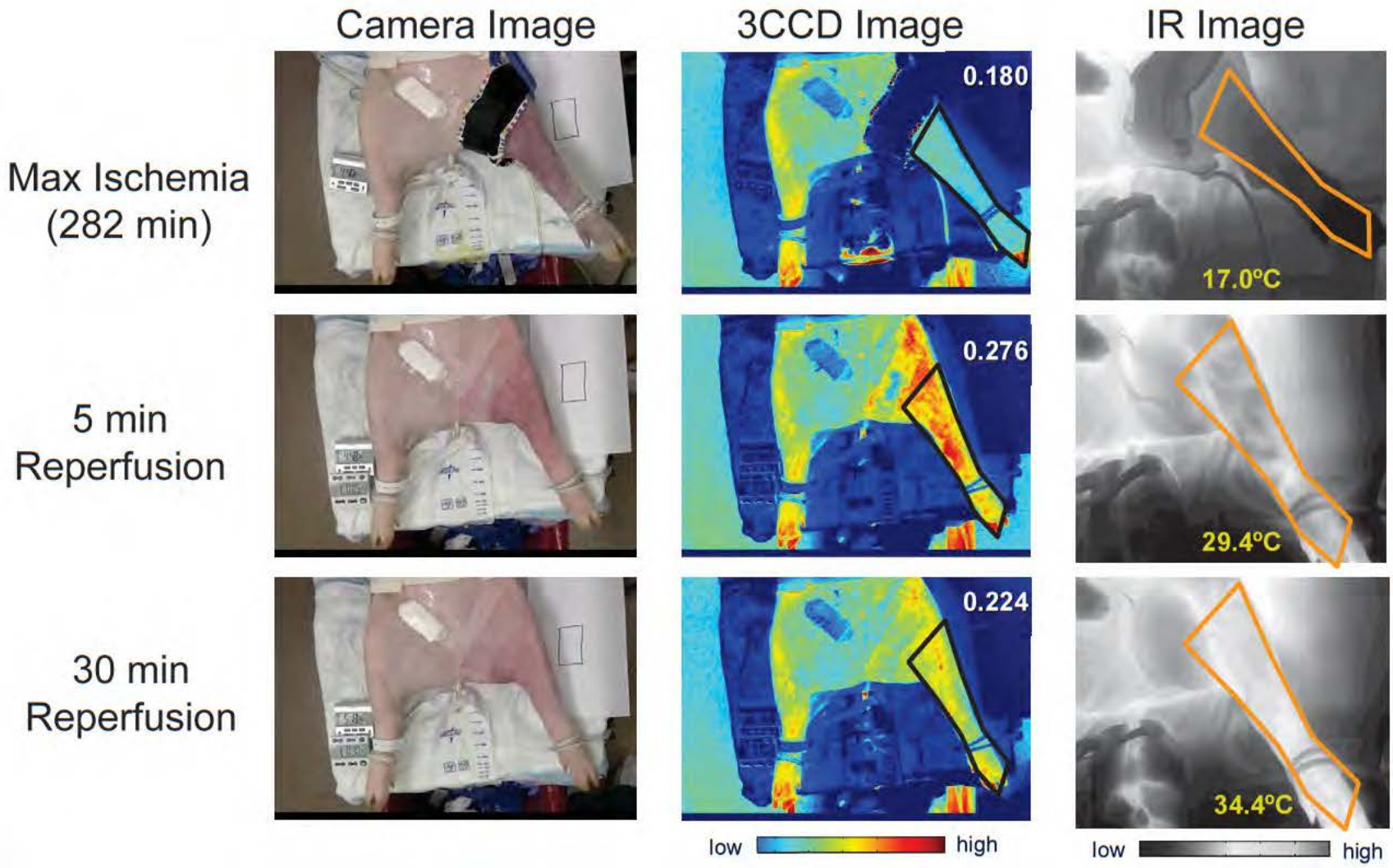

Post-Occlusive Reactive Hyperemia (PORH)

Post-occlusive reactive hyperemia (PORH) is an increase of blood flow after the release of an arterial occlusion, and occurs following the removal of a tourniquet or unclamping an artery during surgery.

The longer the period of occlusion, the greater the metabolic stimulus for vasodilation leading to increases in peak reactive hyperemia and duration of hyperemia. PORH is believed to be a measure of microvascular function.

In our model, the animal that suffer from the largest insult, their microvasculature is most affected, unable to deliver oxygen to the surrounding tissue – in spite of being normally perfused.

Here, we note that tissue perfusion ≠ tissue oxygenation.

PORH can be used to help identify patients with peripheral vascular disease.

Currently, Laser Doppler imaging is used to monitor PORH, but results are poorly reproducible in limbs versus fingers.

Here, we offer a means to monitor PORH in an entire limb.

Monitoring Oxygenation and Perfusion in Real-time

Using commercially available equipment, fused 3CCD and IR images can be co-registered along with their output values in real-time.

Enables simultaneous monitoring of tissue oxygenation and perfusion, which are not always synonymous in diseased tissue.

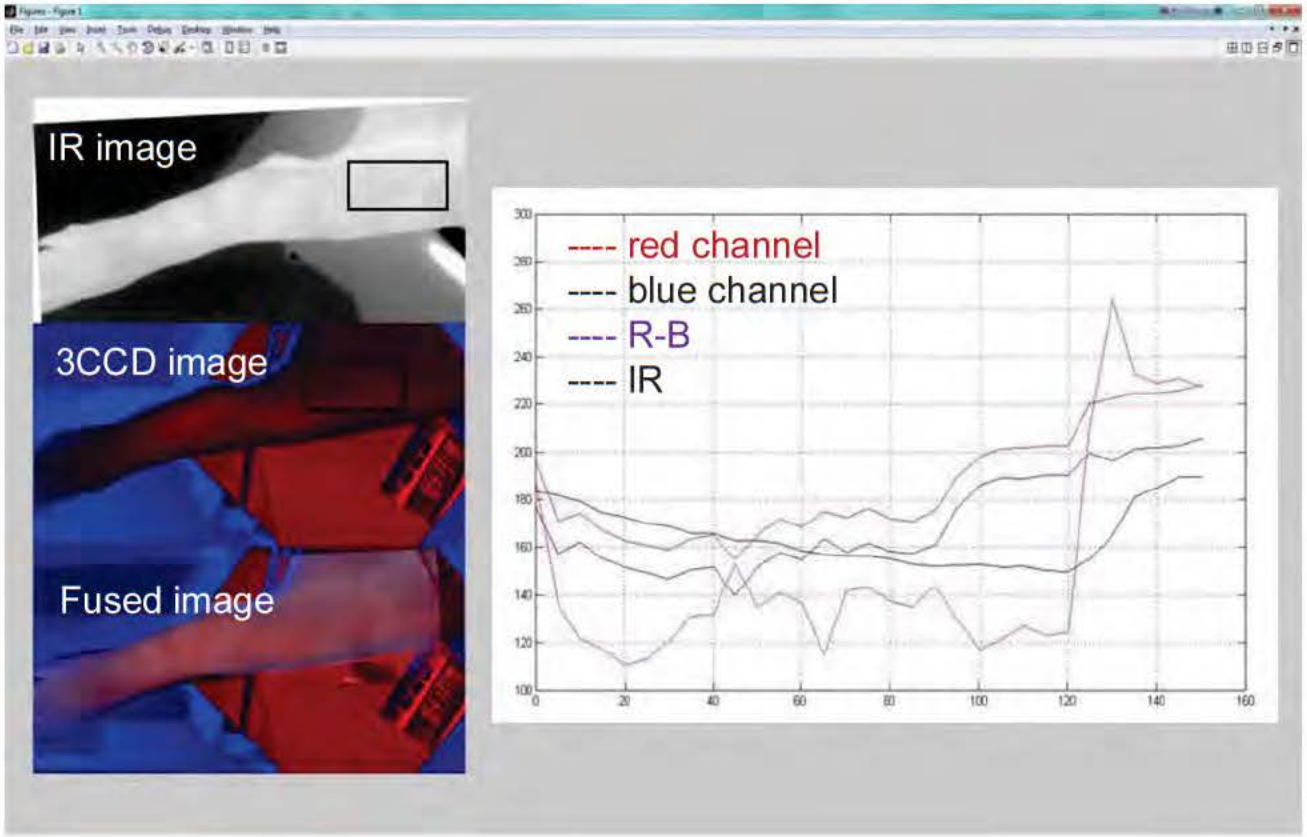

Women in Science

Being a Woman – Gender Bias in Science

In 2012, a journal article published in Proceedings of the National Academy of Sciences (PNAS) reported a gender bias among science faculty.

Faculty were asked to review a resume from a hypothetical student and report how likely they would be to hire or mentor that student, as well as what they would offer as starting salary. Two resumes were distributed randomly to the faculty, only differing in the names at the top of the resume (John or Jennifer).

The male student was rated as significantly more competent, more likely to be hired, and more likely to be mentored.

The median starting salary offered to the male student was greater than $3,000 over the starting salary offered to the female student.

“Two-thirds of the women interviewed, and two-thirds of the women surveyed, reported having to prove themselves over and over again – their successes discounted, their expertise questioned. “People just assume you’re not going to be able to cut it,” a statistician told us, in a typical comment.”

Moss-Racusin, Corinne A.; John F. Dovidiob; Victoria L. Brescollc; Mark J. Grahama; Jo Handelsman (August 2012). "*PNAS* **109** (41): 16395–16396.

Gender Bias in Science – Equality?

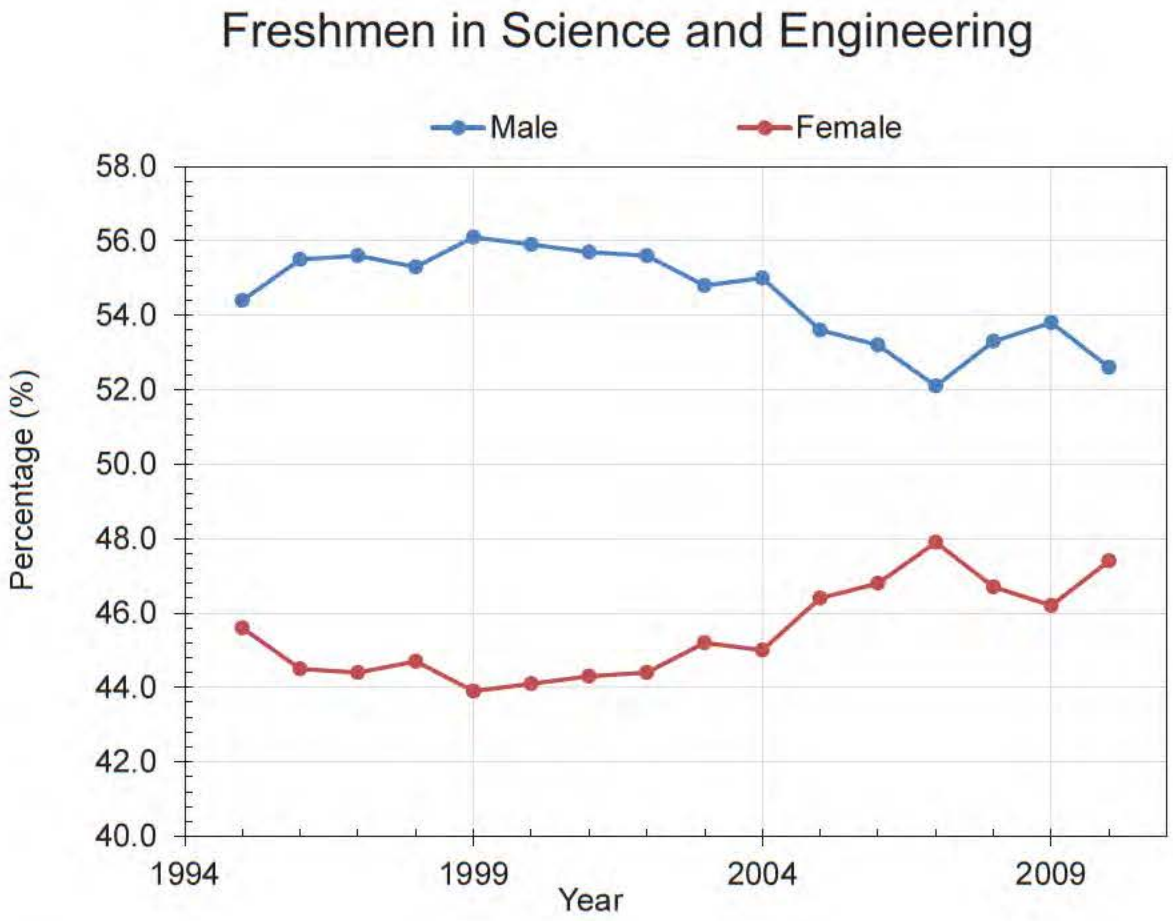

In 2012, U.S. residents were 50.8% female and 49.2% male.

In the Physical Sciences alone, in 2012, 67% of graduate students were male and 33% were female.

http://www.nsf.gov/statistics/wmpd/2013/tables.cfm

Gender Bias in Science – Worth?

For all degrees (2012)

Bachelor's (2012)

Master's (2012)

Doctorate (2012)

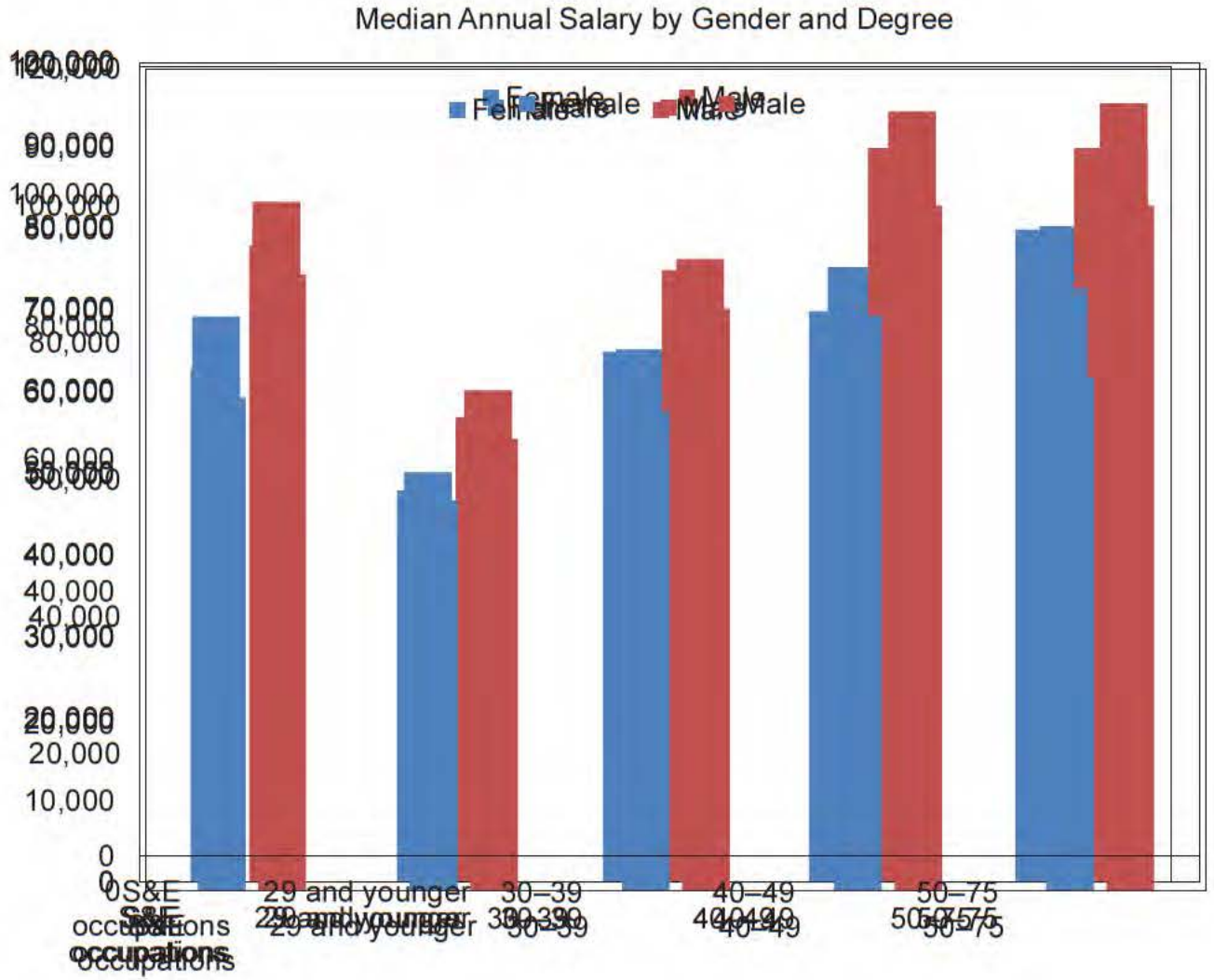

http://www.nsf.gov/statistics/wmpd/2013/tables.cfm

Gender Bias in Science – Proposed Reasons

1. “Women need to behave in masculine ways in order to be seen as competent—but women are expected to be feminine.”

2. “When professional women have children, they often find themselves running into a wall: their commitment and competence are questioned, and opportunities start drying up. ”

3. “Studies show that women who have encountered discrimination early in their careers often distance themselves from other women. An Asian-American statistician described how an older woman who “probably had to go through hell” made sure younger women did, too. This is just one of several ways gender bias can fuel conflict between different generations of women.”

4. “In some cases, the women intentionally kept their personal lives hidden in order to maintain their authority. One scientist said she avoided socializing with her colleagues because “to me, that lessens your authority.”

https://hbr.org/2015/03/the-5-biases-pushing-women-out-of-stem

Motivation and Advice

1. Love what you do - At the heart of it, I believe I have an opportunity to help people. That is my motivation, that is why I go to work every day.

2. My bonus - I really enjoy my research, truly. It is interesting and rewarding. Even more so, I love my interactions with students and employees. Watching them grow is as rewarding as watching my research program grow.

3. My challenges - Bureaucracy is everywhere, but without that infrastructure, I wouldn't have had access to the resources and opportunities that I have. Sometimes you just have to deal with tape.

4. My personal career goal – I hope there comes a day, during my career, when spectroscopic imaging and Raman spectroscopy are used as a common tools in the operating room.

5. Words of wisdom - My mother used to tell me that the sky is limit. I'd still like to believe her. If you let someone limit you, you're limited.

   Don't be afraid to negotiate your self worth and ask for what you want.

Acknowledgements

Regenerative Medicine Dept, NMRC

Jonathan Forsberg, MD
Thomas Davis, PhD
Nicole Crane, PhD
Katherine Cilwa, PhD
Trevor Brown, PhD
Matthew Wagner, PhD
Richard Barth, MS
Ying Cao, MS
Felipe Lisboa, MD
Khairul Anam, PhD
Anthony Foster, PhD
Ammar Qureshi, PhD
Michael Wiley, MBA
Mihret Amare, MS
Alison Tomasino, BS
Nick Clark, BS
Crystal Leonhardt
Fred Gage
Toby Perkins

Orthopaedics Dept, WRNMMCB

Romney Andersen, MD
B. Kyle Potter, MD
Wade Gordon, MD
Jean Claude D'Allyrand, MD
Robert Beer, MD
Mark Fleming, MD
Susan Foster, RN

Department of Surgery, USUHS

Eric Elster, MD FACS
Leon Nesti, MD, PhD
Arnaud Belard, MBA
Rochelle Collantes, PhD
Tiffani Slaughter, BS

REGMED
Shaping the Future of Casualty Care

THANK YOU!

TO HEAL OR NOT TO HEAL? MONITORING COMBAT WOUND OUTCOME USING RAMAN SPECTROSCOPY.

James M. Prieto[1], Sean M. Mock[1], Nicole J Crane[2]
[1]Uniformed Services University of the Health Sciences, Bethesda, MD
[2]Regenerative Medicine Department, Naval Medical Research Center, Silver Spring, MD

Abstract

The management of wounds sustained from combat events has proved to be a major challenge to physicians over the last decade. Recent conflicts have shown to produce a higher proportion of injuries due to blasts and high energy projectiles. Raman spectroscopy may offer a non-invasive technology through which to monitor the healing of these wounds. Given that collagen content has been previously established as the main factor in determining the tensile strength of a wound, it may be beneficial to be able to quantify the collagen deposition in a healing wound bed. Hydroxyproline, which is a major component of collagen, has been associated with a specific band area in the spectra of tissue samples. Using Raman spectroscopy, 76 wounds samples were analyzed, and the band area (843 cm^{-1} - 883 cm^{-1}) known to be associated with hydroxyproline was measured at various time points throughout the healing process. This band area was found to have a statistically significant relationship with the eventual wound outcome (dehisced or healed). Further work is yet to be done confirming whether or not this band area is truly reflective of the amount of hydroxyproline or collagen in the wound bed, yet this demonstrates the potential that Raman spectroscopy has in allowing the physician to non-invasively recognize when a wound may be in danger of failing.

Background

A higher proportion of complex injuries involving blasts and high energy explosives has been noted in recent conflicts. There has also been noted to be an increase in wounds to the extremities as a result of the increasing use of body armor. [1]

The process of wound healing is a dynamic process involving multiple mediators, cells, and extracellular molecules. The healing of these complex wounds has proven to be a challenge to surgeons with respect to successful wound closure.

Preliminary studies have found that Raman Spectroscopy shows promise as a technique to be used to monitor the molecular changes that occur in the wound bed in order to predict the likelihood of successful wound closure. [2]

Collagen content in the wound bed appears to play a major role in establishing the strength of the healed wound. [3] Hydroxyproline is a major component of the collagen molecule and produces a specific band in the Raman Spectra of biological tissue samples. [4]

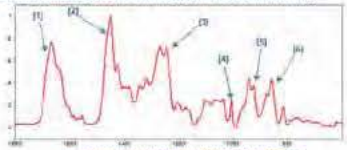

Figure 1: Raman spectra of type I Collagen with critical band assignments highlighted and listed in table below

Number	Raman Shift (cm^{-1})	Band Assignments
1	1665	Amide I
2	1450	Protein CH_2 Deformation
3	1272, 1243	Amide III
4	1003	Phenylalanine
5	920, 858	Proline Backbone
6	873	Hydroxyproline

Band Assignments for Raman spectra of Collagen I shown in Figure 1

[5]

Materials & Methods

Wound tissue biopsies were obtained from IRB approved studies at Walter Reed National Military Medical Center. Approximately 1cm^3 of tissue was collected from the center of the wound bed from combat-wounded patients during each surgical debridement and fixed in formalin.

Fixed biopsies were examined ex vivo using the Raman RXN 1 (785 nm [1]) w/ PHAT Probe; spot size 4.7mm.

The spectra of the first and last biopsies were compared from the healing process of each wound.

Hydroxyproline band area was calculated from the total band area between 843 cm^{-1} and 883 cm^{-1}.

Hydroxyproline band area between first and last biopsy from each wound was compared.

Change in band area for each wound was compared with the eventual outcome of the wound (healed or dehisced). Of note, there were four separate wounds which were classified as "delayed" (longer than 30 days till closure or two standard deviations from the mean). These wounds were excluded from the study.

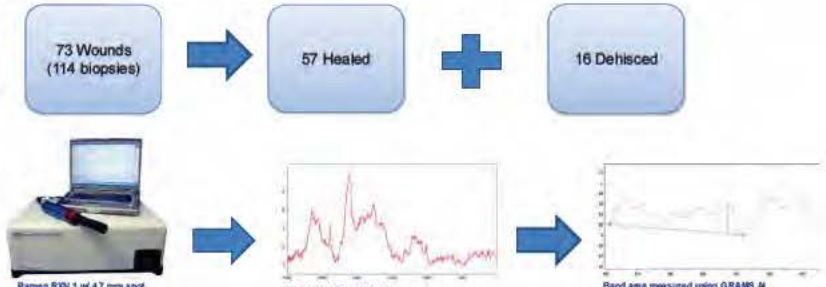

Results

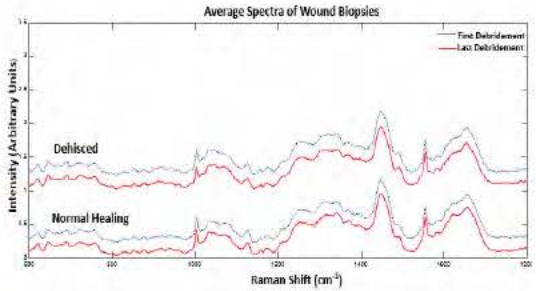

Wound Outcome	Number	Change in Band Area (%) +/- SEM	P-VALUE
Healed	57	33.5 +/- 7.9	
Dehisced	16	-20.4 +/- 4.2	0.001

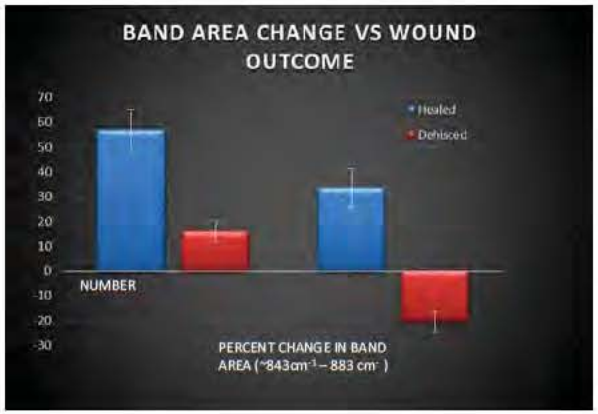

Summary of Results & Conclusions

The average wound spectra for each type of wound (healed vs dehisced and first vs last debridement) were noted to be very similar when averaged and plotted. This illustrates the difficulty in using Raman spectroscopy to detect subtle differences in the molecular makeup of biological tissues.

However, the change in band area between first and last debridement was noted to be significantly different between normal healing and dehisced wounds. The results suggest that the normal healing wounds had an increase in hydroxyproline (collagen) throughout the healing process while dehisced wounds showed a decrease. This would make sense considering that collagen deposition is a known important step in the wound healing process. This data is further supported by the fact that collagen is known to be critical in determining the tensile strength of a wound.

Further work needs to be done to confirm the ability of Raman spectroscopy to detect relative amounts of hydroxyproline in biological tissue samples. Currently, the "gold standard" for such a measurement is high performance liquid chromatography. If this could be established, then perhaps Raman spectroscopy could be reliably used as a non-invasive method to analyze the progress of collagen deposition in a healing wound bed.

References

[1] Owens BD et al,. Combat Wounds in Operation Iraqi Freedom and Operation Enduring Freedom J Trauma. 2008;64:295–299
[2] Crane NJ et al., Monitoring the healing of combat wounds using Raman spectroscopic mapping Wound Rep Reg (2010) 18 409-416
[3] F. C. Brunicardi et al., Eds., Schwartz's Manual of Surgery, 8th ed., McGraw-Hill, New York (2006)
[4] T. T. Nguyen, et.al., "Characterization of Type I and IV Collagens by Raman Microspectroscopy: Identification of Spectral Markers of the Dermo-Epidermal Junction," Spectroscopy: An International Journal, vol. 27, no. 5-6,
[5] Hawksworth et al., Inflammatory Biomarkers in Combat Wound Healing, Annals of Surgery 250(6):1002-1007, December 2009

Total Tourniquet Time and Successful Wound Healing in Acute Combat Wounds

Nicole J. Crane [a], Eric A. Elster[a,b,d], Benjamin K. Potter[a,c,d], Jonathan A. Forsberg[a,c,d], Sean M. Mock

[a]Department of Regenerative Medicine, Naval Medical Research Center, Silver Spring, MD
[b]Department of Surgery, Walter Reed National Military Medical Center (WRNMMC), Bethesda, MD
[c]Orthopaedics and Rehabilitation, Walter Reed National Military Medical Center, Bethesda, MD
[d]Department of Surgery, Uniformed Services University of the Health Sciences, Bethesda, MD

Abstract

The ability of tourniquets to effectively stop arterial hemorrhage has made it a staple of pre-hospital care in combat situations. Increased training in the proper employment of tourniquets reduced pre-hospital deaths from arterial exsanguination, by one author's estimate, from 9% to 7% to 2% of deaths in the armed conflicts in Vietnam, Somalia, and Iraq, respectively.[1,2] Prolonged ischemia from excessive tourniquet use can, however, cause both local and systemic adverse effects. Re-introduction of blood flow to an ischemic limb has the potential to induce an ischemia-reperfusion injury, propagated largely by granulocytes and free radicals.[3] Investigative studies in animal models have observed effects of cycles of tourniquet-induced ischemia and reperfusion in terms of metabolic markers and histological changes to striated muscle.[4,5] There is, however, a paucity of literature on the relationship between total tourniquet exposure and wound healing in humans.

This study sought to statistically determine whether or not there exists a correlation between total tourniquet time and specific wound outcomes within a previously studied population of Wounded Warriors who received traumatic injuries and subsequently underwent wound-revising operations until wound closure. For example, individuals who underwent statistically lower total tourniquet times may be more likely to undergo successful wound healing, while individuals with statistically higher total tourniquet time may be more likely to dehisce or suffer acute wound failure.

Background

The proven effectiveness of tourniquets in preventing death from arterial exsanguination warrants a permanent position for them in our repertoire of life-saving interventions. Given this fact, it is appropriate that we more fully understand the adverse effects which have been documented with the use of tourniquets. Further, we must delve into underlying pathophysiology so as to potentially complement the use of tourniquets with optimizing interventions aimed at minimizing adverse effects.

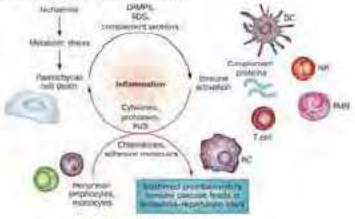

Fig 1 Ischemia-Reperfusion Injury

Adverse effects have been observed from the prolonged occlusion of arterial blood supply to a limb. These consequences can be local, such as edema, compression neuropraxia, bone and soft-tissue necrosis, or compartment syndrome.[6] They can also be systemic, as in acid-base alterations and systemic inflammatory response syndrome.[2] With return of perfusion following removal of a tourniquet, there is an inherent risk of varying degrees of ischemia-reperfusion injury, dependent upon the degree of ischemia which existed initially. This ischemia-reperfusion injury is mitigated largely by granulocytes, such as neutrophils, and free radicals, such as reactive oxygen species.[3] The former create damage in the same manner as in other acute inflammatory reactions.[7] The latter damage surrounding tissue by reacting with cell membranes, among other mechanisms. Both of these facets of injury—the increase in active granulocytes and increase in free radicals—increase upon reperfusion of the area of ischemia. Returning blood brings with it granulocytes that will localize to the area of injury. The blood also returns oxygen to the area in which free radicals were being generated, providing substrates for the formation of reactive oxygen species.[8,9] The inflammatory nature of the ischemia-reperfusion injury can in itself have consequences both locally and at other locations in the body. Tissue that is remote from the site of ischemia, such as liver and lung, can be adversely affected.[6]

Materials & Methods

Through the Joint Trauma System, archived tourniquet time data was acquired from the prehospital and in-patient records of 132 wounds from 83 active duty patients. These subjects were previously enrolled in either of two approved studies at Walter Reed National Military Medical Center observing wound outcomes in Wounded Warriors. Both studies observed a primary clinical outcome of "successful wound healing after definitive closure or coverage."

All subjects were wounded in either Operation Iraqi Freedom or Operation Enduring Freedom.
Wounds were observed for thirty days and received the following standardized care:

- surgical debridement
- pulse lavage
- VAC application

} every 48-72 h, until surgical wound closure or coverage

Wound healing was considered impaired if the wound dehisced after closure or coverage or if closure was delayed (defined as ≥ 21 d after injury, or two standard deviations out of the study's mean normal wound closure time).[10]

Fig 2 The Joint Trauma System

Results

To this point, the data required for analysis in this study remains incomplete. The data available at this point is extremely limited, with data from the pre-hospital care of many subjects presently listed as "unknown" within the Joint Trauma System. The initial time during which a tourniquet was applied to each subject following injury presumably represents the majority of time during which the said individual would have been subject to tourniquet use. As such, analysis cannot be adequately performed at this time.

Discussion

The role that time plays in ischemia-reperfusion injury has been studied in various animal models. One study observed metabolic (lactic acid, creatine phosphokinase, and pH) and histologic changes in the rat hind-limb model during tourniquet-induced ischemia.[4] They observed signs of degeneration by one hour of ischemia, which increased as ischemic time continued. The study showed that the percentage of histologically "normal" striated muscle in affected tissue dropped to near minimal values within the first three hours following tourniquet release, when compared to the percentage differing from normal histology at twenty-four hours post-tourniquet release. Functionally, the study showed similar decreases in contractility of the striated muscle in the first three hours. At twenty-four hours post-ischemia, however, the percentage of contractile tissue increased towards the norm dramatically.

These results held most true up to four hours of ischemia time—within which time range the clinical usage of tourniquet-induced ischemia lies. The study demonstrated that the damage induced by ischemia perpetuates forward in time from when a tourniquet is released. It additionally demonstrates that the return to normal function and histology is limited and time-dependent. Timing of ischemia and reperfusion therefore have effects on histological changes to the tissue itself which only resolve to a certain extent. Ischemia and reperfusion evidently results in a change in the inflammatory state of the tissue and organism involved. Given the limited ability for histological changes caused by ischemia to resolve and the inflammatory changes brought about by ischemia, one may speculate as to whether or not total ischemia time may contribute to inflammatory dysregulation or, more locally, to wound failure.

Summary of Results & Speculation

As mentioned before, this study met challenges with severely limited data on prehospital care of the subjects involved in this study. An outstanding system of prehospital combat casualty data called the Prehospital Trauma Registry (PHTR) exists within the 75th Ranger Regiment[12]. Increased use of innovations such as this and the Casualty Care Card employed under Tactical Combat Casualty Care (TCCC) may hopefully increase prehospital data capture to a point where a study such as this one is more successful.

Fig 3 The TCCC Casualty Card. (*Image adapted from chinookmed.com*)

References

[1]Beekley, AC, et al. "Prehospital Tourniquet Use in Operation Iraqi Freedom: Effect on Hemorrhage Control and Outcomes." The Journal of Trauma: Injury, Infection, and Critical Care. 2008; 64: S28 – S37.

[2]Kragh, JF, et al. "Battle Casualty Survival with Emergency Tourniquet Use to Stop Limb Bleeding." The Journal of Emergency Medicine. Vol. 41, No. 6, pp 590 – 597, 2011.

[3]Gillani, S, et al. "The effect of ischemia reperfusion injury on skeletal muscle." Injury, Int. J. Care Injured 43 (2012) 670 – 675.

[4]Heppenstall, RB, et al. "Pathophysiologic Effects Distal to a Tourniquet in the Dog." The Journal of Trauma. 1979; Vol. 19, No. 4, pp 234 – 238.

[5]Harman, J W, Gwinn, RP. "The Recovery of Skeletal Muscle Fibers from Acute Ischemia as Determined by Histologic and Chemical Methods." American Journal of Pathology. 1949 Jul;25(4) 741-55.

[6]Doyle, GS, Taillac, PP. "Tourniquets: A Review of Current Use with Proposals for Expanded Prehospital Use." Prehospital Emergency Care 2008; 12: 241 – 256.

[7]Tran, TP, et al. "Tourniquet-induced acute ischemia-reperfusion injury in mouse skeletal muscles: Involvement of superoxide." European Journal of Pharmacology 650 (2011) 328 – 334.

[8]Menger, MD, et al. "Microvascular ischemia-reperfusion injury in striated muscle: significance of "reflow paradox." The American Journal of Physiology. 1992 Dec;263(6 Pt 2) H1901-6.

[9]Granger, DN. "Role of xanthine oxidase and granulocytes in ischemia-reperfusion injury." The American Journal of Physiology. 1988 Dec;255(6 Pt 2) H1269 – 75.

[10]Hawksworth, JS, et al. "Inflammatory Biomarkers in Combat Wound Healing." Annals of Surgery. Vol. 250, Number 3, September 2009.

[11]Utz, ER, et al. "Metalloproteinase Expression is Associated with Traumatic Wound Failure." Journal of Surgical Research. 2009; pp1-7.

[12]Kotwal, RS, et al. "Eliminating Preventable Death on the Battlefield." Arch Surg. 2011 Dec;146(12) 1350-8.

Acknowledgements

The views expressed in this presentation are those of the author and do not necessarily reflect the official policy or position of the Department of the Navy, the Department of Defense, nor the U.S. Government. This work was supported/funded by work unit number 602115HP.3720.001.A1015. The study protocols were approved by the Walter Reed National Military Medical Center Institutional Review Board in compliance with all applicable Federal regulations governing the protection of human subjects (WRNMMC 352329, WRNMMC 352334).

Fig. 1 - http://www.nature.com/nrgastro/journal/v10/n2/fig_tab/nrgastro.2012.225_F1.html Fig. 3 - http://www.chinookmed.com
Fig. 2 - http://www.usaisrcamedd.army.mil/10_jts.html

1.0: Scientific Protocol

Title: The effect of inflammatory biomarker expression on decisions to close traumatic wounds

Emory Investigators:

Christopher Dente MD (Principal Investigator)

Allan Kirk MD, PhD (Co-Investigator)

Draft Date: January 1, 2013

2.0: Abstract

Military medicine has been confronted with a significant burden of wounded soldiers during recent conflicts and, as such, has been able to performed detailed analysis of the local and systemic healing milieu in injured patients with war wounds. Indeed, they have created a predictive model, which has the potential to aid surgeons caring for these patients in their decisions to perform definitive closure of these wounds. Surgeons in civilian practice also see a significant number of wounds related to severe trauma or tissue infection and it is not known if and how the healing milieu of these patients is different than patients with war wounds. We propose to perform an observational trial that will involve the collection of tissue and blood samples from patients with significant wounds cared for in our civilian trauma center and have the specimens analyzed for the same genetic markers previously studied by the Naval Medical Research Center. This would allow a predictive model to be created that could assist civilian surgeons with their decisions regarding the timing of wound closure in this setting in the future.

3.0: Introduction and Background

Recent military conflicts have contributed to a large volume of complex wounds that have been managed in military facilities across the world. Oftentimes, serial debridement procedures are required to remove devitalized tissue and decrease bacterial load. This aggressive surgical management combined with copious irrigation

and negative pressure therapy with vacuum-assisted closure (VAC) devices has improved outcomes in soldiers with these grievous wounds.[1,2] Despite these technological advances, however, the basic surgical decision making regarding appropriate timing of wound closure or coverage remains very subjective.

In recent years, the Naval Medical Research Center (NMRC) has demonstrated that local and systemic cytokines and chemokines are objectively associated with acute war wound healing.[3] In addition, they have hypothesized that acute wound failures are a consequence of a dysregulated systemic and local inflammatory response to traumatic injury. Indeed this extensive experience has permitted an algorithm to be developed that allows for objective criteria to assist in the decision to close a wound based on cytokine and chemokine biomarker expression using probabilistic (Bayesian) modeling.

As with these war wounds, many complex wounds in civilian practice require aggressive surgical care. At the Grady Memorial Hospital, a state of Georgia Level 1 trauma center, we admit approximately 3600 trauma patients per year and care for many additional patient with severe tissue infections and open wounds. Indeed, the Emory Department of Surgery treats, on average, 17 patients with necrotizing soft tissue infections, 70 patients requiring fasciotomies, and 41 patients with complex traumatic wounds annually. As with military wounds, these patients require aggressive surgical management oftentimes with multiple debridements prior to final wound closure. Civilian practice is plagued with the same subjective measures of wound closure that exist in the military setting. Furthermore, we have many of the same complications (wound breakdown, secondary infections) that exist in military wounds. Moreover, these patients may undergo multiple, and possibly unnecessary, operative washouts prior to definitive wound closure in an attempt to prevent or minimize these complications.

We propose to partner with the NMRC in translating battlefield knowledge into civilian practice. Specifically, we would like to develop an understanding of the local and systemic milieu in a civilian patient with a complex wound and explore the differences between this patient and a patient with a war wound. To do so, we propose to collect patient specific tissue, fluid and data to help better understand wound dynamics in the

civilian setting which would perhaps eventually allow us to shorten time to recovery and/or help prevent some of the wound breakdown seen in the complex wounds in our practice.

In summary, inflammatory biomarkers in serum and wound fluid correlate with war wound healing and successful closure. Acute wound failures appear to be a consequence of a dysregulation of the local and systemic inflammatory response to injury. Finally, an integrated molecular panel using Bayesian network modeling software effectively discriminates between combat wound healing outcomes and this approach may provide the much-needed objective criteria for acute war wound closure. This methodology appears very promising, and may help to provide a template for the management of severe acute soft tissue injury in civilian trauma. Whether this knowledge gained by the military can be translated into civilian practice is unknown and it is the purpose of this preliminary study to explore these wound dynamics in our population.

4.0 Objectives

Hypothesis:

Serum and wound effluent biomarkers as a measure of local and systemic healing milieu will be similar in military patients with war wounds and in civilian patients with traumatic or surgical wounds.

Objectives:

1. Analyze wound and serum specimens for biomarkers from civilian patients with open wounds and compare these results with results previously obtained from military patients with war wounds.
2. Validate current Bayesian predictive model used for wound management in military wounds for use in the civilian setting or create analogous model for use in civilian setting.

5.0 Study Design and Methods

<u>Study Design and Conduct:</u>

Patients admitted by the Emory Surgical Service at Grady Memorial Hospital will be screened for the entrance criteria listed below. Appropriate patients will be approached for informed consent (see informed consent procedure below). Once patients are enrolled they will have their demographic information placed in the study data base. Each patient will be given a study number to allow for de-identification of transmitted samples. Data collected will include: patient age, date of admission, location (torso vs. extremity), initial size and etiology of the wound, the patient's major co-morbidities, presenting vital signs, injury complex to calculate Injury Severity Score (in trauma patients), date of initial and all subsequent surgeries. They will then be treated with standard of care wound management including all necessary surgical washouts, debridements and bedside dressing changes. Medical data regarding their acute condition will be collected at the time of each dressing change and placed in the study data base. They will have the following blood, wound effluent and tissue samples collected:

The night prior to any scheduled operative wound debridement, a study staff member will place a new Wound Vac canister in the VAC device to begin overnight effluent collection. The patient will then undergo standard of care wound irrigations and debridements provided by the Emory surgical faculty at Grady Hospital. At the time of each debridement, the study staff will obtain at least 1 cm^3 of debrided tissue along with a 10 mL sample of blood drawn from a peripheral site. In most cases, the tissue obtained will be part of the standard of care wound debridement, however, if no tissue requires debridement for clinical reasons, the sample will be taken from the granulating tissue. Since these patients will undergo a variable number of debridements, it is possible that the amount of blood drawn for a particular subject could exceed 50 mL (3mL/kg) over an eight week time period. Finally, the Wound Vac canister from the prior night will be removed and a new canister will be placed. When the VAC system is re-applied to the enrolled patient wound, a two-hour post-debridement effluent collection will begin. Two hours after surgery, study staff will collect the VAC canister and replace it with a new canister and patient will then receive standard wound therapy until the next planned debridement when the above process will be repeated. If the decision is made to close the wound at any surgical procedure, the patient's blood and tissue samples

will constitute the end of sample collection for this patient unless they were to again fulfill entrance criteria on a future date.

In addition, at the time of any bedside wound vac change planned for the study wound, a similar procedure will be undertaken to obtain the same blood smaples, debrided tissue and vac effluent at the bedside.

These samples will be collected and processed by the study staff using the patient's unique study number and transported to the Naval Medical Research Center which will further process and store these samples indefinitely. Results of biomarker assays will be compared to results previously obtained (but de-identified) in military patients with war wounds to ascertain the similarities and differences in the wound and systemic healing dynamics in the two patient populations. All demographic and outcome data will be de-identified prior to transmission to the Naval Medical Research Center. The civilian data will then be use to validate the current predictive model used for military wound management or to create an analogous model for use in the civilian setting.

At each wound debridement, a digital photograph limited to the wound bed will be taken by study staff, dated and stored digitally in the study data base. Also, the wound dimensions will be manually recorded.

Upon discharge, various outcome measures will be recorded and entered into the study data base. These will include: hospital length of stay, intensive care unit length of stay, ventilator days, final outcome of the wound, wound complications, discharge date and discharge disposition. Please see the data collection sheet attached for the types of demographic, wound and outcome data that will be recorded.

6.0 Participant Selection

Entrance Criteria:

The eligible population will be adult male and female patients treated at Grady Memorial Hospital with wounds meeting the criteria listed below and who are being treated with a vacuum assisted closure (VAC) device. This device is in common use at Grady Hospital and is well within the standard of care for these wounds.

1. Surgical or Traumatic Wound ≥ 75cm^2 or traumatic amputation with open wound
2. Wound amendable to VAC treatment
3. Minimum age of 18 years

Exclusion Criteria.

Women who are found to be pregnant and patients who are also prisoners will be excluded.

Sample Size:

Grady Memorial Hospital sees approximately 125 patients with wounds that would meet entrance criteria annually and the study is expected to run over 3 years, leaving a requested sample size of 400 patients. Combined refusal and withdrawal rate is expected to be very low.

Patient Recruitment

a. Patients will be identified by one of the co-investigators by the attendance of general surgery morning report, attendance of trauma bay resuscitations and review of surgical operative logs. The admitting surgeon will be contacted to ensure they are in agreement with patient enrollment prior to approach of the patient. Refusal to participate in the study will not affect the patient's access to care or surgical priority. Patients will be instructed that they can withdraw from the study at any time and for any reason without penalty or adjustments in their care.

b. Subjects will not be compensated for their participation.

Informed Consent:

All patients with wounds that meet inclusion criteria will be approached by study personnel and there will be a detailed discussion with the patient and or the patient's family regarding the aims of the study in addition to the risks and benefits. They will be informed that, based on biomarkers that have been identified in the military setting, that there have been identified certain proteins in the fluid coming from the wounds that is collected in the wound vacuum system and from wound biopsies that is predictive of early or delayed healing in the military setting. A specific discussion with each patient

and family will be carried out informing them that wound biopsies will be analyzed for inflammatory and growth factors using genetic analysis as well as for bacteriologic colonization. It will be stated that we would like to have them participate in this study that will analyze how wounds seen in the civilian setting are similar or different with the intention that these finds may lead to a more detailed understanding of when to best close a wound in future patients. We will explain that the samples taken will be processed and then the results will be analyzed and compared to similar findings from patients with war wounds. We will also inform them that the samples they submit will be stored in the tissue bank of the Emory Transplant Center for potential future evaluation.

In addition, the procedures involved in maintaining privacy and confidentiality will be reviewed with them as outlined in the consent/HIPPA forms to inform them that we will be collecting different personal information about them to see if this personal information may help in determining if the computer program can identify certain factors that may be associated with early or delayed healing and all the personal information will be stored in a secure fireproof filing cabinet so their Protected Health Information is not compromised. Either the principal or co-investigators will be responsible for obtaining informed consent. If the patient is unable to give personal consent for this study, the next-of-kin or health care representative will be approached and consent sought after appropriate discussion.

Photographs of the wounds will be taken during each operating room washout procedure in order to determine the area and volume of each of the enrolled wounds. The area and volume determination of the wounds will be calculated either using a computerized picture area and volume calculating or a laser imaging area and volume calculating method.

7.0 Statistical Analysis

Statistical analyses will be performed mainly by researchers at the Naval Medical Research Center using the statistical models they have previously validated.

8.0 Adverse Event Reporting

All surgical debridements and wound management will be standard of care and no additional procedures will be performed solely for study purposes. The amount of tissue and blood collected from the patient are minimal and constitute insignificant risk, no more than a standard phlebotomy would entail. The wound vac effluent collected would otherwise be considered waste and discarded. There is a minimal risk of loss of confidentiality due to the review and data abstraction from the medical records.

Should a serious adverse event occur, however, the PI within one working day will report the event to the Emory IRB. Unexpected, but not serious adverse events, will be reported within 10 working days after the PI receives notification.

9.0 Data Safety and Monitoring Plan

As no clinical decision will be made with results from the collected specimens, there is no risk that individual patient care will be affected by data obtained in this observational trial. Therefore, no formal DSMP is necessary.

10.0 References

1. Bollero, D., Carnino, R., Risso, D., Gangemi, E.N. & Stella, M. Acute complex traumas of the lower limbs: a modern reconstructive approach with negative pressure therapy. *Wound Repair Regen* **15**:589-594 (2007).

2. Marsh, D.J., Abu-Sitta, G. & Patel, H. The role of vacuum-assisted wound closure in blast injury. *Plast Reconstr Surg* **119**:1978-1979 (2007).

3. Forsberg, J.A.*, et al.* Correlation of procalcitonin and cytokine expression with dehiscence of wartime extremity wounds. *J Bone Joint Surg Am* **90**:580-588 (2008).

Universidad de Emory y Sistema de Salud Grady
Consentimiento para ser un Sujeto de Investigación

Título: El efecto de la expresión de marcadores biológicos inflamatoria sobre las decisiones de cerrar heridas traumáticas.

Investigador principal: Christopher J Dente MD

Colaborador del Estudio: Departamento de Defensa, Centro de Investigación Médica Naval

Introducción

Se le está solicitando estar en un estudio de investigación médica. Este formulario está diseñado para decirle todo en lo que debe pensar antes de decidir consentir (estar de acuerdo) a estar en el estudio o no estar en el estudio. **Es enteramente su decisión. Si decide participar, puede cambiar de opinión más tarde y retirarse del estudio de investigación.** La decision de unirse o no unirse al estudio de investigación no le causará la pérdida de ningún beneficio médico. Si decide no participar en el estudio, su doctor continuará ofreciéndole tratamiento.

Antes de tomar su decisión:

- Por favor lea este formulario o haga que alguien se lo lea cuidadosamente
- Por favor escuche al doctor del estudio o al personal del estudio explicarle el estudio
- Por favor haga preguntas sobre cualquier cosa que no sea clara

Puede quedarse con una copia de este formulario de consentimiento. Siéntase con la libertad de demorarse considerando si le gustaría participar. Quizás quiera discutir su decisión con familia o amigos. No firme este formulario de consentimiento a no ser que haya tenido oportunidad de hacer preguntas y recibir respuestas que para usted tengan sentido. Al firmar este formulario, no está renunciando a ningún derecho legal.

Una descripción de este ensayo clínica estará disponible en http://www.ClinicalTrials.gov, como requiere la ley de Estados Unidos. Esta página Web no incluirá información que lo identifique. Cuando más, la página Web incluirá un resumen de los resultados. Puede explorar esta página Web en cualquier momento.

Descripción del Estudio

El propósito del estudio es entender cómo las heridas grandes sanan en un hospital civil. También nos gustaría aprender si hay cosas que ayudarían a los cirujanos decidir cuándo cerrar una herida. Acciones militares recientes han permitido a los cirujanos que brindan tratamiento a los soldados estudiar sus heridas. Estos cirujanos han creado un método para asistirles en sus decisiones de cerrar algunas de estas heridas. Usan medidas de sustancias pequeñas en la sangre de un paciente y tejido de herida para predecir la cicatrización exitosa de estas heridas. Muchos hospitales civiles enfrentan problemas similares con heridas grandes en pacientes heridos. En efecto, el Hospital Grady Memorial ofrece tratamiento a más de 100 pacientes por año con este tipo de heridas. En este estudio, nos hemos

asociado a un centro de investigación militar para entender mejor cómo las heridas se curan en los hospitales militares. Para hacer esto, le estamos pidiendo que participe en este estudio. Si está de acuerdo, varios especímenes de sangre y tejido suyos y de sus heridas serán recopilados. Estos serán analizados con un enfoque en las mismas sustancias que se ha demostrado predicen cicatrización de heridas exitosa en heridas militares. Se espera que también podamos crear un método de ayudarnos a decidir respecto al cierre de heridas en nuestro hospital. .

Procedimientos: *Ninguna decisión sobre su cuidado o administración de su herida se tomará con base a ningún procedimiento relacionado al estudio. Independientemente de si decide o no participar, experimentará la administración de heridas estándar, la cual consiste de un tratamiento con el sistema de cierre asistido al vacío, desbridamientos de herida estándar y en ocasiones múltiples en el salón de operaciones y cierre de heridas eventual (ya sea con suturas o injerto de piel) tal como lo decidan sus cirujanos. Si decide participar en el estudio, los siguientes eventos ocurrirán:*

1. La noche antes de cada procedimiento o vendaje quirúrgico, el contenedor al vacío en su vendaje será cambiado para permitir la colección de fluidos de la herida previo a cada procedimiento.
2. Durante cada procedimiento quirúrgico, la anestesia o personal del estudio obtendrá un tubo de sangre (estimadamente 10 mL) y sacará un pequeño pedazo de tejido (menor que una moneda de diez centavos) de su escara. El pedazo de tejido removido es tan pequeño que no cambiará la forma en la que su herida sana.
3. Si su herida no cierra durante ese procedimiento, el nuevo contenedor de herida vac será cambiado 2 horas después de la cirugía para permitirles la recolección de fluido de herida inmediatamente después del procedimiento.
4. Una foto digital limitada a la escara será tomada al final de cada procedimiento, justo antes de la aplicación del vendaje quirúrgico. Su herida también será medida en este momento.
5. El mismo proceso se repite durante cada procedimiento quirúrgico subsecuente y por todos los cambios de herida vac junto a la cama.
6. Una vez sus cirujanos decidan cerrar su herida, no habrá que tomarle más muestras.
7. Una vez haya sido dado de alta, su récord médico será revisado para encontrar datos respecto a su cuidado y resultados.
8. Todos los specimens serán etiquetados con un número de estudio (para proteger su identidad) y enviados al Centro de Investigación Médica Naval después de la recolección par ser procesados y guardados.
9. *Los resultados enviados al Centro de Investigación Médica Naval no contendrán información que pueda identificarlo directamente.*

Recopilaremos información sobre usted tal como su género, raza y edad. Esta información será registrada en una base de datos del estudio. Recibirá un número único de estudio. Toda información sobre usted y las muestras de sangre será identificada por este número de estudio. Su nombre no será usado en conexión con la información o las muestras de sangre/tejido.

Alguna de la sangre y tejido que recogemos de usted será guardado por largos periodos de tiempo. Las varias partes de su sangre y tejido serán guardadas individualmente. Además, porciones de su material genético (ADN y ARN) también serán guardadas. Al firmar este formulario, usted estará consintiendo a permitir que sus muestras se guarden y examinen. Parte de su sangre y/u orina podría ser enviada al laboratorio del hospital para exámenes rutinarios que se hacen allá. Una vez más, su muestra será

etiquetada con su número de estudio. El costo de los exámenes administrados será cubierto por el estudio de investigación. Usted no tendrá que pagar por ninguno de estos exámenes.

Usted entiende y está de acuerdo en que cualquier muestra de tejido, sangre, célula u otra muestra biológica que provea como participante en este estudio investigativo son donaciones de estas muestras a la Universidad de Emory. Al realizar su donación, estas muestras, y cualquier data, descubrimientos, materiales u otros productos que provengan de las muestras serán de propiedad exclusiva, permanente de la Universidad de Emory. Usted no tendrá derechos de propiedad sobre las muestras, así como no tendrá ningún derecho de propiedad o estará en derecho de compensación de ningún tipo por cualquier producto, data u otros ítems o información que se desarrolle a partir de las muestras. No obstante, usted puede, en cualquier momento, solicitar que se destruya su muestra, y haremos todos los intentos razonables para honrar su solicitud. Una solicitud escrita se puede enviar al Dr. Christopher J Dente MD, 69 Jesse Hill Jr Drive SE. Rm 307, Atlanta, Ga 30303.

Usted puede cambiar de opinión en cualquier momento y solicitar que sus muestras se destruyan. Si sus muestras no se han procesado, se destruirán a partir de la fecha de su solicitud. Si su(s) muestra(s) han sido procesadas, entonces la información será usada como parte del análisis general del estudio.

Riesgos e Incomodidades

Dado que ninguna decisión relacionada a su cuidado se está haciendo con base en los resultados de este estudio, no hay riesgos comunes o significativos asociados con la participación más allá del riesgo de una muestra de sangre. Este riesgo sería el mismo que presentaría cualquier otra muestra de sangre que haya proveído. El riesgo de sacar sangre es dolor, moretones, infección, enrojecimiento, hinchazón en el lugar donde se introduzca la aguja, mareo y un pequeño chance de desmayo. También está la posibilidad de que un coágulo de sangre se forme en el lugar donde se introduzca la aguja. La cantidad de tejido y sangre removida para efectos del estudio es pequeña y no presenta amenazas a su salud o la habilidad de saneamiento de su herida.

Nueva Información

Es posible que los investigadores aprendan algo nuevo durante el estudio sobre los riesgos de estar en él. Si esto ocurre, se lo comunicarán. Entonces podrá decidir si quiere continuar en el estudio o no. Quizás se le pida firmar un nuevo formulario de consentimiento que incluya la nueva información si usted ha decidido quedarse en el estudio.

Beneficios

Este estudio no está diseñado para beneficiarlo directamente. Su herida puede mejorar mientras esté en este estudio, pero puede que no, e incluso puede empeorar. Este estudio está diseñado para aprender más sobre el saneamiento de heridas y los resultados del estudio pueden ser usados para ayudar a otros en el futuro.

Compensación

No se le será ofrecido pago por estar en este estudio.

Le daremos asistencia médica de emergencia si usted es herido por esta investigación. Sin embargo, Grady Health System no ha dejado de lado fondos para pagar por esta asistencia médica o para

compensar a usted si ocurre un accidente. Si usted cree que ha sido herido por esta investigación, debería contactar Dr. Christopher J Dente (Teléfono 404-616-8915)".

Confidencialidad

Algunas oficinas y personas además de los investigadores podrían mirar tu información médica y récords del estudio. Las agencias gubernamentales y empleados de Emory o Sistema de Salud Grady supervisando la conducta apropiada del estudio pueden revisar sus récords en el estudio. Estas oficinas incluyan la Oficina de Protecciones de Investigación Humana, el Buró de Revisión Institucional de Emory, el Comité de Supervisión de Investigación Grady y la Oficina de Cumplimiento de la Investigación de Emory. Los patrocinadores del estudio también pueden mirar sus récords del estudio. Emory y el Sistema de Salud Grady mantendrán cualquier récord investigativo que creemos al punto en que sea requerido hacerlo por ley. Un número de estudio en vez de su nombre será usado en sus récords de estudio cuando sea posible. Su nombre y otros datos que puedan llevar a usted no aparecerán cuando presentemos este estudio o publiquemos sus resultados.

Los récords de estudio pueden ser abiertos mediante orden judician. También pueden ser producidos en respuesta a una citación o solicitud de producción de documentos.

Información de la Investigación No Aparecerá en el Récord Médico:
Si usted es o ha sido un paciente de Emory o Sistema de Salud Grady, tiene un récord médico de Emory o el Sistema de Salud Grady. Si no es o no ha sido nunca un paciente de Emory o del Sistema de Salud Grady, no tiene uno. Por favor note que un récord médico de Emory o el Sistema de Salud Grady **será** creado si se le realiza cualquier servicio o procedimiento por parte de un proveedor o instalci´øn de Emory o Sistema de Salud Grady para este estudio.

Si usted consiente a estar en este estudio, una copia del formulario de consentimiento y formulario de paciente HIPAA que firme **será** guardada en su récord médico Emory o del Sistema de Salud Grady. Cualquier persona con acceso a su récord médico tendrá la posibilidad de acceder a toda la información del estudio contenida allí. La confidencialidad de la información del estudio en su récord médico será protegida por leyes como la Regla de Privacidad HIPAA. Por otra parte, algunas leyes estatales y federales podrían no proteger la confidencialidad de la información de la investigación .

Emory y el Sistema de Salud Grady no controlan los resultados de exámenes y procedimientos realizados en otros lugares, por lo cual estos resultados no serán depositados en su récord médico de Emory o el Sistema de Salud Grady. Será improbable que estén disponibles para Emory o el Sistema de Salud Grady con motivo de ayudar a su cuidado. Emory y el Sistema de Salud Grady, además, no controlan otros récords médicos que pueda tener con otros proveedores del cuidado de la salud. Emory y el Sistema de Salud Grady no enviarán resultados de ningún examen o procedimiento del estudio a estos proveedores. Si decide estar en el estudio, depende de usted hacerles saber.

Los investigadores revisarán los resultados de ciertos exámenes y procedimientos del estudio sólo por la investigación. Los investigadores **no estarán** revisando los resultados de estos exámenes y procedimientos para tomar decisiones sobre su salud y tratamiento personal. Para este estudio, esas cosas incluyen: los resultados de la administración de su herida, incluyendo el número de veces que haya ido al salón de operaciones y cómo su herida fue cerrada (sutura, injerto de piel); cuánto tiempo estuvo en el hospital; cualquier complicación médica que haya ocurrido mientras estaba en el hospital; qué tipo de herida o infección causó sus heridas y otra información básica sobre su edad y salud general.

Costos

Usted no tendrá ningún costo por participar en este estudio. A usted no se le cobrará por ninguna de las actividades investigativas.

Retiro del Estudio

Usted tiene el derecho de dejar el estudio en cualquier momento sin penalidad

Los investigadores y patrocinador también tienen el derecho de suspender su participación en este estudio sin su consentimiento si:

- Creen que le conviene;
- Usted fuera a objetar a cualquier cambio futuro que se realice en el plan de estudio;
- Por cualquier otra razón.

Información de Contacto

Puede comunicarse con Christopher Dente MD al 404-251-8915:

- Si tiene cualquier pregunta sobre este estudio o su papel en él,
- Si siente que ha tenido un daño relacionado a la investigación o una reacción negativa a la droga del estudio, o
- Si tiene preguntas, preocupaciones o quejas sobre la investigación

Comuníquese con el Buró de Revisión Institucional de Emory al 404-712-0720 o 877-503-9797 o irb@emory.edu:

- Si tiene preguntas sobre sus derechos como participante en la investigación.
- Si tiene preguntas, preocupaciones o quejas sobre la investigación.
- También puede hacerle saber al IRB sobre sus experiencias como participante en la investigación a través de la Encuesta de Participantes de la Investigación: http://www.surveymonkey.com/s/6ZDMW75.

Si usted es un participante del Sistema de Salud Grady, también puede comunicarse con Dr. Curtis Lewis, Senior Vicepresidente de Asuntos Médicos del Sistema de Salud Grady al (404) 616-4261.

Consentimiento

Por favor, escriba en letra de molde su nombre y firme abajo si está de acuerdo con estar en este estudio. Al firmar este formulario de consentimiento, no está renunciando a ninguno de sus derechos legales. Le daremos una copia de este consentimiento firmado, para sus registros.

_____

Nombre del Sujeto

Firma del Sujeto Fecha Hora

Firma de la Persona Conduciendo la Discusión del Consentimiento Informado Fecha Hora

Nombre de la Persona Conduciendo la Discusión del Consentimiento Informado

Firma de Representante Legalmente Autorizado Fecha Hora

Autoridad de Representante Autorizado Legalmente o Relación con Sujeto

You Are Being Asked to Be in a Research Study

What Is a Research Study?

The main purpose of research studies is to gain knowledge. This knowledge may be used to help others. Research studies are not intended to benefit you directly, though some might.

Do I Have to Do This?

No. Being in this study is entirely your choice. If you decide to join this study, you can change your mind later on and withdraw from the research study.

Taking part in a study is separate from medical care. The decision to join or not join the research study will not affect your status as a patient.

What Is This Document?

This form is an informed consent document. It will describe the study risks, procedures, and any costs to you.

This form is also a HIPAA Authorization document. It will describe how your health information will be used and by whom.

Signing this form indicates you are willing to take part in the study and allow your health information to be used.

What Should I Do Next?

1. Read this form, or have it read to you.
2. Make sure the study doctor or study staff explains the study to you.
3. Ask questions (e.g., time commitment, unfamiliar words, specific procedures, etc.)
4. If there will be medical treatment, know which parts are research and which are standard care.
5. Take time to consider this, and talk about it with your family and friends.

Emory University and Grady Health System
Consent to be a Research Subject / HIPAA Authorization

Title: The effect of inflammatory biomarker expression on decisions to close traumatic wounds

Principal Investigator: Christopher J Dente, MD

Study-Supporter: Department of Defense, Naval Medical Research Center

Introduction
You are being asked to be in a medical research study. This form is designed to tell you everything you need to think about before you decide if you want to be a part of the study. **It is entirely your choice. If you decide to take part, you can change your mind later on and withdraw from the research study.** The decision to join or not join the research study will not cause you to lose any medical benefits. If you decide not to take part in this study, your doctor will continue to treat you.

Before making your decision:
- Please carefully read this form or have it read to you
- Please listen to the study doctor or study staff explain the study to you
- Please ask questions about anything that is not clear

You can take a copy of this consent form, to keep. Feel free to take your time thinking about whether you would like to participate. You may wish to discuss your decision with family or friends. Do not sign this consent form unless you have had a chance to ask questions and get answers that make sense to you. By signing this form you will not give up any legal rights.

A description of this clinical trial will be available on http://www.ClinicalTrials.gov, as required by U.S. law. This Web site will not include information that can identify you. At most the Web site will include a summary of the results. You may search this Web site at any time.

What is the purpose of this study?
The purpose of this study is to understand how large wounds heal in a civilian hospital. We would also like to learn if there are things that would help surgeons decide on when to close a wound. Recent military actions have allowed surgeons treating soldiers to study their wounds. These surgeons have created a method to assist in their decisions to close some of these wounds. They use measurements of small substances in a patient's blood and wound tissue to predict the successful closure of these wounds. Many civilian hospitals face similar issues with large wounds in injured patients. Indeed, Grady Memorial Hospital treats more than 100 patients a year with these types of wounds. In this study, we have partnered with a military research center to better understand how wounds heal in civilian hospitals. In order to do so, we are asking you to participate in this study. If you agree, several blood and tissue specimens obtained from you and your wound will be collected. They will be analyzed for the same substances that have been shown to predict successful wound closure in military wounds. It is hoped that we will also be able to create a method to help with our decisions to close wounds in our hospital.

What will I be asked to do?
No decisions regarding your care or your wound management will be made based on any study related procedures. Whether or not you choose to participate, you will undergo the standard wound management which consists of treatment with the "vacuum" dressing, standard and sometimes multiple wound debridements in the operating room

and eventual wound closure (either by sutures or skin grafts) as decided upon by your surgeons. If you choose to participate in the study, the following events will occur:

1. The night before each surgical procedure or dressing change, the vacuum canister on your dressing will be changed to allow for collection of wound fluid prior to each procedure.
2. During each surgical procedure, the anesthesia or study staff will draw one tube of blood (about 10 mL) and will take a small piece of tissue (smaller than a dime) from your wound bed. The piece of tissue removed is so small that it will in no way change the way your wound heals.
3. If your wound is not closed during that procedure, the new wound vac canister will be changed 2 hours after the surgery to allow for collection of wound fluid immediately after the procedure.
4. A digital picture limited to the wound bed will be taken at the end of each procedure, just prior to placement of the surgical dressing. Your wound will also be measured at this time.
5. The same process is repeated during each subsequent surgical procedure and for all bedside wound vac changes.
6. Once your surgeons decide to close your wound, you will have no further samples taken.
7. Upon discharge, your medical record will be reviewed for specific data regarding your care and outcome.
8. All specimens will be labeled with a study number (to protect your identity) and sent to the Naval Medical Research Center after collection to be processed and stored.
9. *Results sent to the Naval Medical Research Center will not contain information that can identify you directly.*

We will collect information about you such as your gender, race, and age. This information will be entered into a study database. You will be given a unique study number. All information about you and the blood samples will be identified by this study number. Your name will not be used in connection with the information or the blood/tissue samples.

Who owns my study information and samples?

If you join this study, you will be donating your samples and study information. You will not receive any compensation if your samples or information to make a new product. If you withdraw from the study, data and samples that were already collected may be still be used for this study.

Some of the blood and tissue we collect from you will be stored for long periods of time. The various parts of your blood and tissue will be stored individually. In addition, portions of your genetic material (DNA and RNA) will also be stored. By signing this form, you will be agreeing to allow storage and testing of your samples. Some of your blood and/or urine may be sent to the hospital laboratory for routine tests that are performed there. Once again, your sample will be labeled with your study number. The costs of the tests that are being run will be paid for by the research study. You will not be billed for any of these tests.

You understand and agree that any tissue, blood, cell, or other biological samples that you provide as a participant in this research study are donations of these samples to Emory University. Upon you donation, these samples, and any data, discoveries, materials or other products that come from the samples will be the exclusive, permanent property of Emory University. You will not have any property rights in the samples, nor will you have any property rights in or be entitled to compensation of any type for any products, data, or other items or information that is developed from the samples. Nevertheless, you may, at any time request that we destroy your sample, and we will make all reasonable attempts to honor your request. A written request can be sent to Dr. Christopher J Dente MD, 69 Jesse Hill Jr Drive SE. Rm 307, Atlanta, Ga 30303.

You can change your mind at any time and ask to have your samples destroyed. If your samples have not been processed, they will be destroyed from the date of your request. If your sample(s) have been processed, then the information will be used as part of the overall study analysis.

What are the possible risks and discomforts?

There may be side effects from the study procedures that are not known at this time.

As no decisions related to your care are being made based on results of this study, there are no common or significant risks associated with participation aside from the risk of a blood draw. This risk would be no different from any other blood draw you have ever had. The amount of tissue and blood removed for study purposes is very small and poses no threat to your health or your ability to heal your wound.

The most common risks and discomforts from having blood drawn are: pain, bruising, infection, redness, swelling at the site of the needle stick and dizziness.
The less common risks and discomforts expected in this study are: a chance of fainting.
Rare but possible risks include: the possibility that a blood clot will form at the needle site.

It is possible that the researchers will learn something new during the study about the risks of being in it. If this happens, they will tell you about it. Then you can decide if you want to continue to be in this study or not. You may be asked to sign a new consent form that includes the new information if you decide to stay in the study.

Will I benefit directly from the study?
This study is not designed to benefit you directly. Your wound may improve while you are in this study but it may not, and it may even get worse. This study is designed to learn more about wound healing and the study results may be used to help others in the future.

Will I be compensated for my time and effort?
You will not be offered compensation for being in this study.

What are my other options?
If you decide not to enter this study, there is care available to you outside of this research study. You do not have to be in this study to be treated for your wound.

How will you protect my private information that you collect in this study?
Emory and Grady Health System will keep any research records that it creates private to the extent that this is required to do so by law. Whenever possible, a study number, rather than your name, will be used on study records. Your name and other identifying information will not appear when we present or publish the study results.

Study records can be opened by court order. They also may be provided in response to a subpoena or a request for the production of documents.

Genetic Information
The Genetic Information Nondiscrimination Act (GINA) is a federal law that protects against genetic discrimination. This law makes it illegal for health insurance companies, group health plans, and most employers to discriminate against you based on your genetic information. This law does not protect you from being discriminated in life insurance, long-term care insurance, or from employers with less than 100 workers.

Medical Record
If you have been an Emory and Grady Health System patient before, then you already have an Emory and Grady Health System medical record. If you have never been an Emory and Grady Health System patient, you do not have one. An Emory and Grady Health System medical record will be made for you if an Emory and Grady Health System provider or facility gives you any services or procedures for this study.

Copies of the consent form/HIPAA authorization that you sign will be put in any Emory and Grady Health System medical record you have now or any time during the study.

The results of some study tests and procedures will be used only for research purposes and will *not* be placed in your medical record. For this study, those items include: results of the research tests done on the blood, tissue and wound fluids that are done only for research purposes.

Tests and procedures done at non-Emory and Grady Health System places may not become part of your Emory and Grady Health System medical record. Also, if you decide to be in this study, it is up to you to let your other health providers know.

In Case of Injury

If you get ill or injured from being in the study, Emory will help you to get medical treatment. Emory and Grady Health System and the sponsor have not, however, set aside any money to pay you or to pay for this medical treatment. The only exception is if it is proven that your injury or illness is directly caused by the negligence of an Emory or sponsor employee. "Negligence" is the failure to follow a standard duty of care.

If you become ill or injured from being in this study, your insurer will be billed for your treatment costs. If you do not have insurance, or if your insurer does not pay, then you will have to pay these costs.

If you believe you have become ill or injured from this research, you should contact Dr. Christopher Dente at telephone number 404-251-8915. You should also let any health care provider who treats you know that you are in a research study.

Costs

There will be no costs to you for participating in this study, other than basic expenses like transportation. You will not be charged for any of the research activities.

Withdrawal from the Study

You have the right to leave a study at any time without penalty.

The researchers also have the right to stop your participation in this study without your consent for any reason, especially if they believe it is in your best interest or if you were to object to any future changes that may be made in the study plan.

Authorization to Use and Disclose Protected Health Information

The privacy of your health information is important to us. We call your health information that identifies you, your "protected health information" or "PHI." To protect your PHI, we will follow federal and state privacy laws, including the Health Insurance Portability and Accountability Act and regulations (HIPAA). We refer to all of these laws as the "Privacy Rules." Here we let you know how we will use and disclose your PHI for the study.

PHI that Will be Used/Disclosed:

The PHI that we will use or share for the main research study includes:

- Medical information about you including your medical history and present/past medications.
- Results of exams, procedures and tests you have before and during the study.
- the number of times you went to the operating room and how your wound was closed (suture, skin graft)
- any medical complications that occurred while you were in the hospital
- what type of injury or infection caused your wounds
- Information about the outcome of your wound and how long you were in the hospital.

Purposes for Which Your PHI Will be Used/Disclosed:
We will use and share your PHI for the conduct and oversight of the research study. We will use and share your PHI to provide you with study related treatment and for payment for such treatment. We will also use and share your PHI to conduct normal business operations. We may share your PHI with other people and places that help us conduct or carry out the study, such as laboratories, data management centers, data monitors, contract research organizations, Institutional Review Boards (IRBs)and other study sites. If you leave the study, we may use your PHI to determine your health, vital status or contact information.

Use and Disclosure of Your Information That is Required by Law:
We will use and disclose your PHI when we are required to do so by law. This includes laws that require us to report child abuse or abuse of elderly or disabled adults. We will also comply with legal requests or orders that require us to disclose your PHI. These include subpoenas or court orders.

Authorization to Use PHI is Required to Participate:
By signing this form, you give us permission to use and share your PHI as described in this document. You do not have to sign this form to authorize the use and disclosure of your PHI. If you do not sign this form, then you may not participate in the research study or receive research-related treatment. You may still receive non-research related treatment.

People Who will Use/Disclose Your PHI:
The following people and groups will use and disclose your PHI in connection with the research study:

- The Principal Investigator and the research staff will use and disclose your PHI to conduct the study and give you study related treatment.
- Emory and Grady Health System may use and disclose your PHI to get payment for study related treatment and to run normal business operations.
- The Principal Investigator and research staff will share your PHI with other people and groups to help conduct the study or to provide oversight for the study.
- The Department of Defense and the Naval Medical Research Center are the Sponsors of the study. The Sponsor may use and disclose your PHI to make sure the research is done correctly and to collect and analyze the results of the research. The Sponsor may disclose your PHI to other people and groups like study monitors to help conduct the study or to provide oversight for the study.
- The following people and groups will use your PHI to make sure the research is done correctly and safely:
    - Emory and Grady Health System offices that are part of the Human Research Participant Protection Program and those that are involved in study administration and billing. These include the Emory IRB, the Emory Research and Healthcare Compliance Offices, and the Emory Office for Clinical Research.
    - Government agencies that regulate the research including: Office for Human Research Protections; Food and Drug Administration
    - Public health agencies.
    - Research monitors and reviewer.
    - Accreditation agencies.

Expiration of Your Authorization
Your PHI will be used until this research study ends.

Revoking Your Authorization

If you sign this form, at any time later you may revoke (take back) your permission to use your information. If you want to do this, you must contact the study team at: Dr. Christopher J Dente, 69 Jesse Hill Jr Drive SE, Department of Surgery, Room 307, Atlanta, Ga 30303.

At that point, the researchers would not collect any more of your PHI. But they may use or disclose the information you already gave them so they can follow the law, protect your safety, or make sure that the study was done properly and the data is correct. If you revoke your authorization you will not be able to stay in the study.

Other Items You Should Know about Your Privacy

Not all people and entities are covered by the Privacy Rules. HIPAA only applies to health care providers, health care payers, and health care clearinghouses. If we disclose your information to people who are not covered by the Privacy Rules, including HIPAA, then your information won't be protected by the Privacy Rules. People who do not have to follow the Privacy rules can use or disclose your information with others without your permission if they are allowed to do so by the laws that cover them.

To maintain the integrity of this research study, you generally will not have access to your PHI related to this research until the study is complete. When the study ends, and at your request, you generally will have access to your PHI that we maintain in a designated record set. A designated record set is data that includes medical information or billing records that your health care providers use to make decisions about you. If it is necessary for your health care, your health information will be provided to your doctor.

We may remove identifying information from your PHI. Once we do this, the remaining information will not be subject to the Privacy Rules. Information without identifiers may be used or disclosed with other people or organizations for purposes besides this study.

Contact Information

Contact Dr. Christopher Dente at 404-251-8915:

- if you have any questions about this study or your part in it,
- if you feel you have had a research-related injury or a bad reaction to the study drug, or
- if you have questions, concerns or complaints about the research

Contact the Emory Institutional Review Board at 404-712-0720 or 877-503-9797 or irb@emory.edu:

- if you have questions about your rights as a research participant.
- if you have questions, concerns or complaints about the research.
- You may also let the IRB know about your experience as a research participant through our Research Participant Survey at http://www.surveymonkey.com/s/6ZDMW75.

If you are a Grady Health System participant, you may also contact Dr. Curtis Lewis, Senior Vice President for Grady Health System Medical Affairs at (404) 616-4261.

Consent and Authorization

Please print your name and sign below if you agree to be in this study. By signing this consent and authorization form, you will not give up any of your legal rights. We will give you a copy of the signed consent to keep.

_____
Name of Subject

_____ _____
Signature of Subject Date Time

_____
Name of Person Conducting Informed Consent Discussion

_____ _____
Signature of Person Conducting Informed Consent Discussion Date Time

_____ _____
Signature of Legally Authorized Representative Date Time
with authority for research decisions

_____
Authority of Legally Authorized Representative or Relationship to Subject

EMORY UNIVERSITY | Institutional Review Board

TO: Chistopher Dente, MD
Principal Investigator
General Su

DATE: November 22, 2013

RE: **Notification of Amendment Approval**
AM4_IRB00058229
IRB00058229
The effect of inflammatory biomarker expression on decisions to close traumatic wounds

Thank you for submitting an amendment request. The Emory IRB reviewed and approved this amendment under the expedited review process on 11/17/2013. This amendment includes the following:

Changes to Consent Form(s): Added Grady DOD Consent, version 7.0, added HIPAA Spanish
Changes to Protocol Document(s): Added Grady Protocol DOD version 7.0
Changes to Study Team members: Added Rondi Gelbard and Thomas Moore

Important note: If this study is NIH-supported, you may need to obtain NIH prior approval for the change(s) contained in this amendment before implementation. Please review the NIH policy directives found at the following links and contact your NIH Program Officer, NIH Grants Management Officer, or the Emory Office of Sponsored Programs if you have questions.

Policy on changes in active awards: http://grants.nih.gov/grants/guide/notice-files/NOT-OD-12-129.html

Policy on delayed onset awards: http://grants.nih.gov/grants/guide/notice-files/NOT-OD-12-130.html

In future correspondence with the IRB about this study, please include the IRB file ID, the name of the Principal Investigator and the study title. Thank you.

Sincerely,

Martha C. Patterson, CIP
Research Protocol Analyst
This letter has been digitally signed

CC	Fuller	Syreese	Winship - Main
	Gelbard	Rondi	Surgery - Main
	Kirk	Allan	Ctr for Transplant'n
	Moore	Thomas	Orthopaedics - Main

Emory University IRB
1599 Clifton Road, 5th Floor - Atlanta, Georgia 30322
Tel: 404.712.0720 - Fax: 404.727.1358 - Email: irb@emory.edu - Web: http://www.irb.emory.edu/

EMORY UNIVERSITY | Institutional Review Board

TO: Chistopher Dente, MD
Principal Investigator
General Su

DATE: December 11, 2013

RE: **Notification of Amendment Approval**
AM5_IRB00058229
IRB00058229
The effect of inflammatory biomarker expression on decisions to close traumatic wounds

Thank you for submitting an amendment request. The Emory IRB reviewed and approved this amendment under the expedited review process on 12/10/2013. This amendment includes the following:

Changes to Consent Form(s): Revised Grady DOD IC, version 8.0
Changes to Study Team members
Changes to funding or funding sources

Important note: If this study is NIH-supported, you may need to obtain NIH prior approval for the change(s) contained in this amendment before implementation. Please review the NIH policy directives found at the following links and contact your NIH Program Officer, NIH Grants Management Officer, or the Emory Office of Sponsored Programs if you have questions.

Policy on changes in active awards: http://grants.nih.gov/grants/guide/notice-files/NOT-OD-12-129.html

Policy on delayed onset awards: http://grants.nih.gov/grants/guide/notice-files/NOT-OD-12-130.html

In future correspondence with the IRB about this study, please include the IRB file ID, the name of the Principal Investigator and the study title. Thank you.

Sincerely,

Martha C. Patterson, CIP
Research Protocol Analyst
This letter has been digitally signed

CC	Fuller	Syreese	Winship - Main
	Gelbard	Rondi	Surgery - Main
	Kirk	Allan	Ctr for Transplant'n
	Moore	Thomas	Orthopaedics - Main

Emory University IRB
1599 Clifton Road, 5th Floor - Atlanta, Georgia 30322
Tel: 404.712.0720 - Fax: 404.727.1358 - Email: irb@emory.edu - Web: http://www.irb.emory.edu/

EMORY UNIVERSITY | Institutional Review Board

TO: Chistopher Dente, MD
Principal Investigator
General Su

DATE: January 23, 2014

RE: **Notification of Amendment Approval**
AM6_IRB00058229
IRB00058229
The effect of inflammatory biomarker expression on decisions to close traumatic wounds

Thank you for submitting an amendment request. The Emory IRB reviewed and approved this amendment under the expedited review process on **1/23/2014**. This amendment includes the following:

Personnel Change only: Adding Elizabeth Beth Begley as study Coordinator, Kevin Scott as other Emory study staff and Julie Lee, Marianne Spevak as Non-Emory study staff.

Important note: If this study is NIH-supported, you may need to obtain NIH prior approval for the change(s) contained in this amendment before implementation. Please review the NIH policy directives found at the following links and contact your NIH Program Officer, NIH Grants Management Officer, or the Emory Office of Sponsored Programs if you have questions.

Policy on changes in active awards: http://grants.nih.gov/grants/guide/notice-files/NOT-OD-12-129.html

Policy on delayed onset awards: http://grants.nih.gov/grants/guide/notice-files/NOT-OD-12-130.html

In future correspondence with the IRB about this study, please include the IRB file ID, the name of the Principal Investigator and the study title. Thank you.

Sincerely,

Donna Thomas
Administrative Assistant
This letter has been digitally signed

CC	Begley	Elizabeth	Information Services
	Fuller	Syreese	Winship - Main
	Gelbard	Rondi	Surgery - Main
	Kirk	Allan	Ctr for Transplant'n
	Moore	Thomas	Orthopaedics - Main

Emory University IRB
1599 Clifton Road, 5th Floor - Atlanta, Georgia 30322
Tel: 404.712.0720 - Fax: 404.727.1358 - Email: irb@emory.edu - Web: http://www.irb.emory.edu/

EMORY UNIVERSITY | Institutional Review Board

TO: Chistopher Dente, MD
Principal Investigator
General Su

DATE: January 31, 2014

RE: **Notification of Amendment Approval**
AM7_IRB00058229
IRB00058229
The effect of inflammatory biomarker expression on decisions to close traumatic wounds

Thank you for submitting an amendment request. The Emory IRB reviewed and approved this amendment under the expedited review process on 01/31/14. This amendment includes the following:

Changes to Consent Forms
Changes to Study Team members:

- Added Bridget Fielder
- Changed the roles for Kevin Scott, Marianne Spevak, and Julie Lee

Documents reviewed with this application:

- Wound biomaker Spanish trans 12.2013 (clean and tracked)

Important note: If this study is NIH-supported, you may need to obtain NIH prior approval for the changes contained in this amendment before implementation. Please review the NIH policy directives found at the following links and contact your NIH Program Officer, NIH Grants Management Officer, or the Emory Office of Sponsored Programs if you have questions.

Policy on changes in active awards: http://grants.nih.gov/grants/guide/notice-files/NOT-OD-12-129.html

Policy on delayed onset awards: http://grants.nih.gov/grants/guide/notice-files/NOT-OD-12-130.html

In future correspondence with the IRB about this study, please include the IRB file ID, the

name of the Principal Investigator and the study title. Thank you.

Sincerely,

Scott S. Katz, MS
Analyst Assistant
This letter has been digitally signed

CC	Begley	Elizabeth	Information Services
	Fielder	Bridget	Winship - Main
	Fuller	Syreese	Winship - Main
	Scott	Kevin	Ctr for Transplant'n
	Gelbard	Rondi	Surgery - Main
	Kirk	Allan	Ctr for Transplant'n
	Moore	Thomas	Orthopaedics - Main

Emory University IRB
1599 Clifton Road, 5th Floor - Atlanta, Georgia 30322
Tel: 404.712.0720 - Fax: 404.727.1358 - Email: irb@emory.edu - Web: http://www.irb.emory.edu/

TO: Chistopher Dente, MD
Principal Investigator
General Su

DATE: March 14, 2014

RE: Notification of Amendment Approval
AM8_IRB00058229
IRB00058229
The effect of inflammatory biomarker expression on decisions to close traumatic wounds

Thank you for submitting an amendment request. The Emory IRB reviewed and approved this amendment under the expedited review process on 3/14/2014. This amendment includes the following:

Personnel Change Only: Adding Wilisha Johnson as other Emory study staff.

Important note: If this study is NIH-supported, you may need to obtain NIH prior approval for the change(s) contained in this amendment before implementation. Please review the NIH policy directives found at the following links and contact your NIH Program Officer, NIH Grants Management Officer, or the Emory Office of Sponsored Programs if you have questions.

Policy on changes in active awards: http://grants.nih.gov/grants/guide/notice-files/NOT-OD-12-129.html

Policy on delayed onset awards: http://grants.nih.gov/grants/guide/notice-files/NOT-OD-12-130.html

In future correspondence with the IRB about this study, please include the IRB file ID, the name of the Principal Investigator and the study title. Thank you.

Sincerely,

Donna Thomas
Administrative Assistant
This letter has been digitally signed

CC	Begley	Elizabeth	Information Services
	Fielder	Bridget	Winship - Main
	Fuller	Syreese	Winship - Main
	Scott	Kevin	Ctr for Transplant'n
	Gelbard	Rondi	Surgery - Main
	Kirk	Allan	Ctr for Transplant'n

Moore Thomas Orthopaedics - Main

Emory University IRB
1599 Clifton Road, 5th Floor - Atlanta, Georgia 30322
Tel: 404.712.0720 - Fax: 404.727.1358 - Email: irb@emory.edu - Web: http://www.irb.emory.edu/
An equal opportunity, affirmative action university

EMORY UNIVERSITY | Institutional Review Board

TO: Chistopher Dente, MD
Principal Investigator

DATE: June 3, 2015

RE: **Notification of Amendment Approval**
AM9_IRB00058229
IRB00058229
The effect of inflammatory biomarker expression on decisions to close traumatic wounds

Dear Dr. Dente,

Thank you for submitting an amendment request. The Emory IRB reviewed and approved this amendment under the expedited review process on **06/03/2015**. This amendment includes the following:

- Changes to the study team:
  - Added: Stephen Dascall
- Change to the Informed Consent form (Version: 05/21/2015)

Important note: If this study is NIH-supported, you may need to obtain NIH prior approval for the change(s) contained in this amendment before implementation. Please review the NIH policy directives found at the following links and contact your NIH Program Officer, NIH Grants Management Officer, or the Emory Office of Sponsored Programs if you have questions.

Policy on changes in active awards: http://grants.nih.gov/grants/guide/notice-files/NOT-OD-12-129.html

Policy on delayed onset awards: http://grants.nih.gov/grants/guide/notice-files/NOT-OD-12-130.html

In future correspondence with the IRB about this study, please include the IRB file ID, the name of the Principal Investigator and the study title. Thank you.

Sincerely,

Steven J. Anzalone, M.S.
IRB Research Protocol Analyst
This letter has been digitally signed

CC	Begley	Elizabeth	Information Services
	Fielder	Bridget	Winship - Main
	Fuller	Syreese	Winship - Main
	Garner	Vanessa	Ctr for Transplant'n
	Knight	Simone	Ctr for Transplant'n
	Gelbard	Rondi	Surgery - Main
	Kirk	Allan	Ctr for Transplant'n
	Moore	Thomas	Orthopaedics - Main

Emory University IRB
1599 Clifton Road, 5th Floor - Atlanta, Georgia 30322
Tel: 404.712.0720 - Fax: 404.727.1358 - Email: irb@emory.edu - Web: http://www.irb.emory.edu/
An equal opportunity, affirmative action university

PDF-XChange
Click to buy NOW!
www.tracker-software.com

EMORY UNIVERSITY | Institutional Review Board

TO: Chistopher Dente, MD
Principal Investigator
General Su

DATE: June 19, 2014

RE: **Continuing Review Expedited Approval**
CR2_IRB00058229

IRB00058229
The effect of inflammatory biomarker expression on decisions to close traumatic wounds

Thank you for submitting a renewal application for this protocol. The Emory IRB reviewed it by the expedited process on 6/19/2014, per 45 CFR 46.110, the Federal Register expeditable categories F4, F5, and F9, and/or 21 CFR 56.110. This reapproval is effective from **7/2/2014** through **7/1/2015** . Thereafter, continuation of human subjects research activities requires the submission of another renewal application, which must be reviewed and approved by the IRB prior to the expiration date noted above.

The following documents were included in this review:

- Grady DOD HIPAA 3.0
- GRADY DOD IC 8.0
- Revocation 2.0
- Wound biomarker Spanish trans 12.2013

Any reportable events (e.g., unanticipated problems involving risk to subjects or others, noncompliance, breaches of confidentiality, HIPAA violations, protocol deviations) must be reported to the IRB according to our Policies & Procedures at www.irb.emory.edu, immediately, promptly, or periodically. Be sure to check the reporting guidance and contact us if you have questions. Terms and conditions of sponsors, if any, also apply to reporting.

Before implementing any change to this protocol (including but not limited to sample size, informed consent, study design), you must submit an amendment request and secure IRB approval.

In future correspondence about this matter, please refer to the IRB file ID, name of the Principal Investigator, and study title. Thank you.

Sincerely,

Martha C. Patterson, CIP
Research Protocol Analyst
This letter has been digitally signed

CC:			
	Begley	Elizabeth	Information Services
	Fielder	Bridget	Winship - Main
	Fuller	Syreese	Winship - Main
	Scott	Kevin	Ctr for Transplant'n
	Gelbard	Rondi	Surgery - Main
	Kirk	Allan	Ctr for Transplant'n
	Moore	Thomas	Orthopaedics - Main

Emory University
1599 Clifton Road, 5th Floor - Atlanta, Georgia 30322
Tel: 404 712 0720 - Fax: 404 727 1358 - Email: irb@emory edu - Web: http://www irb emory edu/
An equal opportunity, affirmative action university

EMORY UNIVERSITY

Date: Thursday, June 19, 2014 2:37:07 PM
View: SF - IRB CR Study Status

Print Close

Continuing Review

Study ID:IRB00058229

Study Name: Biomarker expression in traumatic wounds

1.0 * **Are you continuing to enroll new subjects or obtaining charts/data/specimens?**

Yes, continuing to enroll subjects

2.0 **If the study is closed to enrollment:**

Provide the date the study was closed to enrollment:

Provide the enrollment closure reason:

3.0 * **Did any of the following Internal Events occur within the past approval period?**

Unanticipated problem (related to the research) involving risk to participants or others ○ Yes ◉ **No**

Serious adverse events that were definitely, probably, or possibly related to the research ○ Yes ◉ **No**

Deaths ○ Yes ◉ **No**

Anticipated events that occured with a greater frequency, duration, or severity than what is described in the protocol related documents ○ Yes ◉ **No**

Protocol deviations ○ Yes ◉ **No**

Complaints ○ Yes ◉ **No**

4.0 * **Did any of the following External Events occur within the past approval period?**

Unanticipated problem (related to the research) involving risk to participants or others ○ Yes ◉ **No**

Any event the investigator or sponsor believes changes the risk level of the study? ○ Yes ◉ **No**

5.0 * **Have all reportable events been reported to the IRB as required in this approval period, either previously reported or with this renewal?**

N/A

If no, please submit single events using the Reportable Events activity. To submit a summary report with this renewal, please upload the summary here and any actions taken:

Name	Modified	Version

There are no items to display

6.0 * **Did any events require a change to protocol related documents (e.g., protocol, informed consent document, Investigator's brochure)?** ○ Yes ◉ **No**

If yes, please upload:

Name	Modified	Version

There are no items to display

Enrollment Numbers: A subject is considered to be enrolled in a study when he/she gives informed consent to participate.

1.0 If your study only involves chart reviews, medical records and/or data specimens analysis, enter the number of charts/records/specimens reviewed/analyzed to date:

2.0 How many NEW subjects have been enrolled (per the definition above) in the past approval period?

10

3.0 What is the total number of subjects who have given informed consent to date?

13

4.0 How many subjects completed required screening and began treatment/intervention/participation to date?

13

5.0 Is the number of subjects from 3.0 greater than the number of subjects approved for enrollment by the IRB? ○ **Yes** ◉ **No**

*Number of subjects approved for enrollment by the IRB:*400

If the number of subjects participating is greater than the number approved, please explain the difference:

6.0 Indicate the gender composition of the research subject population you have enrolled during the past approval period:

Unknown or data not collected: ○ Yes ○ No

Female: 2

Male: 8

7.0 How many participants are considered members of specific vulnerable populations?

Please indicate how many participants are vulnerable and under what category (for example, "2 pregnant women and 1 prisoner".)

none

8.0 Indicate the age groups of the research subject population you have enrolled during the past approval period:

18 years old and older

9.0 How many participants were withdrawn from the study during the past approval period? Please attach a brief summary of withdraws.

0

Name	Description

There are no items to display

10.0 Explain any difficulties in recruiting or retaining subjects:

11.0 Is this a VA study: ○ **Yes** ◉ **No**

If yes, please give a minority status of those entered into the protocol.

iew: SF - IRB CR Research

Research Findings and Results

1.0* **Provide a summary of the research findings during the previous approval period:**

10 additional subjects have enrolled in the prior review period. Due to slower than expected enrollment, an amendment was submitted and approved expanding enrollment criteria, in addition a Spanish translation consent was obtained. This has improved pace of enrollment. There has been no interim analysis of data or assays to date.

2.0* **Were there any significant new findings during the previous approval period:**

○ Yes ◉ **No**

If yes, describe the new findings or upload reports:

Name	Description
There are no items to display	

Have current subjects been notified of the significant new findings?

○ Yes ○ No

If no, explain how and when notification will occur:

If yes, explain how and when notification did occur:

3.0* **Have any new findings emerged that may affect the willingness of subjects to continue participation?** ○ Yes ◉ **No**

If yes, please explain:

4.0* **Has the PI's risk-benefit assessment changed based on study results?** ○ Yes ◉ **No**

If yes, explain how and what changes need to be made to the protocol to ensure safety to participants:

5.0* **Has any agency (e.g., FDA or OHRP) or sponsor audited, inspected or otherwise monitored activity at this study site during the past approval period?**

○ Yes ◉ **No**

If yes, upload any correspondence or reports:

Name	Description
There are no items to display	

6.0* **Were there any reports in recent literature, publications and/or abstracts resulting from the conduct of this research? If so, upload copies.**

○ Yes ◉ **No**

Name	Description
There are no items to display	

7.0 **Attach any reports from the data and safety monitoring body and annual IND or IDE reports submitted to FDA. If none are available, please explain (lack of explanation may cause a deferral).**

Name	Description
There are no items to display	

iew: SF - IRB CR Conflict of Interest

Conflict of Interest

- **For more information about Emory COI policies, click here.**

1.0 * Institutional Financial Interest

Is any licensed Emory intellectual property used in this project?:

○ Yes ◉ **No**

2.0 * Investigator Financial Interest

Does the PI/Project Director, any individual listed as Senior/Key Personnel on the grant/contract, and/or any individual identified by the PI/Project Director as having responsibility for and substantial independence in decision making for the design, conduct or reporting of this protocol (including spouse, same-sex domestic partner and/or dependent children, individually or in aggregate) have any of the following financial relationships with (a) the study sponsor; (b) a company whose products or services are used or studied in the research; and/or (c) the technology being studied.

Select YES if any of the following apply:

- Payments of $5,000 or more including salary; consulting fees; honoraria; and/or gifts received within the past 12 months or anticipated for the next 12 months (excluding salary, grant support, and other payments for services received from Emory University)
- Equity or ownership interest (including stock options) valued at $5,000 or more as determined by reference to the entity's publicly listed price (excluding mutual funds)
- Any equity or ownership interest in an entity if the entity's value cannot be determined by reference to publicly listed prices (e.g., privately-held companies, such as start-up companies)
- A position as director, officer, partner, trustee, employee, or any other position of management
- Receipt of licensing fees or royalties from intellectual property rights (patent, copyright, trademark, trade secrets, etc.) that are more than $5,000 annually from an entity or for a technology related to an Investigator's teaching, research, administrative, or clinical duties at Emory
- Any compensation whose value could be affected by the outcome of the research.

Member of the study team has conflict of interest: ○ Yes ◉ **No**

2.0.1 If yes, please provide ID# from the eCOI Proposal Financial Interest in Research Report:

iew: SF - IRB CR Final Page

Summary of Study Status and Next Steps

1.0 Study Status:Yes, continuing to enroll subjects

2.0 Changes in Consent, Waivers, HIPAA or research instruments: no

3.0 Subjects participating is greater than the number of subjects approved: no

You need to submit an **Amendent** if you answered **yes** to any of the questions above.

4.0 Reportable Events since last continuing review:

If you have a single event that needs to be reported, please submit it using the Reportable Event activity. If you have a summary report, please submit it with this continuing review.

5.0 Click the '**Finish**' button to exit this page. Click on the '**Submit**' activity in the project workspace to send to the IRB Office.